UNIVERSITAT DE BARCELONA

Formation and subsequent inversion of extensional salt-detached ramp-syncline basins developed above ramp-flatramp faults

Maria Roma Nuñez

GGAC
Grup de Geodinàmica i Anàlisi de Conques

UNIVERSITAT DE BARCELONA

Institut de Recerca Geomodels

Formation and subsequent inversion of extensional salt-detached ramp-syncline basins developed above ramp-flat-ramp faults

Maria Roma Nuñez

Memòria de Tesi Doctoral

Desembre 2019

Institut de Recerca Geomodels
Grup de Recerca de Geodinàmica i Anàlisi de Conques
Departament de Dinàmica de la Terra i de l'Oceà
Universitat de Barcelona

Supervisors:
Dr. Josep Anton Muñoz de la Fuente
Dr. José Oriol Ferrer Garcia

Institut de Recerca Geomodels

Grup de Recerca de Geodinàmica i Anàlisi de Conques

Departament de Dinàmica de la Terra i de l'Oceà

Universitat de Barcelona

FORMATION AND SUBSEQUENT INVERSION OF EXTENSIONAL SALT-DETACHED RAMP-SYNCLINE BASINS DEVELOPED ABOVE RAMP-FLAT-RAMP FAULTS

Memòria presentada per **Maria Roma Nuñez** per optar al grau de Doctor en Ciències Geològiques per la Universitat de Barcelona.

Aquesta memòria s'ha realitzat dins del Programa de Doctorat de Ciències de la Terra (H0Z01 - HDK09), sota la direcció del **Dr. Josep Antoni Muñoz de la Fuente** i el **Dr. José Oriol Ferrer Garcia.**

Maria Roma Nuñez

Barcelona, Desembre 2019

Dr. Josep Antoni Muñoz de la Fuente

Dr. José Oriol Ferrer Garcia

This PhD thesis has been realized within both, the Grup de Recerca de Geodinàmica i Anàlisi de conques (2014SGR467-2017SGR-596, funded by the Secretaria d'Universitats i Recerca del Departament d'Economia i Coneixement de la Generalitat de Catalunya and the Agènica de Gestió d'Ajuts Universitaris i de Recerca) and the Institut de Recerca Geomodels (funded by the Universtitat de Barcelona and the Fundació Bosch i Gimpera). Most of the work as PhD student has been carried out at the Departament de Dinàmica de la Terra i de l'Oceà (formerly Departament de Geodinàmica i Geofísica) of the Universitat de Barcelona. The research project has also been funded by the projects SALTECRES (CGL2014-54118-C2-1-R-BTE) and SALTCONBELT (CGL2017-85532-P) from the Ministerio de Ciencia e Innovación of the Spanish Government. The research project has been based in two analog modeling experimental programs. The first experimental program was carried out at the SIMGEO-Geomodels Analogue Modelling Laboratory. This laboratory was supported by a Scientific Infrastructures Project (UNBA08-4E-006) co-funded by Statoil and the European Regional Development Fund of the Ministerio de Ciencia e Innovación of the Spanish Government. The second experimental program was carried out at the Royal Holloway University of London, at Fault Dynamics Research Group. This laboratory was funded by the STAR Research Consortium, sponsored by the BG Group, BHPBilliton, ConocoPhilips, Eni, MarathonOil, Nexen, Shell, Talisman Energy, and YFP. The interpretation of experimental data have been done using academic software licenses of GoCad, Move, Petrel and Kingdom Suite provided by Paradigm^{MT}, Midland Valley, Schlumberger and HIS respectively. During the research project, Maria Roma Nuñez benefited from one predoctoral contract (FBG307451) from March 2014 to March 2017. After the research activities carried out by the PhD student have been financially supported by an APIF (Ajuts al Personal Investigador en Formació) predoctoral grant awarded from the Universitat de Barcelona.

a l'avi

If you can't explain it simply, you don't understand it well enough

Albert Einstein

A G R A Ï M E N T S

Sembla que ha arribat el dia de tancar el que vam iniciar fa cinc anys i em costa de creure la quantitat de persones que he conegut i m'han ajudat a fer possible aquesta tesi. Aquests darrers mesos, des de la distància física de viure a l'altre banda de l'Atlànic, he pogut fer balanç del doctorat. Estic molt satisfeta de poder dir que ha estat una experiència que m'ha ajudat a créixer professional i personalment al mateix temps que he gaudit de la geologia i de totes les persones que me l'han ensenyat.

En primer lloc m'agradaria donar les gràcies al meu director de tesi Josep Anton Muñoz per haver-me donat l'oportunitat de treballar en el projecte de Tanzània, de realitzar l'estada de recerca a Egham i d'enviar-me a innumerables congressos al llarg d'aquests anys. Agrair-te també, que encara que en alguns moments no haguem pogut tenir un contacte continuat, sempre has estat a prop en els moments decisius. En aquells moments que requerien de la teva habilitat a l'hora d'aportar idees claus per desfer nusos, habilitat que sempre t'he admirat. Per últim, m'agradaria dir que acompanyar-te al camp ha estat un luxe, al teu costat he après que per entendre qualsevol estructura geològica cal buscar sempre l'explicació més fàcil.

No tinc paraules per agrair-te tot el que has fet per mi Oriol Ferrer. La llista és infinita, però el més important ha estat comptar sempre amb la teva plena confiança. Em vas dirigir el treball final de màster, em vas posar a càrrec dels models analògics del projecte de Tanzània, em vas deixar com a responsable del laboratori de modelització de Geomodels quan vas marxar a Londres, em vas convidar i cuidar durant l'estada de recerca a la Royal Holloway i em vas acompanyar a tots els congressos durant aquella època. A més a més, cal dir que aquesta tesi no hagués arribat tant lluny sense la teva plena disponibilitat. Has prioritzat sempre els meus treballs i les correccions dels articles a la teva pròpia feina. T'has esforçat a ensenyar-me a escriure, a fer bones figures, pòsters i presentacions, i a ser sempre meticulosa amb la feina. Com alumne teva puc dir que créixer al teu costat ha estat una sort, tant es així, que he sigut l'enveja del Frede i l'Uri. Després d'aquests anys, de les mil hores al camp i les mil i una als laboratoris em sembla que m'emporto més que un director de tesi.

Voldria agrair també al meu director postís, l'Eduard Roca, per la confiança dipositada en aquesta tesi des del primer dia, per estar sempre disponible quan m'han sorgit dubtes, per guiar-me i ensenyar-me. He aprés molt al teu costat, sobretot en questa última etapa

compartint despatx. Volia agrair-te especialment tots aquets moments que m'has explicat la geologia estructural amb paciència i des de les bases. També afegir que gràcies al teu suport financer he pogut publicar i divulgar la recerca feta durant aquest anys.

I want to thank you to Professor Ken McClay for bring me the opportunity to do a research internship at Fault Dynamics laboratory, and also thank you for your help during the articles revisions and to support my research since today.

Estoy especialmente agradecida a Marco Snidero por el tiempo que pasamos juntos en Tanzania. Me conociste que ni sabía dónde estaba ni hacia donde iba, pero aun así, creíste en mi. Me quedo con lo especial y importante que siempre me has hecho sentir a tu lado.

Moltes gràcies a l'Òscar Gratacós, per dedicar-me el temps que no tenies, *Gocad* amunt i *Move* avall, pels teus consell dietètics, per gestionar la 226 i fer-ho tot més fàcil.

También quiero darte las gracias Pablo Granado por tus consejos de cómo llevar la tesis, tus críticas constructivas y por sugerirme artículos que me han ayudado mucho.

Agrair també a la Núria Carrera i al Pablo Santolaria per escoltar-me en els deu minuts del cafè, el vostre punt de vista sempre m'ha ajudat a reflexionar i trobar solucions.

Un record especial per la Teresa Beamud, per facilitar-me la feina durant aquests anys, i per la teva companyia en aquests *coffebreaks*, curts però intensos on hem rigut molt i que sens dubte, trobaré a faltar.

Gràcies Oskar Vidal, per no rendir-te durant el procés de publicar el meu primer article i per estar a tota hora disponible responent els meus correus farcits de preguntes.

Un gràcies molt afectuós al Frede i al Miró, pel seu recolzament en moments de dubtes i incerteses, però també en els bons moments. Crec que m'emporto a dos molt bons amics.

Moltes gràcies a la resta de companys, Patricia Cabello, Mireia Butillé, Esther Izquierdo, Joana Mencos, Marina Nebot, Pau Arbués, Marco de Matteis, Fani Górriz, Elisabeth Wilson, Rodolfo Uganda, que sempre heu estat allà per animar-me i disposats a ajudar-me.

Gràcies a tot el Departament de Dinàmica de la Terra i de l'Oceà per mostrar un interès en l'avanç de la tesi. Al seu equip administratiu per donar-me el suport logístic necessari. I a l'administració de la Facultat de Ciències de la Terra, en especial a la Susana, per ajudar-me des de la distància en el procés del dipòsit.

Gràcies a les meves amigues que, tot i que em sembla que a hores d'ara encara no han entès exactament el que faig, sempre m'han recolzat, anima't i sobretot estima't. Moltes gràcies al Francesc, la Montse i al Cesc per estar sempre pendents i a prop per tot el que ha fet falta.

He tingut la sort de néixer en una gran família i sens dubte aquesta tesi és gràcies a vosaltres. Estic molt agraïda als meus pares pel seu suport incondicional, a la meva germana Anna per relativitzar els meus "problemes", al meu germà Aniol per la curiositat en la geologia i preguntar sense parar, i al meu germà Yuri per cuidar-me des de la distància.

Molt especialment agraïda a l'Oriol, company de carrera, parella de màster i marit de tesi. No t'ho he posat fàcil i no se com t'ho has fet, però si sóc aquí és gràcies a tu. T'estimo.

TABLE OF CONTENTS

PREFACE AND THESIS DESCRIPTION

MOTIVATION AND OBJECTIVES

Seismic and field data reveal the existence of extensional synclinal basins not bounded by major faults. Nevertheless, their origin and mechanisms of development still remain unclear. This is because the accommodation space of extensional synclinal basins may be created by basement steps underneath the prekinematic succession or, alternatively, for a given prekinematic layer the position of the extensional faults may be laterally shifted by a decoupling horizon. In any case, the existence of weak horizons in the deformed sedimentary pile, such as salt, enhance the formation of extensional synclinal basins. As a result, most of the examples of these basins are related with salt tectonics. Furthermore, extensional synclinal basins may be masked if these basins are subsequently partially-to-totally inverted and eventually incorporated into fold-and-thrust belts. In such settings, recognizing the existence or the geometry of subsalt extensional faults that created the accommodation space and deciphering the kinematic evolution are not straightforward. Despite improvements in seismic imaging and processing, the structural complexity of these systems still allows for conflicting interpretations.

The Geomodels Research Institute, over many years ago has been dealing with the formation and subsequent inversion of extensional synclinal basins (García-Senz, 2002; Ferrer, 2012, Mencos, 2010; Carola, 2014; Nebot, 2016). Therefore, in order to gain insight into the knowledge of the origin and development of these basins, this thesis has been designed to develop experimental analog modeling with the aim to compare modeling results with case studies based on both field and seismic data. In this sense two experimental programs are included in this thesis.

The Experimental Program 1 has been designed for the understanding of the Columbrets basin, in the Southern Valencia Trough. This is a case study based on the interpretation of the Columbrets Basin seismic dataset, provided by Cairn Energy. This basin formed in a hyperextended domain above a major low-angle extensional subsalt fault. It was subsequently weakly inverted by detachment along the Upper Triassic evaporites. In order to support the interpretation of the Columbrets Basin, the Experimental Program 1 includes 8 final sandbox models developed at the *GEOMODELS Analog Modeling Laboratory (University of Barcelona)*. It consists to reproduce a high degree of extension involving two detachment levels: i) the low-angle extensional fault and ii) the prekinematic Upper Triassic evaporites by

using a plastic sheet and a polymer unit respectively, and then the resulted basin was weakly inverted. The results of the Experimental Program 1 have proved its reproducibility in different climatic conditions, taking advantage of the collaborative project with the *Geomaabara analog modeling laboratory at the Earth Science Department-UDOM*-Tanzania.

The Experimental Program 2 has been designed for the understanding of the structural features observed in basins studied by the Geomodels Group. The majority of the cases are based on field examples of partially-to-totally inverted basins. Thus, the experimental program aims to reproduce two phases of extensional deformation above a pair of ramp-flat faults, with sedimentation of salt between the two extensional phases, and subsequently the resulted basins were inverted recovering the entire amount of extensional displacement. The Experimental Program 2 has developed during the research stay at the *Fault Dynamics Research Group Laboratory (Royal Holloway University of London)*, in order to request the international PhD status.

This thesis presents a wide new variety of analytical techniques based on analog models that increase the visualization of the basin kinematic evolution. These new visualization methodologies also improve the comparison between analogs and other worldwide basins (seismic or outcrop data), thus reducing the uncertainty during interpretation.

Finally, the integration of both experimental programs, the potential analytic tools and the overall discussions; motivated to develop a review of extensional synclinal basins. This review is presented as the introduction chapter of this manuscript.

Accordingly and following the exposed problem approach, this thesis pursues the following main objectives:

- Use scaled analog models as a main tool to resolve the unanswered questions about the formation and kinematic evolution of the extensional synclinal basins detached on salt. The most noteworthy of these questions are: how do these basins are formed, how do they develop and which factors control them during extension and inversion?

- Provide a general guide for improving the interpretation of salt-bearing basins where these styles of extensional salt tectonics develop. This guide is addresses to researchers in

extensional salt tectonics for academic propose, but also to industry geoscientists whose efforts are focused on hydrocarbon exploration and production in subsalt environments.

From these main objectives the following detailed objectives are:

- Provide a review of synclinal basins and a state of the art of extensional analog models.

- Study the role of salt, welding kinematics and synkinematic sedimentation during basin inversion.

- Provide a new structural and kinematic model for the Columbrets Basin (Western Mediterranean) through the integrated understanding of the geometry of both supra and subsalt structures. In addition, acquire a regional cross-section, constructed with the support of seismic data, onshore fieldwork and gravity modeling.

- Provide a general overview of the new advanced analytical techniques in analog modeling and their application to structural interpretation, by quantifying **i)** the salt mobilization from sandbox cross-section restorations, and **ii)** the deformation and the along-strike structural variation with 3D structural models obtained from data capture.

STRUCURE AND ORGANIZATION OF THE THESIS

This memoir is presented as a compendium of three scientific articles published on international journals included in the citation index report. On the basis of the previous outlined approach, the present memoir has been organized in the following chapters:

CHAPTER 1 that provides a summary of the thesis, both in English and Catalan.

CHAPTER 2 This section drives to specify the characteristics and involved mechanisms that define ramp-syncline and salt-detached ramp-syncline basins, together with the origin and kinematic model of ramp-flat-ramp extensional faults. Therefore, this chapter provides an overview of the widespread-recognized salt-detached ramp-syncline basins and the state of the art of extensional analog models. The chapter finishes with the description of the methodology used in this thesis to solve the exposed issues.

In **CHAPTER 3** the general results of this thesis are described. The first section is about the results obtained from the Experimental Program 1 inspired in the Columbrets Basin, the second section shows the analog model results from Experimental Program 2 inspired in extensional basins that have experienced multiple rift phases and subsequently inverted. The results of this second experimental program allow us to analyze the salt mobilization from cross-section kinematic restoration. The third section is based also on the results of the Experimental Program 2, but in that case focused in the involved salt tectonics.

CHAPTER 4 provides an overall summary for the discussions about the results of both experimental programs that have been exposed in the published articles. The chapter pretends answering the questions proposed in the introduction review.

CHAPTER 5 lists the summary of the conclusions of this thesis

CHAPTER 6 lists all the references mentioned throughout the manuscript.

APPENDIX provides a copy of the already published articles.

CHAPTER 1. SUMMARY

ABSTRACT

The widespread extensional deformation that took place during Jurassic to Cretaceous times in Western Europe and the North Atlantic margin resulted in the formation of several rift systems. Some of the resulting basins associated with these rifts show broad synclines detached on pre- or synkinematic Permian or Triassic salts and filled by thick sedimentary successions. They are rarely fault bounded, instead they are bounded by salt structures that are generally parallel to the major subsalt structures. As such, the formation of these extensional systems requires the presence of **i)** a subsalt extensional fault with significant dip changes and **ii)** an evaporitic unit above the extensional fault, which partially or completely decouples the suprasalt basin from the subsalt extensional fault. Moreover, the complexity of these scenarios further increases when some of these basins, during latest Cretaceous and Cenozoic times, were partially inverted or incorporated into fold-and-thrust belt.

Synclinal basins have a significant exploration potential when their extensional geometry is preserved and when they have undergone positive tectonic inversion. However, in some cases, their subsalt geometry may not be fully recognizable, especially when the imaging of the subsalt seismic data is poor. The shape and kinematics of such faults have usually been established using the architecture of synkinematic units and by assuming complete coupling of the hangingwall rocks. Therefore, there are fault interpretations that do not consider the role of deep salt layers, which clearly act as an effective detachment, decoupling sub- and suprasalt deformations.

This thesis provides a review of the formation and evolution extensional synclinal basins and an overview of the widespread-recognized salt-detached ramp-syncline basins. To obtain a deeper understanding of the geometry and kinematic evolution of these salt-detached ramp-syncline basins, the principal aim of this thesis is to decipher the factors that are involved in the development of these basins during both extension and inversion.

To achieve this goal we carried out a deep investigation about the state of the art of extensional analog models, then we performed two experimental programs consisting in different sandbox models. The experimental results, together with the new used analytic tools, reveal that the kinematic evolution of the salt-detached ramp-syncline basins during extension and inversion depends on the interaction of different factors that may function simultaneously. Our results show that the main structure formed at the end of the extension is

a salt-detached ramp-syncline. Its formation and evolution not only depends on the subsalt fault type and geometry, but also on the subsalt fault displacement, salt migration, salt thickness and degree of decoupling. In addition, the inversion of these salt-detached ramp-syncline basins is also controlled by syninversion sedimentation, erosion and the kinematics of the inherited extensional and salt structures (or its equivalent welding). The inversion of these basins resulted in a major thick-skinned fault-bend anticline with thin-skinned contractional structures.

Our results are used to improve the interpretation of the Mesozoic Columbrets Basin (Western Mediterranean) and serve a guide for seismic sections of inverted Mesozoic salt-detached ramp-syncline basins on the Atlantic margins, where subsalt faults are not well-imaged, and thus the suprasalt geometries must be used to infer the subsalt structure.

RESUM EN CATALÀ

L'extensió Juràssica – Cretàcica Inferior que va tenir lloc a l'Europa Occidental i al marge Nord Atlàntic va resultar en la formació de nombrosos sistemes de rift. Les conques associades a aquests rifts es mostres com a sinclinals amples, reomplerts per grans successions sedimentaries i desenganxats a un nivell salí (Pèrmic o Triàsic Superior). Aquestes conques rarament estan directament associades a falles, en canvi es troben limitades per estructures salines que generalment son paral·leles a les estructures del basament. Per tant, la formació d'aquests sistemes extensionals requereix la presencia de **i)** una falla de basament extensiva amb diferents cabussaments i **ii)** una unitat evaporítica a sobre d'aquesta falla, la qual genera un desacoblament parcial o total respecte la conca i la falla extensiva. A més a més, la complexitat d'aquests contextos geològics augmenta quan algunes d'aquestes conques es troben parcialment invertides o fins i tot incorporades en cinturons de plecs i encavalcament durant el Cretaci Superior i Cenozoic.

Les dades sísmiques i de camp permeten precisar la geometria d'aquestes conques sinclinals, però no la de les falles extensionals que las van originar. La geometria i la cinemàtica de las falles extensives associades ha aquestes conques, normalment s'ha establert utilitzant la geometria dels materials més superficials i assumint un acoblament total entre el basament i la cobertora. Aquestes interpretacions no consideren el paper que pot juga un nivell salí profund que clarament desacobla la deformació entre el basament i la cobertora.

L'objectiu principal d'aquesta tesi es investigar els principals factors que controlen la formació i evolució de les conques sinclinals, utilitzant com a eina principal la modelització analògica. Per assolir aquest objectiu s'ha realitzat una revisió sobre conques sinclinals i una revisió de models analògics extensius realitzats fins ara. A partir d'aquests antecedents s'han realitzat dos programes experimentals. Els resultats d'aquests mostren com la formació i evolució de les conques sinclinals depenen de diversos factors que actuen simultàniament durant l'extensió i la posterior inversió.

Aquesta tesi es pot utilitzar com a guia per reduir les incertes durant la interpretació de la geometria del basament associat a conques sinclinals desenvolupades en contextos salins, sobretot en el casos on les dades sísmiques disponibles no tenen bona resolució i cal utilitzar la geometria de la cobertora per reconèixer l'estructura del basament.

CHAPTER 2. GENERAL INTRODUCTION

2.1. SALT-DETACHED RAMP-SYNCLINE BASINS: A REVIEW

Salt-detached ramp-syncline basins are asymmetric synclinal sedimentary basins whose depocenters are not bounded by major faults, instead they appear usually flanked by salt structures. Basin geometry is controlled by the presence of a salt unit and by basement steps, both underneath the synkinematic sediments (Roma et al., 2018b).

Although basins with synclinal geometries have been classically described in contractional settings (e.g., piggy-back basins; Ori and Friend, 1984), syncline basins are also common features in extensional regimes as continental extensional systems or passive margins. They have been well documented worldwide such as in the Basin and Range province (Kruger and Johnson, 1994), Dampier Sub-Basin (McClay, 1996), Gulf of Mexico (Rowan, 2002), Newark Basin (Schlische, 1992), Suez Rift (Khalil and McClay, 2002), Jeanne d'Arc Basin (Withjack and Callaway, 2000), Matalles and Alès Basins (Benidicto et al., 1999; Sanchis and Séranne, 2000), Kvamshesten Basin (Osmundsen et al., 2000), Santos Basin (Pichel et al., 2018), Porcupine Basin (Shannon et al., 2007) among others. Nevertheless, these synclinal basins have been developed by a varied range of mechanisms: **i)** above a ramp-flat extensional fault, **ii)** by salt evacuation, **iii)** by a combination of the previous both mechanisms (involving subsalt basement steps or extensional faults and salt evacuation) or **iv)** by thermal subsidence.

The following section analyzes the mechanism that allow the development of synclinal basins, focused on those developed in the hangingwall of ramp-flat-ramp extensional faults with and without involving salt unit (i.e., ramp-syncline and salt-detached ramp-syncline basins), for their relevance in the main objective of this PhD thesis. Then, this section also provides the key suprasalt observations to distinguish between salt-detached ramp-syncline basins and other geometrically similar salt-bearing synclinal basins developed by different mechanisms.

2.1.1. Synclinal basins on extensional settings

Synclines are common in extensional fault systems and they normally host synkinematic sediments onlapping their limbs. They can develop above single planar extensional faults as extensional fault-propagation folds (Sharp et el., 2000). Extensional synclines have also been described as a fault-bend folds in the hangingwall of ramp-flat-ramp faults in rift systems (Ellis and McClay, 1988; Guimerà et al., 1995; Benedicto et al., 1999;

McDonell et al., 2010; Vetti and Fossen, 2012). In addition, synclinal basins have also been described in salt-bearing rift systems and passive margins (mechanically anisotropic), where the kinematics of these structures is more complex (Jackson and Hudec, 2005; Soto et al., 2007; Pichel et al., 2018; Roma et al., 2018a). In these scenarios, the presence of a viscous layer such as salt or over-pressured shales, promotes the formation of synclinal basins regardless of the subsalt fault type (i.e., planar non-rotational, planar rotational, listric, ramp-flat-ramp). Taking these observations into account, the following section attempts to describe extensional ramp-syncline basins developed in mechanical isotropic and anisotropic stratigraphy, i.e., by active basement fault or by salt evacuation above an active basement fault as a triggering mechanism respectively.

2.1.1.1. *Development of ramp-syncline basins in isotropic stratigraphic sequence*

Ramp-synclines are folds or flexures that form in the hangingwall of extensional faults above non-planar faults, as ramp-flat-ramp faults (Xiao and Suppe, 1992) (**Fig. 2.1**). Deformation of the hangingwall evolves as fault displacement increases and mainly depends on the deformation mechanisms, geometry of the fault, and rheology of the deformed rocks.

The hangingwall deformation of non-planar extensional faults, such as ramp-flat-ramp geometries, results from hangingwall accommodation to the fault geometry during displacement (Fossen, 2016). Hangingwall deformation results in: **i)** a breakaway half-graben above the upper ramp, **ii)** a ramp-synclinal (Xiao and Suppe, 1992) above the lower ramp, and **iii)** a landward (or ramp-anticline) and basinward extensional rollovers respectively associated with the upper and lower ramp-flat pair (Gibbs, 1984; McClay and Ellis, 1987a and b; Ellis and McClay, 1988; McClay, 1990; McClay, 1996; McClay and Scott, 1991; Benedicto et al., 1999). Secondary structures as crestal collapse grabens within the rollovers, curved normal faults above the lower ramp and minor antithetic normal faults within the basinward rollover panel, can be developed depending on the amount of fault displacement (McClay and Scott, 1991) (**Fig. 2.1**). The most basinward planar or sigmoidal antithetic fault separates the rotational block in its hangingwall and the translational block in its footwall.

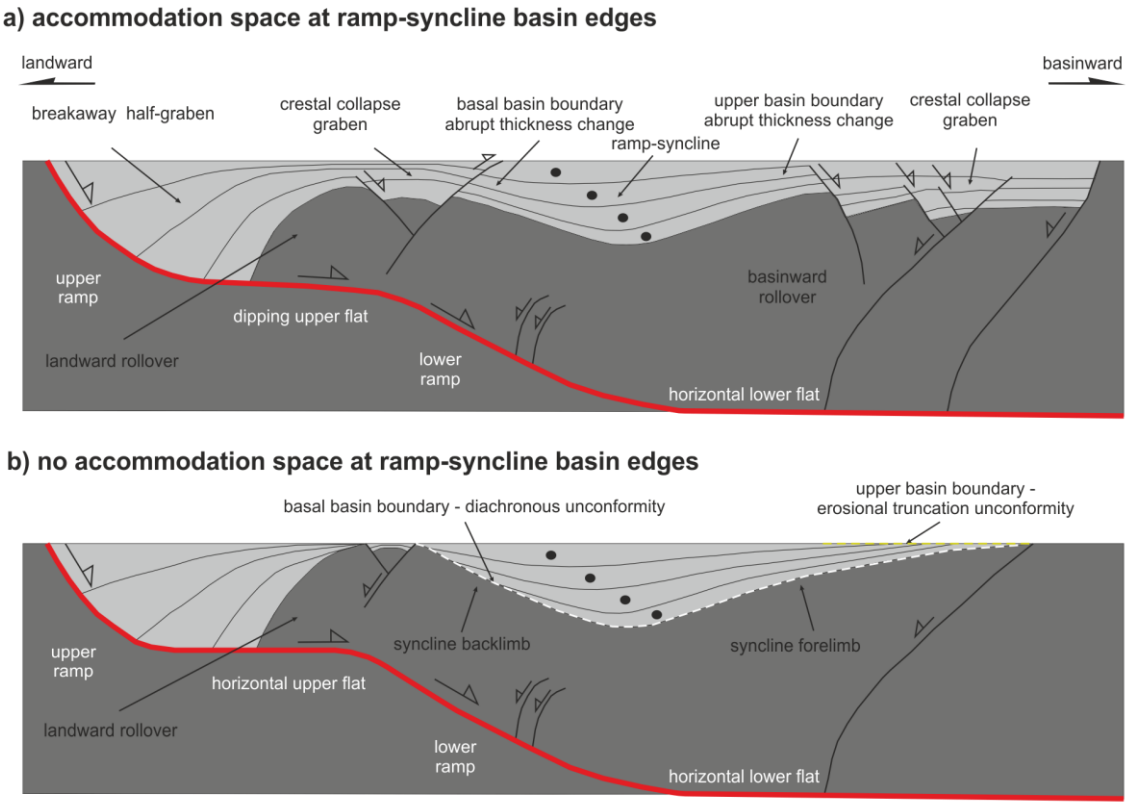

Fig.2.1. Sketch illustrating the structures developed above a ramp-flat-ramp fault (modified from McClay and Scott, 1991). **a)** Accommodation space above the upper footwall flat. **b)** No accommodation space above the upper footwall flat. Note that the accommodation space is directly related with the dipping of the upper footwall flat. The black dots within the asymmetric ramp-syncline basin indicate the progressive landward-shifting of the synextensional depocenters as extension increase.

Synclinal basins developed above a non-planar extensional faults have received several names in the literature depending on the authors: **i)** hangingwall syncline (Gibbs, 1984); **ii)** ramp-syncline basin (Ellis and McClay, 1988; McClay, 1990; McClay and Scott, 1991; McClay, 1996); **iii)** extensional-ramp basin (Guimerà et al., 1995); **iv)** extensional hanging-wall syncline basin (Benedicto et al., 1999; Sanchis and Séranne, 2000); **v)** ramp basin (McDonell et al., 2010); **vi)** hanging-wall basins (Vetti and Fossen, 2012). Taking into account all this terminology to describe the same structure, we will hereinafter refer to ramp-syncline basins for the hangingwall synclines developed above ramp-flat-ramp extensional faults. We think this term is the most accurate to define this type of basins because their development requires the presence of a fault ramp underneath the hangingwall.

Ramp-syncline basins develop by regional extension, but synkinematic sediments are not bounded by shallow major faults. In this sense, whereas both extensional rollovers have fault cutoffs (**Fig. 2.1**), the ramp-syncline basin is an unfaulted growth syncline. During

extension, both rollovers and basins (i.e., half-graben and ramp-syncline) move basinward away from the respective ramp where it initially formed. Its final location depends on the amount of displacement. As the hangingwall slides down above the footwall ramp, the locus of the ramp-syncline depocenter remains fixed over time. This kinematics entailed a progressive migration of the synextensional depocenters as the fault displacement increases producing a characteristic asymmetric ramp-syncline basin (**Fig. 2.1a**).

Ramp-syncline basins exhibit a large variation in size, from major basins (i.e., Columbrets Basin (Roca, 1996) to some local basins (i.e., Alés Basin, Sanchis and Seranne, 2000), and they can contain stratigraphic successions that are more than 3 km thick.

As noted above, one of the key factors to identify ramp-syncline basins is the architecture of the synrift deposits. The basin infill is characterized by progressive landward-shifting of the depocenters, resulting in an asymmetric syncline with a basinward-dipping growth axial surface (**Fig. 2.1**). The synrift beds dip in the opposite direction to the tectonic transport, and have commonly a sigmoidal-shape defining in some cases "pseudo-clinorforms" (**Fig. 2.1b)**. The basin infill onlaps the prekinematic syncline forelimb (limb vergent towards transport direction) (**Fig. 2.1**). Therefore, without being in direct contact with the master fault itself, as occurs in the breakaway half-grabens (Vetti and Fossen, 2012) (**Fig. 2.1**). This unconformable deposition defines the basal boundary of the basin (**Fig. 2.1**).

The geometry of the ramp-syncline basin will be strongly controlled by the relative rate of aggradation (or sediment accommodation space)/erosion, fault geometry and displacement (Withjack and Schidle, 2006). Depending on these factors, the basin boundaries will present: **i)** an abrupt thickness change of the synkinematic unit (Withjack and Schlische, 2006) (**Fig. 2.1a**), or **ii)** a diachronous unconformity (**Fig. 2.1b**) (Jackson and Hudec, 2005). The growth axial surface will remain parallel to the lower ramp only if the thickness above the landward rollover does not change during the extension. In contrast, erosion or aggradation above the landward rollover would decrease or increase the dip of the growth axial surface respectively (Bedenicto et al., 1999).

2.1.1.2. *Development of salt-detached ramp-syncline basins in anisotropic stratigraphic sequence*

Additionally to the previous described scenario, ramp-syncline basins may also develop in mechanical anisotropic stratigraphic sequences (hereinafter salt-detached ramp-synclines). Salt facilities the development of salt-detached ramp-syncline basins above active normal faults by draping the suprasalt layers over basement steps produced by subsalt faults. Formation of such extensional drape folds requires decoupling of the suprasalt layers above the sub-salt succession. Slow basement deformation, thicker and low viscosity evaporites favor decoupling of overburden sediments (Withjack and Callaway, 2000).

In this case, mixed modes of deformation styles may be expected (i.e., thick- versus thin-skinned deformation styles), where at least three factors are interacting: **i)** the accommodation space generated by the fault basement geometry and displacement (thick-skinned deformation); **ii)** the suprasalt lateral translation (thin-skinned deformation) and **iii)** the salt evacuation generated by the differential loading. The interaction among these factors results into different basin geometries and stacking patterns of the synrift depocenters.

Three different types of subsalt extensional faults generate salt-detached ramp-syncline basins: listric, planar-rotational and ramp-flat-ramp extensional faults.

Listric extensional faults

Listric extensional faults involving a salt horizon may develop a syncline in the suprasalt succession decoupled from the underneath rollover (**Fig. 2.2a**). This syncline may host synkinematic strata characterized by basinward-migrating depocenters. As a result, a landward-dipping growth axial surface developed, contrary to the basinward-dipping axial surfaces of the ramp-syncline basins above described. In addition, reactive salt walls may develop near the footwall of the listric fault and above the basinward anticline rollover bordering the basin (Soto et al., 2007).

Planar-rotational extensional faults

The presence of a salt layer during the development of planar-rotational faults also enhances the formation of salt-detached ramp-syncline basins as the hangingwall moves

downwards and rotates. The salt facilitates decoupling and the formation of a drape fold above the tip of the fault. The progressively fault block rotation mainly controls the development of the synclinal geometry (**Fig. 2.2b)**. The architecture of the synclinal basin is characterized by a basinward shifting depocenter (i.,e landward-dipping growth axial surface) and the landward migration of the onlap above the prekinematic succession (**Fig. 2.2b)**. In addition, salt migrates mainly towards the syncline forelimb, where salt structures develop.

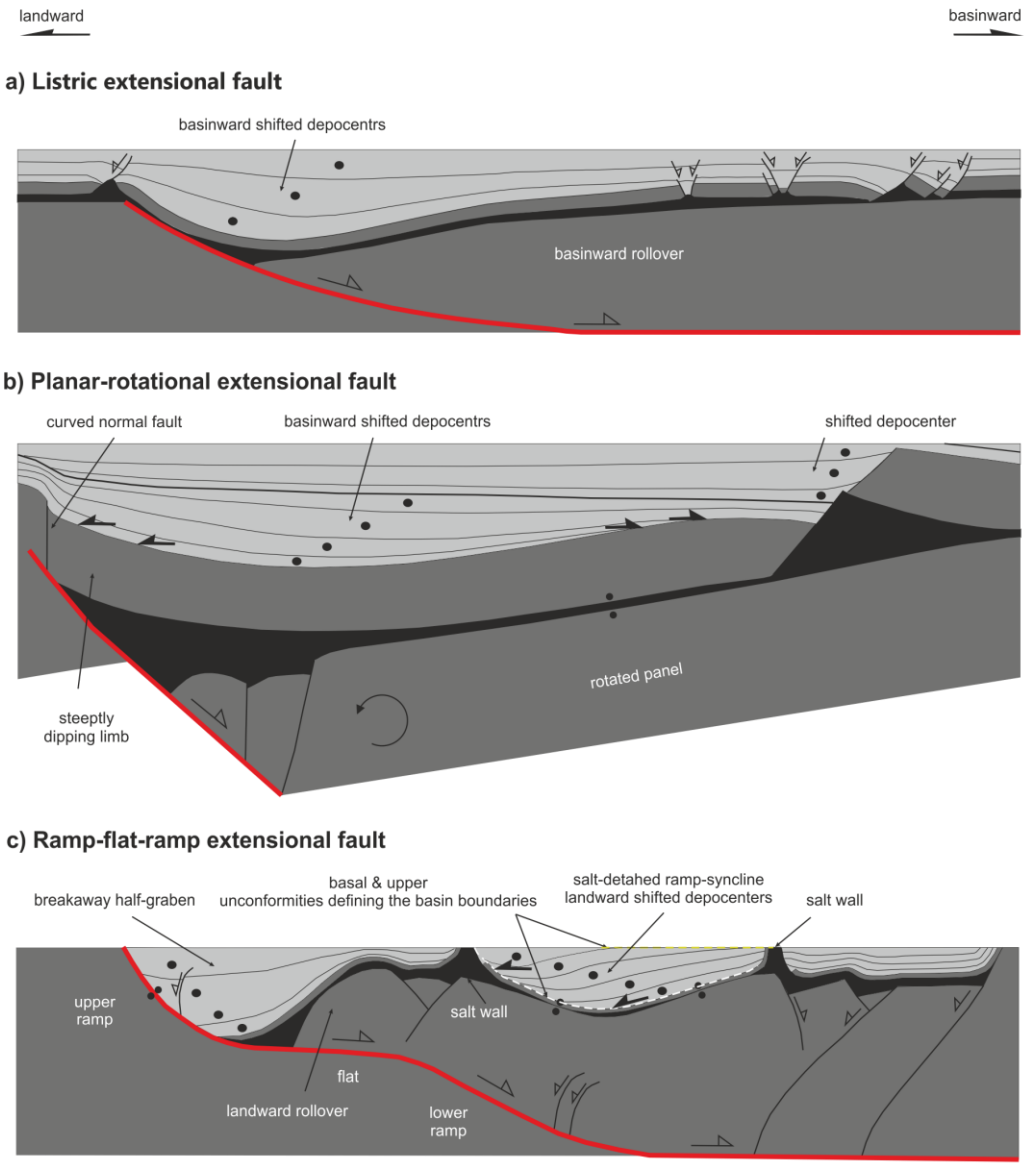

Fig.2.2. Conceptual models of **a)** a synclinal basin developed above a listric fault, modified from Soto et al. (2007), **b)** a synclinal basin developed above a rotational planar fault (sketch courtesy of O. Ferrer) and **c)** a salt-detached ramp-syncline basin developed above a ramp-flat-ramp listric fault (modified from McClay and Scott (1991) and based on Ferrer et al. (2016)). In the three sketches the black polygon corresponds to a pre-extensional polymer equivalent to salt in nature.

Ramp-flat-ramp extensional faults

In this case (**Fig. 2.2c**), the salt-involved fault system is characterized by: **i)** breakaway half-graben, **ii)** subsalt landward and basinward extensional rollovers; **iii)** a salt-detached ramp-syncline basin not bounded by extensional faults, and **iv)** salt structures bounding the basin striking parallel to the major subsalt structures. Secondary structures such as crestal collapse graben in the subsalt extensional rollovers, curved normal faults above the lower ramp and minor antithetic normal faults within the basinward rollover are developed.

Salt-detached ramp-syncline basins develop by regional extension, where the resulted basins are characterized by asymmetric synclines filled by synrift sediments; showing landward-shifting depocenters and basinward-dipping growth axial surfaces (**Fig. 2.2c**). Although, basinward-dipping growth axial surfaces are the result of the displacement of the synclinal basins from the lower ramp to the lower flat (as occurs in previously described classic ramp-syncline basins), such displacement is coeval with flow of the salt. Salt migration can decrease or increase the dip of the growth axial surface, masking the classical shifted depocenter geometry (Roma et al., 2018b). Salt migration is triggered by the lithostatic load produced by synkinematic sediments. Salt flows from the areas with high vertical load (basin depocenter) to the edges of the salt-detached ramp-syncline basin, where the vertical load is lower (e.g., Kehle, 1988; Koyi et al., 1993; Hudec and Jackson, 2007; Ferrer et al., 2014). This can result into salt-inflated areas bounding the salt-detached ramp-syncline basins. As extension progresses, salt-inflated areas can evolve to reactive and passive salt walls (Roma et al., 2018b). Diapirism can accelerate if the overburden of salt-inflated areas is eroded (Rowan and Vendeville, 2006).

Salt-detached ramp-syncline basins are normally decoupled from the subsalt extensional faults, thus in addition to basement extension and salt migration, usually basin translation process is involved, and they can be horizontally translated over the salt for long distances (Coward and Stewart, 1995; Stewart and Clark, 1999; Carola et al., 2015; Roma et al., 2018b).

Geometry of salt-detached ramp-syncline basin depends on sedimentary rate (aggradation or sediment accommodation space), erosion, fault geometry and displacement, but in addition by salt migration and the degree of decoupling. According to these factors, the basin boundaries will present: **i)** an abrupt thickness change of the synkinematic unit (Withjack

and Schlische, 2006) or **ii)** a diachronous unconformity (**Fig. 2.2c**) (Pichel et al., 2018). As the salt-detached ramp-syncline basin evolves and salt migration becomes a more important control factor, diapirism can rotate and even break apart these basin boundaries (Roma et al., 2018b; Pichel et al., 2018). In addition, the formation of primary welds (**Fig. 2.2c**) controls the final stages of the salt-detached ramp-syncline basin, specially because couples the deformation between supra- and subsalt units.

2.1.1.3. *Comparison between basins with synclinal geometries*

In order to promote a well-used terminology, this section shows further basins with synclinal geometries developed in salt-bearing systems, which they are geometrically similar to salt-detached ramp-syncline basins, but they differ in terms of stratal architecture, kinematic, origin and depositional setting in which they from:

i) Sinking minibasins show in most cases a synclinal geometry. However, their geometry differs from the salt-detached ramp-syncline basins. They show an equidimensional geometry and depocenters are vertically stacked (**Fig. 2.3a).**

ii) Salt-detached ramp-syncline basins show some geometrical features that may resemble salt expulsion rollovers, but there are several features that differentiate both of them (**Fig. 2.3b**). The basin boundaries that mark regions of abrupt thickness changes in the salt-detached ramp-syncline are uncharacteristic in salt expulsion rollovers. Salt-detached ramp-syncline basins usually have landward-shifted depocenters, while the best-know examples of expulsion rollovers typically have basinward-shifted depocenters (Ge et al., 1997; Jackson and Hudec, 2005). Moreover, a key observation to distinguish both of them is the position of the salt inflation.

iii) Salt-detached ramp-syncline basins also markedly differ from extensional forced folds developed above a planar non-rotational fault (**Fig. 2.3c**) in terms of salt distribution and stratal geometry. Salt-detached ramp-synclines are asymmetric synclinal basins, while extensional forced folds are upward-widening monoclines. The basinward rollover in salt-detached ramp-syncline basins implies a convex-upward fault bend, while in forced folds it does not exist. The resulting monocline shows vertical stacked synrift depocenters and usually salt structures are only developed at the monocline hinge. Instead, when the extensional system includes two conjugate non-rotational planar normal faults and an effective salt layer,

an extensional forced fold may developes at the tip of each normal fault, resulting in a growth syncline often flanked by salt structures (Dooley et al., 2005).

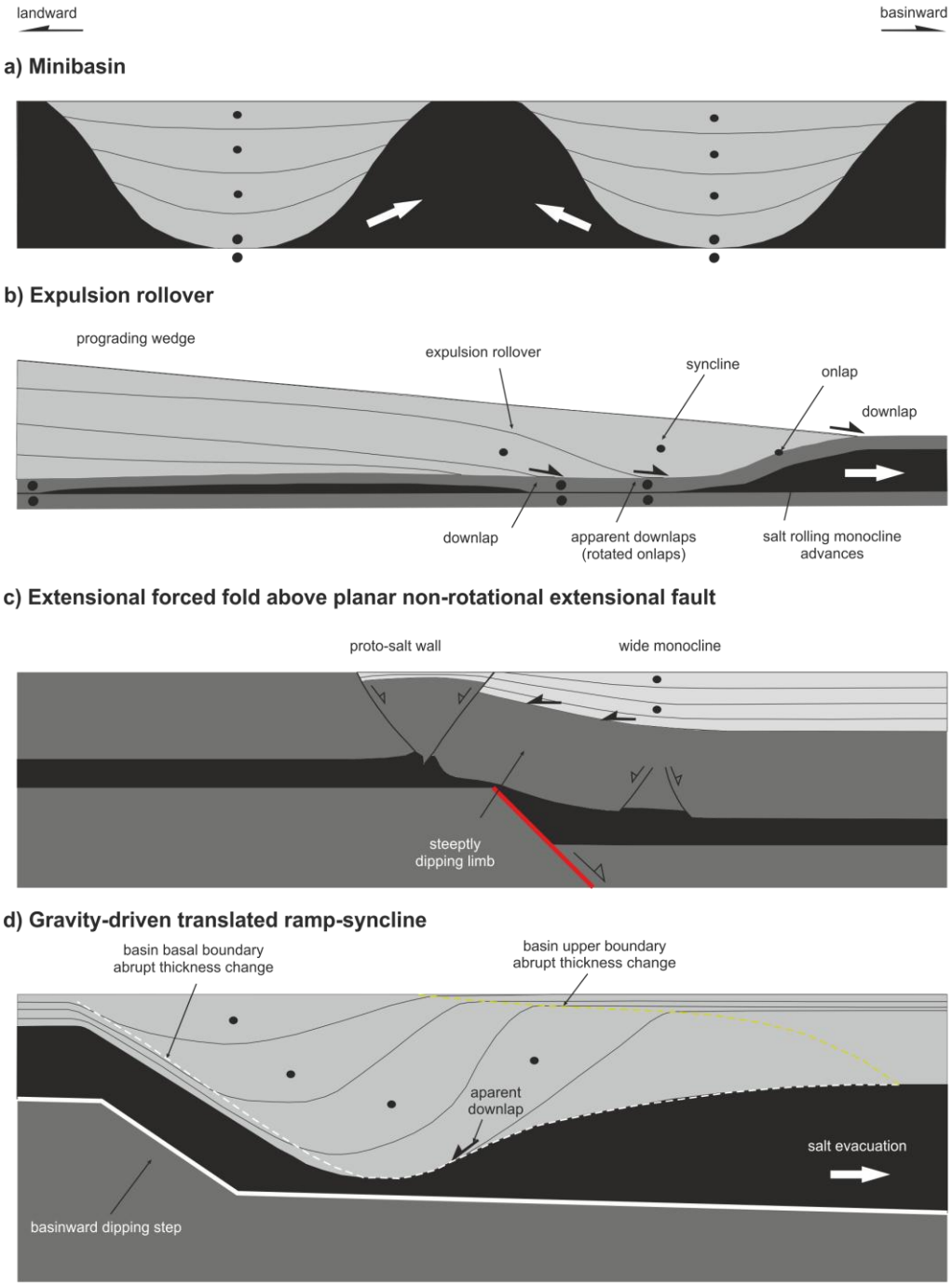

Fig.2.3. Conceptual models of **a)** a minibasin developed in by sinking, **b)** an expulsion rollover developed by deltaic progradation, modified from Ge et al. (1997), **c)** an extensional forced fold developed above a non-rotational planar fault, modified from Withjack and Callaway (2000), and **d)** a gravity-driven translated ramp-syncline developed above a presalt basinward-dipping step in a passive margin, modified from Pichel et al., (2018).

iv) Peel et al. (1998), Jackson and Hudec (2005), Rowan (2014), Jackson and Hudec (2017) and Pichel et al. (2018) identified a second type of ramp-syncline basins developed in

gravity-driven salt-bearing passive margins. They consist of synclinal basins transported basinwards over presalt basinward-dipping steps (**Fig. 2.3d**). These steps are features that can be inherited from a paleotopography or presalt faults. Translation of the ramp-syncline basins occurs in a linked system of gravity-driven extension updip and contraction downdip (Ferrer et al., 2017). I propose hereinafter to refer as translated ramp-synclines for these basins (**Fig. 2.3d**) and restrict the use of salt-detached ramp-synclines for the syncline basins developed in active rift settings (**Fig. 2.2a-c).**

Translated ramp-syncline basins are characterized by asymmetric sigmoidal growth strata dipping and expanding landward (Pichel et al. 2018) (**Fig. 2.3d**). The growth axial surfaces usually dip basinward, becoming steeper upwards. Salt expulsion, diapirism, folding and rotation occur synchronously to translation and syncline basin development (Pichel et al. 2018). The basal and upper boundaries of the basins are generally characterized by abrupt thickness changes and by diachronous unconformities, and the growth axial surface and basin boundaries are sub-parallel (Pichel et al. 2018). In translated ramp-syncline basins the structural style is thin-skinned, while in salt-detached ramp-synclines is thick-skinned with a thin-skinned component, where the amount of translation is usually lesser than in translating ramp-synclines. Secondary structures, such as crestal collapse grabens, extensional rollovers and antithetic normal faults are not developed in translated ramp-syncline basins. Note that basin translation depends on salt thickness, thus the formation of primary welds end up with it.

2.2. ORIGIN OF NATURAL RAMP-FLAT-RAMP EXTENSIONAL FAULTS

Based on the Coulom fracture criterion and Anderson's theory of faulting (Fossen, 2017), extensional faults are commonly thought to initiate with dips around 60° when the maximum stress (σ^1) is vertical and the rock is mechanically isotropic. But I have been described in the previous sections the development of ramp-flat-ramp extensional faults, where a low-angle fault forms by linkage of two steeper segments.

The origin of natural ramp-flat-ramp extensional fault systems has been attributed to different types of mechanisms: **i)** deformation of a pre-existing fault by compaction or isostatic movements (Davison 1987; Buck, 1988; Xiao and Suppe 1989; McClay and Scott, 1991; Vendeville 1991); **ii)** reactivation of thrust faults (Fossen, 2016); **iii)** rotation of pre-existing faults (Fossen, 2016), and **iv)** fault flattening into an intermediate detachment (Gibbs, 1984) or

weak over-pressured zone (Bruce 1984; Bradshaw and Zoback 1988). This last mechanism indicates that ramp-flat-ramp extensional faults can form under a single phase of extension, without to imply pre-existing weak structures from earlier phases of deformation. Thus, the direct formation of low-angle faults in ramp-flat-ramp extensional fault systems requires weak layers. The development of extensional faults flattening at depth into a weak layer has been described from crustal to lithospheric scales.

A mechanically anisotropic stratigraphy favors extensional faults curving and flattening down into interbedded weak layers (**Fig. 2.4a**) such as a salt, over-pressured zones or into pre-existing discontinuities (**Fig. 2.4a**) (Bruce, 1984; Gibbs, 1984; Bradshaw and Zoback, 1988; Ellis and McClay, 1988). In all these cases, they act as effective detachments.

Ramp-flat-ramp extensional faults can also develop at lithospheric scale. Extensional faults can flatten into lower (ductile) - middle (brittle-ductile transition) crust (Sibson, 1977; Wernicke and Burchfiel, 1982; Gibbs, 1984) or Moho discontinuities. These mechanical discontinuities act as a detachments and the fault trajectory may result in a series of flats and ramps (**Fig. 2.4b**). Moreover, exhumed and subsequently serpentinized mantle become a weak layer, which can promotes the formation of extensional low-angle faults (Wernicke, 1985; Wernicke and Axen, 1988).

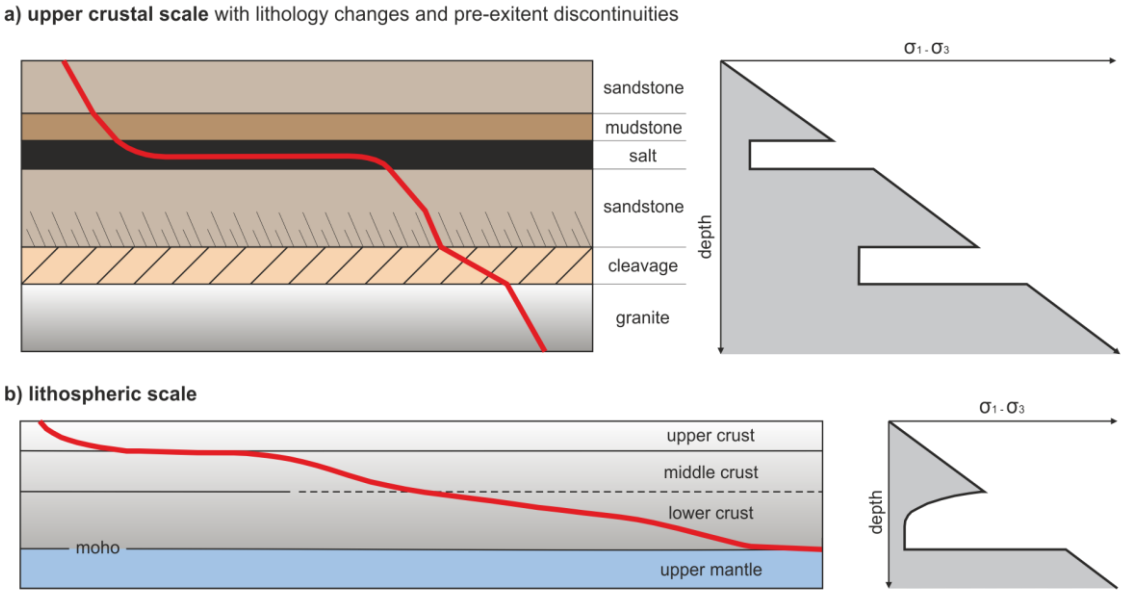

Fig.2.4. a) Development of ramp-flat-ramp extensional fault by lithology changes and pre-existing discontinuities thought the upper crust; **b)** Lithospheric scale major discontinuities that can act as a detachments (modified from Gibss (1987)).

2.3. KINEMATIC MODEL OF RAMP-SYNCLINE AND SALT-DETACHED RAMP-SYNCLINE BASINS

Due to their relevance on this PhD., I have decided to describe the fault-bend folding kinematics during the dip slip of the hangingwall along an extensional fault formed by two ramp-flat couples (**Fig. 2.5a**). Although a listric or a planar fault induce different hangingwall geometries (Faure and Chermette, 1989), the kinematic evolution of the hangingwall in both types of faults is practically equivalent (McClay and Scott, 1991). According to that, and in order to simplify, I have decided to use a planar fault system because both analog experimental programs presented in the following chapter of this manuscript are based on ramp-flat-ramp planar faults.

Results of kinematic models strongly depended on which deformation mechanism was chosen. Deformation mechanisms include constant heave (Gibbs, 1983), constant displacement (Williams and Vann, 1987), constant bed length (Suppe, 1983; Davison, 1986), slip line (Williams and Vann, 1987), and vertical or inclined shear (e.g., Gibbs, 1983; Groshong, 1989; Dula, 1991). Inclined shear is most commonly assumed in normal faulting (Darros de Matos, 1993; Ferril and Morris, 1997, McDonnell et al., 2010). The models of **Fig. 2.5** assume a hangingwall deformation by inclined shear of 60° (from the horizontal), coherent with coulomb fracture orientation, and within the range of most common shear angles in natural systems (Faure and Chermette, 1989; Dula, 1991; Haugue and Grey, 1996).

Six axial surfaces parallel to the shear direction form within the sliding hangingwall. These surfaces defined different dip domains that have moved by translation, subsidence or rotation (**Fig. 2.5b**) (McClay and Scott, 1991). Whereas three axial surfaces are locked to the footwall fault bends (active axial surfaces: x, y and z), the other three were located on the fault panels at a distance equal to the master fault displacement (inactive axial surfaces: x',y' and z') (Xiao and Suppe, 1992) (**Fig. 2.5b**). As fault displacement increases, the landward rollover becomes narrow as is translated above the intermediate flat panel and moving down the lower ramp (compare **Fig. 2.5b** and **c**). The hangingwall rocks rotated when pass through the active axial surfaces during sliding (y and z in **Fig. 2.5c**). As the hangingwall passes through the active and inactive axial surfaces (y-y' and z-z'), it folds as a syncline. The inactive axial surface z' marks the limit of hangingwall rotation, from here to the right the hangingwall is just translated above the lower flat.

The hangingwall flat avobe the footwall lower ramp (i.e., prekinematic unit lying

parallel above the lower ramp fault) is a key feature to identify ramp-flat-ramp faults (**Fig. 2.5d**) since such relationship implies the existence of an intermediate flat panel (Benedito et al., 1999).

The distance between two pairs of equivalent axial surfaces was constant throughout the prekinematic units, but not throughout the synkinematic ones, where the active and the inactive axial surfaces connect (**Fig. 2.5c)**. These inactive axial surfaces are equivalent to the basal and upper basin boundaries. This geometric model shows a diachronous unconformity and an erosional truncation for basal and upper basin boundaries, respectively (**Fig. 2.5c - d**).

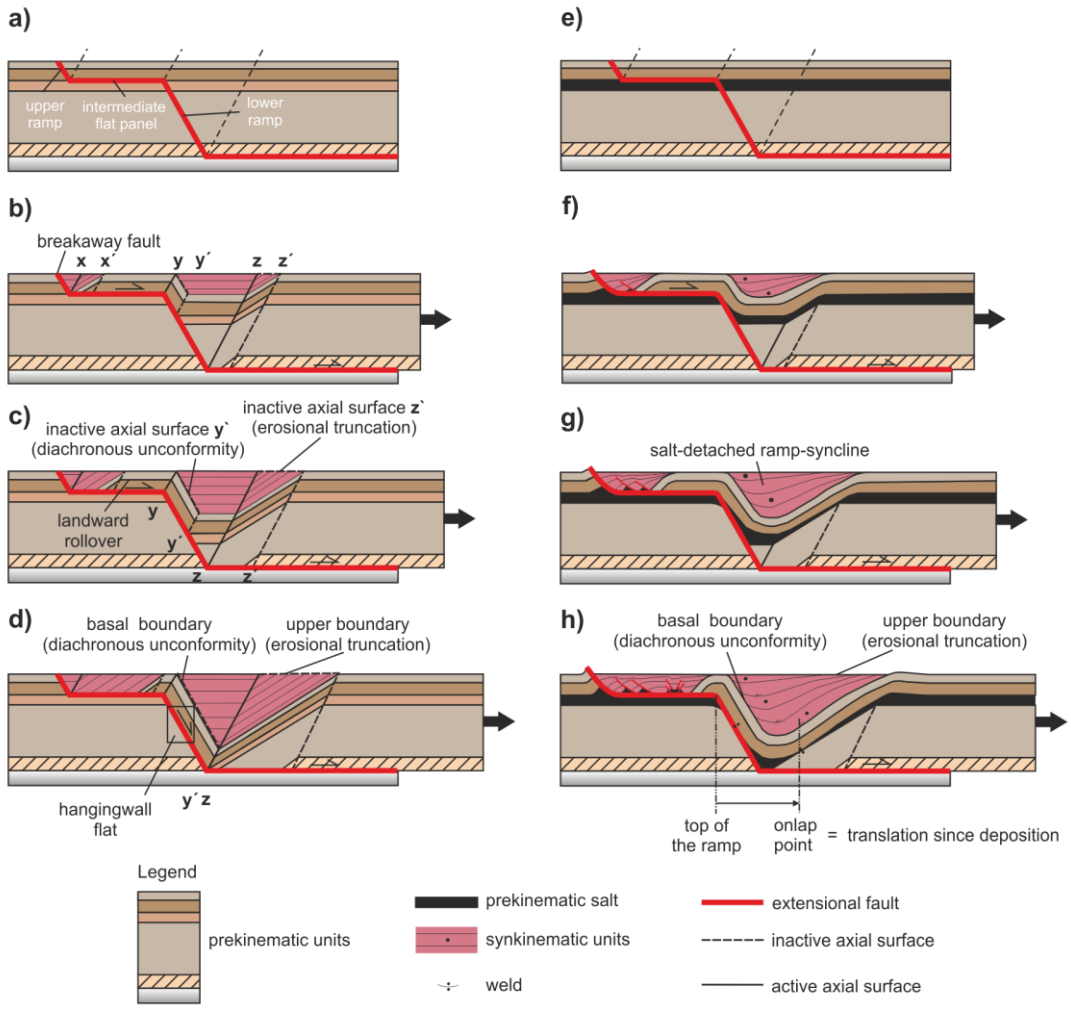

Fig.2.5. Conceptual models of fault-bend folding caused by slip of the hangingwall along an extensional fault system formed by two ramp-flat couples. Note that the conceptual models of the left column are mechanically isotropic (**a – d**), while the conceptual models of the right column (**e – h)** are mechanically anisotropic with an interbedded prekinematic salt layer.

Where the hangingwall rocks slides from the intermediate flat panel to the lower ramp (crossing the active axial surface Y), a subsiding space (i.e., depocenter) is formed and remains

fixed. The progressive basinward translation of the previous filled depocenters, results in an asymmetric ramp-syncline basin (**Fig. 2.5d).** The patterns of vertical movement of the hangingwall are controlled by the shape of the extensional fault. As a consequence the geometry and location of the subsiding depocenter does not change as the system evolves, and the rate of subsidence is directly proportional to the rate of lateral translation, and the translation is proportional to the fault displacement. The growing and deformation of hangingwall synkinematic structures follows the deformation of the prekinematic rocks.

Instead, when the system involves a an interbedded salt layer, the sub- and suprasalt deformation are partially decoupled, thus inhibiting the upwards propagation of the subsalt active and passive axial surfaces into the suprasalt units. The subsalt structures are similar to those developed in systems without a salt layer. In contrast, the deformation style was different for the units overlying the salt (**Fig. 2.5e**). In such case the geometry of the suprasalt units define a salt-detached ramp-syncline basin (**Fig. 2.5h**).

The distance between the active and inactive axial surfaces corresponds to the fault displacement. But usually in decoupled systems the subsalt structure is obscured and these subsalt information is not easy to determine. In such case, the fault displacement can be measured thought the suprasalt synclinal basin (**Fig. 2.5h**). As the salt-detached ramp-syncline basin is always developed basinward of the lower ramp (**Fig. 2.5**), thus the landward edge of the salt-detached ramp-syncline basin corresponds to the top of such subsalt ramp. The distance between the landward edge of the salt-detached ramp-syncline basin and the oldest onlap point records the basin translation (**Fig. 2.5h**) (Jackson and Hudec, 2005). Although this synkinematic observations can help us to infer in the subsalt structure, the following Chapter 4 (overall summary of discussions) shows that this directly extrapolation could results in subsalt misinterpretations.

2.4. BRIEF REVIEW OF WIDESPREAD SALT-DETACHED RAMP-SYNCLINE BASINS

The presence of broad salt-detached ramp-syncline basins is relatively common in the Western Europe (e.g., Norway Devonian basin (Vetti and Fossen, 2012), as well as in their equivalent North-American Atlantic margin (e.g., Newfoundland basins (Balkwill and Legall, 1989) (**Fig. 2.6**) and Western USA Basin and Range (Kruger and Johnson, 1994)). The development of these synclinal basins has been associated to the displacement of lithospheric-scale extensional faults interpreted with ramp-flat, listric or planar-rotational geometries (**Fig.**

2.7). In addition to the control carried out by the basement-involved fault geometry on the development of synclinal basins in those natural examples, the presence and distribution of salt has been critical. The synclinal basins developed in these regions are detached from subsalt faults by Permian (Zechstein Formations) or Late Triassic (Keuper facies and Dagorda Formation) evaporites. In these basins, the salt was deposited at the late stages of extensional deformation related to the breakup of Pangea during Permo-Triassic times (Coward, 1995; Glennie, 1995). As a result, the interaction between the subsalt fault network and the main synrift depocenters is characterized by multiple rift events with deposition of salt during and after extensional phase (i.e., syn- or postrift) (Ziegler, 1988; Balkwill and Legall, 1989; Tankard et al., 1989; Dercourt et al., 1993; Rasmussen et al., 1998; Jackson et al., 2000; Alves et al., 2002). Consequently, these salt units show lateral thickness variations (Jackson and Vendeville, 1994; Coward and Steward, 1995; Ferrer et al., 2008, 2014; Rowan, 2014). In addition to the extensional history, most of these basins were subsequently partially (e.g. Lusitanian (Alves et al., 2002) (**Fig. 2.10a**) or Parentis basins (Mathieu, 1986) (**Fig. 2.10d**)) to totally (e.g. Cameros Basin (Guimerà et al., 1995) (**Fig. 2.10c**)) inverted or even incorporated into a fold-and-thrust belts (e.g. Organyà Basin (Muñoz, 1992)). The distribution and continuity of the salt, or its welded equivalents, played a key role during this late contractional episode (Roma et al 2018c).

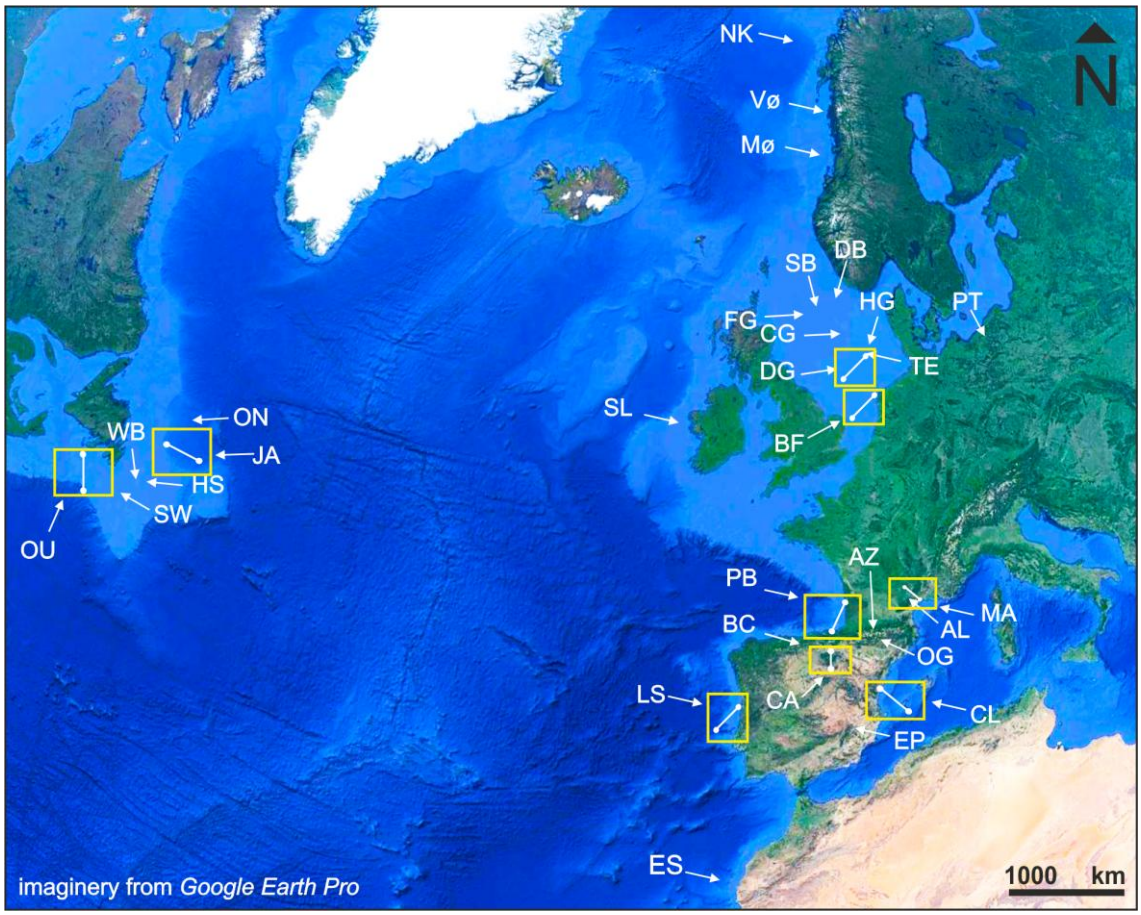

Fig.2.6. Distribution of salt-detached synclinal basins in the Western Europe and North American Atlantic margin. ES Essaouira (Hafid, 2000); LS Lusitania Basin (Alves et al., 2002); EP Eastern Prebetics (Escosa et al., 2018); CL Columbrets Basin (Roma et al., 2018a); CA Cameros Basin (Guimerà et al., 1995); OG Organyà Basin (García-Senz, 2002); BC Basque-Cantabrian Basin (Carola et al., 2015); PB Parentis Basin (Ferrer et al., 2012); AZ Arzacq Basin (Biteau et al., 2006); AL Alès Basin (Sanchis and Séranne, 2000); MA Matelles Basin (Benedicto et al., 1999); SL Slyne Basin; BF Broad Fourteens Basin (Nalpas et al., 1995); DG Dutch Graben (De Jager, 2003); TE Terschelling Basin (Remmelts, 1995); PT Mid-Polish Trough (Krzywiec, 2004); CG Central Graben (Dooley et al., 2005); HG Horn Graben (Nalpas and Brun, 1993); FG Feda Graben (Growers et al., 1993); DB Danish Basin (Stewart and Clark, 1999); SB Sogne Basin (Stewart and Clark, 1999); MØ More Basin (Osmundsen et al., 2002); VØ Voring Basin (Brekke, 2000); NK Nordkapp Basin (Gudlaugsson et al., 1998); OU Orpheus Basin (Durcanin, 2009); Southwhale Basin (Balkwill and Legall, 1989); WB Whale Basin (Balkwill and Legall, 1989); HS Horseshoe Basin (Balkwill and Legall, 1989); JA Jeanne d'Arc Basin (Withjack and Callaway 2000); ON Orphan Basin (Tankar and Welsink, 1989). The white lines inside the yellow rectangles indicate the location of the cross-sections included in **Fig. 2.7.**

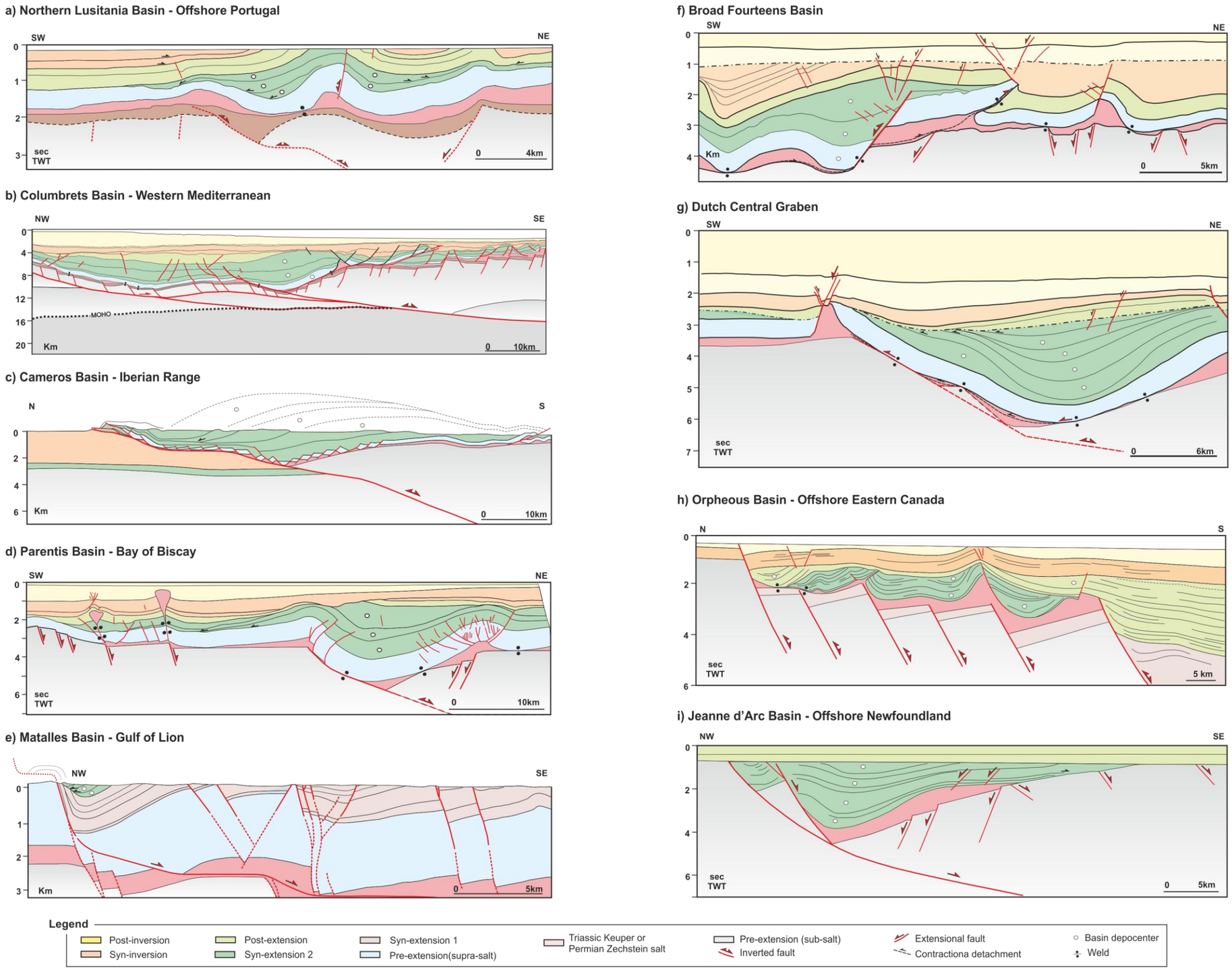

Fig.2.7. Interpreted seismic lines showing salt-detached synclinal basins with different degrees of tectonic inversion (see location on **Fig. 2.6**). **a)** Interpreted seismic line S84-23, of Northern Lusitanian Basin (offshore Portugal) with synstreching salt subsequently affected by a pronounced period of inversion (modified from Alves et al., 2002); **b)** Line drawing of the seismic profile SGV01-107 at the Columbrets Basin (Western Mediterranean) (Roma et al., 2018a); **c)** Cross-section of the Cameros Basin with prekinematic salt totally inverted and incorporated into the Iberian chain as a result of the Alpine orogeny (modified from Soto et al., 2007); **d)** Interpreted line drawing of a composite 2D seismic profile from the eastern Parentis Basin (Bay of Biscay) with a prekinematic salt unit and showing the main features of this slightly inverted basin (modified from Ferrer et al., 2012); **e)** General cross-section of the non-inverted Matalles Basin (Gulf of Lion) (modified from Benedito et al., 1999); **f)** Line drawing of a SW-NE trending seismic profile of the Southern North Sea between the Texel-Ijsselmeer High and the Broad Fourteens Basin(modified from De Jager, 2003); **g)** Line drawing of a regional SW-NE trending profile through salt structures across the eastern part of the Dutch Central Graben (southern North Sea, Netherlands) (seismic from Fugro, source Virtual Seismic Atlas: https://www.seismicatlas.org/entity?id=026b91b3-c042-4f7b-802d-756a4613fa97); **h)** Line drawing from a seismic profile of the inverted Orpheus Basin (offshore eastern Canada) (modified from Durcanin, 2009); **i)** Line drawing of a time-migrated seismic section of the non-inverted Jeanne d'Arc Basin (offshore Newfoundland, Canada) (modified from Withjack and Callaway, 2000).

2.5. STATE OF THE ART EXTENSIONAL ANALOG MODELS AND ANISOTROPIC INVERSION ANALOG MODELS

The extensional deformation of rift systems with and without salt have been intensively studied during the last decades using crustal-scale analog modeling, especially to understand the extensional fault kinematics (Cloos, 1968), the architecture of faults according variable strain directions (Clifton et al., 2000), and the 3D geometry of extensional faults (Yamada and McCLay, 2004). Therefore, the main literature about analog modeling of rift systems focuses its experimental constrains on fault shapes and on the modeling materials. Lithospheric-scale natural-gravity (Brun, 1999) or centrifuge models (Corti, 2012) (performed under an enhanced gravity field) are not treated in the current review.

Two experimental setups have been classically used to simulate the hangingwall deformation of extensional faults in physical modeling: **i)** unconstrained models using a prekinematic sand pack (analog of brittle materials in nature) over two metal or wooden plates (Cloos, 1968; Ellis and McClay, 1988; McClay, 1989; Eisenstadt and Withjack, 1995; Eisenstadt and Sims, 2005; Withjack and Schlische, 2006) that in some literature experiments are separated by a rubber sheet acting as a basal detachment (McClay and White, 1995; McClay et al., 2002; Amilibia et al., 2005) (**Table. 2.1**) or **ii)** completely constrained models (McClay, 1990; Roure et al., 1992) using a rigid block to simulate the master fault geometry. A plastic sheet fixed to a moving wall usually covers the rigid block acting as a main detachment. The brittle hangingwall is simulated by a prekinematic sand pack overlying the plastic sheet (Withjack et al., 1990; Koyi et al., 1993; Nalpas and Brun, 1993; Withjack and Callaway, 2000; Withjack and Schlische, 2006; Burliga et al., 2012).

Unconstrained extensional models were based on simple basement geometries. These experiments produced dominantly planar faults or fault with a slight steepening-upwards geometry (see referenced authors in **Table. 2.1)**. The uniform extension experiments produced series of horst blocks or parallel fault systems between which significant hangingwall accommodation structures were not developed. These experiments do not allow reproduce ramp-flat-ramp extensional faults.

However, in constrained models a great variety of fault geometries have been studied according to the natural prototypes: **i)** planar extensional faults (Vendeville, 1987; Withjack et al., 1990; Withjack and Callaway, 2000; Withjack and Schlische 2006; Ferrer et al., 2014 and

2016); **ii)** rotational planar extensional faults and domino fault systems (Buchanan and McClay, 1992; McClay and Buchanan, 1992; Mitra, 1993; Jagger and McClay, 2016); **iii)** kinked planar faults (convex or concave upward bend) flattening at depth (Withjack et al., 1995; Patton, 2005; Ferrer et al., 2014 and 2016); **iv)** listric extensional faults (Ellis and McClay, 1988; McClay and Ellis, 1987a, b; McClay, 1989; Soto et al., 2007) and **v)** ramp-flat-ramp extensional faults (McClay and Ellis, 1987a,b; Ellis and McClay, 1988; McClay, 1989; McClay and Scott, 1991; Ferrer et al., 2016).

The most common materials to build a crustal-scale isotropic hangingwall block are dry quartz sand, which according to its mechanical properties simulates brittle rocks in nature (McClay and Ellis, 1987a, b; Ellis and McClay, 1988; McClay, 1989; McClay and Scott, 1991; Withjack and Schlische, 2006; Patton, 2005). Other authors used wet clay that is a more cohesive material (Withjack et al., 1995; Eisenstadt and Withjack, 1995; Withjack and Schlische, 2006).

However, Vendeville (1987); Vendeville and Jackson (1992); Jackson and Vendeville (1994); Vendeville et al. (1995); Bonini (1998); Withjack and Callaway (2000); Burliga et al. (2012); Bonini et al. (2012); Dubois et al. (2002); Konstantinovskaya et al. (2007) and Pinto et al. (2010) introduced a silicone polymer at the base of an isotropic sand pack simulating salt or over-pressured shales in nature. In this case, the polymer decouples the deformation between sub- and supra-polymer units in the hangingwall, acting as an effective detachment. Furthermore, Soto et al. (2007) and Ferrer et al. (2014, 2016) (**Table. 2.1**) introduced into the isotropic sand pack an interlayered silicone polymer between the dry quartz sand in constrained models, resulting in an anisotropic hangingwall stratigraphic pile.

All these experimental setups allowed to characterize the main parameters that control the deformation and evolution of rift basins with or without salt during extension. Among these parameters stand out: **i)** the geometry and the dip of the extensional master fault (Vendeville, 1987; Withjack et al., 1990); **ii)** the amount of extension and deformation rate (Koyi et al., 1993; Vendeville et al., 1995); **iii)** the thickness and rheology of the viscous layer (Withjack and Callaway, 2000); **iv)** the thickness and the rheology of the overburden (Withjack and Callaway, 2000) and **v)** the ratio between sedimentation and extension rates (Soto et al., 2007).

ISOTROPIC MODELS	
Extension in unconstrained models	Cloos, 1968; Ellis & McClay, 1988; Allemand et al., 1989; McClay, 1989; McClay, 1990; Alleman & Brun, 1991; Tron & Brun 1991; Eisenstadt & Withjack, 1995; McClay & White, 1995; McClay, 1996; McClay et al., 2002; Medwedeff & Krantz, 2002; Amilibia et al., 2005; Eisenstadt & Sims, 2005; Schreurs et al., 2006; Withjack & Schlische, 2006
Extension in constrained models	
Planar	Lowell, 1974; Koopman et al., 1987; Vendeville, 1987; McClay, 1989; Withjack et al., 1990; Buchanan & McClay, 1991, 1992; Koyi et al., 1993; Nalpas & Brun, 1993; Mitra & Islam, 1994; McClay, 1995; Withjack & Callaway, 2000; Medwedeff & Krantz, 2002; Dooley et al., 2003; Withjack & Schlische 2006; Burliga et al., 2012
Rotated planar	Buchanan & McClay, 1992; McClay & Buchanan, 1992; Mitra, 1993; McClay, 1995; Jagger & McClay, 2016
Kinked	Withjack et al., 1995; Patton, 2005; Ferrer et al., 2014, 2016.
Listric	McClay & Ellis, 1987a, b; Ellis & McClay, 1988; McClay, 1989; McClay, 1990; McClay, 1995; McClay, 1996; Soto et al., 2007; Ferrer et al., 2016
Ramp-flat-ramp	McClay & Ellis, 1987a, b; Ellis & McClay, 1988; McClay, 1989; McClay, 1990; McClay & Scott, 1991; Roure et al., 1992; Mitra & Islam, 1994; McClay, 1995; McClay, 1996; Ferrer et al., 2016
Extension and inversion in unconstrained and constrained models	Koopman et al., 1987; McClay, 1989; Buchanan & McClay, 1991,1992; Mitra & Islam, 1994; Eisenstadt & Withjack, 1995; Keller & McClay, 1995;McClay, 1995; McClay, 1996; Dubois et al., 2002; Yamanda & McClay, 2003a,b-2004; Amilibia et al., 2005; Einstard & Sims, 2005; Panien et al., 2005; Del Venisette et al., 2005-2006; Patton, 2006; Konstantinovskaya et al., 2007; Buiter et al., 2009; Pinto etal., 2010; Bonini et al., 2012; Burliga et al., 2012; Ferrer et al., 2016; Granado et al., 2017
ANISOTROPIC MODELS	
Extension in unconstrained models Basal and interlayered polymer	Ballard et al., 1987; Vendeville & Jackson, 1992; Nalpas & Brun, 1993; Jackson & Vendeville, 1994; Nalpas et al., 1995; Vendeville et al., 1995; Brun & Nalpas, 1996; Bonini, 1998; Withjack & Callaway, 2000; Dubois et al., 2002; Gartrell et al., 2005; Schreurs et al., 2002; Konstantinovskaya et al., 2007; Pinto et al., 2010; Bonini et al., 2012; Burliga et al., 2012
Extension in constrained models Interlayered syn- and pre-kienamtic polymer	Vendeville, 1987; Withjack & Callaway, 2000; Del Venisette et al., 2005, 2006; Dooley et al., 2005; Soto et al., 2007; Ferrer et al., 2014; Ferrer et al., 2016
Extension and inversion in constrained models Interlayered polymer	Dooley et al., 2005; Durcanin, 2009; Burliga et al., 2012; Ferrer et al.,2016; Roma et al., 2018a,b & c.

Table.2.1. Summary of the existing crustal-scale analog modeling literature about constrained and unconstrained models during extension and inversion without (isotropic models) or with (anisotropic models) interlayered pre- or synkinematic polymer.

Nevertheless, while much has been written on analog modeling of rift basins with prerift salt (Vendeville et al., 1995; Withjack and Callaway, 2000; Soto et al., 2007), there is

little published about synrift salt (Ferrer et al., 2014). As in our case studies the salt was deposited during the regional extension, our analog models were designed to reproduce these salt basins with synrift salt (Roma et al., 2018b).

For both techniques (i.e., unconstrained and constrained models) some of these authors have applied shortening after the extensional episode simulating basin inversion in nature (Bonini et al., 2012) (**Table. 2.1**). For unconstrained models, they used to push the moving wall together with the attached plate (**Fig. 2.8a and b**) (Eisenstadt and Withjack, 1995; Einstard and Sims, 2005; Del Venisette et al., 2005 and 2006; Granado et al., 2017), while for constrained models they reverse the motion of: **i)** the moving wall (**Fig. 2.8c and d**) (Buchanan and McClay, 1991 and 1992; Mitra and Islam, 1994; McClay, 1995) or **ii)** the rigid footwall block (**Fig. 2.8e and f**) (Mitra and Islam, 1994; Yamada and McClay, 2004; Burliga et al., 2012). However, those techniques were improved by reversing the motion of: **i)** the moving wall together with the plastic sheet attached on a roller motor, both at the same velocity (**Fig. 2.8g and h**) (Ferrer et al., 2012; Roma et al., 2018a) or **ii)** the rigid block underneath a fixed plastic sheet (**Fig. 2.8i and j**) (Yamanda and McClay, 2003a and b; Ferrer et al., 2016; Roma et al., 2018b). These improvements allow avoiding buttressing effect.

Only recent works considered the inversion phase including a polymer layer interbedded into the pre- or synkinematic sand pack. Del Ventisette et al. (2005) explored the positive inversion as a mechanism of diapiric growth in the edges of the basin simulating the Saiss (Morocco) and Central Graben Basins (North Sea). Using an experimental approach based on the western Central Graben (North Sea), Dooley et al. (2005) investigated the 3D geometries and kinematics of deformation in the overburden above intersecting basement fault systems that were separated by a synrift salt layer. In this work they indicate that this intersecting fault set generates complex 3D flap structures in the overburden that localize diapiric activity. Then, they were subjected to moderate inversion that leads to complete reactivation of the basin boundary fault system and of the diapiric network. The study of Durcanin (2009) was focused on how the deposition of a thick synrift ductile layer affected the deformation patterns of the overburden during the tectonic evolution of the Orpheus rift basin and its subsequent inversion. Ferrer et al. (2014 and 2016) used a rigid footwall blocks to simulate different basement fault geometries with interbedded pre- and synkinematic polymer to understand the role of this parameter on the overburden deformation and salt tectonics during extension and inversion. They summarized the control of the salt layer continuity (or its

welded equivalent) as well as the distribution of inherited salt structures from the extensional episode during the subsequent tectonic inversion.

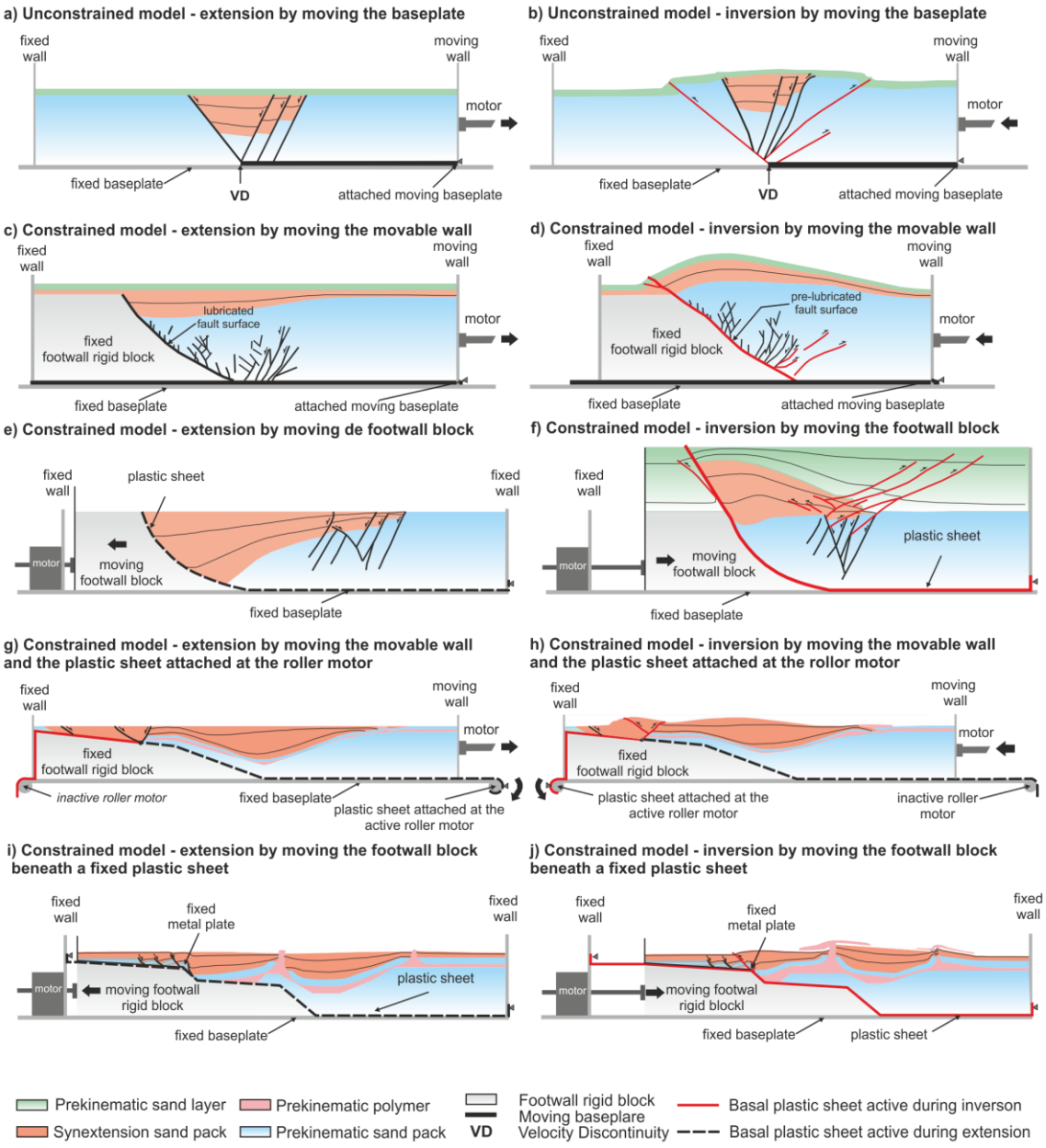

Fig.2.8. Simplified conceptual sketches showing different analog modeling techniques for applying shortening after the extensional episode simulating basin inversion in nature. Unconstrained model at the end of the extension **a)** and at the end of the inversion **b)** (modified from Granado et al., 2017); Constrained models at the end of the extension **c)** and at the end of the inversion **d)** by moving the movable wall (modified from Mitra and Islam, 1994); at the end of extension **e)** and at the end of the inversion **f)** by moving the footwall rigid block (modified from Yamada and McClay, 2004); at the end of the extension **g)** and at the end of the inversion **h)** by moving the movable wall and the plastic sheet (modified from Roma et al., 2018a) and at the end of the extension **i)** and at the end of the inversion **j)** by moving the rigid footwall block (modified from Roma et al., 2018b).

The different experimental programs included in this PhD follows the completely constrained technique considering different fault geometries and a polymer layer acting as an effective decoupling (Roma et al., 2018a, 2018b and 2018c). However, our work differs from Ferrer et al. (2014) because they did not apply any inversion, and from Dooley et al. (2005) because they applied a low degree of inversion. Our experiments supplement the works of Del Ventisette et al. (2005); Durcanin (2009) and Ferrer et al. (2016) by investigating the development of salt-detached ramp-syncline basins above a kinked ramp-flat-ramp rigid wooden footwall block involving pre- and synrift polymer with large amounts of extension simulating multiple rift events and high degrees of inversion. In addition, despite the experiments of Ferrer et al. (2016) considered the effect of inversion, the small amount of previous extension applied did not allow the development of diapirs. In this sense, our experimental programs have allowed the development of diapirs and salt walls piercing the overburden during the extensional episode allowing the polymer migration with the consequent thinning of the source layer and the development of primary welds. The distribution of inherited salt bodies and welds at the end of the extensional episode has been critical during the subsequent inversion.

2.6. PROBLEM APPROACH AND INTRODUCTION TO THE PUBLISHED ARTICLES

The present thesis has been elaborated as a compendium of articles, which are included in the Appendix of this manuscript. The complete references of these articles are the following:

-Roma, M., O. Ferrer, E. Roca, O. Pla, F.O. Escosa, M. Butillé, 2018a. Formation and inversion of salt-detached ramp-syncline basins. Results from analog modeling and application to the Columbrets Basin (Western Mediterranean). Tectonophysics. 745, 214-228, doi: 10.1016/j.tecto.2018.08.012.

-Roma, M., O. Vidal-Royo, K. McClay, O. Ferrer, J.A. Muñoz, 2018b. Tectonic inversion of salt-detached ramp-syncline basins as illustrated by analog modeling and kinematic restoration. Interpretation. 6(1), T127-T144, doi: 10.1190/INT-2017-0073.1.

-Roma, M., O. Ferrer, K.R. McClay, J,A. Muñoz, E. Roca, O. Gratacós, P. Cabello, 2018c. Weld kinematics of synrift salt during basement-involved extension and subsequent inversion:

Results from analog models. Geologica Acta. 16(4), 391-410, doi: 10.1344/GeologicaActa 2018.16.4.4.

To understand how these three articles relate to each other, and therefore the coherence of this manuscript, firstly it is essential to introduce the problem addressed in this thesis.

As previously introduced (**section 2.4.**), the presence of broad extensional synclinal basins not bounded by major faults is relatively common in the Western Mediterranean, Iberian and the Central- and North-Atlantic realms (**Fig. 2.9a**). These basins reach different evolutionary stages during rifting episodes, as well during inversion. This is the case of some of the Iberian basins used as analogues in this PhD. For instance; the Parentis and Columbrets basins developed above a hyperextended crust and then were slightly inverted during the collision between Iberian and Eurasian plates. In contrast, Organyà and Cameros basins were totally inverted and incorporated into the Pyrenees and Iberian chains respectively.

These extensional systems are commonly controlled by the basement-involved extensional fault geometry, but also they are strongly controlled by the presence and distribution of salt layers (**Fig. 2.9b**). The presence of salt may exert strong influences on: **i)** the location of ramps and flat fault systems (**section 2.2.**); **ii)** the geometries of suprasalt folds (**section 2.1.** Soto et al., 2007; Ferrer et al., 2016); **iii)** the along-trike structural variation; **iv)** the degree of coupling/decoupling between sub- and suprasalt deformation (Stewart and Clark, 1999; Withjack and Callaway, 2000), and **v)** the development of salt-related structures (Koyi et al., 1993; Koyi and Petersen, 1993; Nalpas and Brun, 1993; Jackson et al., 1994; Vendeville et al., 1995; Stewart et al., 1996; Helgeson, 1999; Richardson et al., 2005). In addition, the distribution of salt units strongly depends on the period it was deposited with respect to the extensional deformation phases of the basin (i.e., pre- ,syn- or post-extension) (Jackson and Vendeville, 1994; Coward and Steward, 1995; Ferrer et al., 2008; Ferrer et al., 2014). This fact significantly controls the thickness of salt available during the development of salt detached ramp-syncline basins as well as the structural style in many passive margins and extensional provinces (Rowan, 2014).

The Upper Triassic (Keuper facies) evaporites are one of the main detachment levels of both the Mesozoic extensional basins and the fold-and-thrust belts of the Iberian Peninsula (Guimerà et al., 1995; Séranne et al., 1995; Sanchis and Séranne, 2000; Alves et al., 2002;

Biteau et al., 2006; Soto et al., 2007; Ferrer et al., 2008; Roca et al., 2011; Ferrer et al., 2012; Ferrer et al., 2016). Similarly, Permo-Triassic (Zechstein Formations) evaporites are the main detachment in the Western European basins, and particularly in the Southern and Central North Sea, where they play a prominent role in their deformation history (Badley et al., 1989; Nalpas and Brun, 1993; Gowers et al., 1993; Nalpas et al., 1995; Remmelts, 1995; Gudlaugsson et al., 1998; Pascoe et al., 1999; Withjack and Callaway, 2000; Brekke, 2000; Osmundsen et al., 2002; Richardson et al., 2005).

A thick salt layer may facilitate the decoupling of the overbuden above the basement faults resulting into a thin-skinned structural style (Coward and Stewart, 1995; Jackson and Hudec, 2005; Carola et al., 2015; Pichel et al., 2018). In the case of multiple rift events with intervening period of salt deposition, as occurred in the examples above referred, variable lateral and also vertical distributions of salt may occur (Rowan, 2014), and thus mixed modes of styles (i.e., coupled and decoupled systems or thin- and thick-skinned deformation styles) may be expected (**Fig. 2.9c**).

Furthermore, most of these basins have subsequently been partially-to-totally inverted (Mathieu, 1986; Muñoz, 1992; Guimerà et al., 1995; Roca, 2001; Alves et al., 2002; Withjack and Schlische, 2005; Soto et al., 2007; Ferrer et al., 2008 and 2012; Roca et al., 2011; Mencos et al., 2015) (**Fig. 2.9d**). When this occurs, in addition to de inversion degree, other factors such as the synkinematic sedimentation, the continuity of the salt unit as well as the presence of inherited salt structures, strongly influences the structural style developed during this stage.

To sum up (**Fig. 2.9**), salt-detached ramp-syncline basin are widespread developed in different basins worldwide rift systems and passive margins, and may involve deep faults and salt units in their development (**Fig. 2.9a-b**). They can be developed during multiple rift events (**Fig. 2.9c**), with salt deposition before (prekinematic), during (synkinematic) or after the rifting (post-kinematic). Whatever the case, salt decouples the supra- and subsalt deformation, making it difficult to interpret the location and geometry of the subsalt-involved extensional fault. Their interpretation could be much more complex if these basins are subsequently inverted masking those extensional structures (**Fig. 2.9d**).

As already noted, these basins have a significant exploration potential but, despite recent improvements in seismic processing and imaging, the structural complexity of salt-

detached ramp-synclines can lead to interpretations with a high degree of uncertainty (**Fig. 2.9e-f**).

In this scenario, analog (sandbox) models have proven to be a powerful tool to reduce interpretation uncertainties (**Fig. 2.9g**) since they are a good approximation to reproduce geological processes at scale (Ellis and McClay, 1988; McClay, 1989, 1990; Koyi et al., 1993; Dooley et al., 2005; Soto et al., 2007; Durcanin, 2009; Ferrer et al., 2014, 2016). Thus, analog modeling can help in constraining the interpretation of subsalt structures as well as obtain rigorous kinematic models. This also allows the validation of balanced and restored cross-sections including salt structures, understanding the interaction between subsalt faults and the overlying evaporites during the extensional or the overprinted inversion phase.

The three articles included in this thesis manuscript are based on two different experimental programs. The design of those programs is based on different case studies, selected in order to study different degrees of coupling/decoupling, extension and compression.

Using the Mesozoic salt-detached ramp-syncline Columbrets Basin (Western Mediterranean) as a case study, the first article (Roma et al., 2018a) introduces the Experimental Program 1 carried out at the Geomodels Analog Modeling Laboratory (University of Barcelona) consisting of eight different sandbox models. This basin developed in relation with the opening of both the Tethys (Roca et al., 1994) and Atlantic Ocean (Roca, 2001), and belongs to the ancient South Iberian passive margin (Etheve et al., 2018). It is a good example to study a preserved hyperextended rift basin detached on Upper Triassic (Keuper) evaporites and developed above a major ramp-flat-ramp extensional subsalt fault (Roca, 1996). Although this basin was slightly overprinted by a postrift inversion episode, the extensional architecture was perfectly preserved. Hence, the aim of this article is twofold: 1) to decipher the influence of the ramp-flat-ramp extensional fault during the syncline development and the interaction with a prekinematic salt; and 2) to infer how salt-detached ramp-syncline basins are subsequently inverted.

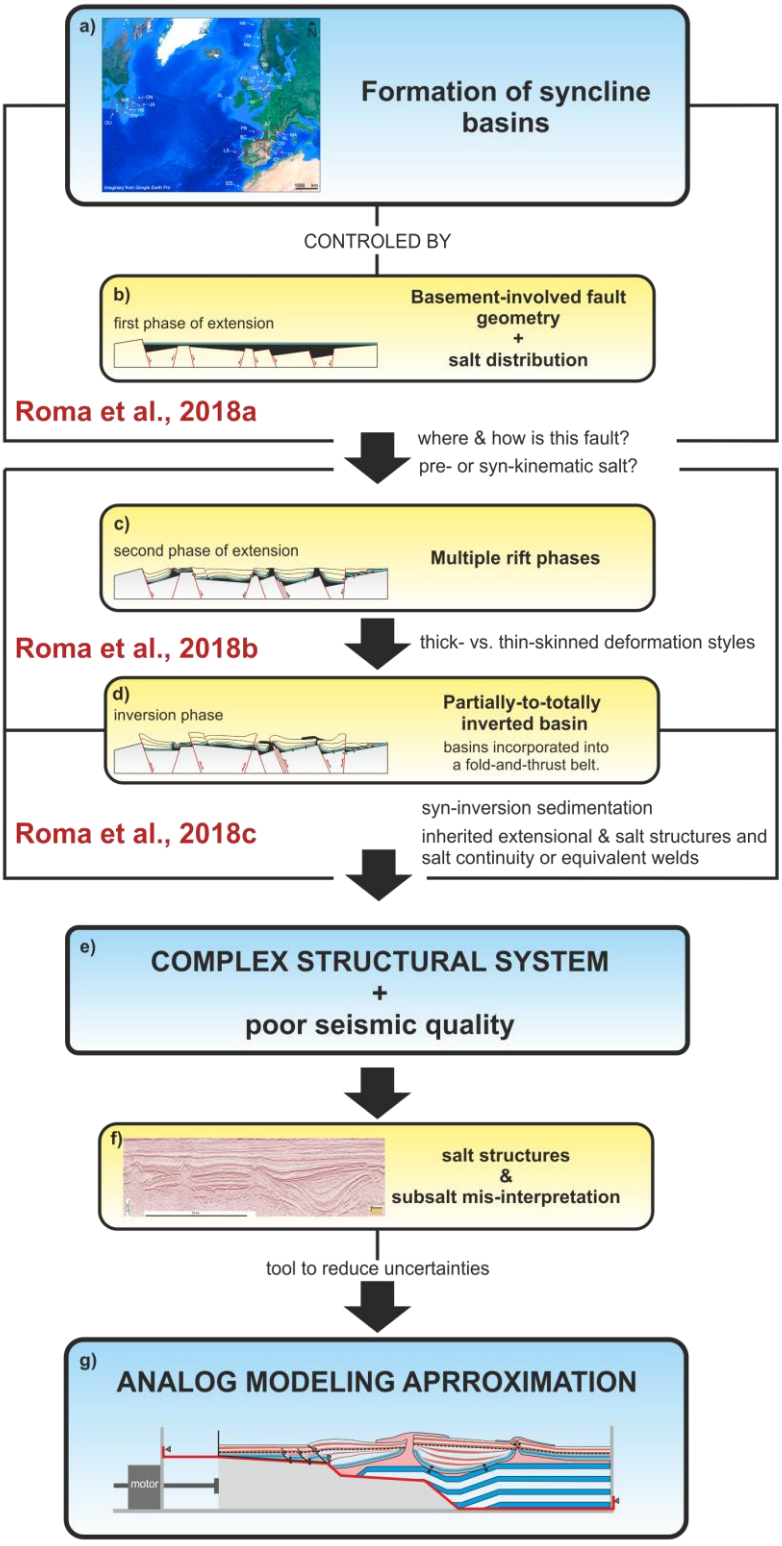

Fig.2.9. Workflow of the problem approach followed in this PhD and the different parts covered by the articles presented in this manuscript.

The second article (Roma et al., 2018b) introduces the Experimental Program 2 carried out during a two-months PhD stay at the Analog Modeling Laboratory of the Royal Holloway University of London. In particular the experiments depicted in this second article were

designed to simulate the kinematic evolution of some Mesozoic salt-detached ramp-syncline basins of the Iberian Peninsula and similar basins worldwide involving synrift salt (i.e. Offshore Portugal, Bay of Biscay, Basque-Cantabrian and Central Pyrenees). These basins are characterized by multiple rifting events and have been partial-to-total inverted. The Experimental Program 2 includes five models that underwent two phases of extension above a ramp-flat-ramp basement fault with synrift polymer deposited between the two extensional phases. These experiments were subsequently shortened simulating later inversion. The aim of this article is to understand the interaction of the main factors involved in extension and inversion, together with quantify salt mobilization thought restoring an analog model with well-known imposed kinematics and boundary conditions. To do it, the article analyses two representative sections across the model with and without well-developed diapirsm. These cross-sections were then sequentially restored with geometric algorithms to illustrate the structural evolution and the variations in sectional area of the salt.

The Experimental Program 2 has also been used as the basis for the third article of this PhD (Roma et al., 2018c). This article expands the experimental program and the methodological analysis previously published in Roma et al. (2018b) in order to provide insights into welding kinematics in basins with synrift salt during both extension and inversion. It also analyzes how syninversion sedimentation affects the regional structure and salt tectonics.

Combining the interpretation of hyperextended basins detached on a prerift salt layer (Roma et al., 2018a), with the interpretation of partially-to-totally inverted salt-detached ramp-syncline basins (Roma et al., 2018b), together with the study of welding kinematics and syninversion sedimentation in this basins (Roma et al., 2018c), the main purpose of this PhD. manuscript is to understand how this basins are developed and which factors control them during extension and inversion based on scaled sandbox models. Therefore, as a whole, these three papers together determine key ideas about the interpretation of these so complex scenarios. Thus, could support published interpretations and serve as a guide for better interpretation of subsalt areas.

2.7. METHODOLOGY

2.7.1. Introduction

This section includes the experimental methodology used in the experimental programs 1 and 2, covering the analog materials (**section 2.7.1.1.),** the scaling between models and nature (**section 2.7.1.2.)**, the experimental limitations **(section 2.7.1.3.)** and the techniques used in the analysis and visualization of the experiments **(section 2.7.1.4.)**.

The most important point of an experimental program is the setup design. The experiments should be scaled in order to be comparable to our natural analogue (Koyi, 1997; Goncharov, 2010) (**Fig. 2.10**). At this point, the dimensions of the experiment, the mechanical properties of the analog materials, or the deformation rates applied to the experiments should be scaled (Hubbert, 1937). During experiment deformation a rigorous methodological workflow must be followed (**Fig. 2.10**) in order to have a high control of experiments evolution and to quantify the effect of each involved parameters. This workflow can be repeated several times changing parameters between each experiment to check their effect in the kinematic evolution of the experiment. Then, the experimental results are compared with natural examples or case studies (**Fig. 2.10**).

This proposed methodology has applied to our experimental programs thanks to the research internship done at the analog modeling laboratory in the Royal Holloway University of London. This workflow is outlined during this following **section 2.7.1.4.**

The Experimental Program 1 includes 10 different analog models (Roma et al., 2018a), while the Experimental Program 2 includes 7 different models (Roma et al., 2018b and 2018c) (**Table. 2.2**). Each experimental program includes a baseline model from which different parameters have been modified until to obtain a range of models large enough to determine the effect of these parameters on the kinematic evolution of the models and in the resulting structural style. In addition, some of the models have been repeated in order to ensure its reproducibility (Driehaus, 2013), during the research stay done at the Geomaabara analog modeling laboratory at the University of Dodoma.

The articles that are part of the main body of this PhD, do not include all the models of each experimental program. Only eight models of the Experimental Program 1 have been

selected for the article by Roma et al. (2018a), and three models of the Experimental Program 2 have been included in the articles by Roma et al. (2018b and 2018c). The experiments presented in the articles correspond to end-members (**Table. 2.2**) that illustrate the evolution of the salt-detached ramp-syncline basins during extension and inversion, paying special attention to the role of salt structures, erosion and synkinematic sedimentation.

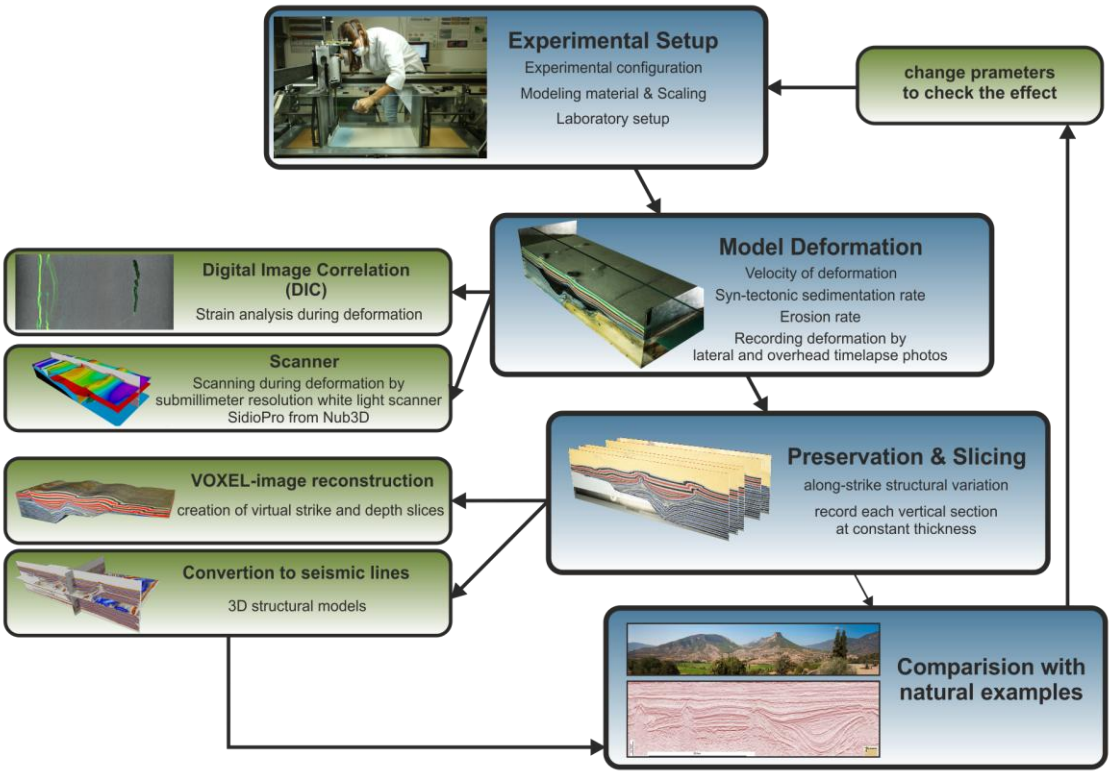

Fig.2.10. General workflow applied in the experimental programs presented in this PhD. Note that the use of each technique may change depending on the considered experimental program.

The analog models included in this PhD were designed using a completely constrained fault technique (**section 2.5.**). The experimental setup for both programs was inspired in the experimental configurations used by Yamada and McClay (2003a and b), which were subsequently improved by Ferrer et al. (2016) for the inversion episode. This configuration consists in a rigid wooden block that constrains the geometry of the main fault, and an overlying plastic sheet to reproduce the fault detachment and to transmit both extensional and contractional deformation (see details and specific configuration in **sections 2.7.2.1. – 2.7.3.1.**).

a) Experimental Program 1

Experiment	Pre-kinematic thickness (cm)	Polymer thickness (cm)	Extension (cm)	Inversion (cm)	Time (hours)
Exp._1.1 (baseline)	11.8	-	20	-	70
Exp._1.2 (baseline)	11.8	-	20	9	93
Exp._1.3	11.8	0.5	20*	-	70
Exp._1.4	11.8	0.5	20*	9	93
Exp._1.5	12.3	1	20*	-	70
Exp._1.6	12.3	1	20*	9	93
Exp._1.7	11.8	0.5	10*	-	35
Exp._1.8	11.8	0.5	20*	9*	93

*erosion during extension or inversion, keeping constant the regional datum at the begining of extension.

b) Experimental Program 2

Experiment	Extension (cm)		Stretching rate (cm/h)	Inversion (cm)	Shortening rate (cm/h)	Sedimentation inversion	Time (hours)
	phase 1	phase 2					
Exp._2.1*	7	8	1	-	-	-	15
Exp._2.2*	7	8	1	8	1	-	23
Exp._2.3*	7	8	1	8	1	5 mm thick / 1 cm	23
Exp._2.4	7	8	0.4	-	-	-	37.5
Exp._2.5	-	9	1	every 5mm of extension the deformation box was tilted 0.5º			9

* experiments presented in detail in this thesis

Table.2.2. Summary table showing the main characteristics of the Experimental Program 1 **a)** and Experimental Program 2 **b).**

2.7.1.1. *Modeling materials*

The materials used for both experimental programs (**Table. 2.3**) were well-sorted, subrounded dry silica sand (nearly pure silica with 199-250 µm of average grain size) and a polydimethylsiloxane polymer (PDMS). The dry sand is an excellent material to simulate brittle deformation of upper crustal sedimentary rocks (Horsfield, 1977; McClay, 1990; Schellart, 2000), and the PDMS polymer (Weijermars, 1986; Couzens-Schult et al., 2003; Dell' Ertole and Schellart, 2013) has been widely used as analogue of viscous salt (Koyi et al., 1993; Nalpas and Brun, 1993; Vendeville et al., 1995; Withjack and Callaway, 2000; Dooley et al., 2005; Soto et al., 2007; Ferrer et al., 2014, 2016). Silica sand has a Mohr-Coulomb behavior at moderate values of normal stress as used in the laboratory (Hubbert, 1951; Mandl et al., 1977). The mechanical properties of poured sand were measured with a ring shear tester at the Fault Dynamics Research Group Laboratory during the first PhD research stay. According to these

mechanical tests, the poured dry sand used in the experimental programs has an angle of internal friction of 34.6° (coefficient of internal friction (μ) of 0.5–0.6), a bulk density (ρ) around 1500 kg·m^{-3}, and a low apparent cohesive strength of 55 Pa. The coefficient of sliding friction between the plastic sheet and the sand pack was μb=0.21-0.37 (Huiqi et al., 1992; Liu et al., 1992; Konstantinovskaia and Malavieille, 2005, Graveleau et al., 2012). On the other hand, the PDMS polymer (Rhodia Rhodorsil Gum FB — PDMS) has a near-perfect Newtonian fluid behavior when deformed at a laboratory strain rate of $1.83 \cdot 10^{-4}$ s^{-1} (Dell'Ertole and Schellart, 2013). It has a very low yield strength (Weijermars, 1986) as halite at geological time and space scales (Dell'Ertole and Schellart, 2013). According to the properties provided by the manufacturer and literature mechanical analysis, it has an effective viscosity (η) of 10^4 Pa·s and a density (ρ) of 972 kg·m^{-3} (Dell'Ertole and Schellart, 2013)

Parameter	Model	Nature	Model/Nature ratio
Length, L (m)	0.01	1000	10^{-5}
Density loose sand, ρ (kg·m^{3})	1500	1900 - 2500	0.8 - 0.6
Angle of internal friction, ϕ (º)	34.6	30 - 40	1.1 - 0.8
Ang. int. friction green sand, ϕ (º)	30	30 - 40	1 - 0.6
Density polymer, ρ (kg·m^{-3})	972	2170 - 2200	0.44
Viscosity polymer, η (Pa·s)*	10^4	10^{18}-10^{19}	10^{-14}-10^{-15}
Velocity, V (model (mm/hour) & nature (mm/year))	1	0.01	625000
Time, t (model (hour) & nature (year))	1	713.000	$1.6 \cdot 10^{-10}$

* Viscosity measured when deformed at a laboratory strain rate of $1.83 \cdot 10^{-4}$ s^{-1}

Table.2.3. Scaling parameters used in both experimental programs

2.7.1.2. *Scaling*

In terms of scaling (**Table.2.3**) and according to Hubbert (1937), 'an analog model is representative of its natural prototype if both systems are geometrically, kinematically and dynamically similar'. Two bodies are said to be geometrically similar when all corresponding lengths are proportional and all corresponding angles of the two bodies are equal. If two geometrically similar bodies undergo geometrically similar changes of shape or positions, or both, the two bodies are said to be kinematically similar provided the time required for any

given change in the one is proportional to that required for the corresponding change in the other (Hubbert, 1937). Two bodies which are geometrically and kinematically similar are also dynamically similar only if the ratio between the forces acting on corresponding particles in the two bodies, compared kind for kind, is constant (Koyi, 1997).

Dynamically similar ones are achieved through dimensionless body forces (gravity and inertia) and surface forces (force to the area acted upon, and is known as the stress).

$F^* = Fm/Fn$

where *F* are forces, *m* means a quantity in the model and *n* means a quantity in nature. The model ratio of forces (F*) is function of mass (m) and gravity (g);

$F = m \cdot g$

However, body forces diminish with size more rapidly than the surface forces, so that if the element of volume is small enough we may completely neglect the body forces for that element (Hubbert, 1937), so $g_{model} = g_{nature}$ and $g^*=1$

$F = m$ **(1)**

Assuming the basic rules of scaling analysis (Hubbert, 1937; Ramberg, 1967; Vendeville, 1987; Withjack and Callaway, 2000; Keppler et al., 2013), the surface forces have to be measured by the model-to-prototype ratio for stress (σ*), that is equal to;

$\sigma^* = F^*/L^{2*}$ **(2)**

where F* and L* are the model-to-prototype ratios for forces and length respectively (ratio of the distances between equivalent points on the model and on the prototype).

From the model ratios of mass (m*) and length (L*), the model ratio of density (ρ*) is obtained directly:

$\rho^* = m^*/L^{*3}$ or; **(3)**

$$m^* = \rho^* \cdot L^{*3} \quad \textbf{(4)}$$

Starting from Eq. (2) and replacing each quantity for Eq. (1), (3) and (4), such Eq. (2) can also be expressed as:

$$\sigma^* = F^*/L^{2*} \ (1,3,4) = \rho^* \cdot L^{*3} / L^{2*} = \rho^* \cdot L^*$$

$$\sigma^* = \rho^* \cdot L^* \cdot \text{“}g^*\text{”} \quad \textbf{(5)}$$

where ρ*, g*, and L* are the model-to-prototype ratios for the density, gravity acceleration, and length, respectively. The density ratio (ρ*) was obtained by assuming an average value for the density ratios for the model materials (sand – polymer) and for natural rocks (siliciclastics – halite) (**Table. 2.3**) ρ*=0.8-0.4 and $L^*=10^{-5}$ (i.e., 1 cm in the model represents 1 km in nature). Taking into account Eq. (5), we obtained $\sigma^*= 6 \cdot 10^{-6}$.

From σ* and viscosity ratio of polymer (η*), the strain rate ratio (ε*) can be calculated as:

$$\varepsilon^* = \sigma^* / \eta^* = 6 \cdot 10^{9} \quad \textbf{(6)}$$

where η* is the model ratio of viscosity (10^{-15}), obtained from the polymer viscosity (10^{4}) and the viscosity for the rock salt (10^{19}) (Weijermars et al., 1993).

The time ratio (t*), which is the inverse of ε*

$$t^* = 1/ \varepsilon^* = 1,6 \cdot 10^{-10}$$

which means that 1 h in the experiments represents about 713.000 years in nature.

Our Experimental Program 1 lasted 70–90 h, equaling a range in geological time of 50–64 My. Our Experimental Program 2 lasted 15-23 h, equaling a range in geological time of 10–16 My.

Finally, since the velocity ratio (V*) can be defined as:

$$V^* = L^* / t^* \quad \textbf{(7)}$$

Then the extension and shortening rate for our models was 4 mm/h during both extension and inversion phases for the Experimental Program 1, equivalent to 0.5 mm/y in nature, and 10 mm/h for the Experimental Program 2 (**Table. 2.2**), equivalent to 1.4 mm/y in nature. The total extension for Experimental Program 1 was 20 cm (20 Km in nature) and the total shortening 9 cm (9 Km in nature). While for Experimental Program 2 the total extension was 15 cm (15 Km in nature) and the total shortening was 8 cm (8 Km in nature)

2.7.1.3. *Modeling limitations*

Scaled physical models are powerful visual tools for the forward modeling of brittle deformation in the upper crust (Dooley et al., 2005; Soto et al., 2007; Corti et al., 2012; Dooley et al., 2017; Ferrer et al., 2017). In particular they can simulate a wide range of tectonic settings from extension, inversion, strike-slip and contraction as well as mobile salt and shale systems. Analog models have distinct advantages over numerical models in that they are visual and 3D and are relatively easy to construct. Serial sectioning at the end of the experiments permit to determine the 2D along-strike variation of structures and geometries. The new analysis techniques based on Particle Image Velocimetry (PIV), 3D voxel imaging, or virtual seismic represent an improvement on the 3D structural characterization (e.g. fault linkages, fault displacements and complex 3D fault geometries). The application of these techniques also allows a direct comparison between analog models and case studies in structurally complex areas (e.g. depth slices in 3D seismic).

Despite the modeling materials simulate the deformation mechanics of brittle sedimentary rocks and viscous salt in the upper crust producing realistic geometric and kinematic structures, there are important limitations which must be considered when interpreting the results of the experimental programs included in this PhD:

i) All modeling approaches (analytical, numerical, analog) imply a simplification of the complexities of the natural process. Especially for analog (sandbox) models, the limited analog materials available to simulate the whole rock properties, difficult to simulate the complex natural rheology and strength profiles, and consequently analog models are greatly simplified (Corti, 2012).

ii) Deformation in sandboxes will always be strongly controlled by the boundary conditions at the base and sides of the model. Great care is needed in the construction of physical models to ensure that the boundary conditions in the model replicate those in nature (McClay, 1996).

iii) Although the use of rigid blocks to force the geometry of normal faults has been widely employed in analog modeling (McClay, 1989 and 1995; Buchanan and McClay, 1991; Roure and Colleta, 1996; Yamada and McClay, 2003a and b), the main disadvantage of this technique is the inability of rigid footwalls to deform (McClay, 1995; Bonini *et al.*, 2012). This fact prevents the formation of basement involved footwall structures as shortcuts or horses as occurs in nature (*e.g.* McClay, 1989 and 1995; Nalpas *et al.*, 1995; Eisenstadt and Sims, 2005). Despite this limitation, our experimental programs combined the rigid footwall and a brittle sub-polymer sand pack to impose topographic variations during deformation, and both were considered as the basement.

iv) For avoiding the use of metal or wooden plates and rigid blocks, centrifuge models imposes a uniform stress field on the models where the distribution of deformation is only controlled by lateral variation in strength and rheology of the analog materials (Corti et al., 2012), without requiring a velocity discontinuity. In this case, the models underwent vertical thinning and lateral expansion in response to the centrifugal forces (Corti, 2004). However, centrifuge models are usually characterized by a limited size and continuous monitoring of deformation is usually not possible limiting the observation of structural evolution.

v) Whereas numerical models are able to simulate complex rheological variations induced by temperature changes (Corti et al., 2003), analog models cannot simulate temperature dependence of rock rheology (Corti et al., 2003; Corti, 2012), flexural and isostatic effects of deformation as occurs in natural systems. Compaction of sediments, fluid flow and the development of over-pressures are also intrinsic limitations of the modeling method (McClay, 1996). Although, magmatic processes has been modeled at crustal- and lithospheric-scale, those process are great simplified since they are far from capturing the complex interaction of magma intrusion, chemical reactions, dyking and faulting observed during continental rifting (Corti, 2012).

vi) In particular, the rigid footwall bocks used in the experimental programs cannot simulate footwall uplift. Footwall uplift may be a very significant deformation mechanism in

extensional scenarios where there is little constraint by synrift sedimentation (Allen and Allen, 2013), and the lack of these effects, therefore, remains as an important limitation to the analog models (McClay and White 1995).

vii) Fault displacement may be expected to occur as a system of faults (Soto et al., 2007; Corti, 2012), whereas in constrained analog models half-graben boundary coincides with a sole main fault.

viii) The models are grain size dependent and grain size effects are noticeable in the width of the shear-fault zones and the limits to which faults are discernible (McClay, 1990; Scholtz, 1990). In particular the faults in the analog models are formed by granular shear processes without grain breakage, a process that does not replicate fault mechanics in nature (Corti et al., 2003)

ix) In the presented models the basin formed during extension is always infilled with synrift sediment, a condition which does not always occur in nature where sedimentation can be interrupted and even periods of erosion are common (McClay, 1990; Soto et al., 2007).

x) Our models have a layered brittle overburden of pure quartz sand, which creates density ratios of sand/silicone that are much higher than those of nature, assuming a siliciclastic overburden above halite (Soto et al., 2007). Exaggerated density ratios erroneously magnify overburden foundering, rise of active diapirs, and expulsion and extrusion of salt (Dooley et al., 2007). Dooley et al. (2007) and Dooley et al. (2009), they used a brittle overburden comprised alternating layers of silica sand and hollow glass beads (Rossi and Storti, 2003). Hollow glass beads have a much lower density than sand, thus scaling the bulk density more accurately. Varying the sand-bead ratio in the brittle section produced an overburden having about the same bulk density as the salt analogue (Dooley et al., 2007).

xi) Higher friction between the glass-side walls and the polymer/sand pack produced a border effect on the structures. In addition, the polymer sticks against the glass-side walls masking the structures' evolution through the glass due to the edge effects.

2.7.1.4. *Data capture, analysis and visualization techniques*

The model's evolution during both extension and inversion was recorded by lateral and overhead time-lapse photographs taken every 60 seconds with high-resolution digital cameras. These photographs were processed using digital image correlation (DIC) software (**Fig. 2.10**) to quantify the strain as well as the displacement vectors for the prekinematic layer and each synkinematic layer (for further details of DIC analysis see Adam et al., 2005). In addition, the surface topography of the models was recorded during both extensional and inversion phases using a sub-millimeter resolution white light scanner (SidioPro from Nub3D; Ferrer et al., 2017) (**Fig. 2.10**).

At the end of the experiment, the models were preserved adding water with a gelling agent that allow the slicing of the model in different cross-sections, at a spacing of 3 mm, parallel to the deformation direction (orthogonal to the main structures in the models included in this PhD) (**Fig. 2.10**). Those vertical serial sections were also recorded using high-resolution digital cameras positioned perpendicularly the experiments in order to analyze the along-strike variations of structures (**Fig. 2.10**). In order to avoid optical deformations due to the lenses, the focal length has been kept constant in each photograph. A 5 cm-wide section was neglected along each glass-side of the experiments during their analyses in order to avoid edge effects.

The short distance between each cross-section (3 mm) allows the application of innovative image or seismic techniques to study the internal structure of the models. The voxel reconstruction image-technique from the interpolation between cross-sections using a medical software for CT scans allows to create a 3D image volume that can be virtually sliced in any direction (**Fig. 2.10**) (Dooley et al., 2009; Ferrer et al., 2016, 2017).

On the other hand, following the methodology proposed by Hammerstein et al. (2014) the final cross-sections photographs can be converted to 2D SEG-Y format that, applying an in-house interpolation methodology, are converted into 3D seismic volumes (**Fig. 2.10**). This allowed an accurate interpretation of each key horizons and faults, paying special attention to the top and bottom of the polymer layer to characterize the along-strike variation of salt structures, quantifying parameters such as thickness variations of the polymer layer or the position of the depocenters throughout the experiments. The 3D seismic interpretation was carried out with Petrel (Schlumberger) and the maps were built using Gocad (Paradigm).

2.7.2. Experimental Program 1

The Experimental Program 1 was carried out at the Geomodels Analog Modeling Laboratory of the University of Barcelona.

2.7.2.1. *Experimental setup*

The analog experiments (**Table. 2.2a**) were carried out in a 90 cm-long, 50 cm-wide, and 35 cm-deep glass-sided deformation box. Two end walls orthogonal to the glass-sided walls made the experiment a closed system. Both glass-sided walls and the left-hand side wall were fixed, whereas the other wall was moved by a servo-motor at a constant velocity (**Fig. 2.11a**). A rigid wooden block attached to the fixed wall was used to simulate the intracrustal fault geometry (**Fig. 2.11a)** of the Columbrets Basin case study, (see **Chapter. 3** for further details). The geometry of this block was characterized by: a 30 cm-long upper panel dipping 5°; a 20 cm-long intermediate panel dipping 20°, and a third horizontal lower panel corresponding to the baseplate (**Fig. 2.11a**). A plastic sheet attached to the roller servo-motor (**Fig. 2.11b**) and overlying both the rigid block and the baseplate reproduced the fault motion. It covered the entire model except for the uppermost 3 cm of the upper panel, simulating the fault breakaway (end of basal plastic sheet, or EBPS in **Fig. 2.11a**).

The extensional deformation was achieved by pulling the moving wall and the plastic sheet away at the same speed and direction (**Fig. 2.11b**). Then, the contractional deformation during inversion was transmitted by reversing the direction of the moving wall and the left-hand side roller motor (where the plastic sheet was fixed only during this episode; **Fig. 2.11c**).

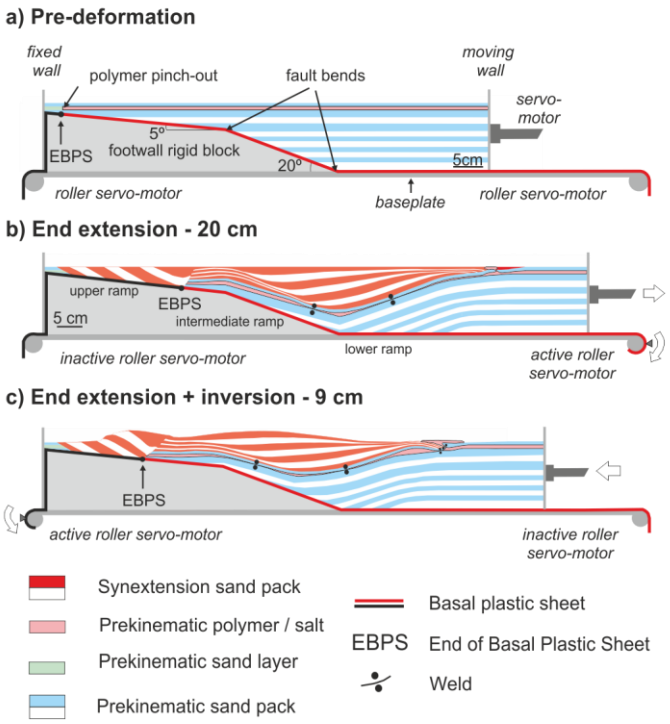

Fig.2.11. Conceptual sketches of the experimental apparatus and materials used in the Experimental Program 1. **a)** sketch of the rig before deformation; **b)** structural pattern at the end of the extension (after 20 cm of extension) and **c)** structural pattern at the end of inversion (after 20 cm of extension and 9 cm of shortening).

2.7.2.2. *Experimental procedure*

The deformation box was filled by manually pouring 3 mm-thick horizontal prekinematic layers of alternating white and colored sand (blue or black). Each layer was labeled using a scraper until reaching a total thickness of 10.7 cm above the baseplate (**Fig. 2.11a**). Depending on the experimental configuration (**Table. 2.2a**), a 0.5 or 1 cm-thick layer of green sand (baseline models) or polymer, overlay the prekinematic sand pack. The polymer covered the area between the EBPS (polymer pinch-out in **Fig. 2.11a**) and the moving wall. Between the EBPS and the fixed wall it was substituted by a green sand layer with the same thickness, simulating the non-presence of salt at the Desert de les Palmes high (Roca et al., 1994, (for further details, see the next **Chapter. 3**). To complete the prekinematic succession both the polymer and the green sand layer were overlaid by two 3 mm-thick layers of white and blue sand (**Fig. 2.11a**). After that, all experiments were extended by 20 cm using a constant deformation rate of 4 mm/h (except Experiment 7, which was extended by 10 cm; **Table. 2.2a**).

Before to start experiments, and according to the natural analogue, it is necessary to define if the pre-deformation regional will be fixed or variable during the experiment or what will be the sedimentation or erosion rate. For this Experimental Program 1, the synkinematic white, black and red sand layers were added at every 1 cm of extension, keeping constant the prekinematic regional datum (**Fig. 2.11b**). This fact also imposed the erosion of any topography above this datum, which was developed by polymer inflation during extension. After extension, all experiments were partially inverted using the same strain rate (4 mm/h). Syninversion sedimentation was not considered in any experiment, and the topography generated during shortening was preserved. Only Experiment 8 tested the role of erosion during inversion (**Table. 2.2a**).

In order to preserve the final topography and to inhibit any polymer movement after inversion the experiments were covered with thick post-kinematic sand.

2.7.3. Experimental Program 2

The Experimental Program 2 was carried out at the Fault Dynamics Research Group Laboratory, Earth Science Department, from the Royal Holloway University of London (RHUL), during the research stay, supervised by Prof. Ken McClay and Dr. Oriol Ferrer.

2.7.3.1. *Experimental setup*

The analog models were carried out in a 63 cm long, 30 cm wide, and 35 cm deep glass-sided deformation box (**Fig. 2.11a**). A rigid wooden block with four kinked fault bends was used as a footwall geometry that imposed a ramp-flat-ramp geometry to the master fault. Both ramps dip at 45°, and they were separated by two panels dipping at 3.5° with an adjacent horizontal basal detachment at the base of the model (**Fig. 2.12a**). We placed a flexible (but not stretchable) plastic sheet above the footwall block to reproduce the master fault motion (**Fig. 2.12a**, solid red line) that acted as a major detachment during both extension and inversion. The plastic sheet remained attached at both end walls during extension and inversion. We fixed a metal plate above the upper footwall flat to form the breakaway fault (**Fig. 2.12a**); here, the plastic sheet went underneath the metal plate. Extension was achieved by pulling the footwall block away using a motor-driven worm screw (**Fig. 2.12d**). For the inversion, the motion of the footwall block was reversed to produce contraction of the hangingwall section (**Fig. 2.12e**).

The extensional and contractional displacement rates of the moving footwall remained constant during the experimental program (10 mm/hour). These deformations and synkinematic sedimentation rates were selected after two testing models in order to favor polymer flow, such as the salt in nature.

2.7.3.2. *Experimental procedure*

The layered prekinematic sand pack for the Experimental Program 2 was formed by pouring 3 mm thick, horizontal white and colored sand layers into the deformation box using a mechanical scraper. This prekinematic unit covered the entire model (i.e., the footwall block and the plastic sheet) with a total thickness of 9.3 cm above the horizontal basal detachment (**Fig. 2.12a**). The models (**Table. 2.2b**) were initially extended 7 cm at a displacement rate of 10 mm per 10 min. No synkinematic strata were added during this first phase of extension (**Fig. 2.12b**). The accommodation space was then infilled by a polymer showing important variable thickness (**Fig. 2.12c**). The polymer has a horizontal upper surface, a thickness of 5 mm on the right section of the model, 37 mm at the deepest depocenter, and it pinches out on the upper footwall flat. The polymer was covered by a 10 mm thick sand layer prior to the second phase of extension (overburden in **Fig. 2.12c**).

Subsequent stretching was applied at a rate of 10 mm per hour (**Fig. 2.12d**) with up to 8 cm of total extension (150 cm, considering both phases). During this phase, synkinematic layers were added by pouring alternating layers of red, white, and black sand after every 5 mm of extension, keeping the prekinematic regional datum constant, equal to the one existing at the beginning of the second extensional phase (**Fig. 2.12c**).

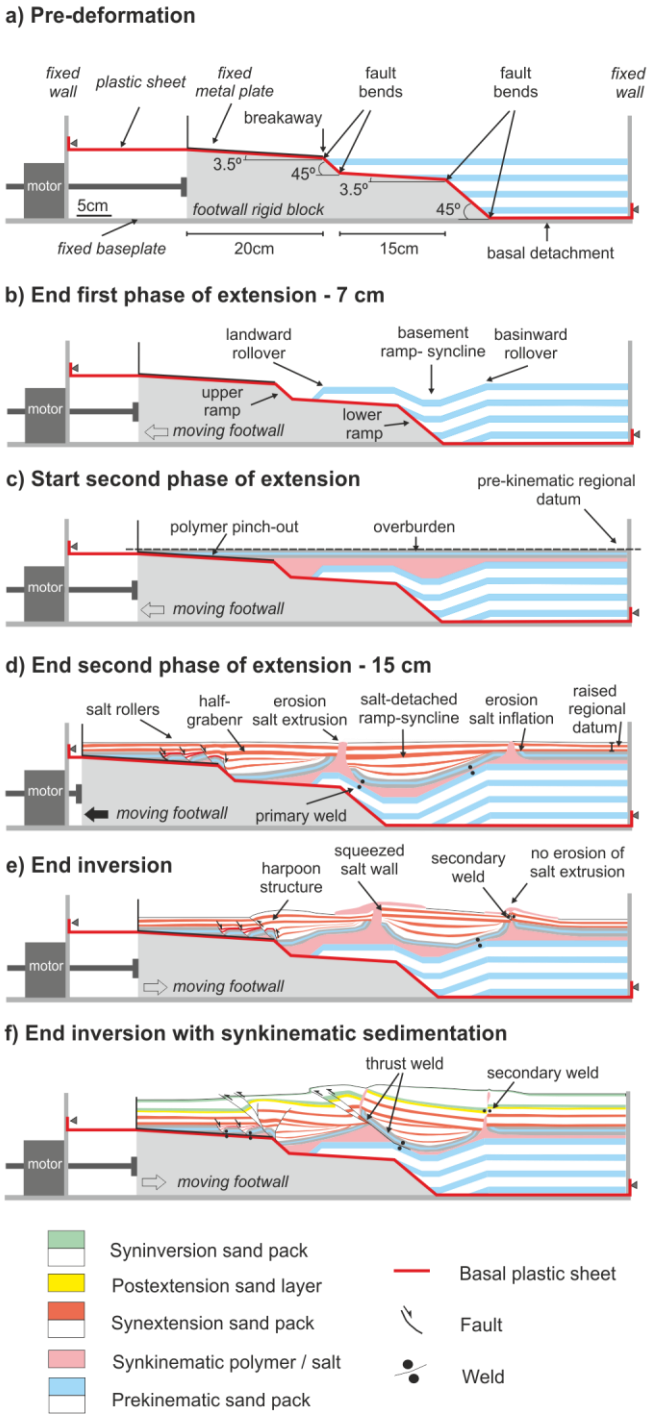

Fig.2.12. Conceptual sketches of the experimental apparatus and materials used in the Experimental Program 2. **a)** pre-deformation configuration - sketch of the rig before deformation, **b)** structural pattern at the end of the first extensional phase (after 7 cm of stretching), **c)** polymer filling the depocenters generated during the first phase of extension, **d)** experimental configuration at the end of the second extensional phase (after an additional 8 cm of stretching), **e)** configuration at the end of the inversion (after 7 cm of shortening) and **f)** structural pattern at the end of the inversion (after 7 cm of shortening), green and white layers represent syninversion sedimentation.

The models were paused for 15 min. during the deposition of each second extensional phase synkinematic sand layer. Synkinematic sedimentation increased the differential load

between basin depocenters and their edges enhancing polymer flow and localizing diapirism. Any topographic highs that had formed by polymer inflation were eroded during the synkinematic layering (**Fig. 2.12d**), thus removing the overburden and enhancing subsequent polymer rise. Once the polymer reached the surface of the experiment through passive diapirs, the regional datum was raised by 3 mm for each subsequent synkinematic layer, thus simulating the passive growth of the salt wall (**Fig. 2.12d**). Overhangs formed by polymer extrusion onto the model's surface were manually removed with a sharpened knife (it has only removed the entire polymer overhang without affecting the diapir stem) during the second phase of extension (simulating salt dissolution and erosion in nature, Rowan and Vendeville, (2006)) before adding a new synkinematic layer (**Fig. 2.12d**). The polymer surface extrusions are also removed to avoid Christmas-tree structures (repeated salt extrusion over the underlying strata, which create stacked salt wings forming a serrated contact). Removing the polymer extrusion, we simplify the extensional geometry of the salt structures and we also reduce the complexity of the subsequent inverted salt structures.

While Exp._2.1 ended after the second extensional phase, Exp._2.2 and 2.3 (**Table. 2.2b**) were subsequently inverted by 8 cm (**Fig. 2.12e-f**) at a shortening rate of 10 mm per hour, until reaching the null point of the second extensional phase. Exp._2.2 did not consider erosion either synkinematic sedimentation during the inversion stage (**Fig. 2.12e**). However, in Exp._2.3, green, white and black syninversion sand layers were added after each 10 mm of shortening raising the regional datum to 5 mm-thick (**Fig. 2.12f**).

Completed models were covered by a thick postkinematic sand layer to preserve the final topography and inhibit any undesired polymer movement.

2.7.3.3. *Restoration procedure*

Structural restoration is a tool that has been used for a number of decades to illustrate the evolution of geological systems through time, based on known principles and horizon-fault relationships (Chamberlin, 1910; Bally et al., 1966; Dahlstrom, 1969). Through the years, the widespread application of these techniques to predict fault and horizon geometry in depth has given rise to more sophisticated algorithms (Groshong et al., 2012; Lingrey and Vidal-Royo, 2015), which allow the restoration of complex, decoupled salt systems as the one presented in this thesis, for the Experimental Program 2 (**Table. 2.2b**). Restoring an analog model with well known, imposed kinematics and boundary conditions gives also the opportunity to investigate

complex three-dimensional processes such as salt (i.e. polymer) mobilization across the model, that would otherwise be obscured by scarcity or even lack of reliable data.

Two final cross-sections of Exp._2.2 (**Table. 2.2b**) were sequentially restored to illustrate the structural evolution of the two main domains across areas with well-developed salt walls and across areas without extruded salt walls. The sequential restoration shows **i)** the change in basin geometry due to extension, positive inversion, and diapirism, and it highlights the different responses to deformation of the sub- and supra-polymer units and **ii)** the variations in the area of the polymer section between the sub- and supra-polymer units at each phase. The sub- and supra-polymer units in the analog models were restored independently using different strain transformations (i.e., restoration methods) for each. The supra-polymer deformation is characterized by folding and faulting as a consequence of extension and compression — triggering polymer mobilization — and therefore flexural slip, unfolding to a known datum (regional) was applied, allowing conservation of the line length and area (Dahlstrom, 1969; Groshong et al., 2012; Lingrey and Vidal-Royo, 2015). The deformation of the sub-polymer sand pack was generated by slip along the master fault, and was restored using the fault parallel flow algorithm in Move™ by applying the measured fault offsets between consecutive restoration phases. Sequential restorations were carried out from the inversion phase and to the start of the second phase of extension after the deposition of the polymer layer.

CHAPTER 3. SUMMARY OF RESULTS

3.1. INTRODUCTION

The general results of this thesis have been summarized in three scientific manuscripts entitled “Formation and inversion of salt-detached ramp-syncline basins. Results from analog modeling and application to the Columbrets Basin (Western Mediterranean)”; “Tectonic inversion of salt-detached ramp-syncline basins as illustrated by analog modeling and kinematic restoration” and “Weld kinematics of synrift salt during basement-involved extension and subsequent inversion: Results from analog models”. The first article was submitted to the journal Tectonophysics, and was focused on the analog modeling of salt-detached ramp-syncline basins with the aim to understand the specific, kinematic evolution of the Columbrets Basin (Western Mediterranean). The second article was submitted as a technical paper to the journal Interpretation, with the aim to demonstrate the powerful tool of analog models as an aid to structural interpretation. The third article was submitted to a special issue of the journal Geologica Acta devoted to “contributions to the geological evolution of the Iberian Peninsula: a tribute to Pere Santanach”. This last article was aimed at gaining insights on welding kinematics using analog models, but also provides a general overview of the advanced techniques in analog modeling. Those three journals are enlisted within the international Journal Citation Index (JCI). In the following, the main results of each of these articles are summarized and illustrated.

3.2. FORMATION AND INVERSION OF SALT-DETACHED RAMP-SYNCLINE BASINS. RESULTS FROM ANALOG MODELING AND APPLICATION TO THE COLUMBRETS BASIN (WESTERN MEDITERRANEAN)

After a general introduction of geological setting of the Columbrets Basin, the setup configuration used for the Experimental Program 1 (geometry of the master faults, stratigraphy, fault displacement, etc) will be justified. Subsequently, a summary of the main obtained results of the sandbox models with and without polymer (Experimental Program 1, **Table. 2.4a**) is described. For broader and detailed overview of the results see the article attached at the Appendix Chapter.

3.2.1. Main structural features of the Columbrets Basin

The Columbrets Basin is located in the southwestern part of the València Trough in the Western Mediterranean (**Fig. 3.1**) and belongs to a NE-trending intracontinental basin that

developed during the Mesozoic on the northwestern margin of the Maghrebian Tethys (Schettino and Turco, 2010). The basin is a 60–80 km-long and 40–50 km-wide asymmetric syncline (**Fig. 3.1**) with a short and steeply dipping southeastern limb (syncline forelimb) and a larger and gently dipping northwestern limb (syncline backlimb; **Fig. 3.2**). It is filled by a thick (up to 8–9 km) succession of uppermost Triassic to Cretaceous carbonate sediments (Roca, 1996) that overlie a hyperextended crust (< 4 km-thick) beneath the syncline hinge (Pascal et al., 1992; Torne et al., 1992; Etheve et al., 2018). The thickness of the uppermost Triassic to Lower Cretaceous basin infill gradually decreases from the syncline hinge towards both edges. This sedimentary succession is affected by extensional and contractional faults detached at the Upper Triassic (Keuper) evaporites that act as a regional decoupling layer. The thickness of this evaporitic unit changes across the basin, becoming thinned until it is welded at the syncline limbs, while thickening by inflation along the syncline edges where salt structures (i.e., diapirs and salt walls) are developed.

Beneath the Upper Triassic salt unit, the top of the basement and the overlying Permian-Lower Triassic rocks depict the same broad synformal geometry but they are affected by a widespread system of extensional faults (**Fig. 3.2)**. Most of these faults do not propagate across the Upper Triassic salt except at the onshore northwestern margin of the basin in the Desert de les Palmes where they form a listric fan system (**Fig. 3.2a**; Zeyen et al., 1985; Martín and Suriñach, 1988; Roca et al., 1994; Vidal et al., 1998; Ayala et al., 2003). Desert de les Palmes belongs to an old NE-SW high, where the Jurassic basal unconformity eroded the Keuper facies (Roca et al., 1994). There, these faults cut through the entire Mesozoic succession and appear detached in the upper crust (2–3 km beneath the top of the Paleozoic basement) as an intracrustal detachment (Roca et al., 1994).

In the Columbrets Basin there is no evidence of any major bounding fault that has created the accommodation space for the basin infill (**Fig. 3.2b**), but the horizontal reflectors of the high reflective middle and lower crust (coming from the Iberian mainland-NW; **Fig. 3.2b**), as well as the Moho reflector, have lateral endings (red points in **Fig. 3.2b**). Taking into account the surface structure in the Desert de les Palmes and the oblique set of reflectors cutting the intracrustal horizontal reflectors (**Fig. 3.2b**), the Columbrets Basin is interpreted as developed in the hangingwall of a south-directed intracrustal low-angle fault with three different dipping panels (**Fig. 3.2a**): an upper horizontal panel (Desert de les Palmes), an intermediate panel dipping towards the southeast, and a southeast dipping lower panel with a lower angle.

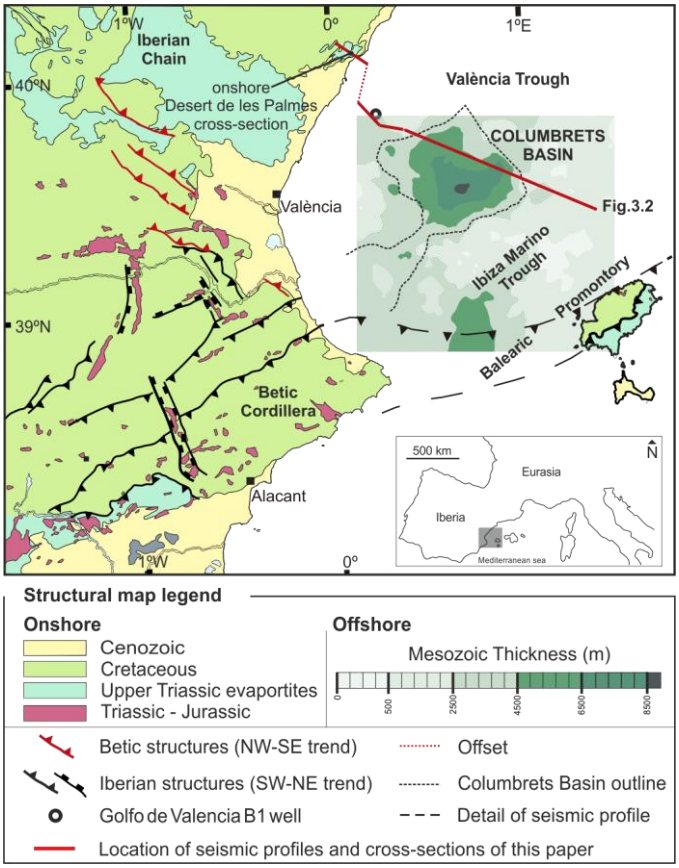

Fig.3.1. Simplified structural map of the south-western València Trough and surrounding onshore areas (modified from Escosa et al., 2018). The Mesozoic isochore map of the Columbrets Basin has been obtained from the interpretation of the SGV01 seismic survey. SW Europe map (insert) shows the geographical location of the structural map.

Based on the fault geometry and the correlation of the footwall and hangingwall upper crustal ramps we have estimated that the extensional displacement of this fault is about 80 km (**Fig. 3.2**).

The presence of a major pre- and middle Miocene unconformity on the top of the basin infill as well as of some thrusts affecting the Paleogene to the lowermost Miocene units in the basin margins, indicate that the Columbrets Basin was tectonically inverted during this period. This inversion, coeval to the formation of the Iberian Chain the northwest of the study area (Álvaro et al., 1979; Guimerà and Álvaro, 1990), was only partial and was accommodated by: **i)** the contractional reactivation of the intracrustal low-angle fault; and, **ii)** the local development of a southeast-directed thrust detached into the Upper Triassic evaporites in the southeastern limb of the basin (**Fig. 3.2**).

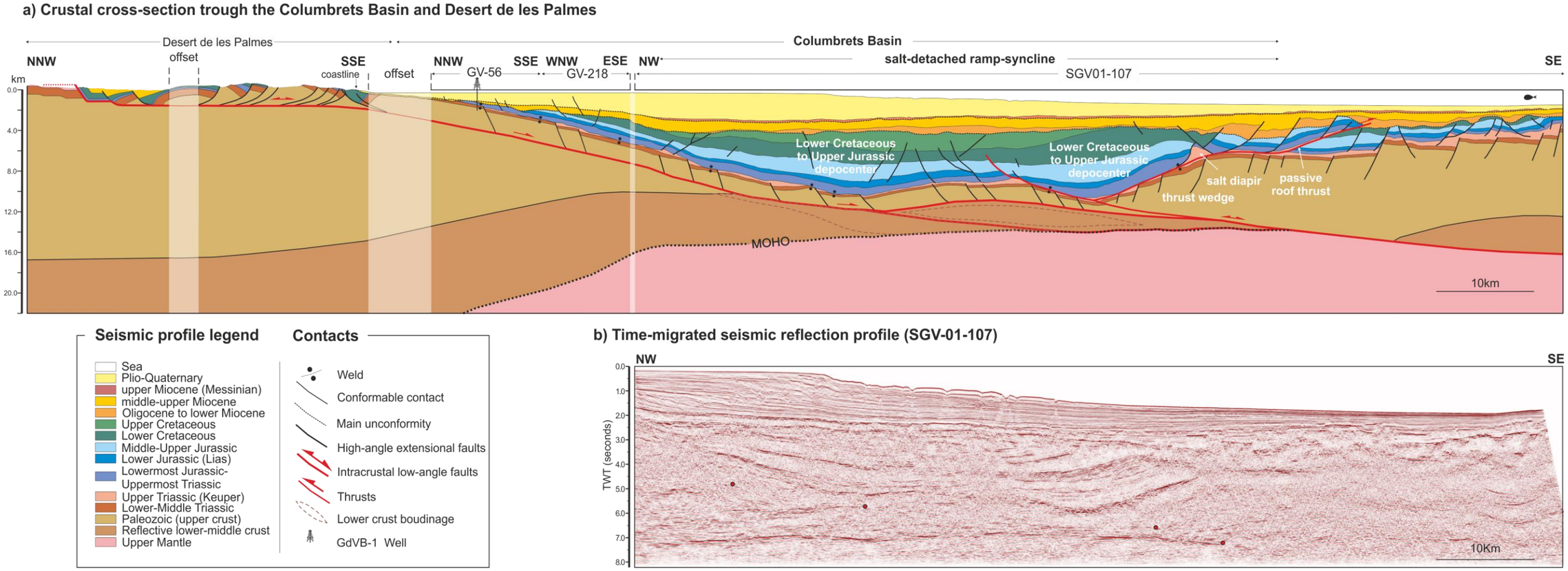

Fig.3.2. a) Crustal cross-section through the Columbrets Basin and the Desert de les Palmes. The interpretation of the Desert de les Palmes is based on Zeyen et al. (1985); Martín and Suriñach (1988); Roca et al. (1994); Vidal et al. (1998) and, Ayala et al. (2003); **b)** Time-migrated seismic line used to define the offshore structure of the Columbrets Basin in the central part of the València Trough (See location in **Fig. 3.1**). The red points indicate the lateral ending of some seismic reflections, which allow interpretation of the south-directed intracrustal low angle fault.

3.2.2. Analog modeling of low-angle intracrustal extensional faults

3.2.2.1. *Baseline Experiment*

The extensional episode in the baseline experiment (**Table. 2.2a**) led to the formation of an asymmetric ramp-syncline above the intermediate panel that was characterized by a slightly angular hinge with depocenters younging landward. The prekinematic sand pack defined an extensional basinward rollover with a crestal collapse graben developed at its hinge (**Figs. 2.2 and 3.3a**). Four axial surfaces defined different dip domains in the ramp-syncline (**Fig. 3.3a**). Note that the inactive axial ones were located on the fault panels at a distance equal to the master fault displacement. Throughout the synkinematic pack, the active and the inactive axial surfaces connect forming the so-called growth axial surface (Xiao and Suppe, 1992).

Together with this ramp-syncline, a landward rollover (also called ramp-anticline) developed above the upper fault bend (**Fig. 3.3a**). This rollover was progressively overlain by horizontal synkinematic layers that filled the accommodation space created by the downward translation of the hangingwall sand pack above the upper fault panel. The width of this rollover progressively decreased as extension progressed and the sand pack crossed the active axial surface A (**Fig. 3.3a**). In addition, at the EBPS (end of basal plastic sheet), over the upper panel) a breakaway half-graben with a width equal to the applied fault displacement developed (**Fig. 3.3a**).

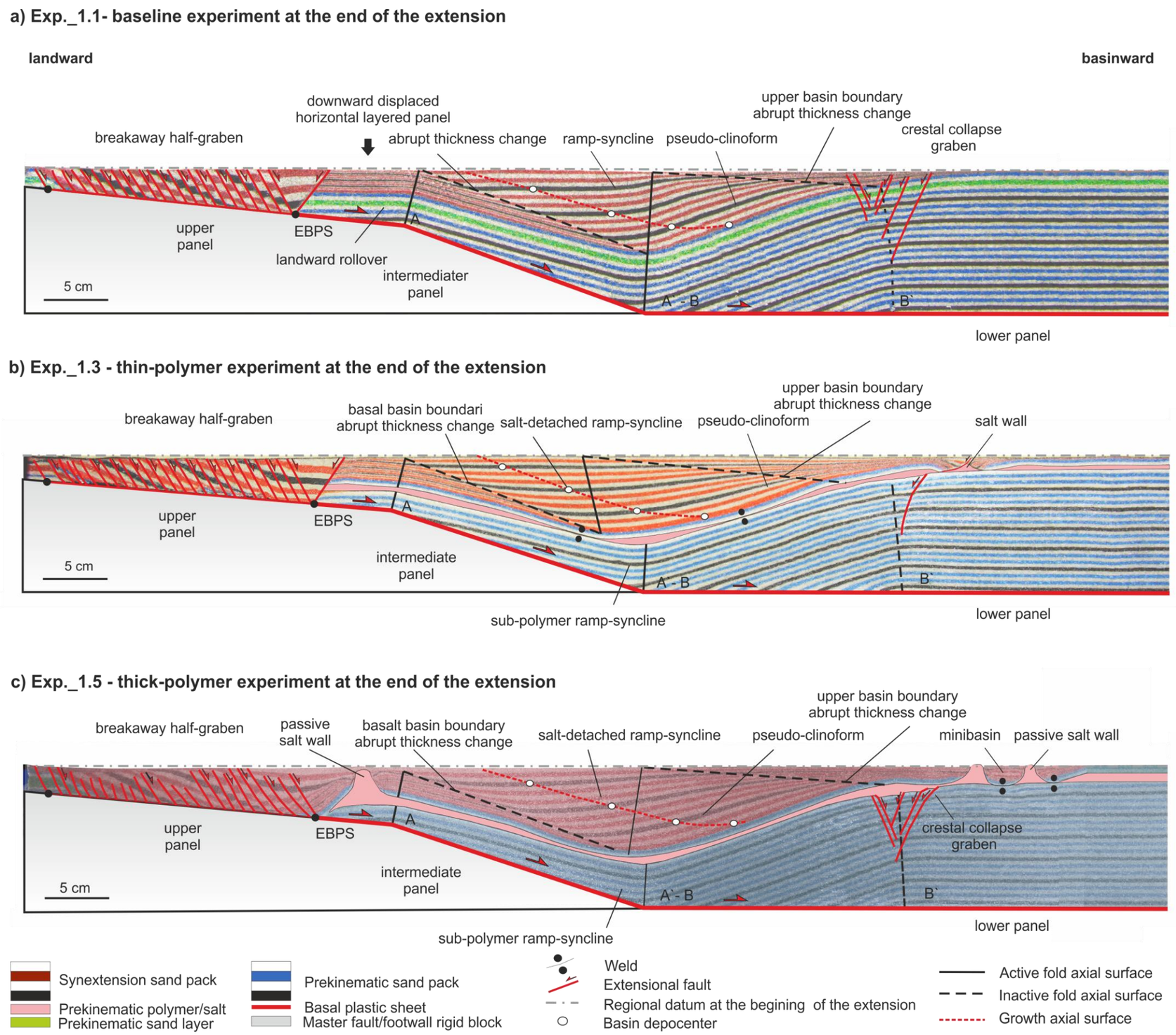

Fig.3.3. Interpreted cross-sections with the structures at the end of extension in different experiments (Exp_1.1, 1.3, and 1.5, see **Table. 2.4a** for more detail) and with the terminology used in this **Chapter 3.**

3.2.2.2. *Experiment with polymer*

The breakaway half-graben and the sub-polymer structure of these experiments (**Fig. 3.3b**) were similar to those developed during the baseline Exp._1.1 (**Fig. 3.3a**). In contrast, the deformation style was different for the units overlying the polymer.

While the baseline experiment shows a slightly angular ramp-syncline (**Fig. 3.3a**), in the experiments with polymer, the curved geometry of the supra-polymer ramp-syncline basin was constrained by the master fault geometry, but also by the polymer layer that acted as a detachment (hereinafter salt-detached ramp-syncline). In this scenario, the synkinematic depocenters also became younger landward, as occurred in the baseline experiment. Nevertheless, in this case the polymer migration modified the depocenter's path (compare Figs. **Fig. 3.3a** and **Fig. 3.3b**) and it developed salt structures bordering the basin parallel to the major “subsalt” structures (i.e., upper fault bend and basinward rollover). In addition, the polymer partially decoupled sub- and supra-polymer successions, inhibiting the upwards propagation of the sub-polymer active axial surfaces (i.e., A & B in **Fig. 3.3b**) into the supra-polymer unit. At the end of the extension in Exp._1.3 (thin-polymer layer; **Table. 2.2a**), the salt-detached ramp-syncline limbs become welded against the sub-polymer ramp-syncline. In contrast, in the thick-polymer experiment (Exp._5 and 6; **Table. 2.4a**) no primary welds formed in equivalent positions during the extensional phase (**Fig. 3.3c**).

Regardless of the polymer thickness, the polymer flow was preferentially towards the basinward rollover hinge where gentle anticline ridges formed by polymer inflation (**Fig. 3.3b**). Finally, once these reactive structures pierced the overburden they evolved into passive walls. In contrast, at the other syncline edge, diapiric structures only developed when the polymer layer is thick (**Fig. 3.3c**).

3.2.3. Inversion of the ramp-syncline basins

3.2.3.1. *Baseline Experiment*

The inversion of the baseline experiment was characterized by the formation of a major fault-bend anticline resulting from the up-dip displacement of the inherited

ramp-syncline along the master fault (**Fig. 3.4a**). This induced the formation of a wide flat-topped up anticline that was flanked by two nearly planar limbs whose boundaries belong to four new axial surfaces: two pinned to the fault bends (active axial surfaces C and D in **Fig. 3.4a**) and two pinned to hangingwall cut-off lines, and consequently displaced by the plastic sheet a distance equal to the applied shortening (inactive axial surfaces C' and D' in **Fig. 3.4a**).

The contractional reactivation of the landward rollover also resulted in a width amplification and the formation of a triangle zone at the EBPS. As shown in **Fig. 3.4a**, this triangle zone was bounded by: **i)** a thrust that cut the previously faulted breakaway half-graben, and **ii)** a backthrust that developed from the inversion of the inherited planar fault that previously bordered the breakaway half-graben (**Fig. 3.3a**).

3.2.3.2. *Experiment with polymer*

The inversion of the polymer experiments also led to the development of a fault-bend anticline, but in this case the basin uplift was minor compared to the baseline experiment (compare synkinematic layers above the regional datum at the end of extension in **Fig. 3.4a and b**).

In addition to the fault shape, the presence of a continuous polymer layer, its welded equivalent, or the diapiric structures at the edges of the syncline basin, were the main factors that governed contractional deformation. At the beginning of the inversion, the polymer withdrew towards the diapirs and walls, located at the edges of the basin, enhancing extrusion. As a consequence, whereas new welds develop in thick-polymer experiments (**Fig. 3.4d**), the welded area under the syncline basin considerably increased in the thin-polymer experiment as shortening progressed (**Fig. 3.4b**).

In a similar way to the baseline experiment, shortening modified the internal architecture of the syncline basin, but also squeezed the polymer ridges.

Fig.3.4. Interpreted cross-sections with the structures at the end of inversion of different experiments (Exp_1.2, 1.4, 1.8, and 1.6, see **Table. 2.4a** for more information) and with the terminology used in this **Chapter 3.**

The contractional deformation also produced the inversion of the breakaway half-graben in a similar way to the baseline experiment, developing a triangle zone at the EBPS (compare **Fig. 3.4a and b**). The inherited extensional fault pinned to the EBPS was inverted, developing a footwall syncline (**Fig. 3.4c**). Instead, with respect to the results of thick-polymer experiment (**Fig. 3.4d**), the geometry of the triangle zone was not controlled by the inherited normal fault pinned to the EBPS, but by the presence of an inherited collapsed salt wall (**Fig. 3.4d**).

3.3. TECTONIC INVERSION OF SALT-DETACHED RAMP-SYNCLINE BASINS AS ILLUSTRATED BY ANALOG MODELING AND KINEMATIC RESTORATION.

This following section outlines the general results obtained from two end-member experiments from the Experimental Program 2 (**Table. 2.2b**). Both experiments have been extended during two phases (Exp._2.1 and 2.2). After the two extensional phases, just one of the experiments (Exp._2.2) was also subjected to inversion. For broader and detailed overview of the results see the article attached at the Appendix Chapter.

3.3.1. Extensional deformation

3.3.1.1. *First phase of extension*

The first phase of extension produced translation of the prekinematic sand pack over the master fault, which generated fault-related folding of the hangingwall. The hangingwall geometry at the end of the first extensional phase was characterized by two major depocenters (breakaway half-graben and ramp-syncline) flanking a structural high (landward rollover). In addition, an extensional basinward rollover formed where the master fault flattened out into the horizontal basal detachment. Minor antithetic normal faults developed within this large extensional rollover panel. All these structures were covered by a polymer layer of variable thickness, at the end of the first extensional phase, simulating synrift salt.

3.3.1.2. *Second phase of extension*

The second phase of the extension reactivated the master fault. The sub-polymer structures developed during the first phase of extension are still recognized during the entire second phase of extension (**Fig. 3.5**). The width of the sub-polymer landward rollover

decreases as the extension progressed; in contrast, the sub-polymer ramp-syncline was amplified as a result (**Fig. 3.5**). With continued extension, an extensional drape fold developed at the breakaway fault, evolves into an extensional fault-propagation fold (**Fig. 3.5a**). During this process, the polymer thinned above the upper ramp favoring the upward propagation of this fault into the synextensional sand pack (**Fig. 3.5**). At the early stages of the second phase of extension, several small listric faults with triangular footwall salt rollers were formed in the upper footwall flat to the left of the breakaway (**Fig. 3.5**).

Upward fault propagation was inhibited, where the polymer was thicker. Continued extension was accommodated by the formation of a salt-detached ramp-syncline basin lying above the polymer unit and above the sub-polymer ramp-syncline (**Fig. 3.5**). The lithostatic load produced by synkinematic sedimentation — combined with the master fault slip — triggered polymer flow from the areas with high vertical load (basin depocenter) to the edges of the salt-detached ramp-syncline basin, where the vertical load was lower. This gave rise to polymer-inflated areas bounding the salt-detached ramp syncline. The erosion of polymer-inflated areas favored the growth of reactive to passive salt walls, at the edges of the salt-detached ramp-syncline basin. The continuity of the source layer was interrupted after the formation of basin welds near the end of the extensional phase (**Fig. 3.5**).

3.3.2. Contractional deformation

Inversion produced the reactivation of the master fault and the polymer flow. A broad frontal harpoon structure was developed by contractional reactivation of the breakaway fault (**Fig. 3.6**). In the footwall of the harpoon structure, a small amplitude faulted detachment fold nucleated. The salt-detached ramp-syncline basin was welded against the sub-polymer structures during the extension phase and became rapidly uplifted, tightened, and narrowed during the inversion. At the end of extension, the weld surfaces at both syncline limbs were narrow and local (**Fig. 3.5**). In contrast, at the same point at the end of the inversion (**Fig. 3.6**), the joining area of the welds increases. The inherited salt wall, above the basinward rollover, at the end of extension was squeezed with the consequent development of secondary welds and the formation of a thrust at the salt wall pedestal (**Fig. 3.6a**). At this point, sub- and supra-polymer deformations became coupled. In contrast, the left side salt walls were squeezed, thereby forcing polymer extrusion, but not the development of secondary welds.

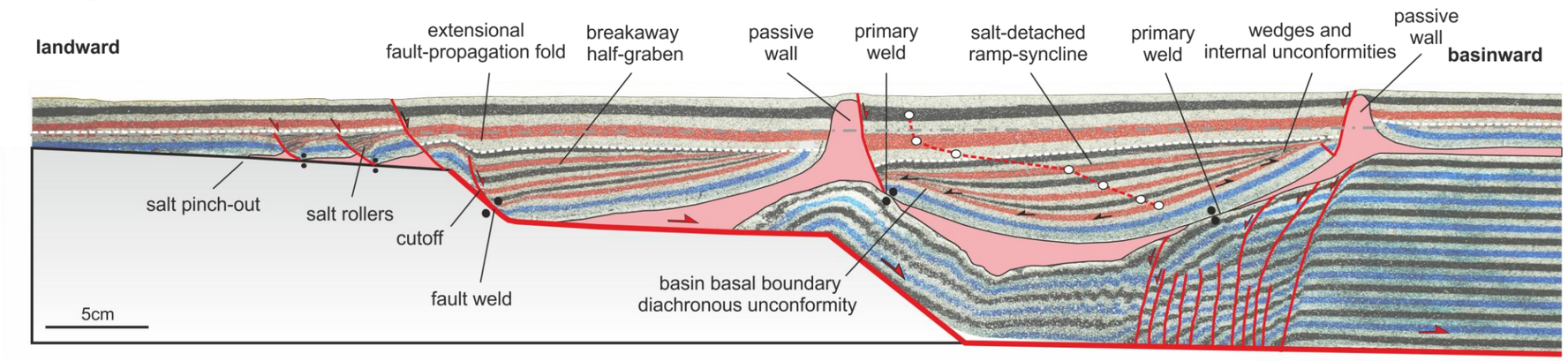

Fig.3.5. Interpreted cross-section of the structures observed in Exp._2.1 at the end of the second phase of extension (after 15 cm of lengthening) and with the terminology used in this chapter. a) central cross-section at the end of the extension and b) lateral cross-sections at the end of the extension.

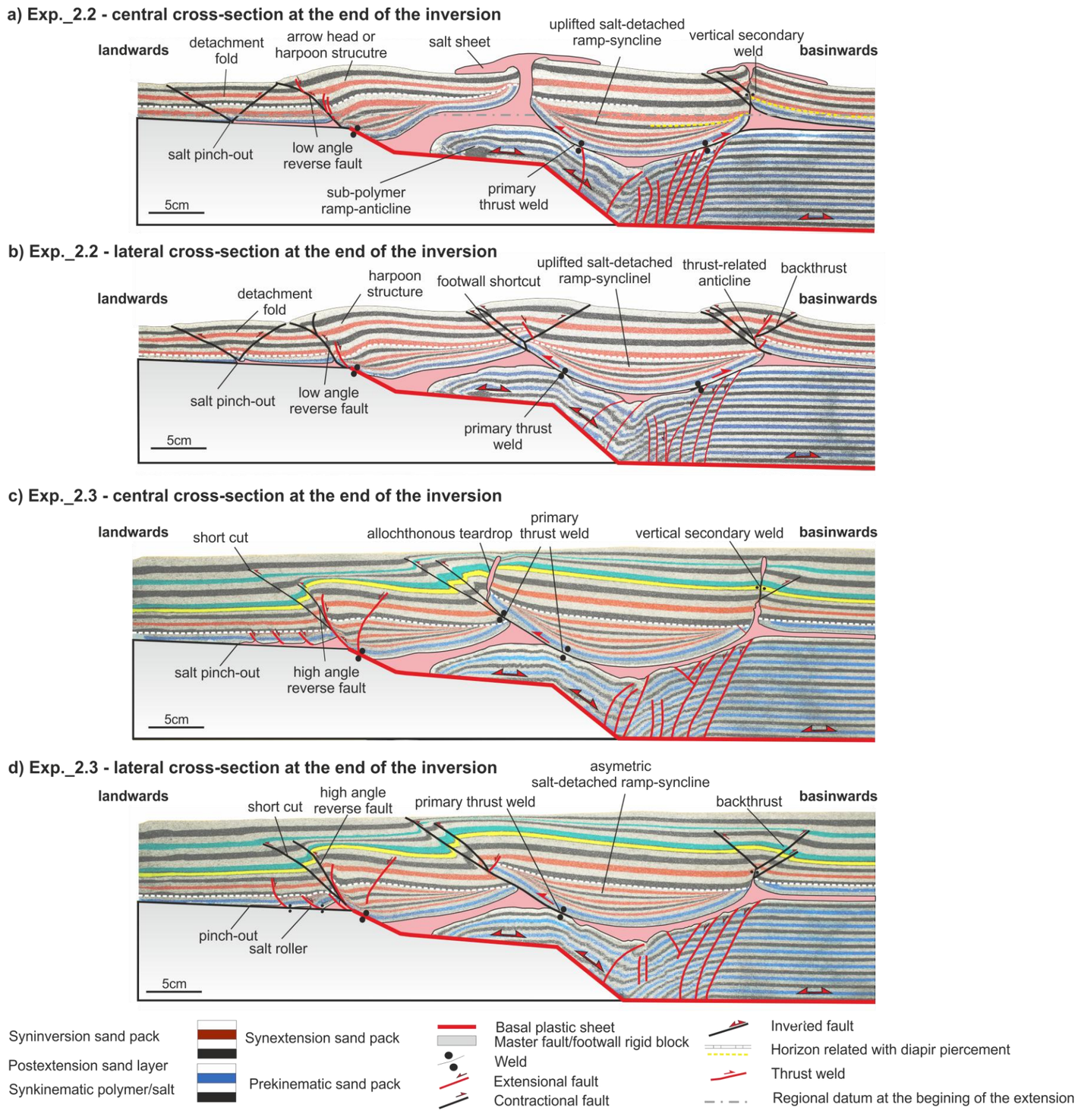

Fig.3.6. a) & **b)** Interpreted cross-section of the structures observed in Exp._2.2 at the end of the inversion (after two phases of extension followed by 8 cm of contraction) and with the terminology used in this paper. **c)** & **d)** Interpreted cross-sections of the Exp._2.3 showing the main structural elements and the different style of salt structures along-strike**. a)** & **c)** central cross-sections at the end of the inversion, **b)** & **d)** lateral cross-sections at the end of the inversion.

3.3.3. Salt mobilization analysis from kinematic restoration

The evolution in geometry and volume (the area in the section plane) of the salt is strictly related to the formation (or lack) of pierced salt walls in the model. **Figs. 3.7 and 3.8** illustrate the variation of salt area through extension and shortening for central and lateral cross-sections, respectively. The estimated initial polymer area on each section should be approximately 98.5 cm^2, assuming that the initial 2773 cm^3 volume of polymer was evenly distributed over the 30 cm wide, homogeneously folded, prekinematic units.

With the onset of the second phase of extension in central section (**Fig. 3.7i**), the main subsided part of the salt-detached ramp-syncline basin caused a progressive loss of salt (**Fig. 3.7ii**). Due to border effects, we can determine that the basin geometry is almost conical (i.e., non-cylindrical); therefore, the basin depocenter coincides with the central part of the model. As a consequence, the salt tends to migrate radially. In this central cross-section, the area of available salt reached its minimum at 12 cm of extension, losing approximately 28.3% (27 cm^2) of the salt in the form of out of section salt mobilization (**Fig. 3.7ii**); it coincided with the end of the reactive diapirism and also with the onset of passive diapirism. At 12 cm of the second extensional phase, the triangular shapes (reactive diapirsm) become open salt walls (passive diapirism), and they grow in width and height. At the end of this second extensional phase (15 cm), the area of available salt has increased by a total of 19.9% (13.6 cm^2 — including all material lost by the effects of extrusion and erosion, which corresponds to 455 cm^3 or 16% of the initial volume of salt volume lost through diapirs during the second extensional phase) (**Fig. 3.7iii**). This value indicates a large volume of salt that mobilized along-strike into the central section from the neighbouring areas (from **Fig. 3.8iii** to **Fig. 3.7iii**). Finally, after the inversion of the basin, the salt area went out of section, which resulted in a decrease of 8.7% (8 cm^2) (**Fig. 3.7iv**). This area of variation is surprisingly low. At this stage (**Fig. 3.7iv**), we would expect to quantify a great loss of salt because **i)** the surface of joining primary welds was increased, **ii)** the formation of secondary welds, and **iii)** the large amount of salt being extruded. However, the key to understanding the small variation in salt volume in central cross-section lies in the neighboring lateral cross-section (**Fig. 3.8**). At this particular stage, there is a large decrease in the salt area where no extrusion takes place (**Fig. 3.8iv**): from 98.9 cm^2 at the end of the second extensional event (**Fig. 3.8iii**), down to 50.8 cm^2 of salt available at the end of the compressional phase (**Fig. 3.8iv**). The difference totals up to 48.6% of the salt area lost (48.1 cm^2) during the inversion of the basin. This indicates that during the extension and inversion phases, a large volume of salt migrates across the model from outer areas (lateral cross-

section, **Fig. 3.6ii** and **Fig. 3.8**) toward the central parts (**Fig. 3.6i** and **Fig. 3.7**) of the model to feed the piercing salt walls. Beyond this, we can observe how the regions without diapirs, welds, and salt extrusion end up regions that have lost more salt volume.

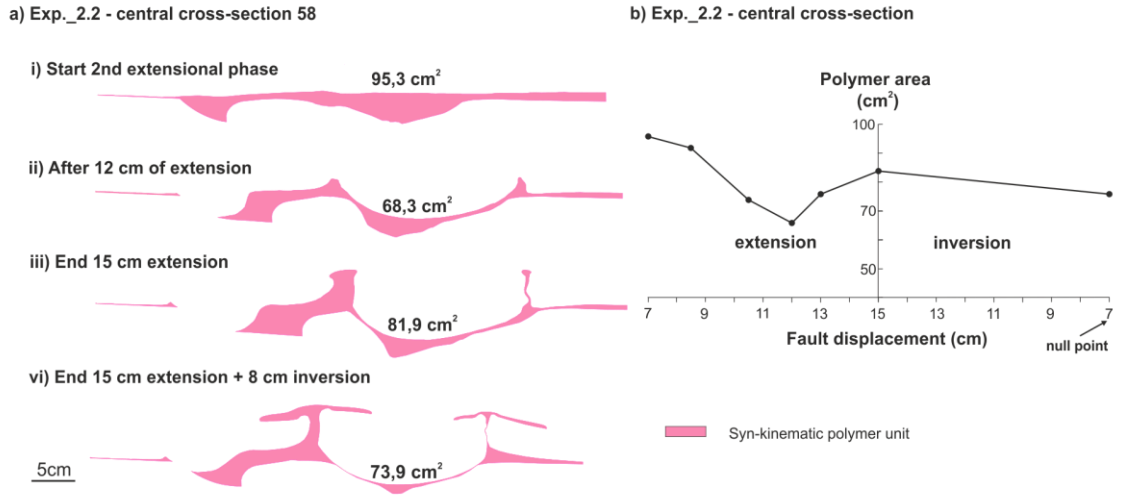

Fig.3.7. a) Restoration of polymer area for section 58 from Exp._2.2 and **b)** plot of polymer area versus fault displacement during extension (left side of the graph) and inversion (right side of the graph).

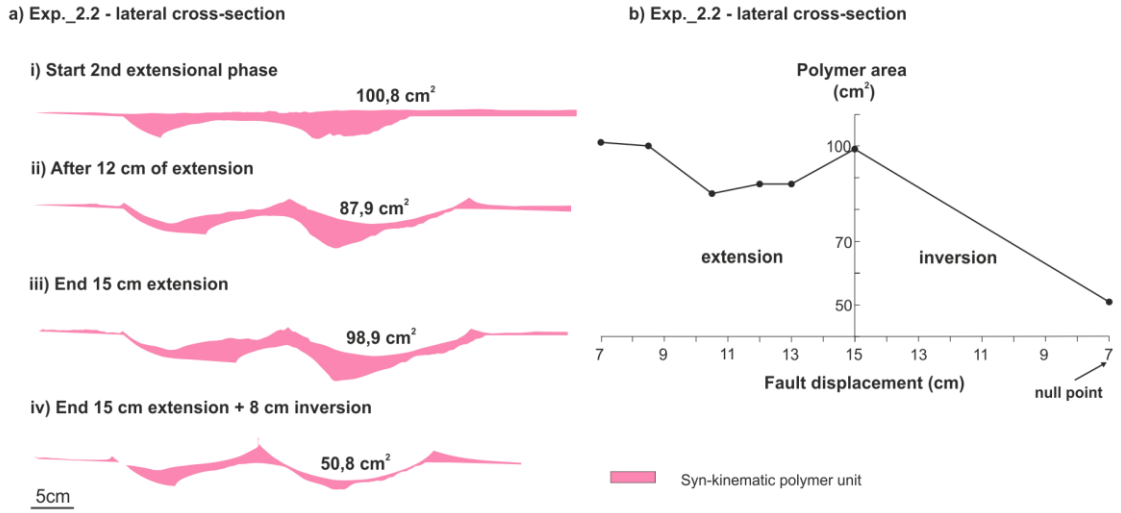

Fig.3.8. a) Restoration of polymer area through the extension and inversion phases for section 87 from Exp._2.2 and **b)** plot of the polymer area versus fault displacement during extension (left side of the graph) and inversion (right side of the graph).

3.3.3.1. *Restoration limitations*

The sub- and supra-polymer units in the analog models were restored independently using different restoration methods for each (**section 2.7.3.3**). As in many restorations, the algorithms used may be only an approximation of the deformation mechanism in the models

(e.g. McClay, 1995; Jagger and McClay, 2016) and do not account for different volume changes during extension (volume increase along fault zones) and inversion (volume decrease due to compaction as the result of higher stresses during contraction). Because of these limitations, the restored sections in **Figs. 3.9 and 3.10** show differences in restored line lengths between the sub- and supra-polymer units. 8.42% of the prekinematic unit was lost during the multi-stage deformation process. That the bed length, resulting from deformation of the model, should be 9.44% larger in order to match the extent of the supra-polymer unit. To explain the differential line length, geological processes that have been described in nature and are replicated by sandbox models include **i)** internal shear and readjustment of particles because of the ongoing deformation regime (LPC – Layer Parallel Compaction); and **ii)** out of section movement due to salt tectonics and transpression (Casas et al., 1996; Koyi, 2000; Koyi and Sans, 2006; Burberry, 2015). While quantifying internal shear, Koyi (2000) and Koyi and Sans (2006) observed that more than 15% of bulk shortening was accommodated by tectonic compaction in the sand overburden before the deformation reached the pinch-out of the ductile unit, and no visible structure was formed. In addition, field studies report up to 35% of shortening being accommodated by internal shear in the foreland of the South-Pyrenean basin before the generation of the first frontal structure (Casas et al., 1996). Consequently, we consider internal shear as the main factor to take into account when it comes to considering bed length and area conservation in the restoration of compressional structures.

Flexural slip and fault parallel flow restoration methods were applied to restore the supra- and sub-polymer deformation sand pack, respectively (**section 2.7.3.3**). Fault-parallel flow only preserves line length when offset occurs along planar faults. The resulting variation in the sub- and supra-polymer and polymer units between the end of inversion (**Figs. 3.9g and 3.10g**) and the final restored stage (at the beginning of the second phase of extension, **Fig. 3.9a and 3.10a**) is below 2% for the in-line length and below 5% for area for both sections. It has determined this by comparing the restored sections with the initial dimensions of the model. Similarly, variations in polymer areas between the restorations and the actual models before the second phase of extension were less than 5%. These small variations are reasonable for valid geometric section reconstructions of analog models (Lingrey and Vidal-Royo, 2015).

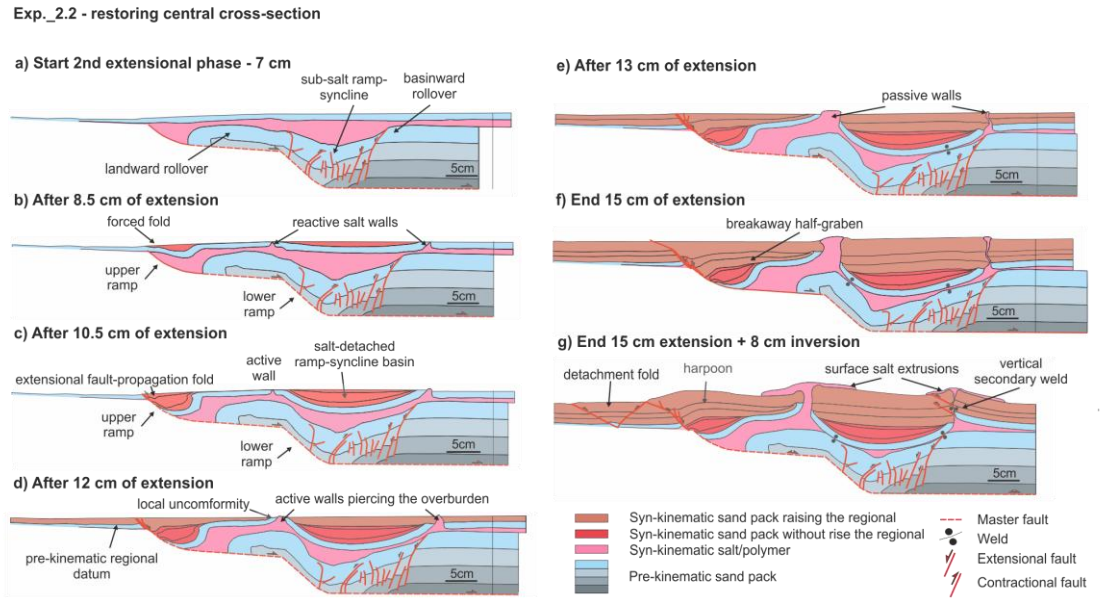

Fig.3.9. Sequential restoration of central cross-section from Exp._2.2 illustrating the structural evolution during the second phase of extension. **a)** During the first phase of extension subsalt structures developed during the first phase of extension; **b)** after 8.5 cm of extension, a suprasalt extensional forced fold above the upper ramp formed and two reactive salt walls developed at both basin edges; **c)** after 10.5 cm of extension, the suprasalt extensional forced fold evolved to an extensional fault-propagation fold and the reactive salt walls become active as diapirs progressed; **d)** after 12 cm of extension, the active salt walls pierced the overburden and consequently the prekinematic regional datum was raised; **e)** after 13 cm of extension, the active salt walls become passive; **f)** after 15 cm of extension, the salt-detached ramp-syncline has already welded against the subsalt structures; and **g)** at the end of 8 cm of inversion — net contraction with regard to the second phase of extension. The evolution of salt structures along time has been constrained with the model's top overhead photographs.

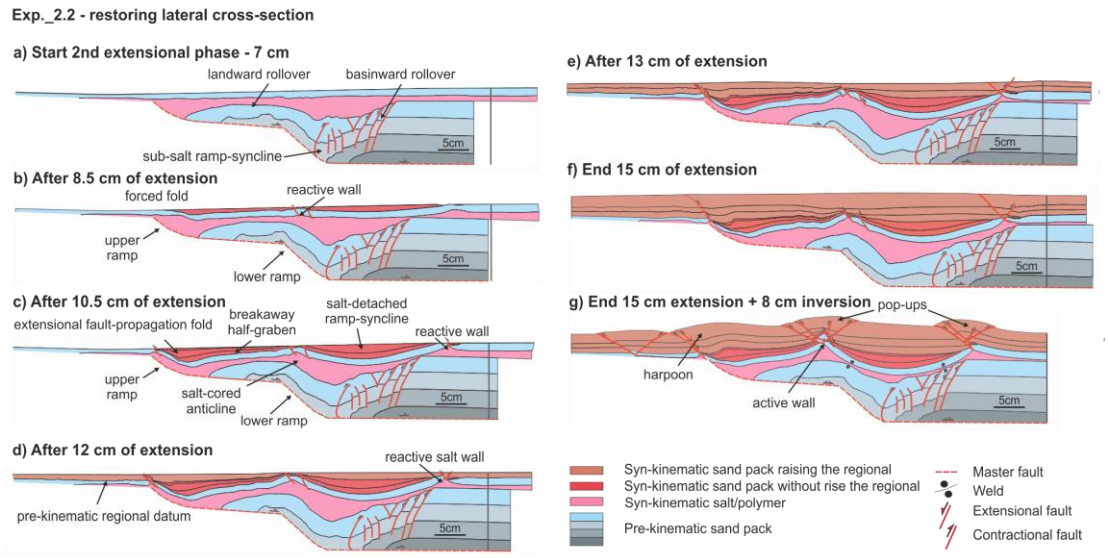

Fig.3.10. Sequential restoration of lateral cross-section from Exp._2.2 illustrating the structural evolution during the second phase of extension. **a)** Prior to the second phase of extension; **b)** after 8.5 cm of extension, a suprasalt forced fold and a reactive salt wall were developed; **c)** after 10.5 cm of extension, the suprasalt forced fold become an extensional fault-propagation fold; **d)** after 12 cm of extension, the prekinematic regional datum was raised; **e)** after 13 cm of extension; **f)** after 15 cm of extension; and **g)** at the end of 8 cm of inversion — net contraction regard to the second phase of extension. The evolution of salt structures along time has been constrained with the model's top overhead photographs.

3.4. WELD KINEMATICS OF SYNRIFT SALT DURING BASEMENT-INVOLVED EXTENSION AND SUBSEQUENT INVERSION: RESULTS FROM ANALOG MODELS.

In this section, we summarize the main results of the three experiments (Exp._2.1, 2.2 and 2.3 in **Table. 2.2b**) from the Experimental Program 2. Although, both end-member experiments have been reported in the previous **section 3.3** (Exp._2.1 and 2.2), in this following section, the results of the Exp._2.1, are focused on how the combination of the geometry of the master fault and the synrift polymer, affects polymer migration and the evolution of the salt structures. The Exp._2.2, in this case, depicts the inherited configuration (polymer and sub-polymer faults) as being contractionally reactivated and rejuvenated during inversion. In addition to the experiments discussed previously in **section 3.3,** a new experiment (Exp._2.3) is herein analyzed to discuss the role of the synkinematic sedimentation during inversion.

3.4.1. Extension above a ramp-flat-ramp basement fault with synrift polymer

Due to the space created by the extensional motion of the hangingwall during the first phase of extension (**Fig. 3.11a**), the polymer exhibits important variations in thickness (**Fig. 3.11b**), being thicker in the two depocenters, constant above the lower flat and pinching out against the upper flat panel (**Fig. 3.11b**). These thickness differences simulate different sub-basins with syn- or inter-rift salt units filling the topography generated during the rift in nature.

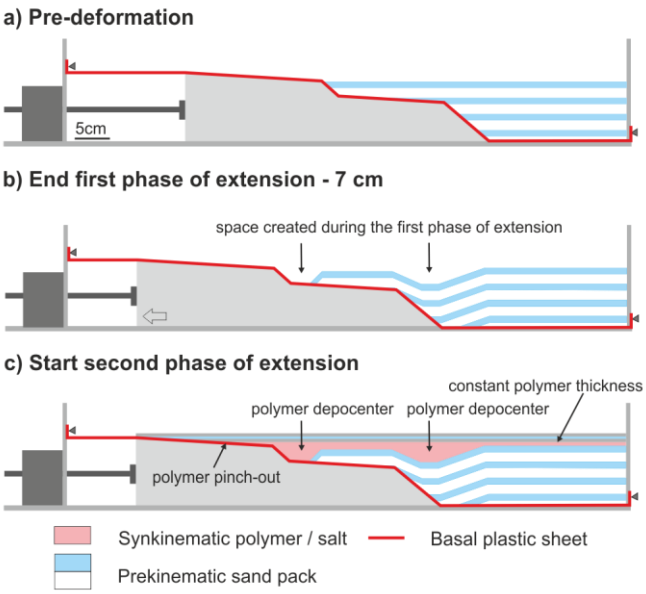

Fig.3.11. Conceptual sketches of the Experimental Program 2. **a)** pre-deformation configuration, **b)** structural pattern at the end of the first extensional phase and **c)** polymer filling the depocenters generated during the first phase of extension. Note how the polymer exhibits an initial configuration with important variation in thickness across the section.

With ongoing extension during the second phase, two different deformation styles characterized the evolution of the overburden above the upper and the lower master fault ramps. These two styles are clearly controlled by the polymer thickness differences:

i) The thin polymer layer above the breakaway fault favored strong coupling between basement and overburden extension. This led to the upwards propagation of the breakaway basement fault through the polymer into the overburden, which constrained the development of the breakaway half-graben (**Fig. 3.5**). As extension progressed, the growth of this half-graben forced the polymer evacuation towards the landward rollover hinge, thus arching the overburden above the pre-extension regional datum by inflation.

ii) Extension also produced the early downdip translation of the overburden over the gently dipping upper flat panel of the rigid block. Consequently, different basinward-dipping polymer-detached listric faults controlled the rise of asymmetric reactive diapirs and salt rollers close to the polymer pinch-out (**Fig. 3.5**).

iii) In contrast where the polymer was thicker, the overburden deformation was initially decoupled from sub-polymer extension. In this case, most of the suprasalt subsidence was related to the polymer migration, which triggered the development of two drape monoclines bounding a salt-detached ramp-syncline in the overburden.

Fig. 3.12a illustrates a structural map of Exp._2.1 at the top of the polymer unit that defines the main structural features of the sand layers above the polymer, whereas the map of **Fig. 3.12b** illustrates the subsalt structure. Note the structural differences between both horizons, which mean that the polymer layer acts as a markedly effective decoupling layer during extension (e.g. Koyi et al., 1993; Vendeville et al., 1995; Stewart and Clark, 1999; Withjack and Callaway, 2000).

During extension, the source layer was progressively stretched, thinned and finally depleted with the development of primary welds (Jackson and Cramez, 1989) (**Fig. 3.5**). Different weld types developed in our experiments associated with **i)** the salt rollers (primary welds), **ii)** below the breakaway half-graben at the hangingwall of the upper ramp (fault weld) and, **iii)** at both limbs of the salt-detached ramp-syncline (primary welds). The formation of these welds, especially at the upper ramp and below the salt-detached ramp-syncline favored coupling between overburden and basement deformation (**Fig. 3.5**).

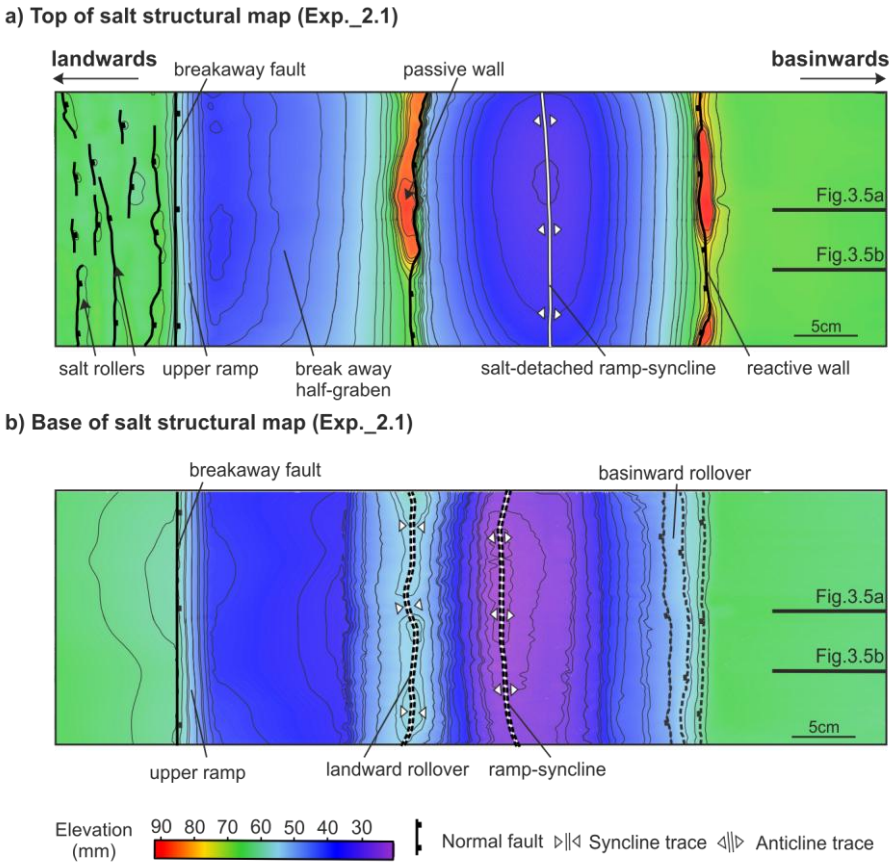

Fig.3.12. a) Structural map of the bottom of the overburden showing the supra-polymer structures and **b)** structural map of the top of the pre-polymer sand package showing the sub-polymer structures (contours in mm). Reddish color indicates a structural high and blue, structural lows. Structures marked with a continuous line correspond to the faults affecting the overburden whereas dashed structures are those affecting the basement (i.e., sub-polymer materials).

3.4.2. Inversion of a ramp-flat-ramp basement fault with synrift polymer

The inherited extensional architecture, the location of salt structures and the presence of primary salt welds dramatically controlled the evolution of the contractional structures during the inversion episode.

As soon as inversion began, the inherited weak salt walls reactivated their growth. The partial closure of the stems drives a significant increase of upwards polymer flow rates producing lateral extrusion and small overhangs on the model surface. During this initial stage, the pre-existing reactive salt walls were contractionally rejuvenated by squeezing, developing anticlines or thrust-related anticlines on top of them (**Fig. 3.6b**). The new topography forces the flow of the extruding polymer, thereby developing salt sheets.

With the ongoing inversion, polymer extrusion continued and parts of the coalesced salt sheets were amalgamated developing symmetric allosutures (Dooley et al., 2012). The different contractional strength along-strike in the salt walls results in curved thrusts (thrust salient at reactive salt walls) that form reentrants towards the squeezed passive walls (Dooley et al., 2009). The development of secondary welds is not coeval at both salt walls and it depends on the polymer available at the source layer, the presence of primary welds, their reactivation and the width of the pre-contractional polymer body. The surface that was primarily welded at the end of the extension at both syncline limbs is larger above the basinward rollover (**Fig. 3.5**). This clearly limited the volume of polymer available to be expulsed during shortening, and therefore, favors a faster secondary welding of the salt wall above the basinward rollover hinge (**Fig. 3.6a**). Secondary welding is also enhanced by the reactivation of primary welds as thrust welds that cause the uplift of the salt-detachment ramp-syncline (**Fig. 3.6b**). The salt-detached ramp-syncline was uplifted with a clockwise rotation pushed by the widening of the landward rollover as inversion progressed (**Fig. 3.6a-b**).

3.4.3. Inversion of a ramp-flat-ramp basement fault with synrift polymer and syninversion sedimentation

At mild inversion, the polymer extrusion rate significantly decreased. This fact is related to the squeezing of diapir stems and the development of secondary welds, isolating the feeder from the source layer (**Fig. 3.6c**). The intense uplifting of the salt-detached ramp-syncline, produces diapir stem closure and concentrates deformation at the two thrusts with opposite vergence, at both basin edges. Then, secondary welds evolve into thrust welds. The salt walls' pinch-off above the landward rollover creates an allochthonous teardrop that is decapitated by thrust welds (**Fig. 3.6c**). Shortcuts nucleated into the thrust weld and then propagated the contractional deformation into the overburden. At this point, the gradual thickness increase of the syninversion sand pack hinders the contractional propagation of the breakaway fault being finally buried as a blinded thrust (**Fig. 3.6c-d**). In contrast to Exp._2.2, the shortening propagation at the footwall of this thrust and the reactivation of the polymer pinch-out is totally inhibited by the thick synkinematic unit (**Fig. 3.6c-d**).

After intense shortening, the only active contractional structure is the thrust related to the salt wall above the landward rollover. The allochthonous teardrop located at the hangingwall of the thrust weld is displaced by up to 4 cm from its original position above its pedestal (**Fig. 3.6c**). In contrast, the syninversion sedimentation buried the salt wall at the

opposite basin edge (**Fig. 3.6c**). It was partially squeezed while developing vertical secondary welds and thrust-related anticlines (**Fig. 3.6c-d**). The welding kinematic differences between the two edges of the salt-detached ramp-syncline basin forced the clockwise rotation of the basin at the hangingwall of the thrust weld (**Fig. 3.6c-d**).

In addition to the structural architecture inherited from the extensional episode, the results of this Exp._2.3 shows how the synkinematic sedimentation plays a key role in strain localization and in the evolution of salt structures during inversion. Furthermore, it is also critical to the timing of contractional structures.

CHAPTER 4. OVERALL SUMMARY OF DISCUSSIONS

4.1. INTRODUCTION

This chapter integrates the outcomes obtained from the sandbox analog models carried out during this thesis. In particular, this chapter deals with a synthesis of the discussions and questions already published in the thesis-related articles. It aims to review the general structural features of salt-detached ramp-syncline basins and provide a guide to a better interpretation of the subsalt structure based on suprasalt geometries. The obtained results not only improve the understanding of the formation of salt-detached ramp-syncline basins, but also supply information that has permitted to deepen into the characterization of the inversion-related features developed during the contractional deformation of salt-detached ramp-syncline basins. The following topics are addressed: **i)** the interaction of the main parameters controlling the geometry and kinematics of salt-detached ramp-syncline basins; **ii)** their subsequent inversion; **iii)** the role of sedimentation and erosion during inversion and **iv)** the kinematics of welding. In addition, the integrated analysis presented in this chapter allows us to compare model results with natural analogs of salt-detached ramp-syncline basins developed under moderate to highly amount of extension and inversion.

4.2. INTERACTION OF THE MAIN PARAMETERS CONTROLLING THE GEOMETRY AND KINEMATICS OF SALT-DETACHED RAMP-SYNCLINE BASINS

4.2.1. Influence of the fault geometry and fault displacement

The formation of ramp-syncline basins without a salt layer requires the presence of a non-planar extensional fault (Gibbs, 1984; Ellis and McClay, 1988; McClay, 1990; McClay and Scott, 1991; Withjack et al., 2002; Soto et al., 2007), more specifically, a fault which includes an upper convex-up fault bend and a lower concave-up bend (i.e., an extensional fault with three differently dipping panels). These authors conclude that the geometry of the ramp-syncline basin depends on the amount of extension, and the shape and dip of the involved-panels of the main extensional fault. For larger fault displacements, there is an increase in the length of the syncline limbs, and therefore in the width and amplitude of the ramp-synclines. The dip of the fault panels constrains the syncline back- and forelimbs' dips (Xiao and Suppe, 1992; Withjack et al., 2002). Models by Ferrer et al. (2016) show that wide, gentle and shallow ramp-synclines developed above a gently dipping intermediate panel (as occurs in our Exp._1.1; **Fig. 3.3a**). In contrast, narrow and deep ramp-synclines developed as a function of steeper intermediate panels (as occurs in our Exp._2.1; **Fig. 3.5**).

Through the conceptual sketches in **Fig. 4.1a – c** we can notice how the dip of the lower panel strongly constrains the geometry of the ramp-synclines. For the same amount of displacement, the length and dip of the syncline forelimb would be greatest for a gently dipping lower panel (symmetric syncline in **Fig. 4.1a**) and progressively shorter and lower as the dip of this panel increases (asymmetric syncline in **Fig. 4.1b - c**). If we turn our focus to the different accommodation spaces created, which are related to the fault geometry, we can notice how the dip of the upper and lower panels control the hangingwall sediment accomodation space. This would be greatest for a highly dipping upper and lower panel (**Fig. 4.1b)**, while would be zero for horizontal upper and lower panels. This is directly related with the ramp-syncline basin boundaries (Withjack and Schlische, 2006; Pichel et al., 2018).

4.2.2. Interaction between salt migration and subsalt fault shape

The dip of the upper and lower fault panels control the accommodation space, and in its turn influences salt migration, as this process is mainly triggered by pressure head differences related to changes in overburden thicknesses (**Fig. 4.1d - f)** (Khele, 1988; Vendeville and Jackson, 1992; Jackson and Vendeville, 1994; Hudec and Jackson, 2007). Thus, in these scenarios the salt migrates from the syncline hinge (thick synkinematic unit and high pressure head; **Fig. 4.1d - f**) to the syncline edges (null or thin synkinematic unit and low pressure; **Fig. 4.1d - f**). So, the preferential salt migration towards the syncline edges is constrained by the thickness difference between the synkinematic unit at both syncline edges, which is in turn controlled by the fault displacement and the dip of the fault panels. For a given fault displacement the preferential salt migration will be controlled by the dip of the fault panels (**Fig. 4.1d - f**).

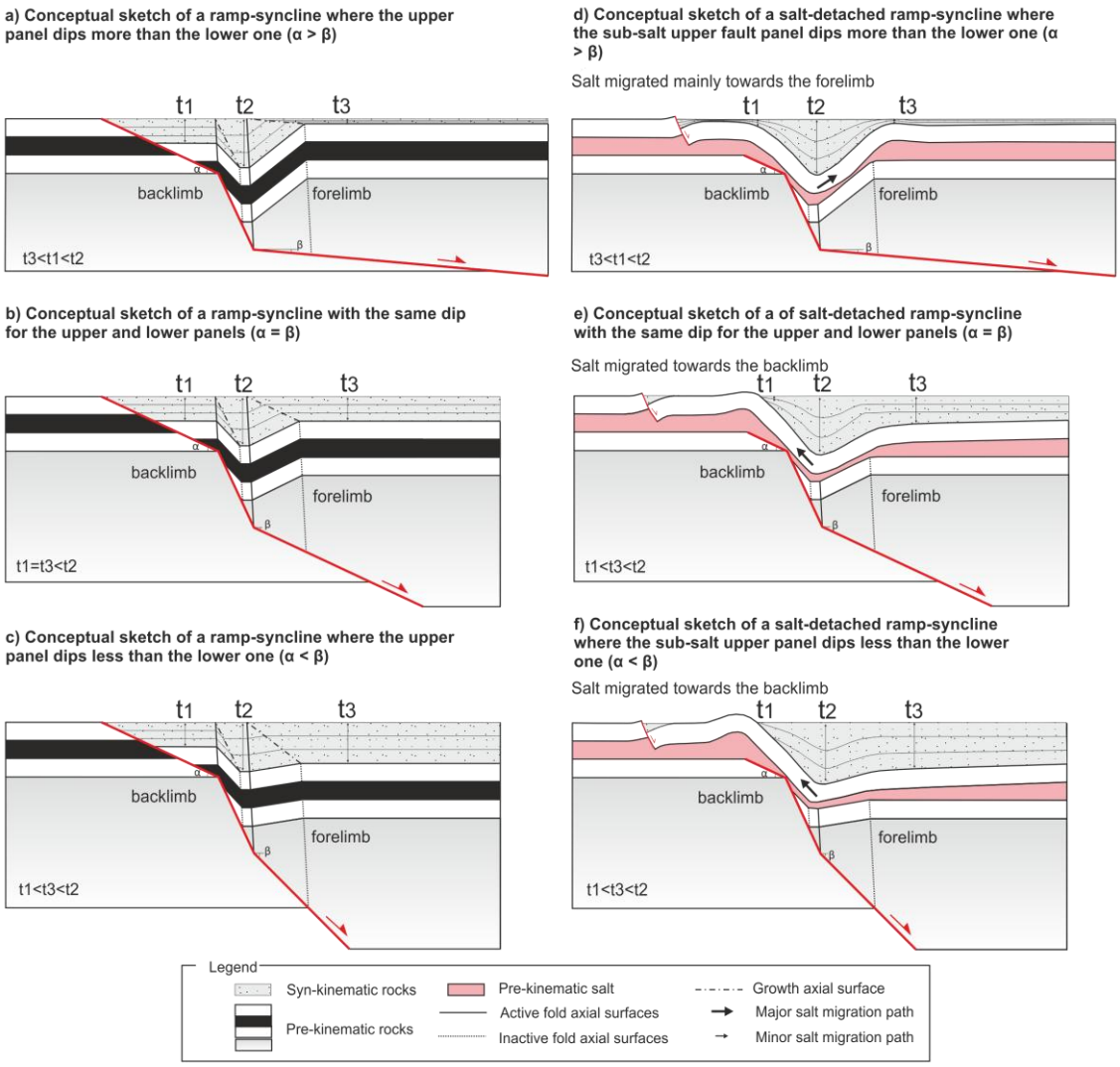

Fig.4.1. Simplified conceptual sketches showing the relationships between different kinked fault geometries, the overburden thicknesses and the salt migration. Note that the intermediate fault panel has the same length, position and dip in all figures.

For gently dipping lower fault panel (**Fig. 4.1d**), the salt will preferentially migrates basinward, where the synkinematic unit is thinner. In contrast, for steeply dipping lower fault panel (**Fig. 4.1e and f**), the accommodation space filled by the synkinematic materials is higher above the lower panel, thus forcing salt migration landward.

According to this conceptual sketch, models of Experimental Program 1 (**Table. 2.4**) the synkinematic sedimentation is null above the lower fault panel but not at the edge above the upper panel, where accommodation space increase as extension progress (above the landward rollover, **Fig. 3.3**). This implies that the polymer preferentially migrates basinward, and where consequently salt inflation and the diapiric structures will easily rise and pierce the cover. In contrast, models of Experimental Program 2 (**Table. 2.4**) both upper and lower panels

are almost horizontal, which means that no accommodation space at the basin edges occurs, so no preferential salt migration due to this.

4.2.3. Influence of initial salt thickness and its distribution

The timing of the salt deposition, pre-, syn-, or postkinematic, during the evolution of the salt-bearing rift basins is one of the main factors controlling the thickness of the salt. Consequently, their structural style (Jackson and Vendeville, 1994; Rowan, 2014), the degree of decoupling between sub- and suprasalt units and salt migration due to sediment loading, mainly depends on salt thickness (e.g., Koyi and Petersen, 1993; Koyi et al., 1993; Vendeville et al., 1995; Richardson et al., 2005) (**Fig. 4.2a**). Although, the most important thickness differences occur if salt is deposited during rifting, the presence of previous topographic irregularities can also determine salt thickness differences (Dooley et al., 2017).

Different deformation styles domains are developed in the same salt-bearing system clearly controlled by salt thickness differences: **i)** thin-skinned; **ii)** thick-skinned and **iii)** mixed modes (**Fig. 4.2b**).

.

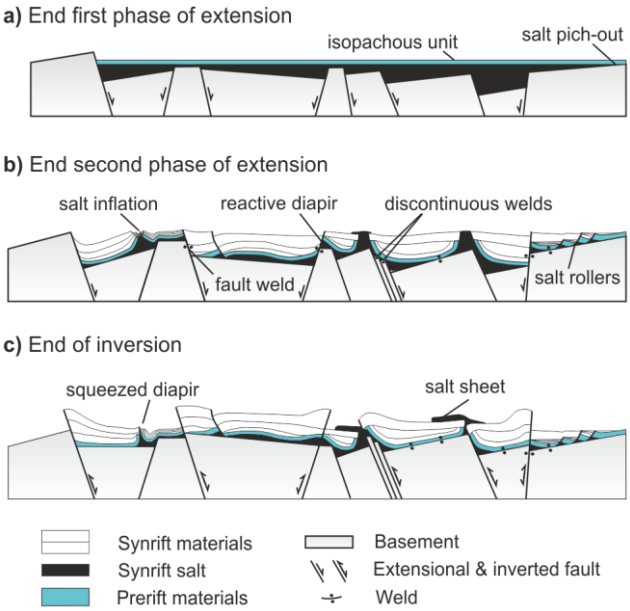

Fig.4.2. Simplified conceptual model on the deformation style of synrift salt basins. **a)** during the first extensional phase synrift salt accumulates in grabens and half-grabens so salt thickness varies; **b)** salt rollers, reactive diapirs, passive diapirs and fault welds form in the synkinematic overburden and **c)** inversion of inherited structures (modified from Jackson and Hudec, 2017).

A thin salt layer enhances a thick-skinned deformation style and consequently, the upward propagation of subsalt basement-involved faults into the suprasalt succession. Drape

folds at the tip of the subsalt fault evolve to extensional fault-propagation folds as subsalt fault displacement increases (**Figs. 3.5 and 4.2b**). The upward propagation of basement-involved subsalt faults may determine the formation of premature salt welds and consequently coupling deformation between sub- and suprasalt units (**Fig. 3.5**), thus controlling the subsequent evolution of the suprasalt basins. Nucleation of curved normal faults attached at the fault ramp, usually occurs after the formation of a fault weld. In addition, thin salt can also enhances thin-skinned deformation. Salt above a slightly tilting panel promotes gravitational gliding (i.e., salt flowing basinward) and consequently overburden translation above salt, that resulting in salt rollers structures detached on thin salt (**Figs. 3.5 and 4.2b**).

Thicker salt unit above an extensional subsalt basement-involved fault favors partially decoupling deformation. In that case, the overburden structure is an indirect reflection of the underlying basement structural patterns (Jackson and Hudec, 2017). In such scenarios mixed thin- and thick-skinned modes of styles are fairly common. In such, both subsalt basement-involved extensional fault (i.e., thick-skinned) and salt unit (i.e., thin-skinned) controls suprasalt basin development (**Figs. 3.5 and 4.2b**). Usually, resulting in the development of salt-detached ramp-syncline basin.

4.2.4. Degree of decoupling between subsalt and suprasalt units

Salt and overburden thickness differences, cohesive strength/ductility of the overburden, displacement amount and displacement rate or salt viscosity have a strong impact on the degree of coupling over time (Coward and Stewart, 1995; Stewart and Clark, 1999; Withjack and Callaway, 2000). The important strength contrasts between salt and other sedimentary rocks favor a partial to fully decoupled deformation between basement and salt overburden during rifting, where salt acts as a highly efficient décollement (e.g. Koyi et al., 1993; Jackson and Vendeville, 1994; Pascoe et al., 1999; Withjack and Callaway, 2000; Dooley et al., 2005; among others). Although partially decoupling is the most common scenario in nature, decoupling along a salt horizon makes difficult deciphering the geometry of the subsalt basement-involved fault system based on the structure of the suprasalt succession.

Our research supports previous modeling works in that the geometry and kinematics of salt-detached ramp-syncline basins are strongly controlled by the subsalt master fault geometry. Nevertheless, our analog models show evidences of decoupling during extension (i.e., basin translation above the salt layer). This means that the salt unit has favored a thin-

skinned deformation above subsalt basement-involved faults, resulting into mixed thin- and thick-skinned deformation styles described in previous section. Therefore, if the amount of extension and the degree of decoupling is significant, the basin can be transported away over the salt unit, from the subsalt fault ramp to above a subsalt fault flat (Carola, et al., 2015, Pichel et al., 2018).

Modeling results show some key geometric elements that allow deciphering the amount of decoupling, such as comparing between **i)** the subsalt fault displacement and **i)** the overbuden translation. The subsalt fault displacement is recorded between the distance of the subsalt active and inactive axial surface. While overburden translation may be estimated by measuring the distance between **i)** the top of the lower ramp and **ii)** the oldest onlap point (c.f. Jackson and Hudec, 2005, Pichel et al., 2018) (**Figs. 4.3a and b**).

Fig. 4.3a2 shows that the amount of suprasalt basin translation is less than the subsalt fault displacement. In contrast, **Fig. 4.3b3** shows that the amount of suprasalt basin translation is more than the subsalt fault displacement. In the first case, such difference is due to the suprasalt basin is translated landward using the salt weld as a detachment (see details in next **section 4.5.**) (Stewart and Clark, 1999). While, in the second case the degree of decoupling is fairly enough to add a thin-skinned component in the global thick-skinned deformation style.

a) salt-detached ramp-syncline basin developed above a low-angle ramp-flat extensional fault and detached on thin-salt

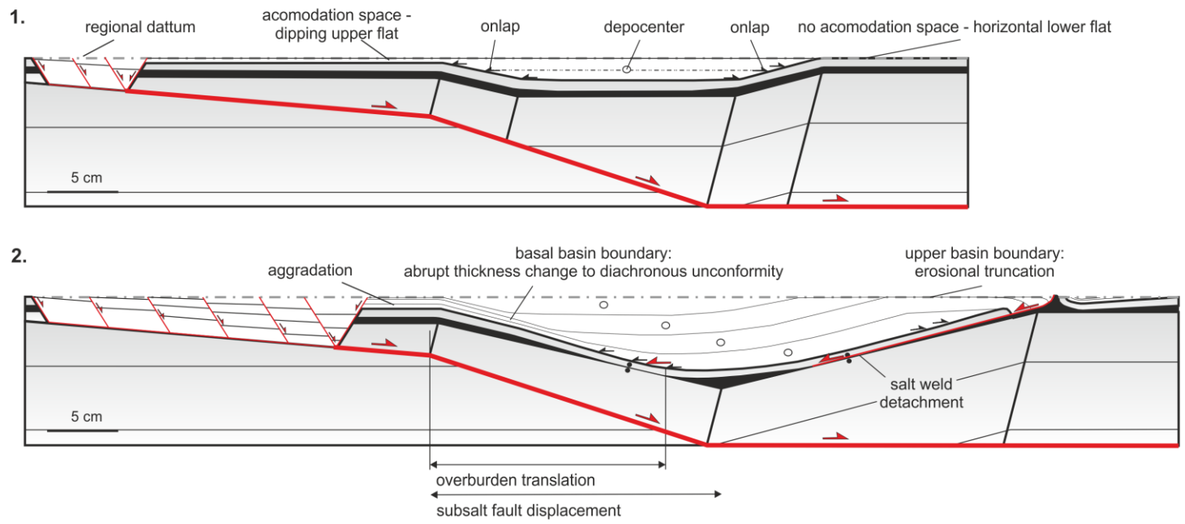

b) salt-detached ramp-syncline developed above a ramp-flat extensional fault and detached on thick-salt

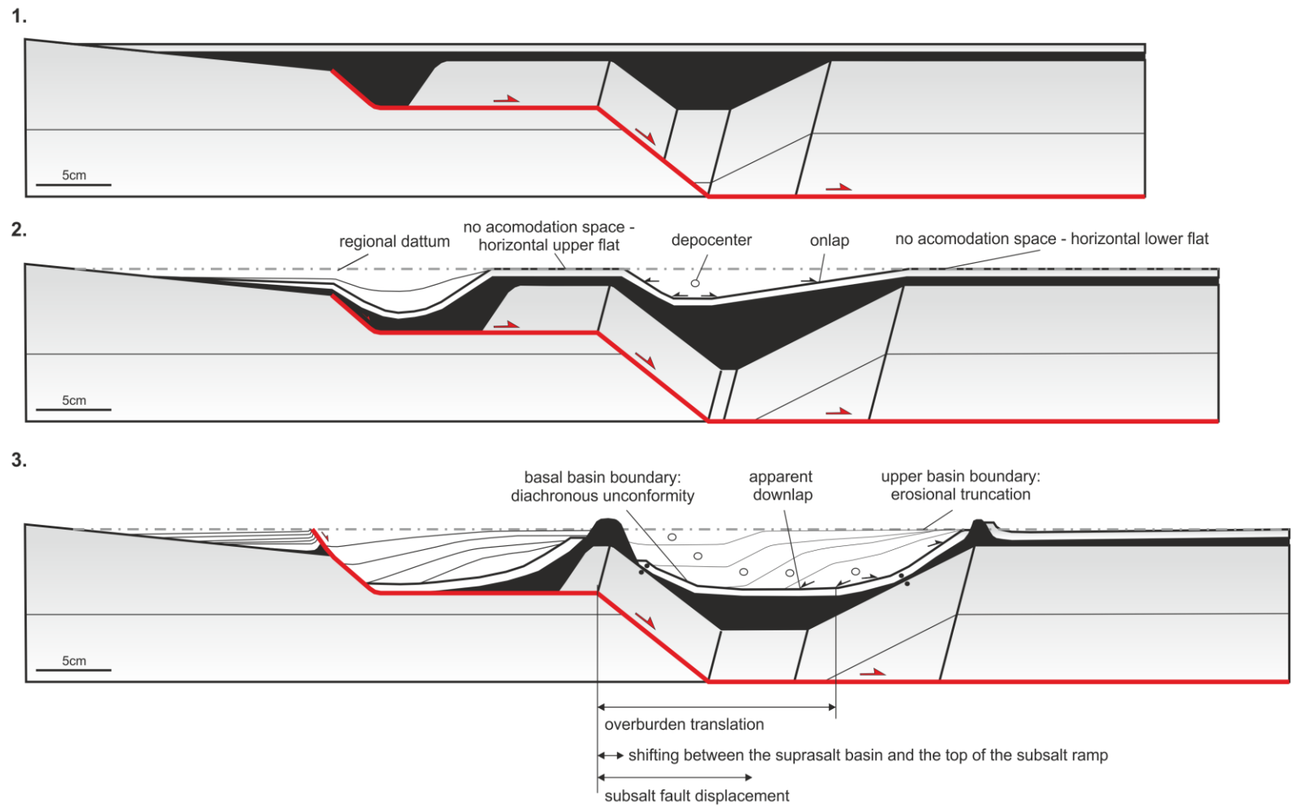

Fig.4.3. Conceptual sketch on the effect of basin translation during extension. **a)** Based on Exp._1.3 from the Experimental Program 1 and **b)** based on Exp._2.1 from the Experimental Program 2. **Figs. 4.3a2 and b3** compare the amounts of fault displacement and suprasalt basin translation for both experimental programs respectively.

4.2.5. Interpretation of the subsalt basement-involved fault

While in ramp-syncline basins the rate of subsidence is directly proportional to the rate of lateral translation, and the translation is proportional to the fault displacement, in salt bearing basins, salt migration increase the rate of subsidence and decoupling adds suprasalt lateral translation. Thus, in salt-bearing basins the subsalt fault displacement is not at all directly proportional to stratigraphic sequence thickness neither basin lateral translation. In such complex scenarios the key observations rest on deciphering the contribution of each factor.

Overall, our investigation shows the interaction between four factors during extension: **i)** the subsalt fault geometry and fault displacement, **ii)** the initial thickness of the salt unit and its distribution, **iii)** the salt migration due to sediment loading, and **iv)** the degree of decoupling between sub- and suprasalt units (Ellis and McClay, 1988; Koyi et al., 1993; Withjack and Callaway, 2000). The interaction between these factors is recorded in the synkinematic basin infill. Therefore, based on the suprasalt basin architecture, (i.e., the stacking pattern of the synrift depocenters and the angular relations of the synrift sediments) we should be able to interpret the subsalt fault geometry, the amount of decoupling and infer for the subsalt fault displacement.

In regions where the subsalt structure is not well imaged, the identification of salt-detached ramp-syncline basin may indicate the presence, location and geometry of subsalt basement-involved fault. Therefore, I propose the main following suprasalt observations:

i) The development of salt-detached ramp-syncline basins during fault displacement is recorded in the synkinematic architecture as a dipping growth axial surface, formed by the lateral shifting of the depocenters. This growth axial surface is mainly the result of the basin displacement above a concave-up fault bend. Depending on the subsalt fault type the growth axial surface would generally dip opposite to subsalt fault (usually landward) when the subsalt fault is listric or planar-rotational or in contrast, it would dip parallel (usually basinward) when the involved-basement subsalt is a ramp-flat fault (**Fig. 4.4**).

ii) Whereas onlaps are most easily discerned for the uppermost basin infill (**Fig. 4.4**), apparent downlaps are typical of the lowermost part of the basin. These apparent downlaps were originally onlaps against the prekinematic sequence above subsalt ramps that were

translated during extension and consequently rotated acquiring an apparent geometry (**Fig. 4.4**).

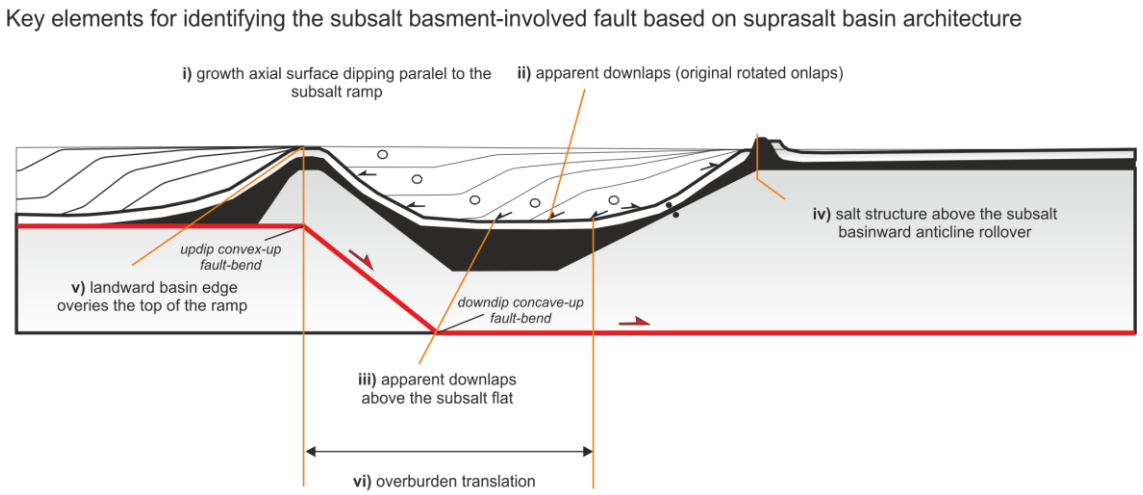

Fig.4.4. Conceptual sketch showing the relationship between the subsalt basement-involved fault and the suprasalt salt-detached ramp-syncline basin. Note that this sketch is based on Exp._2.1 from the Experimental Program 2.

iii) The progressive rotation of original onlap developing apparent downlaps occurred during suprasalt basin translation from a ramp to a horizontal flat (**Fig. 4.4**). So in terms of seismic interpretation the presence of these apparent downlap terminations above a subsalt flat implies a subsalt ramp-flat fault (i.e., a downdip concave-up fault bend).

iv) The position of the salt inflation and/or salt structures in relation with the dip of the synrift pseudo-clinoforms is a key observation to recognize the subsalt extensional basinward and landward anticline rollovers (**Fig. 4.4**).

v) The landward edge of salt-detached ramp syncline basin, usually occurs immediately above the top of the subsalt ramp (updip convex-up fault bend) (**Fig. 4.4**).

vi) The overburden translation may be estimated by measuring the distance between the landward edge of salt-detached ramp-syncline basin and the oldest onlap or apparent dowlap terminations (**Fig. 4.4**). However, our models show that the landward basin edge does not directly overlie the top of the subsalt fault ramp. It is displaced basinward due to the development of a salt structure (**Fig. 4.3b3**). The offset between the top of the subsalt ramp and the landward suprasalt basin edge has a direct implication on the overburden translation (**Fig. 4.3b3**).

vii) The subsalt fault displacement could be similar to the subsidence and basin translation rates. Neverthesess, the additional basin subsidence and overburden translation due to salt migration and decoupling respectively may difficult to predict the subsalt fault displacement (**Fig. 4.3b3**).

4.3. INVERSION OF SALT-DETACHED RAMP-SYNCLINE BASINS

Both experimental programs reveal that the tectonic inversion of salt-detached ramp-syncline basins is mainly characterized by: **i)** the formation of a major fault-bend anticline controlled by thick-skinned deformation, and **ii)** the development of thin-skinned contractional structures (**Figs. 3.4 and 3.6**).

The kinematics and the surface shape of the anticline developed in our experiments during inversion follow the geometric patterns already postulated for fault-bend folds formed above kinked fault thrusts (Suppe, 1983; Medwedeff and Suppe, 1997 or Tavani et al., 2005). Most of the literature of analog models with rigid footwalls subjected to inversion does not contemplate the presence of viscous detachments. Only the works of Durcanin (2009) (synextension polymer on the hangingwall of a listric fault) or Ferrer et al. (2016) (preextension polymer covering the entire models with different faults geometries) analyzed the role of salt during inversion using rigid footwalls. These authors pointed that subsalt and suprasalt contractional deformation could be partially coupled or completely decoupled depending on the inherited salt configuration and the presence of primary welds at the beginning of the inversion. They also denote that preexisting salt structures (diapirs and walls) preferentially absorb contractional deformation during early inversion. This PhD supports these statements, but also illustrates the results of salt-bearing basins involving higher amount of inversion, the salt kinematics during inversion, and how salt influences the resulting structural style.

4.3.1. Thick-skinned contractional structures

The thick-skinned deformation related to the inversion of the flat-ramp-flat master fault resulted in the early uplift of the ramp-synclinal basin and in the subsequent development of a fault-bend anticline. The geometry of this anticline is constrained by the dip of the fault panels, the contractional displacement of the master fault, as well as the length of the intermediate fault panel. However, their architecture differs from the classic geometric

models (i.e., compressional fault-bend folds) because it has an inherited structure in which the hangingwall is not constituted by horizontal layers (**Figs. 3.3 and 3.5**).

This resulting fault-bend anticline is similar to those obtained in the experiments by Durcanin (2009) and Ferrer et al. (2016). They noted that the hangingwall uplift above a kinked planar fault during inversion will be highest as a function of the steepness of the fault panels. Thus, when the most uplifted part occurs above the intermediate panel (i.e., fault ramp) (**Figs. 3.4a, b, and d and Fig. 3.6**), there is an offset between the anticline hinge and the previous ramp-syncline hinge (**Fig. 3.4a**). The position of this transported syncline hinge with respect to the most uplifted part of the hangingwall depends on the fault displacement as well as on the length of the intermediate fault panel. If the displacement is equal to the length of the intermediate panel, the syncline hinge would coincide vertically with the position of the most uplifted part of the hangingwall. Instead, if it is lesser (like our Experimental Program 1 **Figs. 3.4a, b, and d**) or greater (like our Experimental Program 2 **Fig. 3.6**), it would be shifted backwards or frontwards, respectively. This structural style is clearly different to the inversion of half-grabens (**Fig. 3.6**) where the maximum uplift is constrained by the master fault breakaway in a totally coupled deformation developing a classical harpoon structure (Badley et al., 1989). In this case, the maximum uplift coincides with the position of the extensional depocenters (Buchanan and McClay, 1991).

Despite the growth of the fault-bend anticline is mainly controlled by the shape of the master fault, the presence of salt slightly modifies the final inverted structure. Thus, the anticline can reach higher uplift when the system does not include a salt layer (**Fig. 3.4a**). This is because the salt acts as a contractional detachment and migrates during the early inversion stages, hindering the synclinal uplift. As inversion progresses, salt migration produces a local depletion of the source layer enlarging the pre-existing welds or favoring the formation of new ones (compare **Figs. 3.4d - 3.6 with Figs. 3.3b - c and 3.5**). The presence of primary welds at the beginning of the inversion disrupts the continuity of the source layer and prevents salt withdrawal from the salt-detached ramp-syncline depocenter toward the preexisting salt walls (**Fig. 3.5a**). At this point, the system becomes wholly coupled and the up-slip contractional displacement of the subsalt unit along the intermediate ramp of the master fault is transferred into the suprasalt unit favoring uplift, tilting, and clockwise rotation of the salt-detached ramp-syncline basin (**Fig. 3.6a**).

4.3.2. Thin-skinned contractional structures

Regarding the contractional fault-bend anticline formation, thin-skinned structures also develop during the inversion phase. This deformation style is controlled by the inherited synclinal-shape that changes during shortening.

These synclinal-shape changes consist of a progressive length-reduction of the syncline backlimb, and a dip decrease of the syncline forelimb beds. That occurs when the extensional basinward rollover is passively transported and draped from the lower to the intermediate fault panels (**Fig. 3.4a**). Both changes produce a decrease in the syncline interlimb angle (i.e., a reduction of the syncline amplitude) and therefore, shortening of the involved beds and salt evacuation out of section (compare **Figs. 3.9f and 3.9g**). Such amplitude change is especially relevant since it entails length shortening of the synrift layers. In the absence of salt (**Fig. 3.4a**) this process could results in the development of a thin-skinned backthrust above the extensional rollover hinge (Mitra, 2002). Whereas the synclinal-shape changes in salt-detached ramp-syncline basins are characterized by a reduction of the subsalt syncline amplitude, this is not what occurs in the suprasalt syncline. Note that, at the end of the inversion the supra-polymer sand pack is nearly flat with a relatively constant dipping attitude (**Fig. 3.4d**). This gives rise to a reduction of the limb length of the supra-polymer layers. This reduction entails shortening that is added to the global thick-skinned contraction. Consequently, the salt-detached ramp-syncline basins showed more shortening in the suprasalt strata than in ramp-syncline basins without salt.

This additional thin-skinned shortening mainly consists in the reactivation of the salt unit as an effective contractional detachment. Consequently, primary welds are contractionally reactivated as thrust welds (see details in the following **section 4.3.4.**), producing the squeezing of the inherited salt walls. The thin-skinned shortening is mainly localized at the basinward rollover hinge rather than at the syncline backlimb, whereas the inherited diapirs and walls are less squeezed (**Figs. 3.4 and 3.6a - b**).

4.4. ROLE OF SEDIMENTATION AND EROSION DURING INVERSION

In addition to the structural architecture inherited from the extensional episode, the synkinematic sedimentation during inversion plays a key role in strain localization and in the

evolution of salt structures. Furthermore, it also controls the timing of contractional structures (compare **Figs. 3.6a - c and 3.6b - d**).

As documented for fold-and thrust belts, syninversion sedimentation controls the dip and the shape of the reverse fault that propagates into the cover (Baby et al., 1995; Storti and McClay, 1995; Barrier et al., 2013). Usually, a low angle curved reverse fault flattening upwards (**Figs. 3.6a - b**) is developed during the inversion of the half-graben involved-fault. However, this resulting fault is planar and has a high angle when synkinematic sedimentation is involved during the half-graben inversion (**Figs. 3.6c - d**). Another important point is how synkinematic sedimentation favors the back-rotation of the salt-detached ramp-syncline basin during uplift (**Figs. 3.6c - d**) (McClay, 1989, 1995; Buchanan and McClay, 1991; Bonini et al., 2012; Ferrer et al., 2016).

Moreover, it is also well documented for fold-and-thrust belts, that a salt unit can act as a decoupling layer and transfer the contractional deformation (Allen and Beaumont, 2012; Bonini, 2003; Gradmann et al., 2009; Luján et al., 2003; Pla et al., 2019). As those authors pointed, our experiments also show that the salt is extremely efficient when the contractional system has not syninversion sedimentation. In such cases, the foreland salt pinch-out is active since almost the beginning of shortening (**Fig. 4.5a**). In contrast, the foreland salt pinch-out is not effective at all in systems with high syninversion sedimentation rate. In this case, the contractional deformation is usually absorbed in the hinterland. In our models, it is absorbed by the footwall short-cut of the upper ramp, so deformation did not propagate towards the foreland (**Fig. 4.5b**). Similar examples have been described in fault-and-thrust belts where, despite the existence of an effective décollement, synkinematic sedimentation can inhibit the outwards propagation of the deformation front into the foreland (Bonini, 2001; Bonini et al., 2012; Pla et al., 2019).

Our experimental results also demonstrate how the thickening of the syninversion unit directly controls where and how deformation localizes, and therefore, the timing of the contractional kinematics. With increasing sedimentation and burying the frontal contractional structure, the deformation switched backwards towards the hinterland, and is preferentially absorbed by salt structures. In our Exp._2.3 this was favored by the salt layer that acts as a shear zone and transfers the deformation towards the central salt wall developing a fish-tail structure (**Fig. 3.6c - d and Table. 2.2b**, Experimental Program 2) (Letouzey et al., 1995) (**Fig. 4.5**). Similar structures have been interpreted in contractional scenarios with different

detachment layers (Pichot and Nalpas, 2009). In this case, the salt wall related to the landward edge of the salt-detached ramp-syncline absorbed the main contractional deformation and it was squeezed shut. Note that only the basinward basin-edge related-salt-structures were squeezed shut.

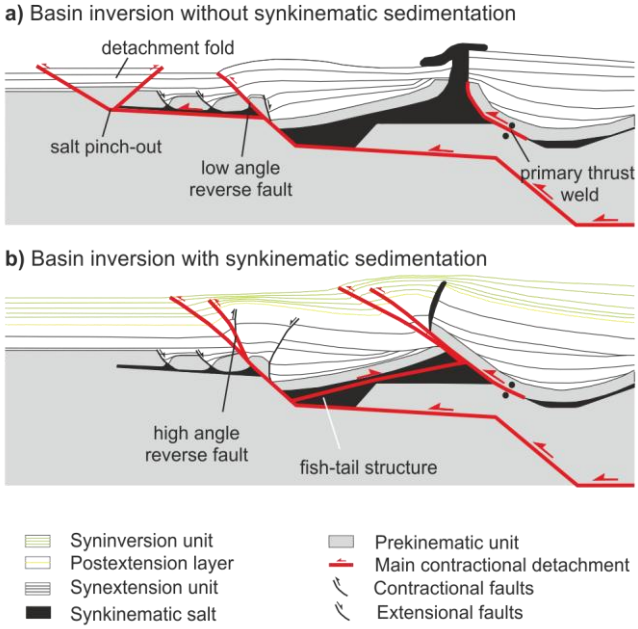

Fig.4.5. Simplified conceptual sketches showing the effect of synkinematic sedimentation during inversion: **a)** basin inversion without synkinematic sedimentation, where the contractional deformation propagates towards the salt pinch-out and it is mainly absorbed by the frontal thrust related to the harpoon structure, and **b)** basin inversion with synkinematic sedimentation where the thrust front has a high angle and the main contractional deformation is absorbed by the pre-existing salt wall also favored by the salt layer transferring deformation towards the salt wall, while developing a fish-tail.

During inversion, the widening of pre-existing welds or the development of new ones, as occurs in our Experiments 1.4 and 1.6 (**Figs. 3.4b and d**) are inhibited or delayed by surface processes such as erosion, by reducing the lithostatic load. Meanwhile, the non-weld development means that the structural style is partially coupled, hence hampering basin uplift (**Fig. 3.4c**).

4.5. WELDING KINEMATICS

4.5.1. Welding kinematics during extension

The subsidence of the salt-detached ramp-syncline basin during extension drives salt flow from the basin depocenter towards its edges where salt inflated anticlines evolve into salt walls. While this occurs, the overburden gradually approaches the underlying basement by

thinning the source layer until they eventually come into contact, depleting salt, and developing primary welds (Jackson and Cramez, 1989). However, unlike what happens when the base of the salt unit is horizontal, the existence of a basement topography constraints welding kinematics.

In salt-bearing basins where the salt unit is relatively thin (500 m thick), welds are quickly developed. Exp._1.3 and Exp._1.7 (**Table. 2.2a, Fig. 4.6**) enable to distinguish two stages of primary welding (**Figs. 4.6b - c**). On the initial one, a primary weld developed at the syncline hinge domain (Weld 1 in **Fig. 4.6b**; between A' and B) by salt migration mainly towards the basinward rollover hinge. As extension progressed the distance between the axial surfaces (A' and B) decreased and Weld 1 crossed the active axial surface B, becoming incorporated within the syncline forelimb (i.e., landward-dipping weld) (**Fig. 4.6c**). This new position of the Weld 1 triggers the further development of salt structures at basin basinward-edge. This is due to the sliding of the synclinal basin (i.e., by landward gravitational gliding) above the landward-dipping Weld 1 (**Fig. 4.6b**) (Coward and Stewart, 1995: Stewart and Clark, 1999). Thus, welding emphasized cover extension and the formation of reactive salt structures by thin-skinned extension (Jackson and Vendeville, 1994; Dooley et al., 2005). The landward sliding uses Weld 1 as a detachment surface and ends up when the primary Weld 2 is developed at the syncline backlimb (basinward-dipping weld) (**Fig. 4.6c**, Weld 2).

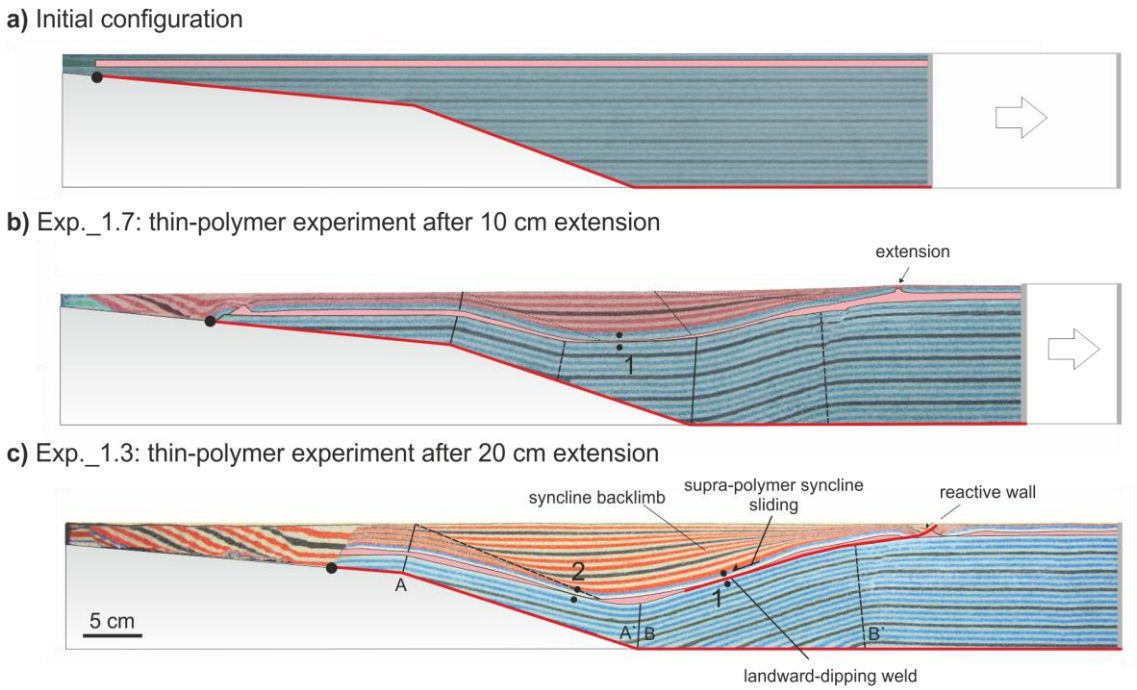

Fig.4.6. Cross-sections of the thin-polymer experiment showing different evolutionary stages (**Table. 2.2a**) **a)** at the beginning of the experiment (stretching 0 cm); **b)** after 10 cm of stretching (Exp._1.7); and **c)** after 20 cm of stretching (Exp._1.3). Numbers 1 and 2 indicate the order of primary weld formation (more detail in the text). See **Fig. 3.3** for legend.

However, when salt is thicker, a larger extension is needed to develop primary welds. In such cases, the first weld developed at the syncline forelimb (Weld 1 in **Fig. 4.7)**. After this landward-dipping primary weld, the salt-detached ramp-syncline basin subsides asymmetrically towards the unwelded limb, expelling salt landward to the adjacent passive diapir. Basin subsidence ceases with the development of the second primary weld against the subsalt syncline backlimb (Weld 2, **Fig. 4.7**). From here, the salt walls (**Fig. 4.7**) act as an extensional fault producing a counter-clockwise rotation of the salt-detached ramp-syncline basin and controlling the further basin depocenter (post-weld depocenter in **Fig. 4.7**). Both, salt wall-fault and basin sliding above the landward-dipping detachment weld (**Fig. 4.7**) results in a slightly antiformaly folded suprasalt basin (**Fig. 4.7**). Despite the length of this new weld 2 is shorter than the previous one (**Fig. 4.8a**), it is enough to interrupt diapir feeding. At this point, the overburden stucks to the subsalt basement. Further extension will increase the width of the subsalt ramp-syncline thus dragging the overburden, and widening the passive diapir (cryptic extension).

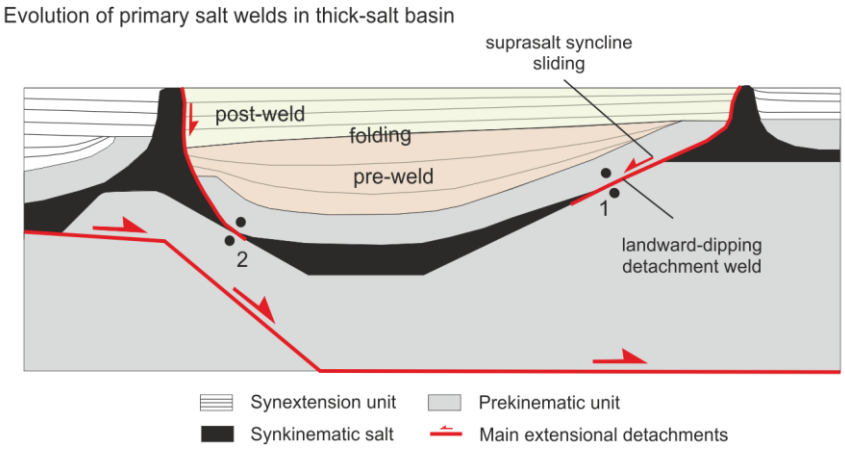

Fig.4.7. Simplified conceptual sketch of the effect of primary welding during extension based on the evolution of Exp._2.1 from the Experimental Program 2.

The basin fill of a salt-detached ramp-syncline shows different sedimentary architectures (i.e., depocenter stacking pattern and stratal geometries) at both basin edges (**Figs. 3.5 and 3.3c)**. From abrupt thickness changes (**Fig. 3.3c)** to progressive onlaps against the syncline backlimb (**Fig. 3.5)**, or wedges with different internal unconformities at the syncline forelimb (**Fig. 3.5**). This architecture dramatically changes with the formation of the first primary weld. The development of this primary weld is recorded in the basin architecture as an abrupt depocenter shifting that matches with a significant reduction of the salt extrusion rate. Glidding shifts the sub- and suprasalt syncline hinges (**Fig. 4.6c**), and a salt remnant with a clear asymmetric shape in cross-section is preserved between the two welds (**Fig. 4.5c**). However,

when welds are not developed, the offset between supra- and subsalt syncline hinges is less than in welded-salt basins.

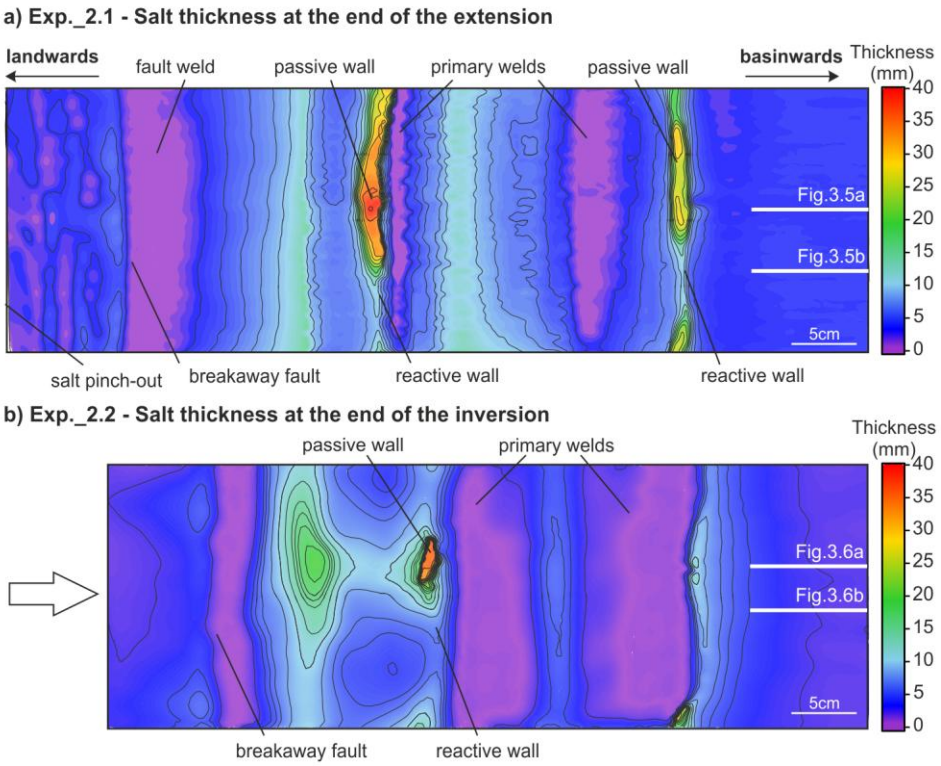

Fig.4.8. a) Thickness maps of salt at the end of the extensional phase for Exp._2.1 and **b)** at the end of the inversion for Exp._2.2. purple colors indicate the areas where salt was depleted thus developing primary welds, whereas yellowish colors correspond to the salt walls with maximum salt thicknesses. White lines correspond to the cross-section locations of **Figs. 3.5a-b and 3.6a-b**.

In addition to the primary welds developed below the salt-detached ramp-syncline basin, other types of welds are usually developed: primary welds associated with salt rollers **(Fig. 3.5)**, and fault welds developed where the salt is thin above the extensional fault **(Fig. 3.5)**. The formation of these welds, favored a strong coupling between overburden and basement deformation.

4.5.2. Welding kinematics during inversion

Primary welds at the end of the extension strongly contrast with those observed at the end of the inversion (**Figs. 3.4 and 3.6**). Inversion implies important basement topographic variations, such as the gradual uplift of the basin. This uplift is associated with a width reduction of the subsalt ramp-syncline (compare **Figs. 3.3 - 3.4 and Figs. 3.5 - 3.6**). Width reduction implies an asymmetric uplift of the salt-detachment ramp-syncline basin pushed by basement topographic variations above the lower ramp – intermediate panel (**Figs. 3.4 and**

3.6). This reduction entails shortening that is superimposed to the global thick-skinned contraction and lead to a change in the weld kinematics. This additional thin-skinned shortening mainly consists on the salt unit reactivation as an effective contractional detachment. As a consequence, the progressive primary welds' are contractionally reactivated as a thrust welds, involving shear along their surfaces, and favoring the squeezing of passive diapirs located at the basin edges with associated salt extrusion (**Figs. 4.9b - c**). This primary thrust weld has not been previously described in any natural case, since according with Rowan et al. (1999) a thrust weld will develop from a secondary weld.

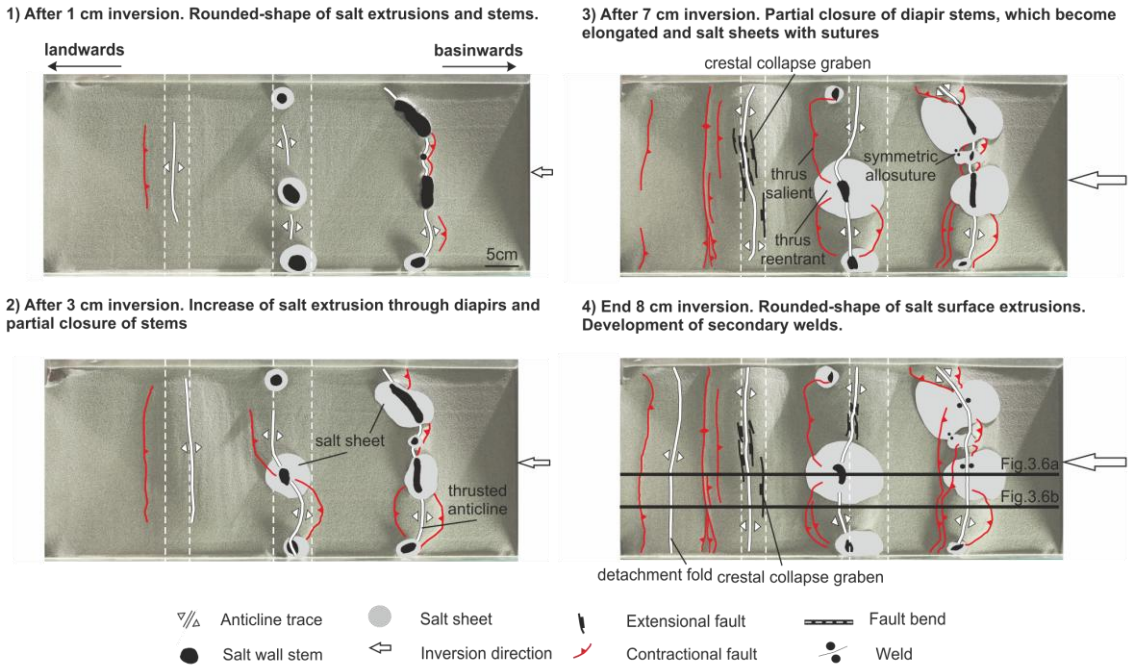

Fig.4.9. Interpreted overhead photographs showing the evolution of Exp._2.2 during inversion without syninversion sedimentation after 1 cm **1)**, 3 cm **2),** 7 cm **3)** and 8 cm **4)** of inversion. Continuous black lines in correspond to the cross-section locations of **Fig. 3.6a-b**. In all the photographs illumination is from the right and surfaces in shadow are dipping to the left.

The comparison of salt thickness maps between Exp._2.1 and Exp._2.2 (**Fig. 4.7**) clearly depicts that: **i)** the length of the primary welds below the salt-detached ramp-syncline progressively increase during shortening, and **ii)** it is reduced for the fault weld related to the breakaway fault.

As has already pointed in previous section (**section 4.3.2.**), despite both salt walls at the edges of the basin are squeezed, only the one located above the basinward rollover hinge (**Figs. 3.4b - c and 3.6a**) usually absorbed the main contractional deformation, and could be totally squeezed hence developing secondary vertical welds (**Figs. 3.4b and 3.6a**). The contractional deformation promotes the development formation of thin-skinned structures

related to the syncline-shape changes during shortening. Such thin-skinned shortening produced by the landward-dipping weld is more effective than the basinward-dipping one. This is due to the landward-dipping thrust weld can be interpreted as a passive roof thrust placed at the top of a thrust wedge (i.e., all the prekinematic sand pack that constituted the basinward rollover). Thus, this thrust wedge is bounded by, the reactivated subsalt master fault (i.e., lower panel) and a related splay which correspond to such landward-dipping thrust weld.

These are the geometric responses that are expected to occur in all inverted extensional basins containing an extensional rollover.

4.6. DEVELOPMENT AND CONTRACTION OF SALT STRUCTURES AT SALT-DETACHED RAMP-SYNCLINE EDGES

As has been already defined, as extension progress, the interplay between susalt basement extension and lithostatic load produced by synkinematic sedimentation, forced salt migration from the basin depocenters towards their edges where salt-inflated ridges occurs (e.g. Kehle, 1988; Koyi et al.,1993; Hudec and Jackson, 2007; Ferrer et al., 2014) (**Fig. 4.10a - b**).

After a few amount of subsalt extension, the salt-inflated ridges show its overburden folded and subsequently stretched by crestal collapse grabens (**Figs. 4.10c and 4.11a**). As extension progress, this crestal collapse graben evolves into a half-graben (**Figs. 4.10d and 4.11b**) and makes room for a reactive diapir to rise. Progressive erosion of topographic highs (**Figs. 4.10c and 4.11b**) favors salt piercement and extrusion (**Figs. 4.11c**). A different timing of salt extrusion could occur, caused by the differences in erosion rates of the salt-inflated areas (**Fig. 4.11b - c**).

Normal fault displacement varies along the strike, reaching its maximum displacement at its central part while displacement decreases with increasing distance from the central part (Withjack et al., 2002). This displacement differences in faults associated with a reactive diapir, generate an along-strike transition thought salt walls (**Figs. 4.10e.1- e2 and 4.11c**), from being passive salt walls at the central part of the associated fault (**Fig. 4.12**) or being reactive towards the fault edges (**Fig. 4.12**).

Thus, mixed mechanisms enhance salt diapir growth: salt inflation, erosion, reactive - active diapirism, the amount of associated fault displacement, welding and passive diapirism.

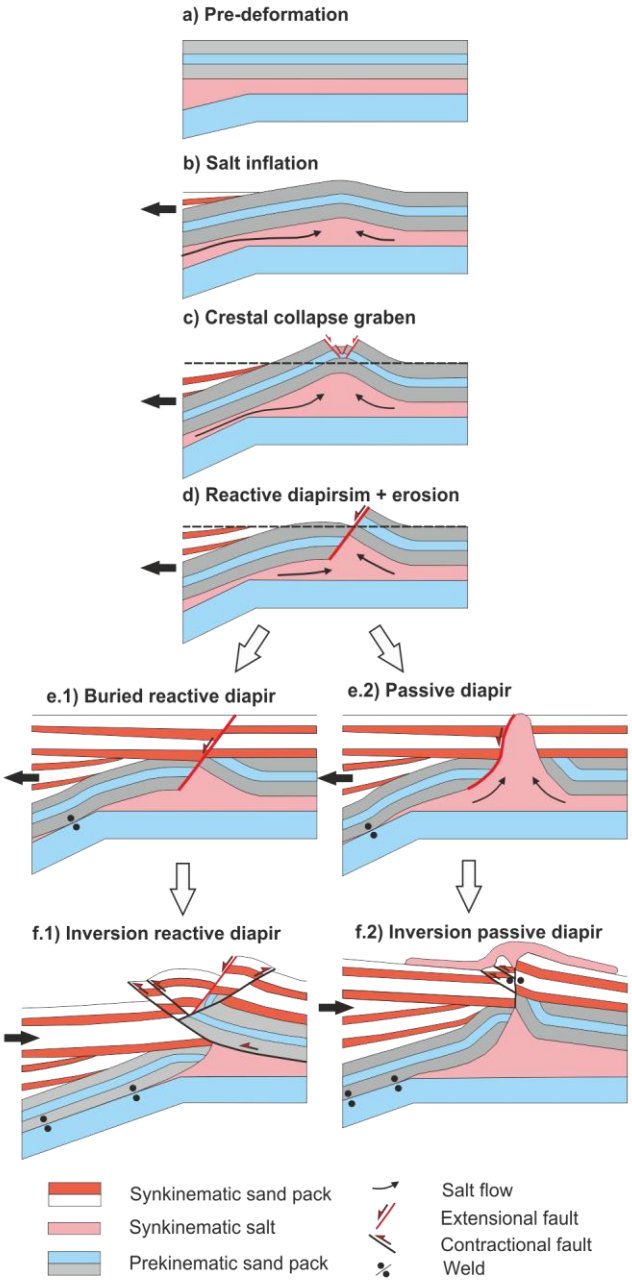

Fig.4.10. Synoptic model showing the different stages of salt structures evolution at the edges of the salt-detached ramp-syncline basin: **a)** Pre-deformational stage, **b)** at the beginning of extension with salt inflated areas fed by the flow from below the basin towards its edges, **c)** as extension progressed, collapse grabens develop at the salt-inflated anticlines, **d)** evolving into basinward-dipping normal faults as a reactive diapir. From this point the reactive diapir could be buried **(e.1)** or could evolve as a passive diapir **(e.2).** With ongoing inversion, an early pop-up structure flanked by opposite-verging thrusts developed above the buried reactive diapir **(f.1).** As shortening progressed the right flank of this diapir was thrusted basinward. In contrast, the passive diapir was squeezed, developing a secondary weld **(f.2).**

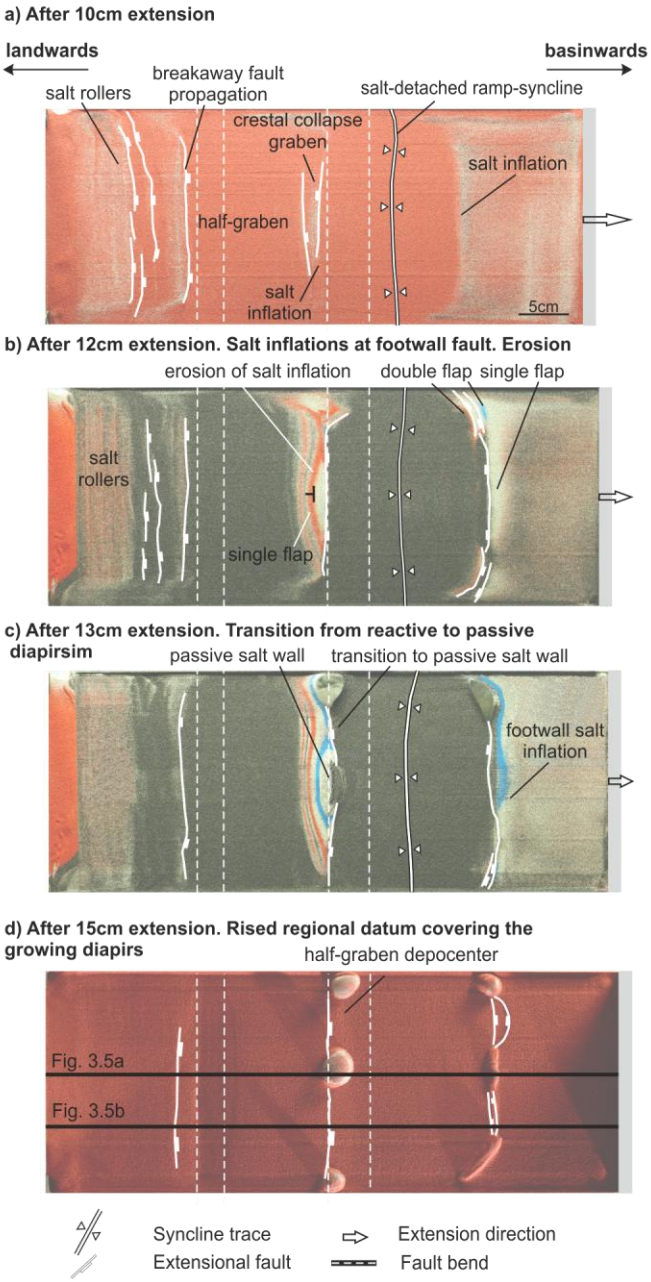

Fig.4.11. Interpreted overhead photographs showing the extensional evolution of Exp._2.1 (illumination is from the right) after **a)** 10 cm, **b)** 12 cm, **c)** 13 cm and **d)** 15 cm of extension. Continuous black lines in **Fig. 4.11d** correspond to the cross-section locations of **Fig. 3.5**.

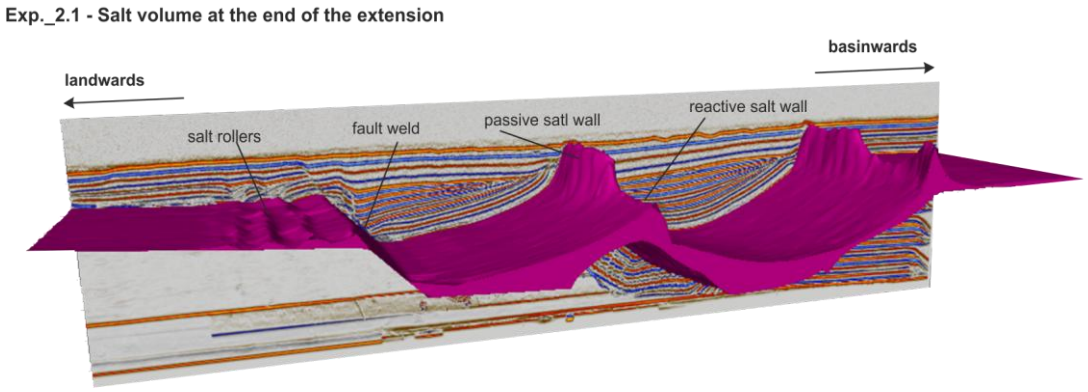

Fig.4.12. 3D view of the along-strike transition of both salt walls bounding the salt-detached ramp-syncline basin in Exp._2.1.

Salt structures are inherently weaker than other parts of the basin; because of this diapirs react sensitively to contraction long before any surrounding rocks (Letouzey et al., 1995, Letouzey and Sherkati, 2004; Rowan and Vendeville, 2006; Callot et al., 2007; Callot et al., 2012; Dooley et al., 2015). Initial shortening is visibly focused on salt structures, whereas surrounding areas deform by lateral compaction (LPC – Layer Parallel Compaction) (Vendeville and Nilsen, 1995; Nilsen et al., 1995; Cramez and Jackson, 2000; Rowan et al., 2000 and 2004).

Salt structures are contractionally rejuvenated by squeezing. Squeezing form thrusts and folds, which trend away in map view due to the 3D strain compatibility differences between salt and adjacent rocks (along-strike variation for the same salt wall, **Fig. 4.13a - b**). These differences constrain the development of: **i)** fold amplification and development of detachment folds with variable vergences where the inherited salt structures were salt ridges (structure A in **Fig. 4.14**), **ii)** reverse faults or thrust anticlines where the inherited salt wall are reactive (**Figs. 4.15a and e**) and **iii)** such reverse fault progressively curve towards the inherited passive salt walls forming thrust reentrants (**Figs. 4.13.a, 4.15b - c and d**).

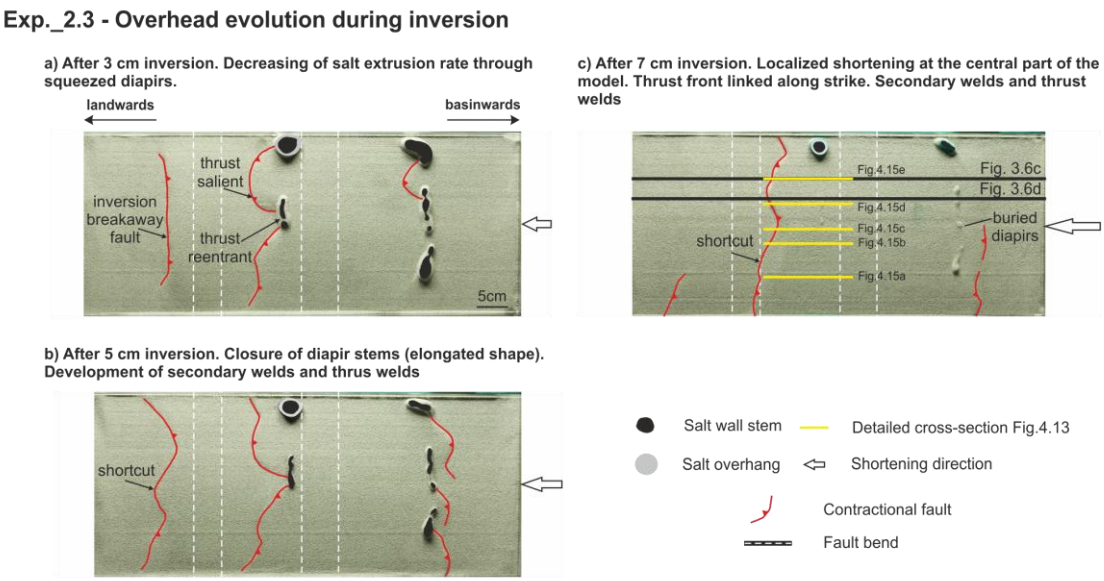

Fig.4.13. Interpreted overhead photographs showing the evolution of Exp.2.3 (with syninversion sedimentation) after 3 cm **a),** 5 cm **b)** and 7 cm **c)** of inversion. Continuous black correspond to the cross-section locations of **Fig. 3.6c-d**. Yellow lines correspond to the different detailed cross-sections of **Fig. 4.15**. In all the photographs illumination is from the right and surfaces in shadow are dipping to the left.

When these passive salt walls are squeezed, occurs an increase in the extrusion rate entailing the formation of a large salt sheet (**Figs. 4.9, 4.13** and structure C in **Fig. 4.14**). This squeezing produce elongated-shape (plan-view) of the salt walls, indicating partial closure of the salt wall stems, and finally the subsequent development of secondary welds (structure B in **Fig. 4.14**). The formation of secondary welds is usually indicated by a broad uplift and folding above the regional datum **(Figs. 3.6 and 4.9).** If inversion continues after secondary welding (**Fig. 4.15c**), the contractional deformation is absorbed by the diapir, and squeezed passive diapirs are separated from their original pedestal (decapitated diapir) (**Fig. 4.15b**) or developed thrust welds (**Figs. 3.6a, 3.4b, 4.9d, 4.14.a – c and 4.15c - d**) (Rowan et al., 1999) with different vergences (structure D in **Fig. 4.14**) nucleated at the upper part of salt wall pedestals (**Fig. 4.10.f2**). In contrast, squeezing of pre-existing reactive diapirs results in asymmetric anticlines, developed along-strike at the hangingwall of the imbricate thrust system (**Fig. 3.6b**), nucleated at the apex of the reactive salt wall and detached at the viscous layer (**Fig. 4.10.f1**).

Finally, after completely squeezed salt structures the structural style change radically, and thrust reentrants become inactive and progressively develops a smoothed-straight thrust front (**Fig. 4.13c**). This evolution is consistent with the models presented by Rowan et al. (1999) or Dooley et al. (2009).

This along-strike transition thought salt walls, have also an important implication in salt mobilization. The restoration of our models show that salt mobilization during shortening is strictly related to the presence or lack of pierced inherited salt walls (**Figs. 3.7 and 3.8**). When the basin has already welded before inversion, no salt migration along plane section occurs, therefore passive salt walls are feed by out of section salt. Usually a large volume of salt migrates from areas without developed passive salt structures toward the areas with well-developed passive salt wall. A key observation is finding large losses of salt volume at regions without developed passive diapirs (**Figs. 3.7 and 3.8**).

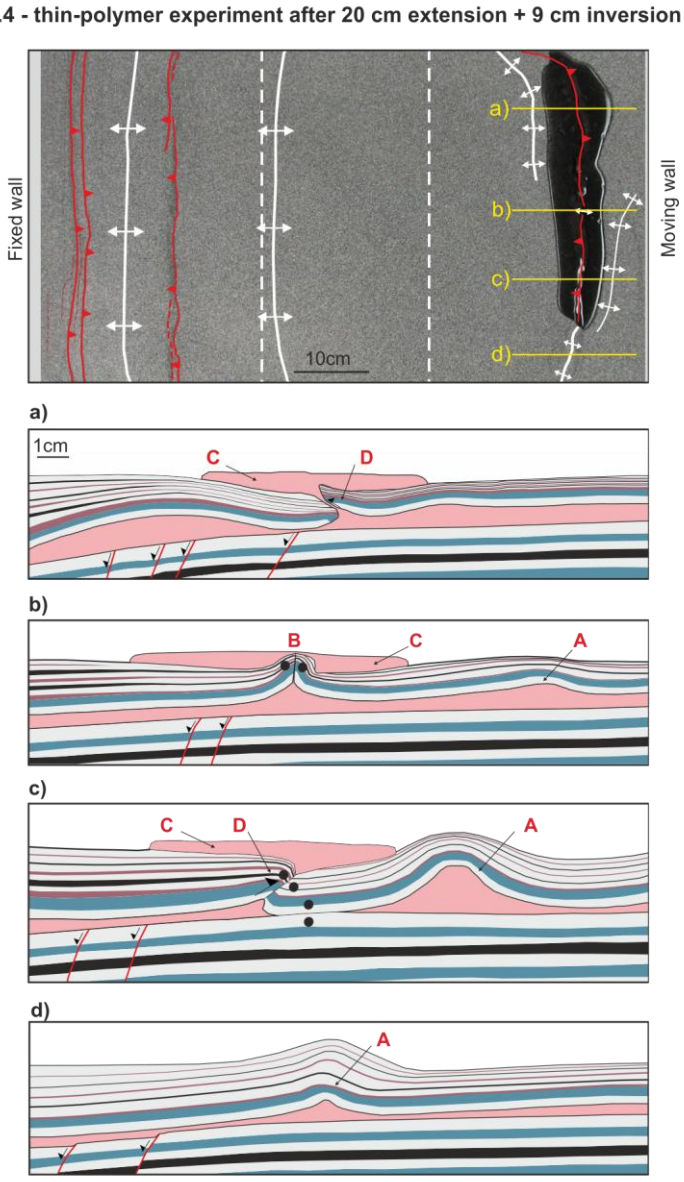

Fig.4.14. Top view of Exp._1.4 at the end of inversion with the location of four serial cross-sections **a) to b)** across a contractionally reactivated salt wall developed near the subsalt basinward extensional rollover hinge. In red: **A)** detachment anticline; **B)** squeezed diapir with vertical secondary weld; **C)** polymer sheet; **D)** thrust-weld with different vergences. See **Fig. 3.4** for legend.

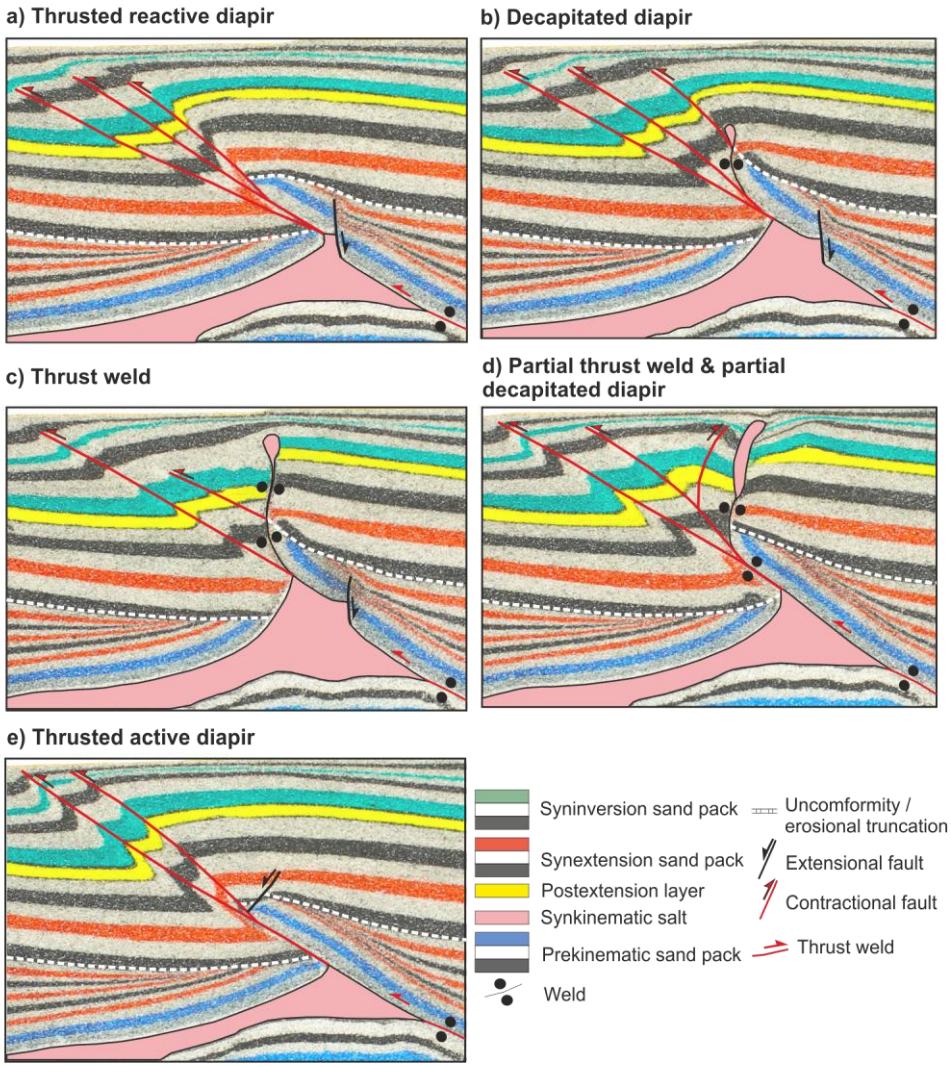

Fig.4.15. Serial detailed cross-sections of Exp._2.3 showing how inversion increases towards the weak diapir inherited from the extensional phase where shortening was focused. Note the along-strike variation of the inverted salt wall above the subsalt landward rollover. **a)** Thrusts nucleating at the apex of a pre-existing reactive diapir, **b)** squeezed passive diapir with a vertical secondary weld subsequently decapitated, **c)** squeezed passive diapir with a vertical secondary weld that evolves to a thrust weld when shortening continues, **d)** partial thrust weld and decapitated diapir and **e)** thrusts nucleating at the apex of a pre-existing reactive diapir. The inherited structure (reactive or passive diapir) and syninversion sedimentation are the main factors controlling the structural evolution during inversion. See **Fig. 4.13** for location.

4.7. COMPARISION WITH NATURAL ANALOGS

The widespread extensional deformation that took place in the Western Europe and North-Atlantic margins during Jurassic to Cretaceous times, results in the formation of several salt-bearing basins developed following with mixed thick- and thin-skinned deformation styles. Among the basins with a salt-detached ramp-syncline stand out the Lusitania Basin (Alves et al., 2002), the Columbrets Basin (Roma et al., 2018a), the Cameros Basin (Soto et al., 2007), the Parentis Basin (Ferrer et al., 2012), the Matalles Basin (Benedicto et al., 1999), the Dutch

Central Graben (Roma et al., 2018c), the Orpheus Basin (Durcanin, 2009), the Jeanne d'Arc Basin (Withjack and Callaway, 2000) and the Organyà Basin (Mencos et al., 2015) (**Figs. 2.6 and 2.7**). They are not bounded by major faults and show a broad synclinal-shape detached on pre- or synkinematic salt (Permian - Zechstein Formations, Late Triassic - Keuper facies or Late Triassic - Dagorda Formation). They are also characterized by thick sedimentary infill that can reach more than 8 km thick in the Columbrets Basin (Roca, 1996). Regardless of the presence and the thickness of salt, the development of these basins was also constrained by the geometry and displacement of the major extensional subsalt fault, which in turn controls the dip and length of the salt-detached ramp-syncline limbs and determines the syncline geometry and the extensional accommodation space generated at both syncline edges.

Subsequently to the extensional phase, some of these basins underwent different degrees of positive tectonic inversion (e.g. Columbrets and Parentis basins), or were totally inverted and incorporated into fold-and-thrust belts (e.g. Organyà Basin into the Pyrenees).

While the Columbrets (**Fig. 2.7b**) (Roma et al., 2018a) or the Cameros (**Fig. 4.15e**) basins (Soto et al., 2007) show wide, gentle and shallow salt-detached-ramp-synclines basins developed above a gently dipping intermediate panel, the Parentis or the Dutch Central Graben basins (**Fig. 4.16b - c**) (Ferrer et al., 2012; De Jager, 2003) show narrow and deep salt-detached ramp-synclines developed as a consequence of the steeper intermediate panel. These basins also have in common the development of extensional rollovers, whose imply a dip-variation geometry of the ramp fault at depth, and the existence of a basal detachment.

The Lusitania, Parentis, Matalles and Dutch Central Graben basins (**Figs. 2.7a, d, e and g**) show a synrift depocenter with a basinward dipping growth axial surface, suggesting the presence of a ramp-flat subsalt fault geometry at depth. In constrast, the Jeanne d'Arc basin and the Orpheous basin show a depocenter-staking-pattern which suggest the presence of a listric and planar-rotational faults respectively (**Figs. 2.7i and h)**.

The internal architecture of the synrift unit also records the interaction of others involving factors. For instance, the Lusitania basin shows a well-developed onlaps and apparent downlaps within its synrift units (**Fig. 2.7a**). Such, geometries suggest that this basin maid significantly translated above the salt.

In the analog experiments presented in this PhD, thick-skinned extension forced salt migration from the syncline hinge towards edges, feeding the growth of salt structures. A similar salt migration pattern has been also interpreted in the Jeanne d'Arc, Parentis, Dutch Central Graben or Columbrets basins (**Fig. 2.7**). In Columbrets Basin (**Fig. 2.7b**), the synkinematic sedimentation is practically nil at the syncline edge above the lower fault panel. This implies that the salt preferentially migrates towards the syncline edge located above the lower fault panel (the one with the lowest dipping attitude) where salt structures developed.

Primary salt weld develop at the syncline limbs after the depletion of the source layer, leaving a salt remnant at the syncline hinge as occurs in Jeanne d'Arc, Parentis, Dutch Central Graben or Columbrets basins (**Figs. 2.7i, g and b)**. Welding at the fault ramp during extension can force the development of curved normal faults as has been interpreted in the Parentis Basin (Ferrer et al., 2012) modifying the trend of the synextensional depocenter path (**Fig. 2.7d**). In contrast, in the Dutch Central Graben (**Fig. 2.7g**) is difficult to identify this abrupt depocenter shifting forced by primary welding. In this case, the development of primary weld during extension can be inferred from the extensional collapse of salt structures bounding the basin (**Fig. 2.7g**).

In Lusitania and Broad Fourteens basins (**Figs. 2.7a and f**) the deposition of salt occurs between several extensional phases (Alves et al., 2002; De Jager, 2003). Consequently, the salt unit shows lateral thickness variation that is another control factor on the structural style of the basin. While thick salt promotes decoupling between suprasalt and subsalt units and the development of wide salt-detached ramp-syncline basins (among **Fig. 2.7**, the Alés Basins in the Gulf of Lion (Sanchis and Séranne, 2000), the Nordkapp Basin in Norwegian Barens Sea (Gudlaugsson et al., 1998) or the Slyne Basin in offshore Ireland), thin-salt favors coupled deformation, the upwards propagation of subsalt faults, and constrains the development of early extensional fault-propagation folds or half-grabens (**Fig. 4.16a)**. Equivalent structures have been also interpreted in the Stavenger fault system in the North Sea (Lewis et al., 2013), in the Central Suez Rift (Withjack and Callaway, 2000) or the Haltenbanken area offshore Norway (Richardson et al., 2005). In a similar way, the imbricate listric fault system outcropping at the Desert de les Palmes (northwest part of the Columbrets Basin) (**Fig. 4.16d**), is equivalent to the breakaway half-graben developed at the updip basin margin of the Exp._1.4 (**Fig. 4.16d**) where salt is not involved and the fault system is detached on an intracrustal detachment (Roca et al., 1994).

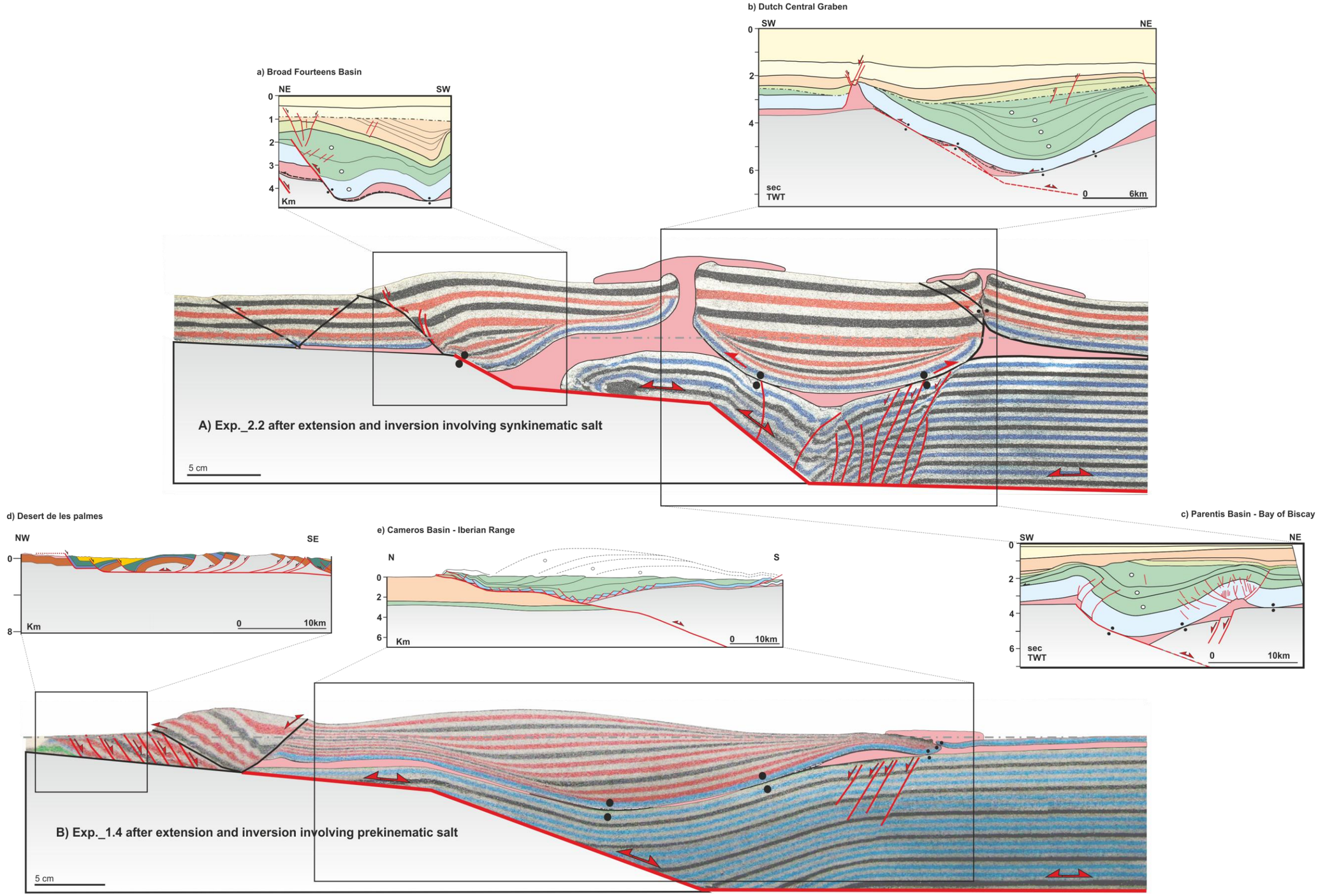

Fig.4.16. Summary of results integrating both case examples and the experimental models. **a)** Broad Forteens Basin, **b)** Dutch Central Graben, **c)** Parentis Basin, **d)** Desert de les Palmes, **e)** Cameros Basin (see legend at **Fig. 2.7**). A) and B) corresponds to Exp._2.2 and Exp._1.4 respectively (see legend for the analog cross-section in **Figs. 3.6 and 3.4**)

Furthermore, several of the previous basins were subsequently inverted during Uppermost Cretaceous to Cenozoic times, developing both thick- and thin-skinned contractional structures. The balanced cross-section of the Cameros Basin (**Fig. 4.16e**) (Soto et al., 2007) or the Organyà Basin (Mencos et al., 2015), show the development of a thick-skinned fault-bend anticline. In contrast, the other basins in **Fig. 2.7** are slightly inverted and this clearly inversion features has not been developed, but the presence of a major unconformity on the top of the basins infill denotes that there were tectonically inverted.

The contractional deformation promotes the formation of thin-skinned structures related to the syncline-shape changes during shortening. These geometric responses are expected to occur in all inverted extensional basins containing an extensional rollover. An example of this occurs in the Cameros Basin (**Fig. 4.16e**), where the southern basin margin is characterized by an inverted thin-skinned backthrust developed above the extensional rollover and detached on the Upper Triassic salt (Soto et al., 2007). The Columbrets Basin (**Fig. 2.7b)** also shows a SE-verging thin-skinned backthrust above the syncline forelimb detached also on the Upper Triassic salt (Roma et al., 2018a). In that case, this backthrust controls the inversion of the basin. In contrast, the inversion of Cameros Basin is mainly controlled by the thick-skinned fault-bend anticline. In this sense, in Columbrets Basin most of the shortening is related to the emplacement of a crustal thrust wedge bounded by the mentioned thin-skinned backthrust (which acted as a passive roof thrust) and the south-east dipping floor thrust. Equivalent thin-skinned contractional structures can also be seen in the Parentis Basin and Dutch Central Graben (**Figs. 4.16c - b**), where the thin-skinned contraction produced the amplification of salt-cored basin-bounding structures by squeezing, using the salt or its equivalent primary weld as a contractional detachment or thrust weld respectively. Only scarce examples of dipping primary welds reactivated as thrust welds have been provided in the literature. These types of structures should develop in inverted rift basins with syn- or postrift salt filling pre-existing relief in which the source layer can have an original dip. The inversion of the northern sector of the Broad Fourteens Basin resulted in a striking thrust weld probably developed from an inherited squeezed salt structure (**Fig. 2.7f**).

In addition, the Broad Fourteens Basin shows the effect of the inversion of sectors where the salt was thin and completely disconnected (i.e., primary fault weld) during the extensional phase. The inversion of the basin with this inherited configuration favors the development of the harpoon structures (**Fig. 4.16a**).

Both the erosion of the Columbrets Basin (Marin et al., 2019) and the welding of the syncline backlimb during inversion, favor contractional deformation accommodated at the thin-skinned backthrust (**Fig. 2.7b**). In contrast, in the Cameros Basin the high rate of synkinematic sedimentation during inversion plays a key role in strain localization. The synkinematic sedimentation buried the thrust front and inhibits the outwards propagation of the deformation front into the foreland (**Fig. 4.16e**). As a consequence basin uplift absorbed the main contractional deformation. In contrast, the Parentis Basin is less affected by syninversion sedimentation (**Fig. 2.7d**), and salt walls developed above the footwall fault are totally squeezed, which means that the salt layer was reactivated as a contractional detachment above the footwall master fault.

All these structural similarities have been also interpreted through an experimental approximation based on analog models (**Fig. 4.16**). Moreover the evolution of the analog models allows to reduce the uncertainty on the origin and kinematics of this salt-detached ramp-syncline basins during both extension and inversion. In that case, the analog models results provide insights and supports the processes that can explain the geometries observed for the previous interpretations.

Our results can be used as a guide for improving the interpretation of seismic lines in other salt-bearing basins, where these styles of extensional salt tectonics develop. In this sense, this PhD. offers alternative interpretations based on the insights found in the coupled subsalt and suprasalt deformation observed in the analog models. Therefore, new constraints for the subsalt extensional master fault interpretation were also presented in this thesis. Our analog results can be useful: **1)** to support published interpretations whit similar geometries to the ones in our models, **2)** assist in the reinterpretation of seismic sections in subsalt areas where imaging is problematic, and **3)** serve as a guide for other similar salt basins.

CHAPTER 5. SUMMARY OF CONCLUSIONS

- A salt-detached ramp-syncline basin is a synclinal sedimentary basin formed above an active extensional fault ramp and detached from this fault by a salt unit. It develops by regional extension but is not bounded by major faults. Instead, it can be flanked by salt structures whose generally nucleated parallel to the major subsalt structures. The sliding of the hangingwall above the footwall fault produces the drape folding of the prekinematic sequence and a locus of subsidence seaward of the fault ramp. This locus remains fixed in space, but its previous sediment fill is progressively moved away from it, producing a characteristic asymmetric synclinal basin. Thus, a salt-detached ramp-syncline is characterized by a dipping growth axial surface defined by the progressive shifting of the synrift depocenters as the extension increase.

- The formation of salt-detached ramp-syncline basins is basically constrained by the geometry of the subsalt fault, but also by the presence, distribution and thickness of salt. Both salt migration and its effectiveness as a detachment allow a thin-skinned deformation in a thick-skinned system, decoupling sub- and suprasalt deformation. In such cases mixed modes of deformation styles are expected, and this scenario become ideal for the development of a salt-detached ramp-syncline basins.

- The synkinematic basin infill architecture of salt-detached ramp-synclines is controlled by the interaction between parameters as: **i)** the subsalt fault displacement and its geometry, **ii)** salt migration, **iii)** the initial thickness of the salt unit and its distribution, and **iv)** the degree of decoupling between the sub- and suprasalt units:

  i) The salt-detached ramp-syncline geometry depends on the amount of extension, shape and dip of the involved-subsalt-fault ramps. For a given flat-ramp-flat fault (i.e., where the ramp is the intermediate panel) wide, gentle and shallow salt-detached ramp-syncline basin

develops above a gently dipping intermediate panel. In contrast, narrow and deep salt-detached ramp-syncline basin develops as a function of steeper intermediate panels. The dip of the upper and lower panels controls the accommodation space at both synclinal basin edges. This will be recorded in the syncline basal and upper boundaries, as an abrupt thickness changes (accommodation space) or as a diachronous unconformity (no accommodation space).

ii) Salt migrates from the syncline depocenter towards its edges. But the preferential salt migration is constrained by the thickness difference between both syncline edges, which in turn is controlled by the fault displacement and dip of the subsalt fault panels. The preferential salt migration is recognized by the development of inflated areas and diapiric structures. The developed passive salt structures are also feeded by salt that migrates along-strike (out-of-section), from neighborhood regions without developed salt structures.

iii) Thick salt promotes decoupling and consequently favors mixed thin- and thick-skinned deformation styles.

iv) Thick salt favors high degree of decoupling, and therefore translation over the salt of the salt-detached ramp-syncline basins.

- Based on the suprasalt basin architecture, it is possible to infer in **i)** the subsalt fault geometry, **ii)** the amount of decoupling, **iii)** the subsalt fault displacement and **iv)** the timing of salt welds formation:

i) For a given listric or planar-rotational subsalt faults the resulting synkinematic growth axial surface will generally dip landwards. In contrast, the growth axial surface will dip basinwards when the subsalt basement-involved fault is a ramp-flat fault. Moreover, the presence of apparent downlaps implies a subsalt ramp-flat fault (i.e., downdip concave-up fault bend). In addition, to determine the updip convex-up fault bend, usually the landward basin edge must occur directly above it. However, salt structures can shift this relationship. Then, secondary structures like extensional rollovers are also useful features to determine the subsalt fault geometry.

ii) The overburden translation may be estimated by measuring the distance between the landward edge of salt-detached ramp-syncline basin and the oldest onlap.

iii) The subsalt fault displacement is recorded between the distance of the subsalt active and inactive axial surfaces. In regions where the subsalt structure is not well imaged, the suprasalt basin translation rate may be used as an approximation. However, the basin translation rate can be more (with high degree of decoupling) or less (with a landward-dipping detachment salt weld) than the subsalt fault displacement.

iv) Decoupling and salt migration will be interrupted after the formation of basin primary welds. The evolution of the salt-detached ramp-syncline basins infers in the timing of welding formation and welding kinematics. The formation of a landward-dipping weld (i.e., primary salt weld incorporated within the syncline forelimb) favors the basinward sliding of

the suprasalt synclinal basin. This sliding resulted in the formation of the primary weld at the syncline backlimb, consequently shifting the sub- and suprasalt syncline hinges. This fact can mask the bulk suprasalt basin translation, by reducing this value. At this point the salt walls, flanking the basin, can act as extensional faults controlling the further basin depocenter. Both, salt wall-fault and basin sliding above the landward-dipping detachment weld, results in a slightly antiformaly folded suprasalt basin. Therefore, an abrupt depocenter's trajectory variations in synkinematic sediments, a salt remnant, an offset between syncline hinges, basin rotation, folding and development of curved normal faults are key geometries that demonstrate welding formation.

- The interaction between different factors as: **i)** the subsalt fault geometry and fault displacement, **ii)** the pre-existing structures (extensional and salt structure), **iii)** salt continuity and the presence of primary welds, **iv)** the salt migration, **v)** the degree of coupling between subsalt and suprasalt units, and **vi)** the synkinematic sedimentation and erosion, controls the structural style, the kinematic evolution and the welding evolution during inversion.

    - The tectonic inversion of salt-detached ramp-syncline basins is mainly characterized by the formation of a major fault-bend anticline controlled by thick-skinned deformation.
    - Simultaneously, basin inversion also produces a reduction in the amplitude of the inherited syncline, which triggered thin-skinned shortening and reactivates the salt layer as an effective contractional detachment. The experimental results show that during inversion, basinward- and landward-dipping primary welds are contractionally reactivated as thrust welds, transferring the contractional deformation to the to the suprasalt unit. This has not been previously described in

any natural case. Depending on the geometry of the inherited salt bodies (reactive or passive salt walls), such thin-skinned shortening favors: **i)** the contractional rejuvenation of the reactive salt walls as a thrust salient (in plan-view) and **ii)** the formation of thrust reentrants (in plan-view) towards the squeezed passive salt walls, increasing salt extrusion and favoring the development of secondary vertical welds and small thrusts nucleating at the diapir's pedestals.

- Such thin-skinned shortening produced by the landward-dipping weld is more effective than the basinward-dipping one, consequently salt structures developed above the basinward extensional rollover hinge absorbed the main contractional deformation. This is due to the landward-dipping weld acts as a passive roof thrust placed at the top of a thrust wedge. These geometric responses are expected to occur in all inverted extensional basins containing an extensional rollover.
- Syninversion sedimentation is a key factor controlling where, when, and how the strain is localized. It also controls the evolution of inherited salt structures. While salt pinch-outs usually serve as nucleation points of thrust fault, synkinematic sedimentation during inversion inhibits the propagation of the contractional deformation towards the salt pinch-out. In that case, the thrust front is translated backwards and is characterized by high angle reverse faults. For instance, synkinematic sedimentation during inversion may seals the thrust front and therefore forces contractional deformation to switch further backwards, where pre-existing salt structures can absorb the main shortening. Meanwhile, primary thrust welds and salt layers act as contractional detachments transferring the deformation towards the inherited diapirs until to develop of secondary welds, thrust welds or decapitated diapirs. During inversion, the widening of pre-existing welds or the development of new ones are inhibited or delayed by reducing the lithostatic load by surface processes such as erosion.

- The analog results can be useful **i)** to support published interpretations where geometries similar to the ones in our models can be observed, **ii)** assist in the reinterpretation of seismic sections in subsalt areas where imaging is problematic, and **iii)** serve as a template for other similar salt basins.

CHAPTER 6. REFERENCES

Adam, J., Urai, J., Wieneke, B., Oncken, O., Pfeiffer, K., Kukowski, N., Lohrmann, J., Hoth, S., Van der Zee, W., Schmatz, j., 2005. Shear localisation and strain distribution during tectonic faulting — New insights from granular-flow experiments and high-resolution optical image correlation techniques. *Journal of Structural Geology*, **27**, 283–301. Doi: 10.1016/j.jsg.2004.08.008.

Allen, J., Beaumont, C., 2012. Impact of inconsistent density scaling on physical analogue models of continental margin scale salt tectonics. *Journal of Geophysical Research*, **17**, 1-22.

Allen, P.A., Allen, J.R., 2013. Basin analysis: Principles and application to petroleum play assessment, 3rd edition. Wiley-Blackwell, John Wiley & Sons.

Álvaro, M., Capote, R., Vegas, R., 1979. Un modelo de evolución geotectónica para la Cadena Celtibérica. *Acta Geologica Hispanica*, **14**, 172–177.

Alves, T.M., Gawthorpe, R.L., Hunt, D.W., Monteiro, J.H., 2002. Jurassic tectono-sedimentary evolution of the Northern Lusitanian Basin (offshore Portugal). *Marine and Petroleum Geology*, **19**, 727-754. Doi: 10.1016/S0264-8172(02)00036-3

Amilibia, A., McClay, K.R., Sabat, F., Munoz, J.A., Roca, E., 2005. Analogue modelling of inverted oblique rift systems. *Geologica Acta*, **3(3)**, 251-271.

Ayala, C., Torne, M., Pous, J., 2003. The lithosphere-astenosphere boundary in the western Mediterranean from 3D joint gravity and geoid modeling: tectonic implications. *Earth and Planetary Science Letters*, **209**, 275–290. Doi: 10.1016/S0012-821X(03)00093-1.

Baby, P., Colletta, B., Zubieta, D., 1995. Etude géométrique et expérimentale d'un bassin transporté: exemple du synclinorium de l'Alto Beni (Andes centrales). *Bulletin de la Société Géologique de France*, *166(6)*, 797-811.

Badley, M., Prince, J.D., Backshall, L.C., 1989. Inversion, reactivated faults and related structures, seismic examples from the Southern North Sea. *The Geological Society of London*, *Special Publications*, **44**, 201-219. Doi: 10.1144/GSL.SP.1989.044.01.12

Balkwill, H.R., Legall, F.D., 1989. Whale Basin, offshore Newfoundland: extension and salt diapirism. Extensional Tectonics and Stratigraphy of the North Atlantic Margins. *American Association of Petroleum Geologists Memoir*, **46**, 233-246.

Bally, A.W., Gordy, P.L., Stewart, G.A., 1966. Structure, seismic data, and orogenic evolution of southern Canadian Rocky Mountains. *Bulletin of Canadian Petroleum Geology*, **14(3)**, 337-381.

Barrier, L., Nalpas, T., Gapais, D., Proust, J.-N., 2013. Impact of synkinematic sedimentation on the geometry and dynamics of compressive growth structures: Insights from analogue modelling. *Tectonophysics*, **608**, 737-752. Doi: 10.1016/j.tecto.2013.08.005

Benedicto, A., Séguret, M., Labaume, P., 1999. Interaction between faulting, drainage and sedimentation in extensional hanging-wall syncline basins: examples of Oligocene Matelles basin (Gulf of Lion rifted margin, SE France). In: Duran, B., Jolivet, L., Horváth, F., Séranne, M., (eds.). The Mediterranean Basins: Tertiary Extension within the Alpine Orogen. *Geological Society of London, Special Publications*, **156**, 81-108. Doi: 10.1144/GSL.SP.1999.156.01.06

Biteau, J.J., Le Marrec, A., Le Vot, M., Masset, J.M., 2006. The aquitaine basin. *Petroleum Geoscience*, **12(3),** 247-273. Doi: 10.1144/1354-079305-674

Bonini, M., 1998. Chronology of deformation and analogue modelling of the Plio-Pleistocene 'Tiber Basin': implications for the evolution of the Northern Apennines (Italy). *Tectonophysics*, **285**, 147–165.

Bonini, M., 2001. Passive roof thrusting and forelandward fold propagation in scaled brittle-ductile physical models of thrust wedges. *Journal of Geophysical Research*, **106(B2)**, 2291-2311.

Bonini, M., Corti, G., Sokoutis, D., Vannucci, G., Gasperini, P., Cloetingh, S., 2003. Insights from scaled analogue modelling into the seismotectonics of the Iranian region. Tectonophysics, 376(3-4), 137–149. Doi:10.1016/j.tecto.2003.07.002

Bonini, M., Sani, F., Antonielli, B., 2012. Basin inversion and contractional reactivation of inherited normal faults: a review based on previous and new experimental models. *Tectonophysics*, **522-523**, 55-88. Doi: 10.1016/j.tecto.2011.11.014

Badley, M., Prince, J.D., Backshall, L.C., 1989. Inversion, reactivated faults and related structures, seismic examples from the Southern North Sea. *The Geological Society of London, Special Publications*, **44**, 201-219. Doi: 10.1144/GSL.SP.1989.044.01.12

Bradshaw, G.A., Zoback, M.D., 1988. Listric normal faulting, stress refraction, and the state of the stress refraction, and the state of the stress in the Gulf Coast basin. *Geology*, **16**, 271-274.

Brekke, H., 2000. The tectonic evolution of the Norwegian Sea continental margin, with emphasis on the Voring and More basins. *Geological Society of London, Special Publication*, **167**, 327-378.

Bruce, C.H., 1984. Smectite dehydration: its relation to structural development and hydrocarbon accumulation in northern Gulf of Mexico Basin. *American Association of Petroleum Geologists Bulletin*, **68**, 673-683.

Brun, J.P., 1999. Narrow rifts versus wide rifts: inferences for the mechanics of rifting from laboratory experiments. *Philosophical Transactions Royal Society London, Series* A, **357**, 695–712.

Brun, J.P., Nalpas, T., 1996. Graben inversion in nature and experiments. *Tectonics*,**15(3)**, 677-687. Doi:10.1029/95TC03853

Buchanan, P.G., McClay, K.R., 1991. Sandbox experiments of inverted listric and planar fault Systems. *Tectonophysics*, **188(1-2)**, 97-115. Doi: 10.1016/0040-1951(91)90317-L

Buchanan, P.G., McClay, K.R., 1992. Experiments on basin inversion above reactivated domino faults. *Marine and Petroleum Geology*, **9**, 486–500.

Buck, W.R., 1988. Flexural rotation of normal faults. Tectonics, 7(5), 959–973. Doi:10.1029/tc007i005p00959

Burberry, C.M., 2015. Spatial and temporal variation in penetrative strain during compression: Insights from analog models. *Lithosphere*, **7(6)**, 611-624. Doi: 10.1130/L454.1

Burliga, S., Koyi, H.A., Krzywiec, P., 2012. Modelling cover deformation and decoupling during inversion, using the Mid-Polish trough as a case study. *Journal of Structural Geology*, **42**, 62–73.

Callot, J.P., Jahani, S., Letouzey, J., 2007. The role of pre-existing diapirs in fold and thrust belt development. In: Lacombe, O., Roure, F., Lavé, J., Vergés, J., (eds.). Thrust Belts and Foreland Basins. Frontiers in Earth Sciences. Berlin, Heidelberg, Springer, 309-325. Doi:10.1007/978-3-540-69426-7_16

Callot, J.P., Trocmé, V., Letouzey, J., Albouy, E., Jahani, S., Sherkati, S., 2012. Pre-existing salt structures and the folding of the Zagros Mountains. *Geological Society of London, Special Publications*, **363**, 545-561. Doi: 10.1144/SP363.27

Carola, E., 2014. The transition between thin- to thick-skinned styles of deformation in the Western Pyrenean Belt. Doctoral dissertation, Universitat de Barcelona, Barcelona, Spain.

Carola, E., Muñoz, J.A., Roca, E., 2015. The transition from thick-skinned to thin-skinned tectonics in the Basque-Cantabrian Pyrenees: the Burgalesa Platform and surroundings. *International Journal of Earth Sciences*, **104(8)**, 2215-2239.

Casas, J.M., Durney, J.S., Ferret, J., Muñoz, J.A., 1996. Determinación de la deformación finita en la vertiente sur del Pirineo oriental a lo largo de la transversal del rio Ter. *Geogaceta*, **20**, 803-805.

Chamberlin, R.T., 1910. The Appalachian folds of central Pennsylvania. *Journal of Geology*, **18(3)**, 228-251.

Clifton, A.E., Schlische, R.W., Withjack, M.O., Ackermann, R.V., 2000. Influence of rift obliquity on fault-population systematics: results of clay modeling experiment. *Journal of Structural Geology*, **22**, 1491–1509.

Cloos, E., 1968. Experimental analysis of Gulf Coast fracture patterns. *American Association of Petroleum Geologists Bulletin*, **52(3)**, 420-444. Doi: 10.1306/5D25C2E5-16C1-11D7-8645000102C1865D

Corti, G., 2004. Centrifuge modelling of the influence of crustal fabrics on the development of transfer zones: insights into the mechanics of continental rifting architecture. *Tectonophysics*, **384**, 191–208.

Corti, G., Bonini, M., Conticelli, S., Innocenti, F., Manetti, P., Sokoutis, D., 2003. Analogue modelling of continental extension: a review focused on the relations between the patterns of deformation and the presence of magma. *Earth-Science Reviews*, **63**, 169–247.

Corti, G., 2012. Evolution and characteristics of continental rifting: Analog modeling-inspired view and comparison with examples from the East African Rift System. *Tectonophysics*, **522**, 1-33.

Couzens-Schult, B., Vendeville, B., Wiltschko, D., 2003. Duplex style and triangle zone formation: insights from physical modeling. *Journal of Structural Geology*, **25**, 1623–1644. Doi: 10.1016/S0191-8141(03)00004-X.

Coward, M.P., 1995. Structural and tectonic setting of the Permo-Triassic basins of northwest Europe. *Geological Society of London, Special Publications*, **91(1)**, 7-39. Doi: 10.1144/GSL.SP.1995.091.01.02

Coward, M., Stewart, S., 1995. Salt-influenced structures in the Mesozoic-Tertiary cover of the Southern North Sea, U.K. In: Jackson, M.P.A., Roberts, D.G., Snelson, S., (eds.). Salt Tectonics: a global perspective. *American Association of Petroleum Geologist Memoir*, **65**, 229-250.

Cramez, C., Jackson, M.P.A., 2000. Superposed deformation straddling the continental-oceanic transition in deep-water Angola. *Marine and Petroleum Geology*, **17(10)**, 1095-1109. Doi: 10.1016/S0264-8172(00)00053-2

Dahlstrom, C.D.A., 1969. Balanced cross sections. *Canadian Journal of Earth Sciences*, **6(4)**, 743-757. doi: 10.1139/e69-069

Darros de Matos, R.M., 1993. Geometry of the hanging wall above a system of listric normal faults; a numerical solution. *American Association of Petroleum Geologist Bulletin*, **77 (11)**, 1839-1859.

Davison, I., 1986. Listric normal fault profiles; calculation using bed-length balance and fault displacement. *Journal of Structural Geology*, **8 (2)**, 209-210.

Davison, I., 1987. Normal fault geometry related to sediment compaction and burial. *Journal of Structural Geology*, **9**, 393-401.

De Jager, J., 2003. Inverted basins in the Netherlands, similarities and differences. *Netherlands Journal of Geoscienes*, **82(4)**, 355-366. Doi: 10.1017/S0016774600020175

Dell' Ertole, T., Schellart, W., 2013. The development of sheath folds in viscously stratified materials in simple shear conditions: an analogue approach. *Journal of Structural Geology*, **56**, 129–141. Doi: 10.1016/j.jsg.2013.09.002.

Del Ventisette, C.D., Montanari, D., Bonini, M., Sani, F., 2005. Positive fault inversion triggering 'intrusive diapirism': an analogue modelling perspective. *Terra Nova*, **17(5)**, 478-485. Doi: 10.1111/j.1365-3121.2005.00637.x

Del Ventisette, C., Montanari, D., Sani, F., Bonini, M., 2006. Basin inversion and fault reactivation in laboratory experiments. In: Tavarnelli, E., Butler, R., Grasso, M., (eds.). Tectonic Inversion Processes and Structural Inheritance in Mountain Belts. *Journal of Structural Geology*, **28**, 2067–2083.

Dercourt, J., Ricou, L.E., Vrielynck, B., 1993. Atlas Tethys Palaeoenvironmental Maps. Gauthier-Villars, Paris, France.

Dooley, T.P., McClay, KR., Hempton, M., Smit, D., 2005. Salt tectonics above complex basement extensional fault systems: Results from analogue modeling. North-west Europe and global perspectives. Proceedings of the 6th Petroleum Geology Conference. Petroleum Geology Conferences Ltd. and the Geological Society of London, 1631- 1648.

Dooley, T.P., Jackson, M.P.A., Hudec, M.R., 2007. Initiation and growth of salt-based thrust belts on passive margins: results from physical models. *Basin Research*, **19**, 165–177.

Dooley, T.P., Jackson, M.P.A., Hudec, M.R., 2009. Inflation and deflation of deeply buried salt stocks during lateral shortening. *Journal of structural geology*, **31**, 582-600. Doi: 10.1016/j.jsg.2009.03.013

Dooley, T.P., Hudec, M.R., Jackson, M.P.A., 2012. The structure and evolution of sutures in allochthonous salt. *American Association of Petroleum Geologists Bulletin*, **96**, 1045-1070. Doi: 10.1306/09231111036

Dooley, T.P., Jackson, M.P.A., Jackson, C.A.L., Hudec, M.R., Rodriguez, C.R,. 2015. Enigmatic structures within salt walls of the Santos Basin—Part 2: Mechanical explanation from physical modelling. *Journal of Structural Geology*, **75**, 163-187. Doi: 10.1016/j.jsg.2015.01.009

Dooley, T.P., Hudec, M.R., Carruthers, D., Jackson, M.P.A., Luo, G., 2017. The effects of base-salt relief on salt flow and suprasalt deformation patterns—Part 1: Flow across simple steps in the base of salt. *Interpretation*, **5(1)**, SD1-SD23. Doi:10.1190/INT-2016-0087.1

Driehaus, L., 2013. Modelización analogical de la deformación en las zonas de compresión y subducción. Doctoral dissertation, Universitat de Barcelona - Université de Rennes, Barcelona – Rennes, Spain - France.

Dubois, A., Odonne, F., Massonnat, G., Lebourg, T., Fabre, R., 2002. Analogue modeling of fault reactivation: tectonic inversion and oblique remobilisation of grabens. *Journal of Structural Geology*, **24**, 1741–1752.

Dula, W.E., 1991. Geometric models of listric normal faults and rollovers. *American Association of Petroleum Geologists Bulletin*, **75**, 1609-1625.

Durcanin, M.A., 2009. Influence of synrift salt on rift-basin development: application to the Orpheus Basin, offshore Canada. Doctoral dissertation, The State University of New Jersey, New Jersey, United States of America.

Eisenstadt, G., Sims, D., 2005. Evaluating sand and clay models: do rheological differences matter?. *Journal of Structural Geology*, **27**, 1399**-**1412. Doi: 10.1016/j.jsg.2005.04.010

Eisenstadt, G., Withjack, M.O., 1995. Estimating inversion: results from clay models. In: Buchanan, J.G., Buchanan, P.G., (eds.). Basin inversion. *Geological Society of London, Special Publication*, **88**, 119–136.

Ellis, P.G., McClay, K.R., 1988. Listric extensional fault system-results of analogue model experiments. *Basin Research*, **1**, 55-70. Doi: 10.1111/j.1365-2117.1988.tb00005.x

Escosa, F.O., Roca, E., Ferrer, O., 2018. Testing thin-skinned inversion of a prerift saltbearing passive margin (Eastern Prebetic Zone, SE Iberia). *Journal of Structural Geology*, **109**, 55-73. Doi: 10.1016/j.jsg.2018.01.004

Etheve, N., Mohn, G., Frizon de Lamotte, D., Roca, E., Tugend, J., Gómez-Romeu, J., 2018. Extreme Mesozoic crustal thinning in the eastern Iberia margin: the example of the Columbrets Basin (Valencia Trough). *Tectonics*, **37**, 636–662. Doi: 10.1002/2017TC004613

Faure, J.L., Chermette, J.C., 1989. Deformation of tilted blocks, consequences on block geometry and extension measurements. *Bulletin de la Société géologique de France*, **8(3)**, 461-476.

Ferrer, O., Roca, E., Vendeville, B.C., 2008. Influence of a syntectonic viscous salt layer on the structural evolution of extensional kinked-fault systems. *Bollettino di Geofisica Teorica ed Applicata*, **49 (2)**, 371-375.

Ferrer, O., 2012. Salt tectonics in the Parentis Basin (Eastern Bay of Biscay): Origin and Kinematics of salt structures in a hyperextended margin affected by subsequent contractional deformation. Doctoral dissertation, Universitat de Barcelona, Barcelona, Spain.

Ferrer, O., Jackson, M.P.A., Roca, E., Rubinat, M., 2012. Evolution of salt structures during extension and inversion of the Offshore Parentis Basin (Eastern Bay of Biscay). In: Alsop, G.I., Archer, S.G., Hartley, A.J., Grant, N.T., Hodgkinson, R., (eds.), Salt Tectonics, Sediments and Prospectivity. *Geological Society of London, Special Publications*, **363**, 361-380. Doi: 10.1144/SP363.16

Ferrer, O., Roca, E., Vendeville, B.C., 2014. The role of salt layers in the hangingwall deformation of kinked-planar extensional faults. Insights from 3D analogue models and comparison with the Parentis Basin. *Tectonophysics*, **636**, 338-350. Doi: 10.1016/j.tecto.2014.09.013

Ferrer, O., McClay, K.R., Sellier, N.C., 2016. Influence of fault geometries and mechanical anisotropies on the growth and inversion of hangingwall synclinal basins: insights from sandbox models and natural examples. In: Child, C., Holdsworth, R.E., Jackson, C.A.L., Manzocchi, T., Walsh, J.J., Yieldings, G., (eds.) The Geometry and Growth of Normal Faults. *Geological Society of London, Special Publications,* **439**. Doi: 10.1144/SP439.8.

Ferrer, O., Gratacós, O., Roca, E., Muñoz, J.A., 2017. Modeling the interaction between presalt seamounts and gravitational failure in salt-bearing passive margins: The Messinian case in the northwestern Mediterranean Basin. *Interpretation*, **5(1)**, SD99-SD117. Doi: 10.1190/INT-2016-0096.1

Ferril, D.A., Morris, A.P., 1997. Geometric considerations of deformation above curved normal faults and salt evacuation surfaces. *The Leading Edge August*, 1129-1133.

Fossen, H., 2016. Structural geology. United Kingdom, Cambridge University Press.

García-Senz, J.M., 2002. Cuencas extensivas del Cretácico Inferior en los Pirineos centrales, formación y subsecuente inversión. Doctoral dissertation, Universitat de Barcelona, Barcelona, Spain.

Ge, H., Jackson, M.P.A., Vendeville, B.C., 1995. Extensional origin of breached Paradox Basin diapirs, Utah and Colorado: Field observations and scaled physical models. In: Huffman, A.C., Lund, W.R.Jr., Godwin, H.L. (eds.). Geology and resources of the Paradox basin: Salt Lake City, UT. *Utah Geological Association, Guidebook*, **25**, 285-293.

Ge, H., Jackson, M.P.A., Vendeville, B.C., 1997. Kinematics and dynamics of salt tectonics driven by progradation. *American Association of Petroleum Geologists Bulletin*, **81**, 398–423.

Gibbs, A.D., 1983. Balanced cross-section construction from seismic sections in areas of extensional tectonics. Journal of Structural Geology, **5(2)**, 153-160.

Gibbs, A.D., 1984. Structural evolution of extensional basin margins. *Geological Society of London Journal*, **141**, 609–620. Doi: 10.1144/gsjgs.141.4.0609

Glennie, K.W., 1995. Permian and Triassic rifting in northwest Europe. *Geological Society of London, Special Publications*, **91(1)**, 1–5. Doi: 10.1144/GSL.SP.1995.091.01.01

Goncharov, M.A., 2010. Applicability of similarity conditions to analogue modelling of tectonic structures. *Geodynamics & Tectonophysics*, **1(2)**, 148-168.

Gowers, M.B., Holtar, E., Swensson, E., 1993. The structure of the Norwegian Central Trough (Central Graben area). In: Parker, J.R. (ed.). Petroleum Geology of Northwest Europe: Proceedings of the 4th Conference. *Geological Society of London*, 1245–1254. Doi: 10.1144/0041245.

Gradmann, S., Beaumont, C., Albertz, M., 2009. Factors controlling the evolution of the Perdido Fold Belt, northwestern Gulf of Mexico, determined from numerical models. Tectonics, 28(2). Doi: 10.1029/2008TC002326

Granado, P., Ferrer, O., Muñoz, J.A., Thöny, W., Strauss, P., 2017. Basin inversion in tectonic wedges: Insights from analogue modelling and the Alpine-Carpathian fold-and-thrust belt. *Tectonophysics*, **703**, 50-68. Doi: 10.1016/j.tecto.2017.02.022

Graveleau, F., Malavieille, J., Dominguez, S., 2012. Experimental modelling of orogenic wedges: A review. Tectonophysics, 538, 1-66.

Groshong, R.H., 1989. Half-graben structures: balanced models of extensional fault-bend folds. *American Association of Petroleum Geologists Bulletin*, **101**, 96–105. Doi: 10.1130/0016-7606(1989)101<0096:HGSBMO>2.3.CO;2.

Groshong, R.H., Jr.C. Bond, A. Gibbs, R. Ratliff, and D. V. Wiltschko, 2012, Preface: Structural balancing at the start of the 21st century: 100 years since Chamberlin: Journal of Structural Geology, **41**, doi: 10.1016/j.jsg.2012.03.010.

Gowers, M.B., Holtar, E., Swensson, E., 1993. The structure of the Norwegian Central Trough (Central Graben area). In: Parker, J.R. (ed.). Petroleum Geology of Northwest Europe: Proceedings of the 4th Conference. *Geological Society of London*, 1245–1254. Doi: 10.1144/0041245.

Gudlaugsson, S.T., Faleide, J.I., Johansen, S.E., Breivik, A.J., 1998. Late Palaeozoic structural development of the south-western Barents Sea. *Marine and Petroleum Geology*, **15(1)**, 73-102.

Guimerà, J., Álvaro, M., 1990. Structure et évolution de la compression alpine dans le Chaîne Ibérique et la Chaîne Côtière Catalane (Espagne). *Bulletin de la Société géologique de France*, **8**, 339–348.

Guimerà, J., Alonso, Á., Mas, J.R., 1995. Inversion of an extensional-ramp basin by a newly formed thrust: the Cameros basin (N. Spain). *Geological Society of London, Special Publications*, **88(1)**, 433-453. Doi: 10.1144/GSL.SP.1995.088.01.23

Hafid, M., 2000. Triassic-early Jurassic extensional systems and their Tertiary inversion, Essaouira basin (Morocco). *Marine Petroleum Geology*, **17**, 409-429. Doi: 10.1016/S0264-8172(98)00081-6

Hammerstein, J., Truelove, L., McClay, K.R., 2014. Additional methods for the analysis of seismic data and risk reduction through the interpretation and reservoir modelling of scaled analogue models. Ideas and Innovation: Fuel for the Energy Capital. Annual Conference and Exhibition. American Association of Petroleum Geologists, Datapages/Search and Discovery Article #90189,lastaccessed:November2019,website: http://www.searchanddiscovery.com/abstracts/html/2014/90189ace/abstracts/1841538

Haugue, T.A., Gray, G.G., 1996. A critique of techniques for modelling normal-fault and rollover geometries. In: Buchaman, P.G., Nieuwland, D.A., (eds.). Modern Developments in Structural Interpretation, Validation and Modelling. *Geological Society of London, Special Publications*, **99**, 89-97.

Helgeson, D.E., 1999. Structural development and trap formation in the Central North Sea HP/HT play. *Geological Society of London, Petroleum Geology Conference series*, **5(1)**, 1029-1034. Doi: 10.1144/0051029

Horsfield, W.T., 1977. An experimental approach to basement controlled faulting: *Geologie en Mijnbouw*, **56**, 363-370.

Hubbert, M.K., 1937. Theory of scaled models as applied to the study of geological structures. *Geological Society of America Bulletin*, **48**, 1459-1520. Doi: 10.1130/GSAB-48-1459

Hubbert, M.K., 1951. Mechanical basis for certain familiar geologic structures. *Geological Society of America Bulletin*, **62**, 355–372.

Hudec, M.R., Jackson, M.P.A., 2007. Terra infirma: understanding salt tectonics. *Earth Science Reviews*, **82**, 1-28. Doi: 10.1016/j.earscirev.2007.01.001

Huiqi, L., McClay, K.R., Powell, D., 1992. Physical models of thrusts wedges. In: McClay, K.R., (ed.). Thrust Tectonics. London, Chapman and Hall, 71-81.

Jackson, M.P.A., Cramez, C., 1989. Seismic recognition of salt welds in salt tectonics regimes. Gulf of Mexico salt tectonics, associated processes and exploration potential. 10th annual research conference program and abstracts. Society of Economic Paleontologists and Mineralogists Gulf Coast Section, 66-71.

Jackson, M.P.A., Vendeville, B.C., 1994. Regional extension as a geologic trigger for diapirism. *Geological society of America bulletin*, **106(1)**, 57-73. Doi: 10.1130/0016-7606(1994)106<0057:REAAGT>2.3.CO;2

Jackson, M.P.A., Vendeville, B.C., Schultz-Ela, D.D., 1994. Structural dynamics of salt systems. *Annual Review of Earth and Planetary Sciences*, **22**, 93-117.

Jackson, M.P.A., Cramez, C., Fonck, J.M., 2000. Role of subaerial volcanic rocks and mantle plumes in creation of South Atlantic margins: implications for salt tectonics and source rocks. *Marine and Petroleum Geology*, **17(4)**, 477-498. Doi: 10.1016/S0264-8172(00)00006-4

Jackson, M.P.A., Hudec, M.R., 2005. Stratigraphic record of translation down ramps in a passive-margin salt detachment. *Journal of Structural Geology*, 27, 889-911. Doi: 10.1016/j.jsg.2005.01.010

Jackson, M.P.A., Hudec, M.R., 2017. Salt Tectonics: Principles and Practice. Cambridge, Cambridge University Press.

Jagger, L.J., McClay, K.R., 2016. Analogue modelling of inverted domino-style basement fault systems. *Basin Research*, **30**, 363-381. Doi:10.1111/bre.12224

Kehle, R.O., 1988. The origin of salt structures. In: Schreiber, B.C., (ed.). Evaporites and Hydrocarbons. Columbia University Press, 345-403.

Keppler, R., Rosas, F.M., Nagel, T.J., 2013. Thin viscous middle-crust and evolving fault distribution during continental rifting: insights from analog modeling experiments. *Tectonophysics*, **608**, 161-175. Doi; 10.1016/j.tecto.2013.10.001.

Khalil, S.M., McClay, K.R., 2002. Extensional fault-related folding, northwestern Red Sea, Egypt. *Journal of Structural Geology*, **24(4)**, 743-762. Doi: 10.1016/S0191-8141(01)00118-3

Konstantinovskaia, E., Malavielle, J., 2005. Erosion and exhumation in acreationary orogens. Experimental and geological approaches. *Geochemistry, Geophysics and Geosystems*, **6(2)**, 1-25. Doi: 10.1029/2004GC000794

Konstantinovskaya, E.A., Harris, L.B., Poulin, J., Ivanov, G.M., 2007. Transfer zones and fault reactivation in inverted rift basins: insights from physical modelling. *Tectonophysics*, **441**, 1–26.

Koyi, H., 1997. Analogue modelling; from a qualitative to a quantitative technique, a historical outline. *Journal of Petroleum Geology*, 20, 233–238.

Koyi, H., Jenyon, M.K., Petersen, K., 1993. The effect of basement faulting on diapirism. *Journal of Petroleum Geology*, **16(3)**, 285-312.

Koyi, H., Petersen, K., 1993. Influence of basement faults on the development of salt structures in the Danish Basin. *Marine and Petroleum Geology*, **10(2)**, 82-94. Doi: 10.1016/0264-8172(93)90015K

Koyi, H., 2000. Towards Dynamic Restoration of Geologic Profiles: Some Lessons from Analogue Modelling. In Mohriak, W., Taiwani, M., (eds.). Atlantic Rifts and Continental Margins. *American Geophysical Union, Geophysical Monograph Series*, **115**, 317–329. Doi: 10.1029/GM115p0317doi: 10.1029/GM115p0317.

Koyi, H., Sans, M., 2006. Deformation transfer in viscous detachments: Comparison of sandbox models to the South Pyrenean Triangle Zone. *Geological Society of London, Special Publications*, **253(1)**, 117-134. Doi: 10.1144/GSL.SP.2006.253.01.06

Kruger, J.M., Johnson, R.A., 1994. Raft model of crustal extension: Evidence from seismic reflection data in southeast Arizona. *Geology*, **22(4)**, 351-354.

Krzywiec, P., 2004. Triassic evolution of the Kłodawa salt structure: basement-controlled salt tectonics within the Mid-Polish Trough (Central Poland). *Geological Quarterly*, **48(2)**, 123-134.

Letouzey, J., Colletta, B., Vially, R., Chermette, J.C., 1995. Evolution of Salt-Related Structures in Compressional Settings. In: Jackson, M.P.A., Roberts, D.G., Snelson, S., (eds.). Salt Tectonics: a global perspective. *American Association of Petroleum Geologists Memoir*, **65**, 41-60.

Letouzey, J., Sherkati, S., 2004. Salt Movement, Tectonic Events, and Structural Style in the Central Zagros Fold and Thrust Belt (Iran). Salt-sediments interactions and hydrocarbon prospectivity: Concepts, applications, and case studies for the 21st century. 24th annual research conference program and abstracts. Society of Economic Paleontologist and Mineralogist Gulf Coast Section, 753-778.

Lewis, M.M., Jackson, C.A.L., Gawthorpe, R.L., 2013. Salt-influences normal fault growth and forced folding: The Stavenger Fault System, North Sea. *Journal of structural geology*, **54**, 156-173. Doi: 10.1016/j.jsg.2013.07.015

Lingrey, S., Vidal-Royo, O., 2015. Evaluating the quality of bed length and area balance in 2D structural restorations. *Interpretation*, **3(4)**. Doi: 10.1190/INT-2015-0126.1

Liu, H., McClay, K.R., Powell, D., 1992. Physical models of thrust wedges. In: McClay, K.R., (ed.). Thrust Tectonics. London, Chapman and Hall, 71–81.

Luján, M., Storti, F., Balanyá, J-C., Crespo-Blanc, A., Rossetti, F., 2003. Role of décollement material with different rheological properties in the structure of the Aljibe thrust imbricate (Flysch Trough, Gibraltar Arc): an analogue modelling approach. *Journal of structural geology*, **25**, 867-881.

Mandl, G., De Jong, L.N.J., Maltha, A., 1977. Shear zones in granular material. *Rock Mechanics*, **9**, 98–144.

Marin, M., Schenk, O., Roca, E., Ferrer, O., Roma, M., Cabrera, L., 2019. Thermal modeling and maturity assessment of the Columbrets Basin (south Valencia Trough, Western Mediterranean). EGU General Assembly 2019 -10556. SSP2.14 - New frontiers in thermal evolution of sedimentary basins: tools and applications. Abstract for a poster session. https://meetingorganizer.copernicus.org/EGU2019/EGU2019-10556.pdf

Martín, P., Suriñach, E., 1988. Estructura de la corteza en la zona entre Ibiza y Castellón. Primeros resultados. In: C.I.R.I.T., (ed.). Xarxes sísmiques. Instrumentació i aplicació a la sismotectònica, Barcelona, 521–537.

Mathieu, C., 1986. Histoire géologique du sous-bassin de Parentis. *Bulletin des Centres Recherche Exploration-Production Elf-Aquitaine*, **10**, 22-47.

McClay, K.R., 1989. Analogue models of inversion tectonics. *Geological Society of London, Special Publications*, **44(1)**, 41-59. Doi: 10.1144/GSL.SP.1989.044.01.04

McClay, K.R., 1990. Extensional fault systems in sedimentary basins: a review of analogue model studies. *Marine and petroleum Geology*, **7(3)**, 206-233. Doi: 10.1016/0264-8172(90)90001-W

McClay, K.R., 1995. The geometries and kinematics of inverted fault systems: a review of analogue models studies. In: Buchanan, J.G., Buchanan, P.G., (eds.). Basin Inversion. *Geological Society of London, Special Publications*, **88**, 97-118. Doi: 10.1144/GSL.SP.1995.088.01.07

McClay, K.R., 1996. Recent advances in analogue modelling: uses in section interpretation and validation. In: Buchanan, P.G., Nieuwland, D.A., (eds.). Modern Developments in Structural Interpretaion, Validation and Modelling. *Geological Society of London, Special Publications*, **99**, 201-225.

McClay, K.R., Eillis, P.G., 1987a. Geometries of extensional fault systems developed in model experiments. *Geology*, **1**, 341-344

McClay, K.R., Eillis, P.G., 1987b. Analogue models of extensional fault geometries. In: Coward, M.R., Dewey, J.E., Hancock, R.L., (eds.). Continental Extension Tectonics. *Geological Society of London, Special Publications*, **28**, 109-125.

McClay, K.R., Scott, A.D., 1991. Experimental models of hangingwall deformation in ramp-flat listric extensional fault systems. *Tectonophysics*, **188**, 85–96. Doi: 10.1016/0040-1951(91)90316-K.

McClay, K.R., Buchanan, P.G., 1992. Thrust faults in inverted extensional basin. In: McClay, K.R., (ed.). Thrust Tectonics. London, Chapman and Hall, 93–104.

McClay, K.R., White, M.J., 1995. Analogue modelling of orthogonal and oblique rifting. *Marine and Petroleum Geology*, **12**, 137–151.

McClay, K.R., Dooley, T., Whitehouse, P., Mills, M., 2002. 4-D evolution of rift systems: Insights from scaled physical models. *American Association of Petroleum Geologists Bulletin*, **86**, 935–959.

McDonnell, A., Jackson, M.P.A., Hudec, M.R., 2010. Origin of transverse folds in an extensional growth-fault setting: Evidence from an extensive seismic volume in the western Gulf of Mexico. *Marine and Petroleum Geology*, **27(7)**, 1494-1507. Doi: 10.1016/j.marpetgeo.2010.03.006

Medwedeff, D.A., Suppe, J., 1997. Multibend fault-bend folding. *Journal of Structural Geology*, **19**, 279–292. Doi: 10.1016/S0191-8141(97)83026-X.

Mencos, J., 2010. Metodologies de reconstrucció i modelització 3D d'estructures geològiques: anticlinal de Sant Corneli - Bóixols (Pirineus centrals). Doctoral dissertation, Universitat de Barcelona, Barcelona, Spain.

Mencos, J., Carrera, N., Muñoz, J.A., 2015. Influence of rift basin geometry on the subsequent postrift sedimentation and basin inversion: the Organyà Basin and the Bóixols thrust sheet (south central Pyrenees). *Tectonics*, **34(7)**, 1452–1474. Doi: 10.1002/2014TC003692.

Mitra, S., 1993. Geometry and kinematic evolution of inversion structures. *American Association of Petroleum Geologists Bulletin,* **77**, 1159–1191.

Mitra, S., 2002. Fold-accommodation faults. *American Association of Petroleum Geologists Bulletin*, **86(4)**, 671–693.

Mitra, S., Islam, Q.T., 1994. Experimental (clay) models of inversion structures. *Tectonophysics*, **230**, 211–222.

Muñoz, J.A., 1992, Evolution of a continental collision belt: ECORS-Pyrenees crustal balanced cross-section. In McClay, K.R., (ed.). Thrust tectonics. New York, Chapman and Hall, 235–246.

Nalpas, T., Brun, J.P., 1993. Salt flow and diapirism related to extension at crustal scale. *Tectonophysics*, **228**, 349-362. Doi: 10.1016/0040-1951(93)90348-N

Nalpas, T., Le Douran, S., Brun, J.O., Untrnehr, P., Richert, J.P., 1995. Inversion of the Broad Fourteens Basin (offshore Netherlands), a small-scale model investigation. *Sedimentary Geology*, **95**, 237-250. Doi: 10.1016/0037-0738(94)00113-9

Nebot, M., 2016. Mesozoic extension and Cenozoic contraction in the Eastern Iberian Chain (Maestrat Basin). Doctoral dissertation, Universitat de Barcelona, Barcelona, Spain.

Nilsen, K.T., Vendeville, B.C., Johansen, J.-T., 1995. Influence of regional tectonics on halokinesis in the Nordkapp Basin, Barents Sea. In: Jackson, M.P.A., Roberts, D.G., Snelson, S., (eds.). Salt tectonics: a global perspective. *American Association of Petroleum Geologists Memoir*, **65**, 413-436.

Ori, G.G., Friend, P.F., 1984. Sedimentary basins formed and carried piggyback on active thrust sheets. *Geology*, **12(8)**, 475-478. Doi: 10.1130/0091-7613(1984)12<475:SBFACP>2.0.CO;2

Osmundsen, P.T., Bakke, B., Svendby, A.K., Andersen, T.B., 2000. Architecture of the Middle Devonian Kvamshesten Group, western Norway: sedimentary response to deformation above a ramp-flat extensional fault. In: Friend, P.F., Williams, B.P.J., (eds.). New Perspectives on the Old Red Sandstone. *Geological Society of London, Special Publications*, **180**, 503–535.

Osmundsen, P.T., Sommaruga, A., Skilbrei, J.R., Olesen, O., 2002. Deep structure of the Mid Norway rifted margin. *Norwegian Journal of Geology/Norsk Geologisk Forening*, **82(4)**.

Pascal, G., Torne, M., Buhl, P., Watts, A.B., Mauffret, A., 1992. Crustal and velocity structure of the Valencia trough (western Mediterranean), part II: detailed interpretation of five expanded spread profiles. *Tectonophysics*, **203,** 21–35. Doi: 10.1016/0040-1951(92)90213-P

Pascoe, R., Hooper, R., Storhaug, K., Harper, H., 1999. Evolution of extensional styles at the southern termination of the Nordland Ridge, Mid-Norway: a response to variations in coupling above Triassic salt. In: Fleet, A.J., Boldy, S.A.R., (eds.). Petroleum Geology of northwest Europe: Proceeding of the 5th Conference. *Geological Society of London*, **5**, 83-90.

Patton, T.L., 2005. Sandbox models of downward-steepening normal faults. *American Association of Petroleum Geologists Bulletin*, **89(6)**, 781-797.

Peel, F., Jackson, M., Ormerod, D., 1998. Influence of major steps in the base of salt on the structural style of overlying thin-skinned structures in deep water Angola. International Conference and Exhibition. American Association of Petroleum Geologists, extended abstracts volume, 366–367.

Pichel, L.M., Peel, F., Jackson, C.A., Huuse, M., 2018. Geometry and kinematics of salt-detached ramp syncline basins. *Journal of Structural Geology*, **115,** 208-230.

Pichot, T., Nalpas, T., 2009. Influence of synkinematic sedimentation in a thrust system with two decollement levels; analogue modelling. *Tectonophysics*, **206(2-3)**, 371-388.

Pinto, L., Muñoz, C., Nalpas, T., Charrier, R., 2010. Role of sedimentation during basin inversión in analogue modelling. *Journal of Structural Geology*, **32**, 554–565.

Pla, O., Roca, E., Xie, H., Izquierdo-Llavall, E., Muñoz, J.A., Rowan, M.G., Ferrer, O., Gratacós, O., Yuan, N., Huang, S., 2019. Influence of Syntectonic Sedimentation and Décollement Rheology on the Geometry and Evolution of Orogenic Wedges: Analog Modeling of the Kuqa Fold-and-Thrust Belt (NW China). *Tectonics*, **38(8)**. Doi: 10.1029/2018TC005386

Ramberg, H., 1967. Model experimentation of the effect of gravity on tectonic processes. *Geophysical Journal International*, **14(1-4)**, 307–329.

Rasmussen, E.S., Lomholt, S., Andersen, C., Vejbæk, O.V., 1998. Aspects of the structural evolution of the Lusitanian Basin in Portugal and the shelf and slope area offshore Portugal. *Tectonophysics*, **300(1)**, 199-225. Doi: 10.1016/S0040-1951(98)00241-8

Remmelts, G., 1995. Fault-related salt tectonics in the Southern North Sea, the Netherlands. In: Jackson, M.P.A., Roberts, D.G., Snelson, S., (eds.). Salt Tectonics: A Global Perspective. *American Association of Petroleum Geologists Memoir*, **65**, 261-272.

Richardson, N.J., Underhill, J.R., Lewis, G., 2005. The role of evaporite mobility in modifying subsidence patterns during normal fault growth and linkage, Halten Terrace, Mid-Norway. *Basin Research*, **17(2)**, 203-223. Doi: 10.1111/j.1365-2117.2005.00250.x

Roca, E., 1996. La Cubeta mesozoica de las Columbrets: aportaciones al conocimiento de la estructura del surco de Valencia*. Geogaceta*, **20(7)**, 1711–1714.

Roca, E., 2001. The Northwest Mediterranean Basin (Valencia Trough, Gulf of Lions and Liguro-Provençal basins): structure and geodynamic evolution. In: Ziegler, P.A., Cavazza, W., Robertson, A.H.F., Crasquin-Soleau, S., (eds.). Peri-Thetys Memoir 6: Peri-Tethyan Rift/wrench Basins and Passive Margins. *Mémoires du Muséum National d'Histoire Naturelle*, **186**, 671 706.

Roca, E., Guimerà, J., Salas, R., 1994. Mesozoic extensional tectonics in the southeast Iberian Chain. *Geological Magazine*, **131(2)**, 155–168. Doi: 10.1017/S0016756800010694.

Roca, E., Muñoz, J.A., Ferrer, O., Ellouz, N., 2011. The role of the Bay of Biscay Mesozoic extensional structure in the configuration of the Pyrenean orogen: Constraints from the MARCONI deep seismic reflection survey. *Tectonics*, **30(2)**.

Roma, M., Ferrer, O., Roca, E., Pla, O., Escosa, F.O., Butillé, M., 2018a. Formation and inversion of salt-detached ramp-syncline basins. Results from analog modeling and application to the Columbrets Basin (Western Mediterranean). *Tectonophysics*, **745**, 214-228. Doi:10.1016/j.tecto.2018.08.012

Roma, M., Vidal-Royo, O., McClay, K.R., Ferrer, O., Muñoz, J.A., 2018b. Tectonic inversion of salt-detached ramp-syncline basins as illustrated by analog modeling and kinematic restoration. *Interpretation,* **6(1),** 127–144. Doi: 10.1190/int-2017-0073.1.

Roma, M., Ferrer, O., McClay, K.R., Muñoz, J.A., Roca, E., Gratacós, O., Cabello, P., 2018c. Weld kinematics of syn-rift salt during basement-involved extension and subsequent inversion: Results from analog models. *Geologica Acta*, **16(4)**, 391-410. Doi: 10.1344/GeologicaActa2018.16.4.4

Rossi, D., Storti, F., 2003. New artificial granular materials for analogue laboratory experiments: aluminium and siliceous microspheres. *Journal of Structural Geology*, **25**, 1893–1899.

Roure, F., Brun, J.O., Colletta, B., Van Den Driessche, J., 1992. Geometry and kinematics of extensional structures in the Alpine foreland basin of southeastern France. *Journal of Structural Geology*, **14(5)**, 503-519. Doi: 10.1016/0191-8141(92)90153-N

Roure, F., Colletta, B., 1996. Cenozoic inversion structures in the foreland of the Pyrenees and Alps. *Mémoires du Muséum national d'histoire naturelle*, **170**, 173-209.

Rowan, M.G., Jackson, M.P.A., Trudgill, B.D., 1999. Salt-related fault families and fault welds in the northern Gulf of Mexico. *American Association of Petroleum Geologists Bulletin*, **83(9)**, 1454-1484.

Rowan, M.G., Trudgill, B.D., Fiduk, J.C., 2000. Deep-water, salt-cored foldbelts: Lessons from Mississippi fan and Perdido foldbelts; northen Gulf of Mexico. In: Mohriak, W., Talwani, M., (eds.). Atlantic rifts and continental margins, Washington D.C., *American Geophysical Union, Geophysical Monograph*, **115**, 173-191.

Rowan, M.G., 2002. Salt-related accommodation in the Gulf of Mexico deepwater: Withdrawal or inflation, autochthonous or allochthonous?. *American Association of Petroleum Geologists Datapages, Gulf Coast Association of Geological Societies Transactions*, **52**, 861-869.

Rowan, M.G., Peel, F.J., Vendeville, B.C., 2004. Gravity-driven fold belts on passive margins. In: McClay, K.R., (ed.). Thrust Tectonics and Hydrocarbon Systems. *American Association of Petroleum Geologists Memoir*, 82, 157–182.

Rowan, M.G., Vendeville, B.C., 2006. Foldbelts with early salt withdrawal and diapirism: physical model and examples from the northern Gulf of Mexico and the Flinders Ranges, Australia. *Marine and Petroleum Geology*, **23(9)**, 871-891. Doi: 10.1016/j.marpetgeo.2006.08.003

Rowan, M.G., 2014. Passive-margin salt basins: hyperextension, evaporite deposition, and salt tectonics. *Basin Research*, **26**, 154-182. Doi: 10.1111/bre.12043

Sanchis, E., Séranne, M., 2000. Structural style and tectonic evolution of a polyphase extensional basin of the Gulf of Lion passive margin: the Tertiary Ales basin, southern France. *Tectonophysics*, **322(3)**, 219-242. Doi: 10.1016/S0040-1951(00)00097-4

Schellart, W.P., 2000. Shear test results for cohesion and friction coefficients for different granular materials: scaling implications for their usage in analogue modeling. *Tectonophysics*, **324**, 1-16. Doi: 10.1016/S0040-1951(00)00111-6

Schettino, A., Turco, E., 2010. Tectonic history of the western Thetys since the Late Triassic. *Geological Society of America Bulletin*, **123**, 89–105. Doi: 10.1130/B30064.1.

Schlische, R.W., 1992. Structural and stratigraphic development of the Newark extensional basin, eastern North America: implications for the growth of the basin and its bounding structures. *Geological Society of America Bulletin*, **104**, 1246–1263.

Scholz, C.H., 1990. The mechanics of earthquakes and faulting. New York, Cambridge University Press.

Schreurs, G., Buiter, S.J.H., Corti, G., Costa, E., Hoth, S., Koyi, H., Kukowski, N., Lohrmann, J., Schlische, R.W., Withjack, M., Boutelier, D., Cavozzi, C., Cruden, A., Daniel, J.-M., Del Ventisette, C., Elder Brady, J.A., Hoffmann-Rothe, A., Mengus, J.-M., Montanari, D., Nilforoushan, F., Ravaglia, A., Yamada, Y., 2006. Analogue benchmarks of shortening and extension experiments. In: Buiter, S.J.H., Schreurs, G., (eds.). Analogue and Numerical Modelling of Crustal-Scale Processes. *Geological Society of London, Special Publications*, **253**, 1–27.

Séranne, M., Benedicto, A., Truffert, C., Pascal, G., Labaume, P., 1995. Structural style and evolution of the Gulf of Lion Oligo-Miocene rifting: Role of the Pyrenean orogeny. *Marine and Petroleum Geology, Special issue IBS*, **12**.

Shannon, P.M., McDonnell, A., Bailey, W.R., 2007. The evolution of the Porcupine and Rockall basins, offshore Ireland: the geological template for carbonate mound development. *International Journal of Earth Sciences*, **96(1)**, 21-35.

Sharp, I.R., Gawthorpe, R.L., Underhill, J.R., Gupta, S., 2000. Fault-propagation folding in extensional settings: Examples of structural style and synrift sedimentary response from the Suez rift, Sinai, Egypt. Geological Society of America Bulletin, 112(12), 1877–1899. Doi:10.1130/0016-7606(2000)112<1877:fpfies>2.0.co;2

Sibson, R.H., 1977. Fault rocks and fault mechanisms. *Geological Society of London*, **133(3)**, 191-213.

Soto, R., Casas-Sainz, M., Del Río, P., 2007. Geometry of half-grabens containing a mid-level viscous décollement. *Basin Research*, **19**, 437-450. Doi: 10.1111/j.1365-2117.2007.00328.x

Stewart, S.A., Clark, J.A., 1999. Impact of salt on the structure of the Central North Sea hydrocarbon fairways. *Geological Society of London*, *Petroleum Geology Conference series,* **5**, 179-200. Doi: 10.1144/0050179

Stewart, S.A., Harvey, M.J., Otto, S.C., Weston, P.J., 1996. Influence of salt on fault geometry: examples from the UK salt basins. *Geological Society of London, Special Publications*, **100(1)**, 175-202. Doi: 10.1144/GSL.SP.1996.100.01.12

Storti, F., McClay, K., 1995. Influence of syntectonic sedimentation on thrust wedges in analogue models. *Geology*, **11**, 999–1002.

Suppe, J., 1983. Geometry and kinematics of fault bend folding. *American Journal of Science*, **283**, 684–721.

Tankard, A.J., Welsink, H.J., Jenkins, W.A.M., 1989. Structural styles and stratigraphy of the Jeanne d'Arc Basin, Grand Banks of Newfoundland. Extensional tectonics and stratigraphy of the North Atlantic margins. *American Association of Petroleum Geologists Memoir*, **46**, 265-282.

Tavani, S., Storti, F., Salvini, F., 2005. Rounding hinges to fault-bend folding: geometric and kinematic implications. *Journal of Structural Geology*, **27**, 3–22. Doi: 10.1016/j.jsg.2004.07.005.

Torne, M., Pascal, G., Buhl, P., Watts, A.B., Mauffret, A., 1992. Crustal and velocity structure of the Valencia trough (western Mediterranean), part I. A combined refraction/wide angle reflection and near-vertical reflection study. *Tectonophysics*, **203**, 1–20. Doi: 10.1016/0040-1951(92)90212-O

Vendeville, B., 1987. Champs de failles et tectonique en extension: modélisation expérimentale. Doctoral dissertation, Université de Rennes 1, Rennes, France.

Vendeville, B.C., Jackson, M.P.A., 1992. The rise of diapirs during thin-skinned extension. *Marine and Petroleum Geology*, **9**, 331–353. Doi: 10.1016/0264-8172(92)90047-I

Vendeville, B.C., Nilsen, K.T., 1995. Episodic growth of salt diapirs driven by horizontal shortening. Salt, sediment, and hydrocarbons. 16th annual research conference program and abstracts. Society of Economic Paleontologist and Mineralogist Gulf Coast Section, 285-295.

Vendeville, B.C., Ge, H., Jackson, M.P.A., 1995. Scale models of salt tectonics during basement-involved extension. *Petroleum Geoscience*, **1(2)**, 179-183. Doi: 10.1144/petgeo.1.2.179

Vetti, V.V., Fossen, H., 2012. Origin of contrasting Devonian supradetachment basin types in the Scandinavian Caledonides. *Geology*, **40(6)**, 571-574.

Vidal, N., Gallart, J., Dañobeitia, J.J., 1998. A deep seismic crustal transect from the NE Iberian Peninsula to the western Mediterranean. *Journal of Geophysical Research-Solid Earth*, **103**, 12381–12396. Doi: 10.1029/98JB00076.

Weijermars, R., 1986. Flow behaviour and physical chemistry of bouncing putties and related polymers in view of tectonic laboratory applications. *Tectonophysics*, **123**, 325-358. Doi: 10.1016/0040-1951(86)90208-8

Weijermars, R., Jackson, M.P.A., Vendeville, B.C., 1993. Rheological and tectonic modeling of salt provinces. *Tectonophysics*, **217**, 143–174

Wernicke, B., 1985. Uniform-sense normal simple shear of the continental lithosphere. *Canadian Journal of Earth Sciences*, **22**, 108–125.

Wernicke, B., Burchfiel, B.C., 1982. Modes of extensional tectonics. *Journal of Structural Geology*, **4(2)**, 105-115.

Wernicke, B., Axen, G.J., 1988. On the role of isostasy in the evolution of normal fault systems. *Geology*, **16(9)**, 848-851.

Williams, G., Vann, I., 1987. The geometry of listric normal faults and deformation in their hanging walls. *Journal of Structural Geology*, **9(7)**, 789-795.

Withjack, M.O., Olson, J., Peterson, E., 1990. Experimental models of extensional forced folds. *American Association of Petroleum Geologists Bulletin*, **74**, 1038-1054.

Withjack, M.O., Islam, Q.T., La Pointe, P.R., 1995. Normal faults and their hanging wall deformation; an experimental study. *American Association of Petroleum Geologists Bulletin*,**79(1)**, 1-18.

Withjack, M.O., Callaway, S., 2000. Active normal faulting beneath a salt layer: an experimental study of deformation patterns in the cover sequence. *American Association of Petroleum Geologists Bulletin*, **84(5)**, 627-651.

Withjack, M.O., Schlische, R.W., Olsen, P.E., 2002. Rift-basin Structure and Its Influence on Sedimentary Systems. *American Association of Petroleum Geologists, Special Publication of SEPM*, **73**. 57–81.

Withjack, M.O., Schlische, R.W., 2005. A review of tectonic events on the passive margin of eastern North America. Petroleum Systems of Divergent Continental Margin Basins. 25th annual research conference program and abstracts. Society of Economic Paleontologist and Mineralogist Gulf Coast Section, 203–235.

Withjack, M.O., Schlische, R.W., 2006. Geometric and experimental models of extensional fault-bend folds. In: Buiter, S.J.H., Schreurs, G. (eds.). Analogue and Numerical Modelling of Crustal-scale Processes. *Geological Society of London, Special Publications*, **235**, 208–305. Doi: 10.1144/GSL.SP.2006.253.01.15.

Xiao, H., Suppe, J., 1989. Role of compaction in listric shape of growth normal faults. *American Association of Petroleum Geologists Bulletin,* **73**, 777-786.

Xiao, H., Suppe, J., 1992. Origin of rollover. *American Association of Petroleum Geologists Bulletin*, **76(4)**, 509–529.

Yamada, Y., McClay, K.R., 2003a. Application of geometric models to inverted listric fault systems in sandbox experiments. Paper 1: 2D hanging wall deformation and section restoration. *Journal of Structural Geology*, **25(9)**, 1551-1560. Doi: 10.1016/S0191-8141(02)00181-5

Yamada, Y., McClay, K.R., 2003b. Application of geometric models to inverted listric fault systems in sandbox experiments. Paper 1: 2D hanging wall deformation and section restoration. *Journal of Structural Geology*, **25(8)**, 1331-1336. Doi:10.1016/S0191-8141(02)00160-8

Yamada, Y., McClay, K.R., 2004. 3-D Analog modeling of inversion thrust structures. In: McClay, K.R., (ed.). Thrust tectonics and hydrocarbon systems. *American Association of Petroleum Geologists Memoir,* **82**, 276– 301.

Zeyen, H.J., Banda, E., Gallart, J., Ansorge, J., 1985. A wide angle seismic reconnaissance survey of the crust and upper mantle in the Celtiberian Chain of eastern Spain. *Earth and Planetary Science Letters,* **75**, 393–402. Doi: 10.1016/0012-821X(85)90182-7

Ziegler, P.A., 1988. Evolution of the Arctic-North Atlantic and the Western Tethys: A visual presentation of a series of paleogeographic-paleotectonic maps. *American Association of Petroleum Geologists Memoir*, **43**, 164-196.

APPENDIX

APPENDIX I

Formation and inversion of salt-detached ramp-syncline basins. Results from analog modeling and application to the Columbrets Basin (Western Mediterranean)

Roma, M., E. Roca, O. Ferrer, O. Pla and M. Butillé, 2018a. Tectonophysics. 745, 214-228, doi: 10.1016/j.tecto.2018.08.012

Tectonophysics 745 (2018) 214–228

Contents lists available at ScienceDirect

Tectonophysics

journal homepage: www.elsevier.com/locate/tecto

Formation and inversion of salt-detached ramp-syncline basins. Results from analog modeling and application to the Columbrets Basin (Western Mediterranean)

Maria Roma*, Oriol Ferrer, Eduard Roca, Oriol Pla, Frederic O. Escosa, Mireia Butillé

GEOMODELS Research Institute, Grup de Geodinàmica i Anàlisi de Conques, Departament de Dinàmica de la Terra i de l'Oceà, Facultat de Ciències de la Terra, Universitat de Barcelona, C/ Martí i Franquès s/n, 08028 Barcelona, Spain

ARTICLE INFO

Keywords:
Salt-detached ramp-syncline basins
Tectonic inversion
Salt tectonics
Analog modeling
Western Mediterranean

ABSTRACT

The widespread extensional deformation that took place during Jurassic to Cretaceous times in Western Europe and the North Atlantic margin resulted in the formation of several rift systems. Some of the resulting basins associated with these rifts show broad synclines detached on pre- or syn-kinematic Permian or Triassic salts, and are filled by thick sedimentary successions. The development of these salt-detached ramp-syncline basins has been associated to the extensional motion of ramp/flat extensional sub-salt faults. The shape and kinematics of such faults have usually been established using the architecture of syn-kinematic units and by assuming complete coupling of the hanging wall rocks. Therefore, there are fault interpretations that do not consider the role played by the deep salt layers, which clearly act as an effective detachment, decoupling sub- and supra-salt deformations. Moreover, the complexity of these scenarios further increases due to some of these basins, which, during latest Cretaceous and Cenozoic times, were partially inverted and were often incorporated into fold-and-thrust belts.

Based on analog models and using the Mesozoic Columbrets Basin (Western Mediterranean) as a case study, the aim of this research is: to decipher the influence of the ramp/flat extensional fault during the syncline development and the interaction with a pre-kinematic salt; and to infer how salt-detached ramp-syncline basins are subsequently inverted.

To achieve this goal we carried out an experimental program consisting of eight different sandbox models. Our results show that the main structure formed at the end of the extension is a salt-detached ramp-syncline and that its geometry not only depends on the dip and length of the fault panels, but also on the fault displacement and salt thickness. The inversion of these salt-detached ramp-synclines resulted in a major thick-skinned fault-bend anticline with minor thin-skinned contractional structures.

1. Introduction

The presence of broad synclinal basins is relatively common in Western Europe and the Central and North Atlantic margins (e.g., Jeanne d'Arc, Matalles, Parentis, Orpheus or Cameros basins) (Fig. 1). These extensional basins are characterized as not being bounded by major faults, and by usually being detached on pre- or syn-extension evaporite units (Permian Zechtein or Upper Triassic Keuper salt; Coward and Stewart, 1995; Clark et al., 1998; Rank-Friend and Elders, 2004; Salvany and Bastida, 2004; Ferrer et al., 2012; Ortí et al., 2017). In some cases these basins have subsequently been partially-to-totally inverted (e.g., Orpheus; Withjack and Schlische, 2005) (Fig. 1d) or the Columbrets basins (Roca, 2001), even incorporated into fold-and-thrust belts (e.g., Organyà-Central Pyrenees; Mencos et al., 2015), or the Cameros basins (Guimerà et al., 1995) (Fig. 1e).

The mechanisms proposed to explain the formation of synclinal basins have been described as extensional fault-bend folding associated with ramp/flat extensional faults, developing ramp-syncline basins with an asymmetric depocenter growth axial trace (Fig. 2a; Gibbs, 1984; Groshong, 1989; McClay and Scott, 1991; Benedicto et al., 1999; Sanchis and Séranne, 2000). But when the system includes a salt layer, an extensional forced fold is associated with the ramp/flat extensional fault and a salt layer accommodates the difference in geometry (Jackson and Hudec, 2005; Soto et al., 2007; Ferrer et al., 2016), thus

Abbreviations: EBPS, End of Basal Plastic Sheet

* Corresponding author.
E-mail address: mariaroma@ub.edu (M. Roma).

https://doi.org/10.1016/j.tecto.2018.08.012
Received 7 January 2018; Received in revised form 15 August 2018; Accepted 16 August 2018
Available online 25 August 2018

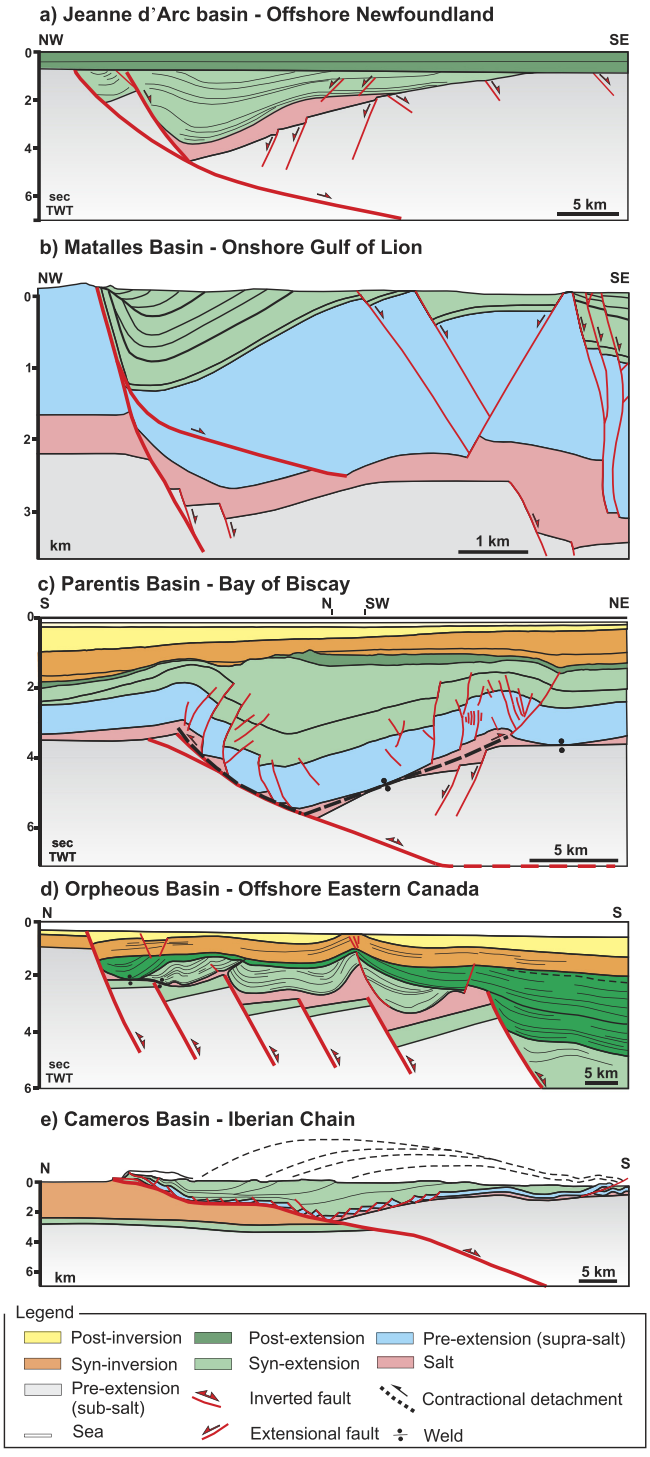

Fig. 1. Natural examples of salt-detached ramp-syncline basins with different degrees of tectonic inversion. a) Line drawing of time-migrated seismic section of non-inverted Jeanne d' Arc Basin (offshore Newfoundland), modified from Withjack and Callaway (2000); b) Cross-section of the non-inverted Matalles Basin (onshore Gulf of Lion), modified from Benedicto et al. (1999); c) Interpreted line drawing of a composite 2D seismic profile from the eastern Parentis Basin (Bay of Biscay) showing the main features of this moderately inverted basin, modified from Ferrer et al. (2012); d) Line drawing from a seismic profile of the inverted Orpheus Basin (offshore eastern Canada), modified from Durcanin (2009); e) Cross-section of the strongly-inverted Cameros Basin (Iberian chain, northern Spain), modified from Soto et al. (2007).

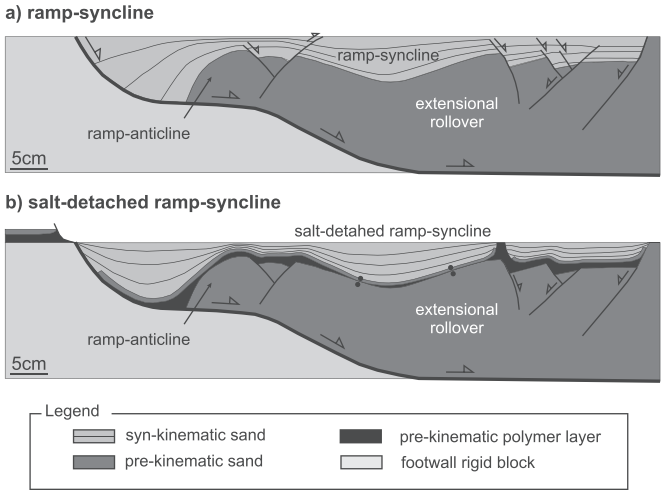

Fig. 2. Simplified cross-sections of sandbox models illustrating the geometries resulting from: a) ramp-syncline developed above a ramp-flat-ramp listric fault in an isotropic sand model (modified from McClay and Scott (1991)); and b) salt-detached ramp-syncline basin developed above a ramp-flat-ramp listric fault with a pre-kinematic polymer layer (modified from McClay and Scott (1991) and based on Soto et al. (2007) & Ferrer et al. (2016)).

developing salt-detached ramp-syncline basins (Fig. 2b; Roma et al., 2018).

Recognizing the existence or the shape of sub-salt extensional faults controlling the formation and kinematic evolution of salt-detached ramp-syncline basins may be complex. This was so far established based on the geometry of the shallow folded supra-salt strata and by assuming complete coupling between them (White, 1992; Guimerà et al., 1995; Benedicto et al., 1999). This assumption nevertheless neglects the decoupling role of the salt, acting as an effective detachment, resulting in a potential mis-interpretation of sub-salt extensional faults (Koyi and Petersen, 1993; De Ruig, 1995; Stewart and Clark, 1999; Withjack and Callaway, 2000; Mohr et al., 2005; Ings and Shimeld, 2006; Soto et al., 2007; Ferrer et al., 2012, 2014, 2016; Krzywiec, 2012; Harding and Huuse, 2015). Furthermore, extensional structures may be masked if these basins were subsequently inverted.

Despite improvements in seismic processing and imaging, the structural complexity of these systems still allows for conflicting interpretations. In order to reduce uncertainties, useful insights may be provided by crustal-scale analog models (Ellis and McClay, 1988; McClay, 1989, 1990; Koyi et al., 1993; Dooley et al., 2005; Soto et al., 2007; Durcanin, 2009; Ferrer et al., 2014, 2016). Using dedicated analog models, this study aims to understand the specific, kinematic evolution of the Columbrets Basin (Western Mediterranean), which belongs to a partially inverted ramp-syncline basin detached on Upper Triassic evaporites (Roca, 1996) and developed above a major low-angle extensional sub-salt fault.

2. The Columbrets Basin

The Columbrets Basin is located in the southwestern part of the València Trough in the Western Mediterranean (Fig. 3) and belongs to a NE-trending intracontinental basin that developed during the Mesozoic on the northwestern margin of the Maghrebian Tethys (Schettino and Turco, 2010). The basin is a 60–80 km-long and 40–50 km-wide asymmetric syncline (Fig. 3) with a short and steeply dipping southeastern limb (syncline forelimb) and a larger and gently dipping northwestern limb (syncline backlimb; Figs. 4 & 5). It is filled by a thick (up to 8–9 km) succession of uppermost Triassic to Cretaceous carbonate sediments (Roca, 1996) that overlie a hyperextended crust (< 4 km-thick) beneath the syncline hinge (Pascal et al., 1992; Torne et al., 1992; Etheve et al., 2018). The thickness of the uppermost

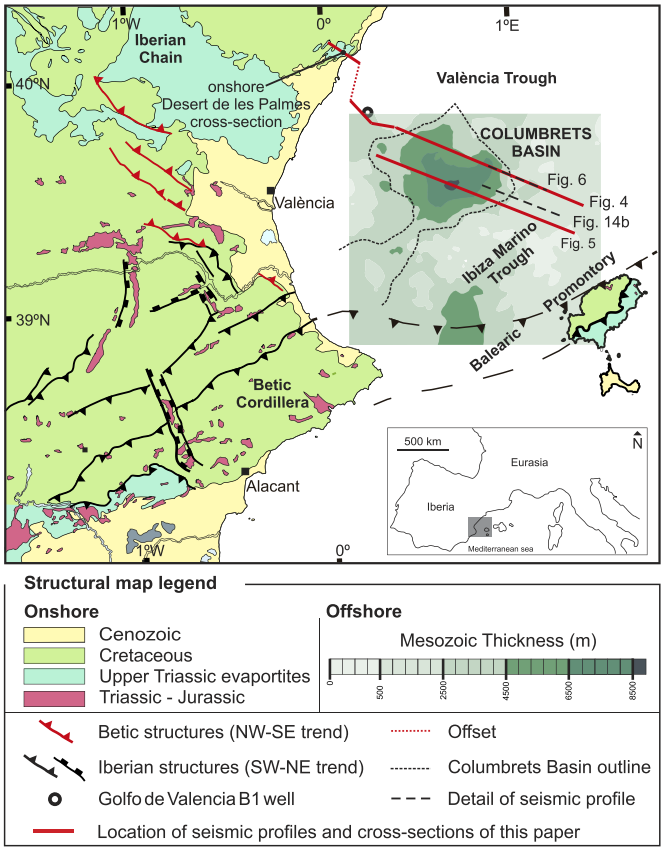

Fig. 3. Simplified structural map of the south-western València Trough and surrounding onshore areas (modified from Escosa et al., 2018). The Mesozoic isochore map of the Columbrets Basin has been obtained from the interpretation of the SGV01 seismic survey. SW Europe map (insert) shows the geographical location of the structural map.

Triassic to Lower Cretaceous basin infill gradually decreases from the syncline hinge towards both edges. This sedimentary succession is affected by extensional and contractional faults detached at the Upper Triassic (Keuper) evaporites that act as a regional decoupling layer. The thickness of this evaporitic unit changes across the basin, becoming thinned until it is welded at the syncline limbs, while thickening by inflation along the syncline edges where salt structures (i.e., diapirs and salt walls) are developed (Fig. 4a).

Beneath the Upper Triassic salt unit, the basement and the overlying Permian-Lower Triassic rocks depict the same broad synclinal geometry but they are affected by a widespread system of extensional faults. Most of these faults do not propagate across the Upper Triassic salt except at the onshore northwestern margin of the basin in the Desert de les Palmes where they form a listric fan system (Fig. 4a; Zeyen et al., 1985; Martín and Suriñach, 1988; Roca et al., 1994; Vidal et al., 1998; Ayala et al., 2003). Desert de les Palmes belongs to an old NE-SW high, where the Jurassic basal unconformity eroded the Keuper facies (Roca et al., 1994). There, these faults cut through the entire Mesozoic succession and appear detached in the upper crust (2–3 km beneath the top of the Paleozoic basement) as an intracrustal detachment (Roca et al., 1994).

In the Columbrets Basin there is no evidence of any major bounding fault as a principal mechanism related to basin formation (Fig. 3). In contrast with Granado et al. (2016) and Etheve et al. (2018) SGV01 seismic interpretations, our Fig. 4b shows how the horizontal reflectors of the high reflective middle and lower crust (coming from the Iberian mainland-NW; Fig. 4b), as well as the Moho reflector, has lateral endings (red points in Fig. 4b). Together with the Desert de les Palmes structure, and while taking into account the surface that obliquely cuts the horizontal reflectors (Fig. 4b), the Columbrets Basin is interpreted as having had developed over a south-directed intracrustal low-angle fault with three different dipping panels (Fig. 4a): an upper horizontal panel (Desert de les Palmes), an intermediate panel dipping towards the southeast, and a southeast dipping lower panel with a lower angle. Based on the fault geometry and the equivalent footwall and hanging wall upper crustal ramps we have been established that the extensional displacement of this fault is about 80 km (Fig. 4). The synclinal geometry results from the displacement of the basin above the intermediate panel to the lower one and the coeval Upper Triassic salt migration. Accordingly, we can define the Columbrets Basin as a salt-detached ramp-syncline basin. In addition, the Mesozoic isochore map in Fig. 3 illustrates two depocenters at the northern part of the basin (compare Figs. 4 & 5). The development of such a second depocenter denotes a local change in the intracrustal fault geometry that is probably linked to the development of an extensional duplex that formed by migration of the footwall's major fault (Gibbs, 1984) or by thermal crustal thinning leading to lower crust boudinage (Reston, 2007).

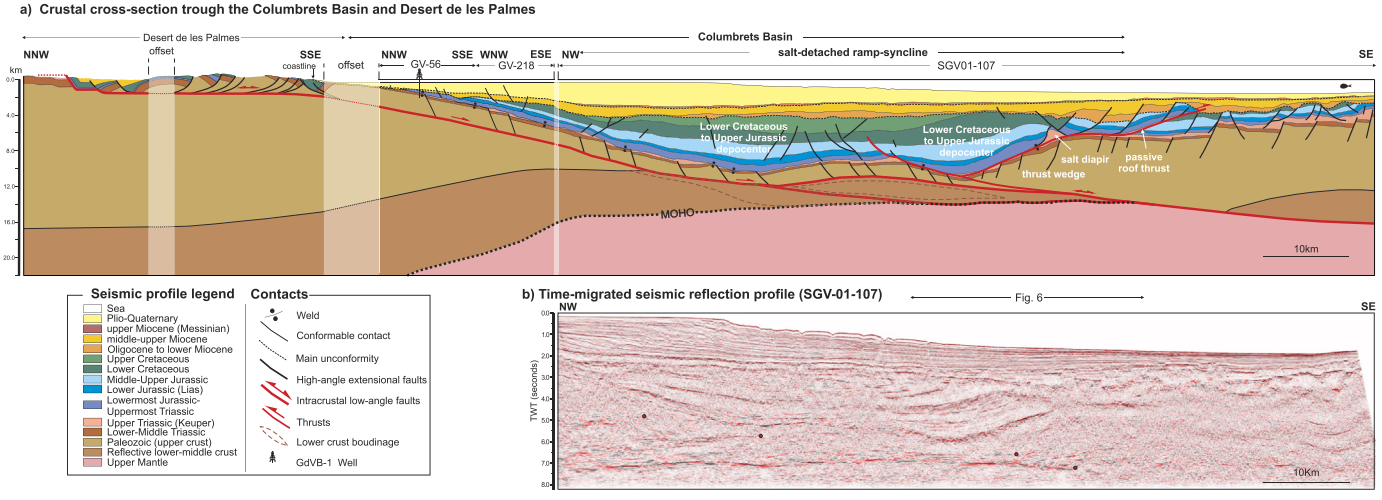

Fig. 4. a) Crustal cross-section through the Columbrets Basin and the Desert de les Palmes. The interpretation of the Desert de les Palmes is based on Zeyen et al. (1985); Martín and Suriñach (1988); Roca et al. (1994); Vidal et al. (1998) and, Ayala et al. (2003); b) Time-migrated seismic line used to define the offshore structure of the Columbrets Basin in the central part of the València Trough (See location in Fig. 3). The red points indicate the lateral ending of some seismic reflections coming from the Iberian mainland-NW, which allow interpretation of the south-directed intracrustal low angle fault. (For interpretation of the references to color in this figure legend, the reader is referred to the web version of this article.)

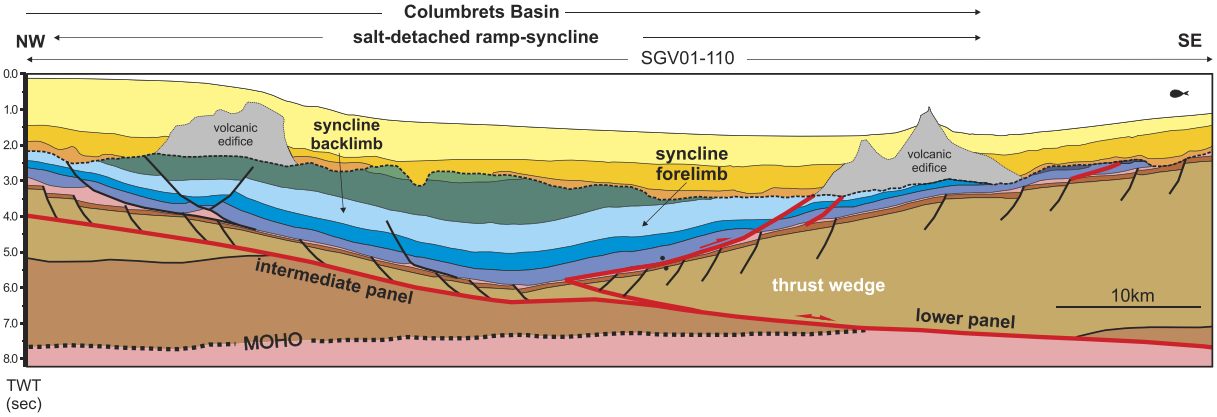

Fig. 5. Crustal cross-section through the Columbrets Basin. See Fig. 3 for location and Fig. 4 for legend.

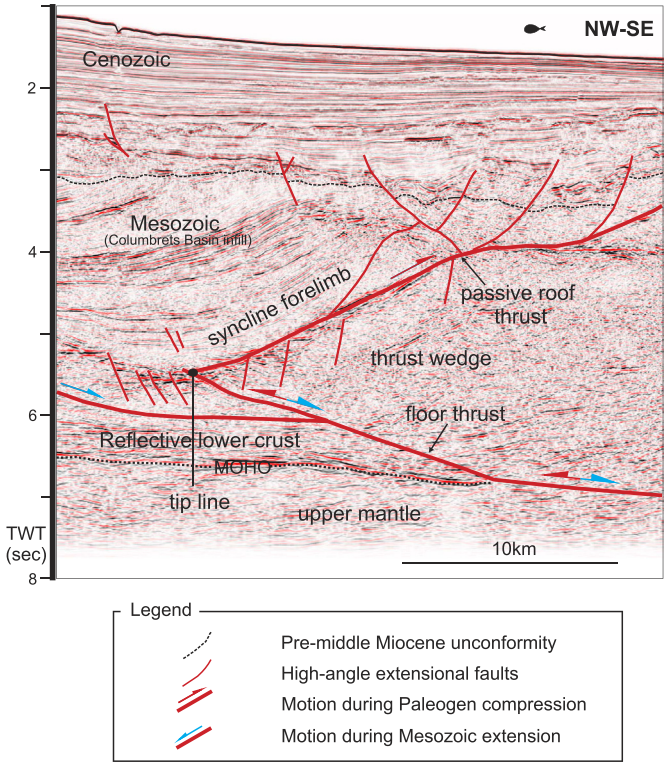

Fig. 6. Geoseismic section (SGV01-107) showing the structure of the southeastern limb of the Columbrets Basin. See Figs. 3 & 4 for location.

The presence of a major pre- and middle Miocene unconformity on the top of the basin infill as well as of some thrusts affecting the Paleogene to the lowermost Miocene units in the basin margins, indicates that the Columbrets Basin was tectonically inverted during this period. This inversion, coeval to the formation of the Iberian Chain at the northwest of the study area (Álvaro et al., 1979; Guimerà and Álvaro, 1990), was only partial and was accommodated by: i) the contractional reactivation of the intracrustal low-angle fault; and, ii) the local development of a thin-skinned southeast-directed thrust detached at the Upper Triassic evaporites in the southeastern limb of the basin (Fig. 6). This last thrust is interpreted as a passive roof thrust (Fig. 6) placed at the top of a thrust wedge bounded at the base by the reactivated intracrustal low angle fault and a related splay. With a tip line located at the syncline hinge (Fig. 6), the motion of this passive roof thrust shifted the Mesozoic basin depocenter southeastwards and led to a major uplift of the southeastern syncline limb, which appears more eroded than the northwestern one (Figs. 4 & 5).

Table 1
Summary table showing the main characteristics of the experimental program of this research.

Experimental program					
Experiment	Pre-kinematic thickness (cm)	Polymer thickness (cm)	Extension (cm)	Inversion (cm)	Time (hours)
1 (baseline)	11.8	–	20[a]	–	70
2 (baseline)	11.8	–	20	9	93
3	11.8	0.5	20[a]	–	70
4	11.8	0.5	20	9	93
5	12.3	1	20[a]	–	70
6	12.3	1	20	9	93
7	11.8	0.5	10[a]	–	35
8	11.8	0.5	20[a]	9[a]	93

[a] Erosion during extension or inversion, keeping constant the regional datum at the beginning of extension.

3. Experimental program

3.1. Model design

The analog experiments (Table 1) were carried out in a 90 cm-long, 50 cm-wide, and 35 cm-deep glass-sided deformation box. Two end walls that were orthogonal to the glass walls made the experiment a closed system. Both glass walls and the left-hand side wall were fixed, whereas the other wall was moved by a servo-motor at a constant velocity (Fig. 7a). A rigid wooden block attached to the fixed wall during all the experiments was used to simulate the intracrustal fault geometry of the Columbrets Basin case study (hereinafter, the master fault; Fig. 7a). The geometry of this block was characterized by: a 30 cm-long upper panel dipping 5°; a 20 cm-long intermediate panel dipping 20°, and a third horizontal lower panel corresponding to the baseplate (Fig. 7a). A plastic sheet placed above the rigid block and the baseplate reproduced the master fault motion. It covered the entire model except for the uppermost 3 cm of the upper panel, simulating the fault breakaway (end of basal plastic sheet, or EBPS in Fig. 7a). The extensional deformation was achieved by pulling the moving wall and the plastic sheet away at the same speed and direction (Fig. 7b). Finally, the contractional deformation during inversion was transmitted by reversing the direction of the moving wall and the left-hand side roller motor (where the plastic sheet was fixed only during this episode; Fig. 7c).

3.2. Analog materials and scaling

Well-sorted and rounded dry silica sand is an excellent analog material for brittle rocks in the upper continental crust (Schellart, 2000):

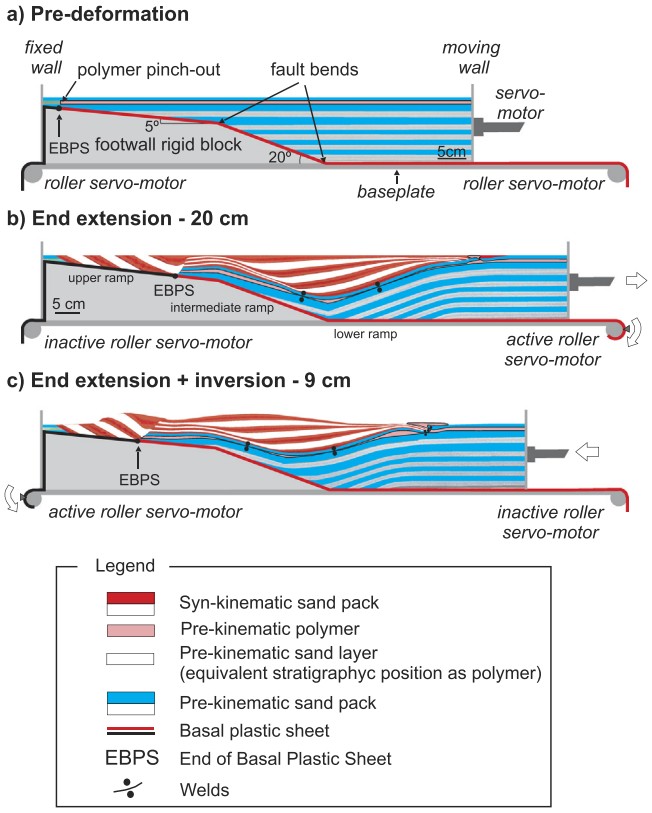

Fig. 7. Conceptual sketches of the experimental apparatus and materials used in the experimental program. a) sketch of the rig before deformation; b) sketch at the end of the extension (after 20 cm of extension); c) sketch at the end of inversion (after 20 cm of extension and 9 cm of shortening).

Table 2
Scaling parameters used in the experimental program.

Parameter	Model	Nature	Model/nature ration
Length, L (m)	0.01	1000	10^{-5}
Gravity acceleration, g ($m \cdot s^{-2}$)	9.8	9.8	1
Density loose sand, ρ ($kg \cdot m^3$)	1500	1900–2500	0.8–0.6
Angle of internal friction, ϕ (°)	34.6	30–40	1.1–0.8
Cohesion loose sand, σ (Pa)	55	10^7	$5.5 \cdot 10^{-6}$
Angle of internal friction green sand, ϕ (°)	30	30–40	1–0.6
Cohesion green sand, σ (Pa)	60	10^7	$6 \cdot 10^{-6}$
Density polymer, ρ ($kg \cdot m^3$)	972	2170–2200	0.44
Viscosity polymer, η (Pa·s)[a]	10^4	10^{19}	10^{-15}
Time, t (model (hour) & nature (years))	1	628,000	$1.8 \cdot 10^{-10}$

[a] Viscosity measured when deformed at a laboratory strain rate of $1.83 \cdot 10^{-4}\ s^{-1}$.

we used a polydimethylsiloxane (PDMS) polymer as the analog for viscous salt (Weijermars, 1986; Couzens-Schult et al., 2003; Dell' Ertole and Schellart, 2013). The silica sand (white, blue, black, and red in color) with an average grain size of 199 μm obeys a Mohr-Coulomb criterion of failure (Hubbert, 1951; Mandl et al., 1977). We determined their properties with a ring-shear tester, resulting in a coefficient of internal friction (μ) of 0.5–0.6, a bulk density (ρ) around 1500 $kg \cdot m^{-3}$, and a low cohesion of 55 Pa. The coefficient of sliding friction between the plastic sheet and the sand pack was μb = 0.21 (Biagi, 1988; Konstantinovskaia and Malavieille, 2005; Liu et al., 1992). On the other hand, the polymer (Rhodia Rhodorsil Gum FB — PDMS) behaves as a Newtonian fluid under laboratory conditions (strain ranges of $1.83 \cdot 10^{-4}\ s^{-1}$ at 20 °C; Dell' Ertole and Schellart, 2013), and has a density (ρ) of 972 $kg \cdot m^{-3}$, and an effective viscosity (η) of about 10^4 Pa·s. In terms of scaling (Table 2) and according to Hubbert (1937), 'an analog model is representative of its natural prototype if both systems are geometrically, kinematically and dynamically similar'. Dynamically similar ones are achieved through dimensionless forces (inertia and surface forces). However, in our analog experiments the inertial forces were negligible due to the fact that the acceleration in our models was very small. Assuming the basic rules of scaling analysis (Hubbert, 1937; Ramberg, 1967; Vendeville et al., 1987; Withjack and Callaway, 2000; Keppler et al., 2013), the surface forces have to be measured by the model-to-prototype ratio for stress (σ*), which corresponds to:

$$\sigma^* = \rho^* \cdot g^* \cdot L^* \quad (1)$$

where ρ*, g*, and L* are the model-to-prototype ratios for the density, gravity acceleration, and length (ratio of the distances between equivalent points on the model and on the prototype), respectively. The density and length ratios were obtained by assuming an average value for the density of the sedimentary rocks and for the halite (Table 2), and given the dimensions of the model and the corresponding dimensions in nature (Table 2); $\rho^* = 0.55 \pm 0.15$ and $L^* = 10^{-5}$ (i.e., 1 cm in the model represents 1 km in nature). Taking into account Eq. (1), we obtained $\sigma^* = 5.5 \cdot 10^{-6}$.

The time ratio (t*) was calculated from the strain rate equation and is expressed as:

$$\eta^* = \rho^* \cdot L^* \cdot t^* \quad (2)$$

where η* is the model ratio of viscosity (10^{-15}), obtained from the polymer viscosity (10^4) and the viscosity for the rock salt (10^{19}) (Weijermars et al., 1993). By assuming the values from Eq. (1) for Eq. (2), the time ratio (t*) is readily obtained:

$t^* = 1{,}8 \cdot 10^{-10}$, which means that 1 h in the experiments represents about 628.000 years in nature. Our experiments lasted 70–90 h, equaling a range in geological time of 44–75 My.

Finally, since the velocity ratio (V*) can be defined as:

$$V^* = L^*/t^* \quad (3)$$

then the extension and shortening rate for our models was 4 mm/h equivalent to 0.6 mm/y in nature.

3.3. Experimental procedure

The deformation box was filled by manually pouring 3 mm-thick horizontal pre-kinematic layers of alternating white and colored sand (blue or black). Each layer was labeled using a scraper until reaching a total thickness of 10.7 cm above the baseplate (Fig. 7a). Depending on the experimental configuration (Table 1), a 0.5 or 1 cm-thick layer of green sand (baseline models) or polymer, overlay the pre-kinematic sand pack. The polymer covered the area between the EBPS (polymer pinch-out in Fig. 7a) and the moving wall. Between the EBPS and the fixed wall it was substituted by a green sand layer with the same thickness, simulating the non-presence of salt at the Desert de les Palmes high (Roca et al., 1994). To complete the pre-kinematic succession, both the polymer and the green sand layer were overlaid by two 3 mm-thick layers of white and blue sand (Fig. 7a). After that, all experiments were extended by 20 cm using a constant deformation rate of 4 mm/h (except Experiment 7, which was extended by 10 cm; Table 1).

Syn-kinematic white, black and red sand layers were added at every 1 cm of extension, keeping constant the pre-kinematic regional datum (Fig. 7b). This fact also imposed the erosion of any topography above this datum, which was developed by polymer inflation during extension. After extension, all experiments were partially inverted using the same strain rate (4 mm/h). Syn-inversion sedimentation was not considered in any experiment, and the topography generated during shortening was preserved. Only Experiment 8 tested the role of erosion

during inversion (Table 1).

In order to preserve the final topography and to inhibit any polymer movement after inversion the experiments were covered with thick post-kinematic sand. Later, the experiments were preserved and serially sectioned into 1 cm-thick vertical slices parallel to the deformation direction.

3.4. Experimental record

The model's evolution was recorded by lateral and overhead time-lapse photographs taken every 6 min, in combination with a model surface topography, recorded during the inversion phase using a sub-millimeter resolution white light scanner (SidioPro from Nub3D; Ferrer et al., 2017). The vertical serial sections carried out at the end of the experiments were also recorded using high-resolution digital cameras positioned perpendicularly the experiments in order to analyze the variation in the structures along strike. A 4 cm-wide section along each side of the experiments was omitted in the analysis to avoid border effects related to the friction between glass sidewalls and the sand pack.

4. Experimental results

This section outlines the main results of sandbox models with and without polymer (Table 1), comparing first for extension and then for inversion. The nomenclature used in the description of the experimental results is summarized in Fig. 8.

4.1. Extensional deformation

4.1.1. Baseline experiment

The extensional episode in the baseline experiment (Table 1) led to the formation of an asymmetric ramp-syncline above the intermediate panel that was characterized by a slightly angular hinge with depocenters younging landwards. The pre-kinematic sand pack defined an extensional rollover with a crestal collapse graben developed at the rollover hinge (Figs. 2a & 9a). Four axial surfaces defined different dip domains in the ramp-syncline. Whereas two of them were pinned to the fault bends (active axial surfaces A and B in Fig. 9a), the other two were located on the fault panels at a distance equal to the master fault displacement (inactive axial surfaces A′ and B′ in Fig. 9a; Xiao and Suppe, 1992). Therefore, such a distance between two pairs of equivalent axial surfaces was constant throughout the pre-kinematic sand layers, but not throughout the syn-kinematic ones, where the active and the inactive axial surfaces connect (Fig. 9a), forming the so-called growth axial surface (Xiao and Suppe, 1992), or outer limit of folding (Withjack and Schlische, 2006).

Together with this ramp-syncline, a ramp-anticline developed above the upper fault bend (Figs. 8 & 9a). This anticline was progressively overlain by horizontal syn-kinematic layers that filled the accommodation space created by the downward translation of the hanging wall sand pack above the upper fault panel. The width of this anticline progressively decreased as extension progressed and the sand pack crossed the active axial surface A (Fig. 9a). In addition, at the EBPS (over the upper panel) a breakaway half-graben with a width equal to the applied fault displacement developed (Figs. 8 & 9a). The syn-kinematic layers in the breakaway half-graben formed a rollover that dipped towards the EBPS. This rollover was cut by a pervasive system of planar synthetic extensional faults attesting to a depocenter migration towards the EBPS during extension (Fig. 9a).

4.1.2. Experiments with polymer

The breakaway half-graben and the sub-polymer structure of these experiments (Fig. 9b) were similar to those developed during the baseline Experiment 1 (Fig. 9a). In contrast, the deformation style was different for the units overlying the polymer.

While the baseline experiment shows a slightly angular ramp-syncline (Fig. 9a), in the experiments with polymer, the curved geometry of the supra-polymer ramp-syncline basin was constrained by the master fault geometry, but also by the polymer layer that acted as a detachment (hereinafter salt-detached ramp-syncline; Roma et al., 2018). In this scenario, the syn-kinematic depocenters also became younger landwards, as occurred in the baseline experiment. Nevertheless, in this case the polymer migration modified the depocenter's path (compare Figs. 9a & 9b) and it developed polymer (i.e., salt) structures bordering the basin parallel to the major sub-polymer structures (i.e., upper fault bend and extensional rollover). In addition, the polymer partially decoupled sub- and supra-polymer deformations, thus inhibiting the upwards propagation of the sub-polymer active axial surfaces (i.e., A & B in Fig. 9b) into the supra-polymer unit.

Experiments 3 (thin-polymer layer; Table 1) and 7 (thin-polymer layer and half extended; Table 1) enable us to distinguish two stages of welding (Fig. 10b & c). The initial one, developed a primary weld at the syncline hinge domain (Weld 1 in Fig. 10b; between A′ & B) by polymer migration towards the extensional rollover hinge; that the weld was enhanced by syn-kinematic sedimentation. As extension progressed the distance between the axial surfaces (A′ & B) decreased and Weld 1 crossed the active axial surface B, becoming incorporated within the syncline forelimb (Fig. 10c). During this episode a secondary stage of welding occurred with the formation of a new primary weld on the syncline backlimb (Weld 2 in Fig. 10c). As a consequence, the hinge of the salt-detached ramp-syncline appeared to be shifted landwards with respect to the sub-polymer ramp-syncline (Fig. 9b & c). A polymer remnant with a clear asymmetric shape in cross-section is preserved between these two welds (Fig. 10c). In contrast, in the thick-polymer experiment (Experiments 5 & 6; Table 1) no primary welds formed in equivalent positions during the extensional phase (Fig. 9c).

Regardless of the polymer thickness, the polymer flow was preferentially towards the extensional rollover hinge where gentle anticline ridges formed by polymer inflation (Figs. 9b, c, 11a & b). The growth of these polymer structures in the models with a thin-polymer layer was enhanced by the development of the primary Weld 1 that coupled supra- and sub-polymer deformations. Welding also

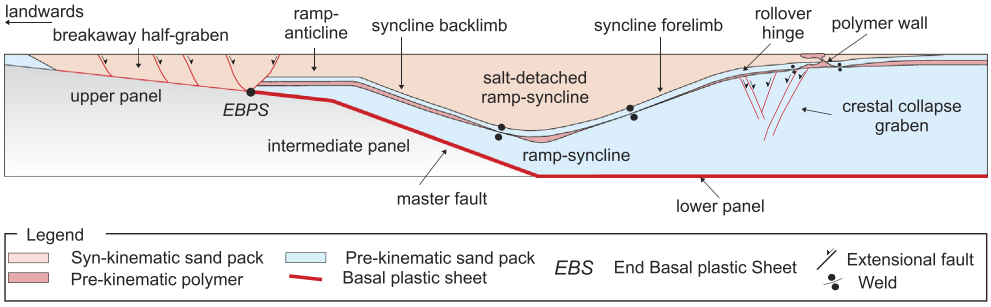

Fig. 8. Simplified sketch of Experiment 3 with a pre-kinematic polymer layer at the end of extension with the nomenclature used in the description of the experimental results.

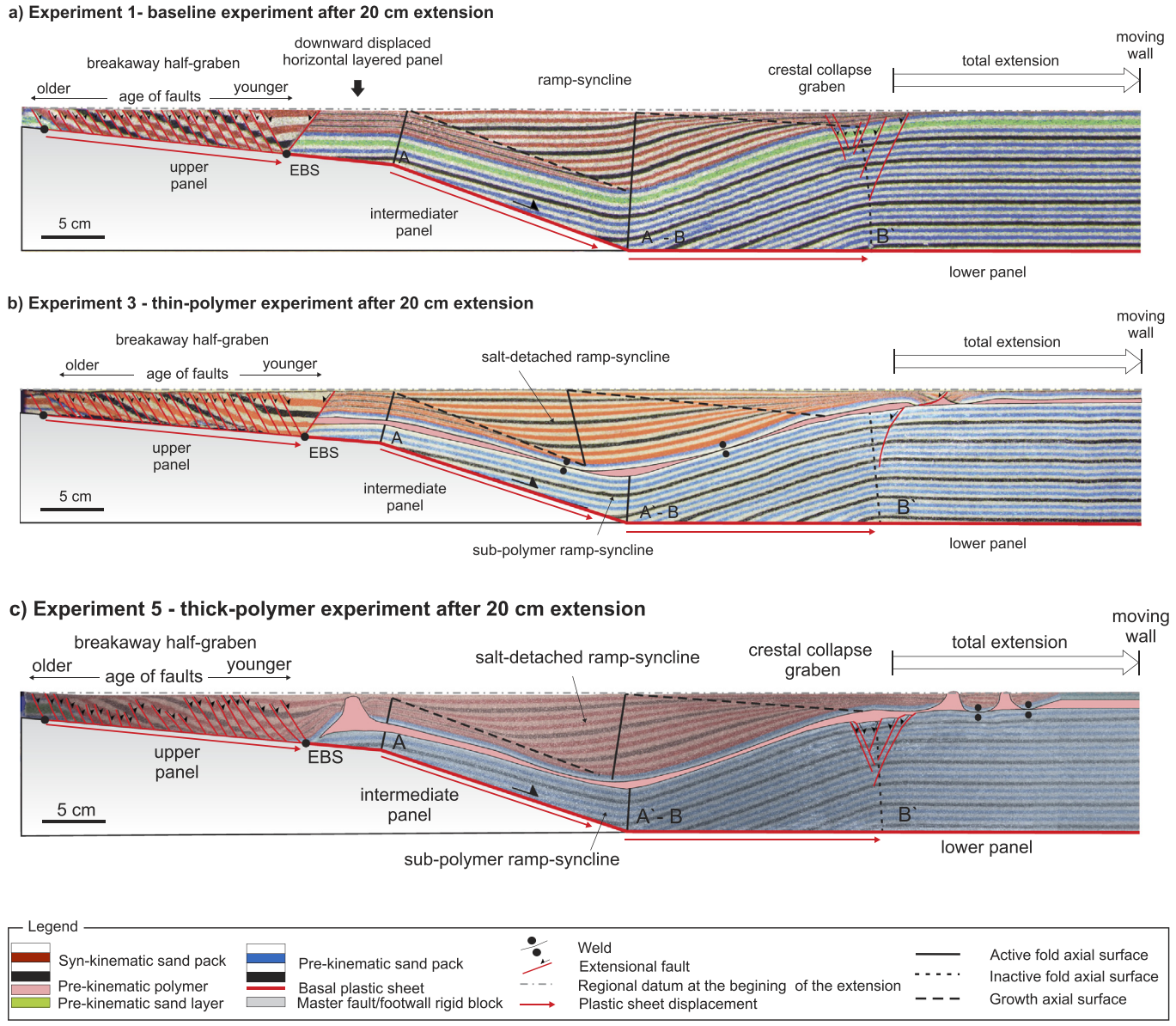

Fig. 9. Interpreted cross-sections with the structures at the end of extension in different experiments (Experiments 1, 3, and 5, see Table 1 for more detail).

emphasized cover extension and the formation of reactive polymer structures (Fig. 11a) from the inflated areas by thin-skinned extension (Jackson and Vendeville, 1994; Dooley et al., 2005). Finally, once these reactive structures pierced the overburden they evolved into passive walls (Fig. 11a). In contrast, at the other syncline edge, diapiric structures only developed when the polymer layer is thick (Figs. 9c & 11b).

4.2. Contractional deformation (basin inversion)

Experiments 2, 4, 6, and 8 (Fig. 12) showed many of the fundamental features of inversion tectonics, agreeing with the classification proposed by Bally (1984) for inverted basins.

4.2.1. Baseline experiment

The inversion of the baseline experiment was characterized by the formation of a major fault-bend anticline resulting from the up-dip displacement of the inherited ramp-syncline along the master fault (Fig. 12a). This induced the formation of a wide flat-topped up anticline that was flanked by two nearly planar limbs whose boundaries belong to four new axial surfaces: two pinned to the fault bends (active axial surfaces C & D in Fig. 12a) and two pinned to the fault plane, but displaced by the plastic sheet motion direction at a distance equal to the applied shortening (inactive axial surfaces C′ & D′ in Fig. 12a). It should be emphasized that the inherited ramp-syncline deformed during contraction, not only laterally and upwards, but also by changing its synclinal-shape (i.e., changing the length and dip of back- and forelimbs). The synclinal-shape change related shortening mainly resulted in the development of a small backthrust (Fig. 12a).

The contractional reactivation of the ramp-anticline also resulted in a width amplification and the formation of a frontal thrust double-wedge at the EBPS. As shown in Fig. 12a, this frontal thrust-double wedge was bounded by: i) a thrust that cut the previously faulted breakaway half-graben, and ii) a backthrust that developed from the inversion of the inherited planar fault that previously bordered the breakaway half-graben (Fig. 9a).

4.2.2. Experiments with polymer

The inversion of the polymer experiments also led to the development of a fault-bend anticline, but in this case the basin uplift was minor compared to the baseline experiment (compare syn-kinematic

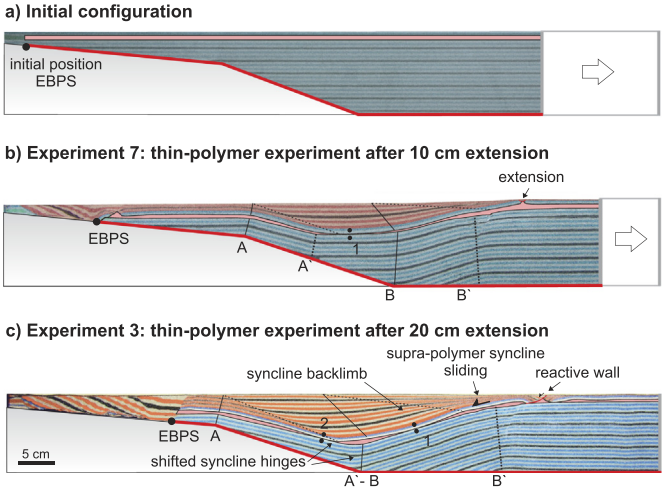

Fig. 10. Cross-sections of the thin-polymer experiment showing different evolutionary stages; a) at the beginning of the experiment (stretching 0 cm); b) after 10 cm of stretching (Experiment 7); and c) after 20 cm of stretching (Experiment 3). 1 & 2 indicates the order of primary weld formation (more detail in the text). See Fig. 9 for legend.

layers above the regional datum at the end of extension in Fig. 12a & b).

In addition to the fault shape (Section 4.2.1), the presence of a continuous polymer layer, its welded equivalent, or the diapiric structures at the edges of the syncline basin, were the main factors that governed contractional deformation. At the beginning of the inversion, the polymer withdrew towards the diapirs and walls, located at the edges of the basin, enhancing extrusion. As a consequence, whereas new welds develop in thick-polymer experiments (Fig. 12d), the welded area under the syncline basin considerably increased in the thin-polymer experiment as shortening progressed (Fig. 12b).

In a similar way to the baseline experiment, shortening modified the internal architecture of the syncline basin, but also squeezed the polymer ridges leading to fold amplification and the formation of detachment folds with variable vergences (Structure A in Fig. 13.2 to .4). In contrast, the squeezing of a polymer wall was characterized by an increase in the extrusion rate, entailing the formation of a large polymer sheet (Fig. 11c & d or Structure C in Fig. 13.1 to .3). The amount of shortening applied to our experiments produced the total squeezing of the stems with the consequent development of secondary welds (Structure B in Fig. 13.2). After that, contractional deformation was absorbed by thrust welds (Rowan et al., 1999) with different vergences (Structure D in Fig. 13.1 & .3).

The contractional deformation also produced the inversion of the breakaway half-graben in a similar way to the baseline experiment, developing a frontal thrust double-wedge at the EBPS (compare Fig. 12a & b). The inherited extensional fault pinned to the EBPS was inverted, developing a footwall syncline (Fig. 12c). Instead, with respect to the results of thick-polymer experiment (Fig. 12d), the geometry of the frontal thrust double-wedge was not controlled by the inherited normal fault pinned to the EBPS, but by the presence of an inherited collapsed polymer wall (Figs. 11d & 12d).

5. Discussion

5.1. Influence of the fault shape on the ramp-syncline geometry

The formation of ramp-syncline basins without a salt layer requires the presence of a non-planar extensional fault (Gibbs, 1984; Ellis and McClay, 1988; McClay, 1990; McClay and Scott, 1991; Withjack et al., 2002; Soto et al., 2007; Ferrer et al., 2016), more specifically, a fault which includes an upper convex-up fault bend and a lower concave-up bend (i.e., an extensional fault with three differently dipping panels). The aforementioned previous authors studied how the geometry of the extensional faults controls the geometry of the ramp-syncline. According to them, the ramp-syncline geometry depends on the amount of extension, and the shape and dip of the panels of the main extensional fault. For larger fault displacements, there is an increase in the length of the syncline limbs, and therefore in the width and amplitude of the ramp-syncline. A ramp-syncline is much better defined with an intermediate and long flat panel (McClay and Scott, 1991), and moreover strongly depends on the curvature when the related extensional fault is listric (Soto et al., 2007). The dip of the fault panels constrains the syncline back- and forelimbs' dips (Xiao and Suppe, 1992; Withjack et al., 2002). Models by Ferrer et al. (2016) show wide, gentle and shallow ramp-synclines developed above a gently dipping intermediate panel. In contrast, narrow and deep ramp-synclines developed as a function of steeper intermediate panels.

Our models and the previous published models have used the baseplate to reproduce the lower fault panel. Through the conceptual sketches in Fig. 14a–c one can notice how the dip of the lower panel strongly constrains the geometry of the syncline. For the same amount of displacement, the length and dip of the syncline forelimb would be greatest for a gently dipping lower panel (symmetric syncline in Fig. 14a) and progressively shorter as the dip of this panel increases (asymmetric syncline in Fig. 14b & c).

5.2. Interaction between the pre-kinematic salt and the sub-salt fault shape

From these observations (Section 5.1), we turn our focus to the different accommodation spaces created, which are related to the fault geometry. Fig. 14 shows how the dip of the lower fault panel can generate more or less accommodation space at the basin margins, and in turn how it influences salt migration. Salt migration is mainly triggered by pressure head differences related to changes in overburden thicknesses (Khele, 1988; Vendeville and Jackson, 1992; Jackson and Vendeville, 1994; Hudec and Jackson, 2007; Ferrer et al., 2014). Thus, the polymer, or its equivalent salt in nature, migrates from the syncline hinge (thick syn-kinematic unit and high pressure head; Fig. 14d to f) to the syncline edges (null or thin syn-kinematic unit and low pressure; Fig. 14d to f). So, the preferential salt migration towards the syncline edges is constrained by the thickness difference between the syn-kinematic unit at both syncline edges, which is in turn controlled by the fault displacement and the dip of the fault panels. When the fault displacement is constant, the preferential salt migration will be controlled by the dip of the fault panels, specifically the lower one (Fig. 14d to f). For the steeply dipping lower fault panel (Fig. 14e & f), the accommodation space filled by the syn-kinematic materials is higher at the syncline forelimb edge, thus forcing salt migration towards the backlimb. In contrast, for gently dipping lower panel (Fig. 14d), the salt will preferentially migrate towards the syncline forelimb where the syn-kinematic unit is thinner. According to this, in our experiments the syn-kinematic sedimentation is null at the syncline edge above the lower fault panel but not at the edge above the upper panel, where it thickens as extension progress (above the ramp-anticline, Fig. 9). This implies that the polymer in our experiments preferentially migrates towards the synclinal edge located above the lower panel (extensional roll-over)—which is the one with the lowest dipping attitude, and where consequently polymer inflation and the resulting diapiric structures will easily rise and pierce the cover.

Secondly, as has been widely reported, the salt unit acts as a detachment during extension (Jackson and Vendeville, 1994; Withjack and Callaway, 2000; Dooley et al., 2005; Ferrer et al., 2008, 2014, 2016). Our models demonstrate that where the salt is thin welds quickly develop (Fig. 10b, Weld 1) favoring cover extension above the extensional rollover hinge (Fig. 10b), thereby enhancing reactive diapirism (Dooley et al., 2005). Nevertheless, when the extension progresses (Fig. 10c), Weld 1 is incorporated into the syncline forelimb; further development of these salt structures (reactive to passive diapirism) is

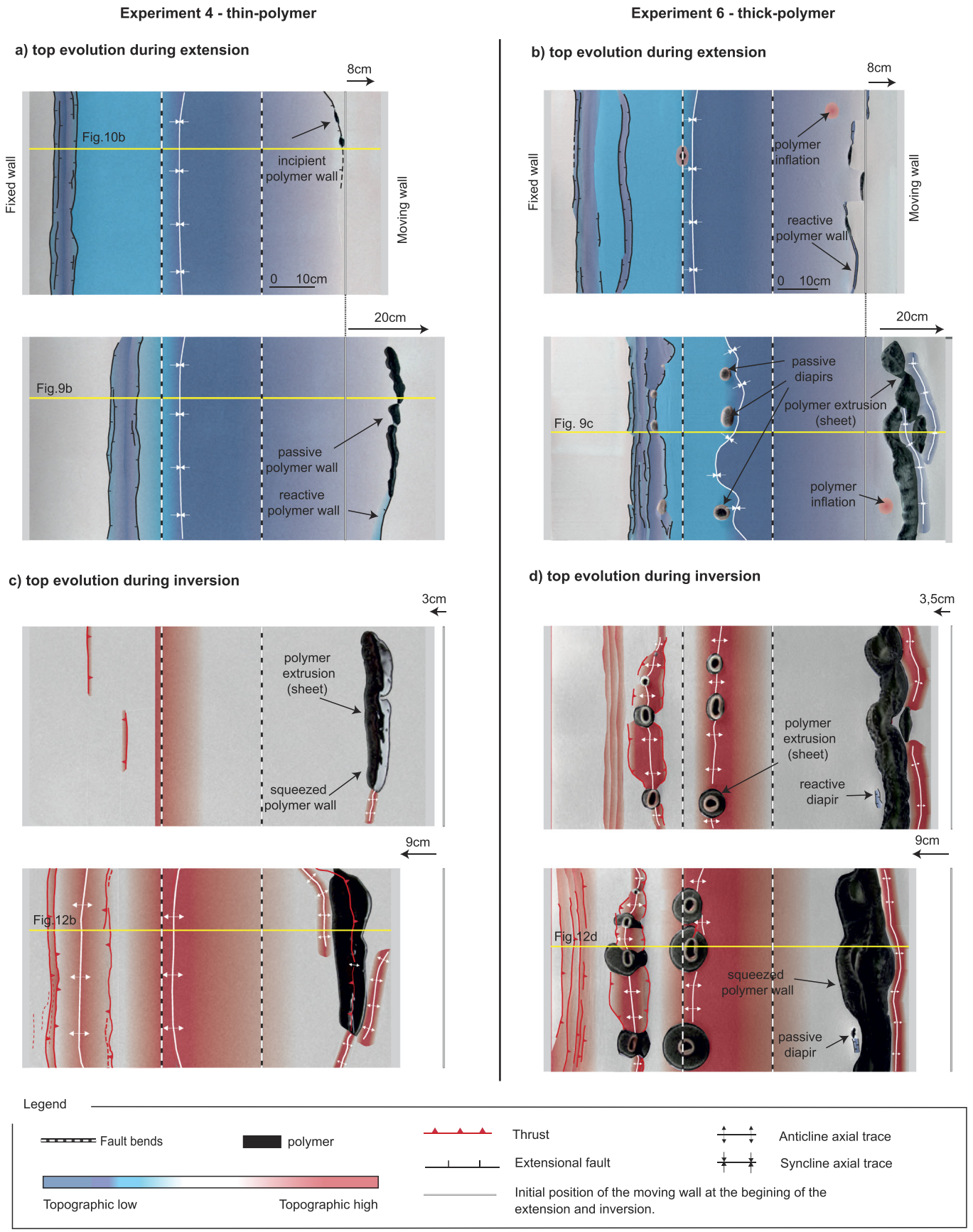

Fig. 11. Interpreted overhead photographs illustrating the structural evolution of Experiments 4 & 6 including a pre-kinematic polymer layer of 0.5 cm-thick and 1 cm-thick, respectively during extension (a & b) and subsequent inversion (c & d).

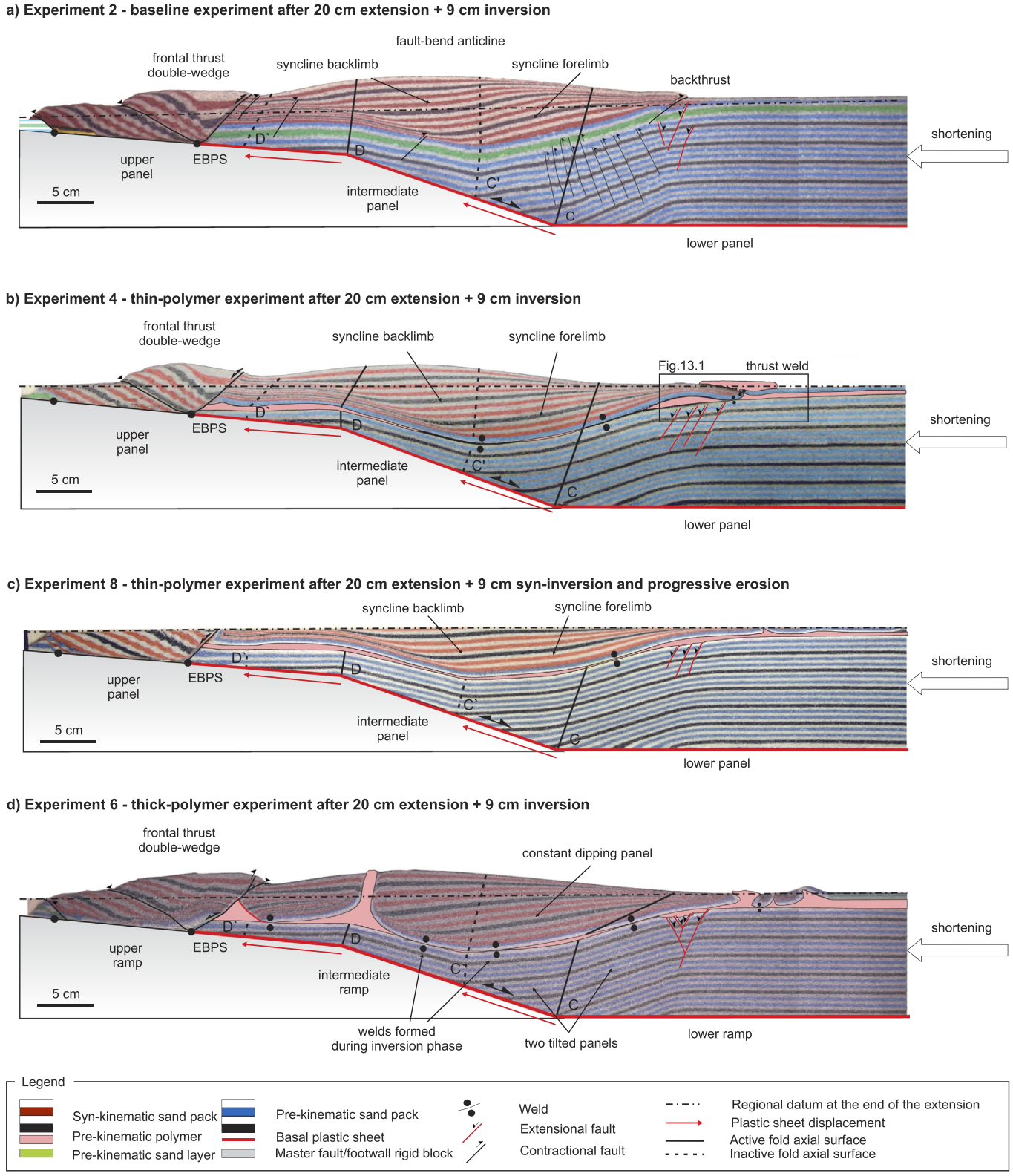

Fig. 12. Interpreted cross-sections with the structures at the end of inversion of different experiments (Experiments 2, 4, 8, and 6, see Table 1 for more information).

also favored by sliding (i.e., by landwards gravitational gliding) of the synclinal basin above the salt (Coward and Stewart, 1995: Stewart and Clark, 1999). The landwards sliding uses Weld 1 as a detachment surface and ends when the primary Weld 2 is developed at the syncline backlimb (Fig. 10c, Weld 2). The resultant glide tectonics shifts the sub- and supra-salt syncline hinges (Fig. 10c). However, when the salt is thick and welds are not developed (Fig. 9c), the offset between supra- and sub-salt syncline hinges is less than in thin-salt basins (Fig. 9c).

5.3. *Inversion of salt-detached ramp-syncline basins*

The experiments reveal that the tectonic inversion of salt-detached

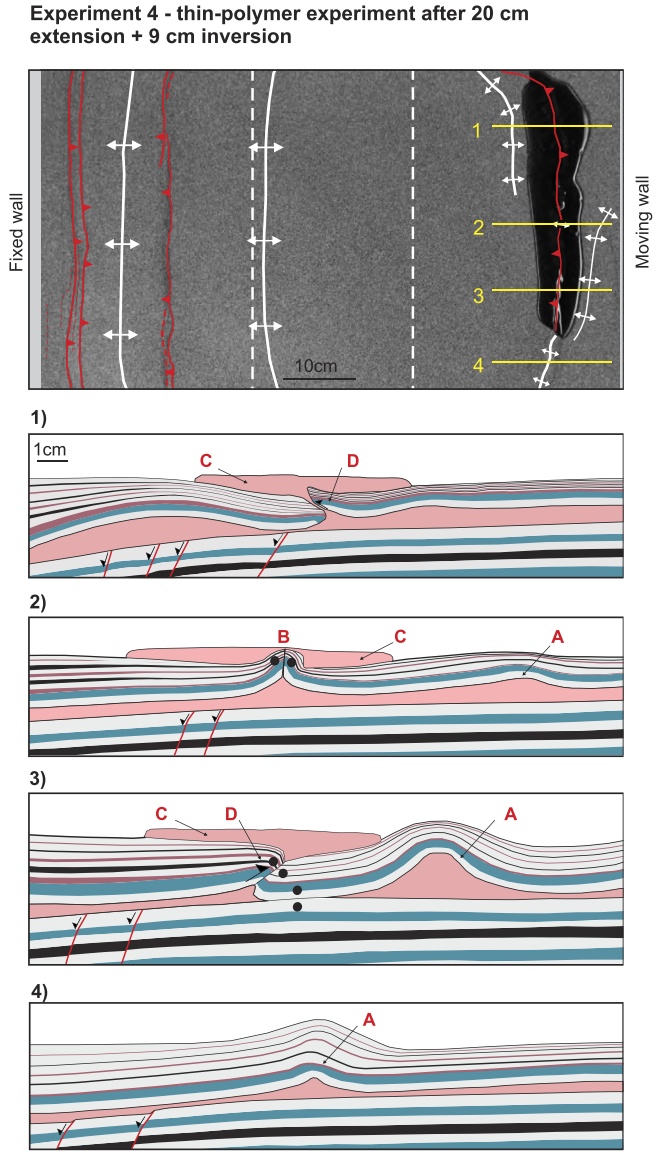

Fig. 13. Top view of Experiment 4 at the end of inversion with the location of four serial cross-sections (1 to 4) across a contractionally reactivated wall developed near the rollover hinge of the master fault. In red: A) detachment anticline; B) squeezed diapir with vertical secondary weld; C) polymer sheet; D) thrust-weld with different vergences. See Figs. 9 and 11 for legend. (For interpretation of the references to color in this figure legend, the reader is referred to the web version of this article.)

ramp-syncline basins is mainly characterized by: i) the formation of a major fault-bend anticline controlled by thick-skinned deformation, and ii) the development of thin-skinned contractional structures (Fig. 12).

5.3.1. Thick-skinned contractional structures

The thick-skinned deformation related to the inversion of the master fault resulted in the early uplift of the synclinal basin and in the subsequent development of a fault-bend anticline. The kinematics and the surface shape of the anticline developed in our experiments follow the geometric patterns already postulated for fault-bend folds formed above kinked fault thrusts (Suppe, 1983; Medwedeff and Suppe, 1997 or Tavani et al., 2005). Thus, the geometry of this anticline is constrained by the dip of the fault panels, the contractional displacement of the master fault, as well as the length of the intermediate fault panel. However, their architecture differs from the geometric models because it departs from the inherited structure in which the hanging wall is not constituted by horizontal layers (Fig. 9a).

This fault-bend anticline is similar to those obtained in the experiments by Durcanin (2009); Ferrer et al. (2016), Roma et al. (2018) and Ferrer et al. (2016) noted that the hanging wall uplift above a kinked planar fault during inversion will be highest as a function of the steepness of the fault panels. Thus, in our experiments the most uplifted part is focused above the intermediate panel (Fig. 12a, b, & d), resulting in an offset between the anticline and the previous syncline hinges (Fig. 12a). The position of this transported syncline hinge with respect to the most uplifted part of the hanging wall depends on the fault displacement as well as on the length of the intermediate fault panel. If the displacement is equal to the length of the intermediate panel, the syncline hinge would coincide vertically with the position of the most uplifted part of the hanging wall. Instead, if it is lesser (like our experiments, Fig. 12a, b, & d) or greater, it would be shifted backwards or frontwards, respectively. This is clearly different to the inversion of half-grabens where the maximum uplift is constrained by the master fault breakaway thus developing the classical harpoon structure (Badley et al., 1989). In this case the maximum uplift coincides with the position of the extensional depocenters (Buchanan and McClay, 1991).

Despite the growth of the fault-bend anticline is mainly controlled by the shape of the master fault; the presence of salt slightly modifies the final inverted structure. Thus, the anticline uplift at the end of the inversion is higher for the ramp-syncline without salt (Fig. 12a) than in salt-detached ramp-syncline basins (Fig. 12b–d). This is because the salt acts as a contractional detachment and migrates during the early inversion stages, therefore counteracting the synclinal uplift. As inversion progresses, salt migration produces the local depletion of the source layer enlarging the pre-existing welds or favoring the formation of new ones (Fig. 12d). At this point the system becomes totally coupled and the basin uplift is more effective. This process is similar to those described in the experiments of Ferrer et al. (2016) and Roma et al. (2018).

5.3.2. Thin-skinned contractional structures

Regarding the contractional fault-bend anticline formation, thin-skinned structures also develop during the inversion phase. This deformation style is controlled by the inherited synclinal-shape that changes during shortening.

These synclinal-shape changes consist of a progressive length-reduction of the syncline backlimb, and a dip decrease of the syncline forelimb beds. That occurs when the extensional rollover is passively transported from the lower to the intermediate fault panels (Fig. 12a). Both changes produce a decrease in the syncline interlimb angle (i.e., a reduction of the syncline amplitude) and therefore, a shortening of the involved beds. Taking into consideration that the distance between the moving wall and the EBPS remained constant during the entire experiment, such an amplitude change is especially relevant since it entails length shortening of the sand layers. In the absence of salt (Fig. 12a) this process results in the development of a thin-skinned backthrust above the extensional rollover hinge (Mitra, 2002). Whereas the synclinal-shape changes in salt-detached ramp-syncline basins show a reduction of the sub-salt syncline amplitude, this is not what occurs in the supra-salt syncline. Note that, at the end of the inversion of our models the supra-polymer sand pack is nearly flat with a relatively constant dipping attitude (Fig. 12d). This gives rise to a reduction of the limb length of the supra-polymer layers. This reduction entails shortening that is added to the global thick-skinned contraction. Consequently, the salt-detached ramp-syncline basins showed more shortening in the supra-salt strata than in ramp-syncline basins without salt. This additional thin-skinned shortening mainly consists in the reactivation of the salt unit as an effective contractional detachment, producing the squeezing of the inherited salt walls above the extensional rollover hinge with the subsequent development of secondary welds. Further inversion causes those secondary welds to evolve into thrust welds (Figs. 12b, 13.1, & .3). Unquestionably, the thin-skinned

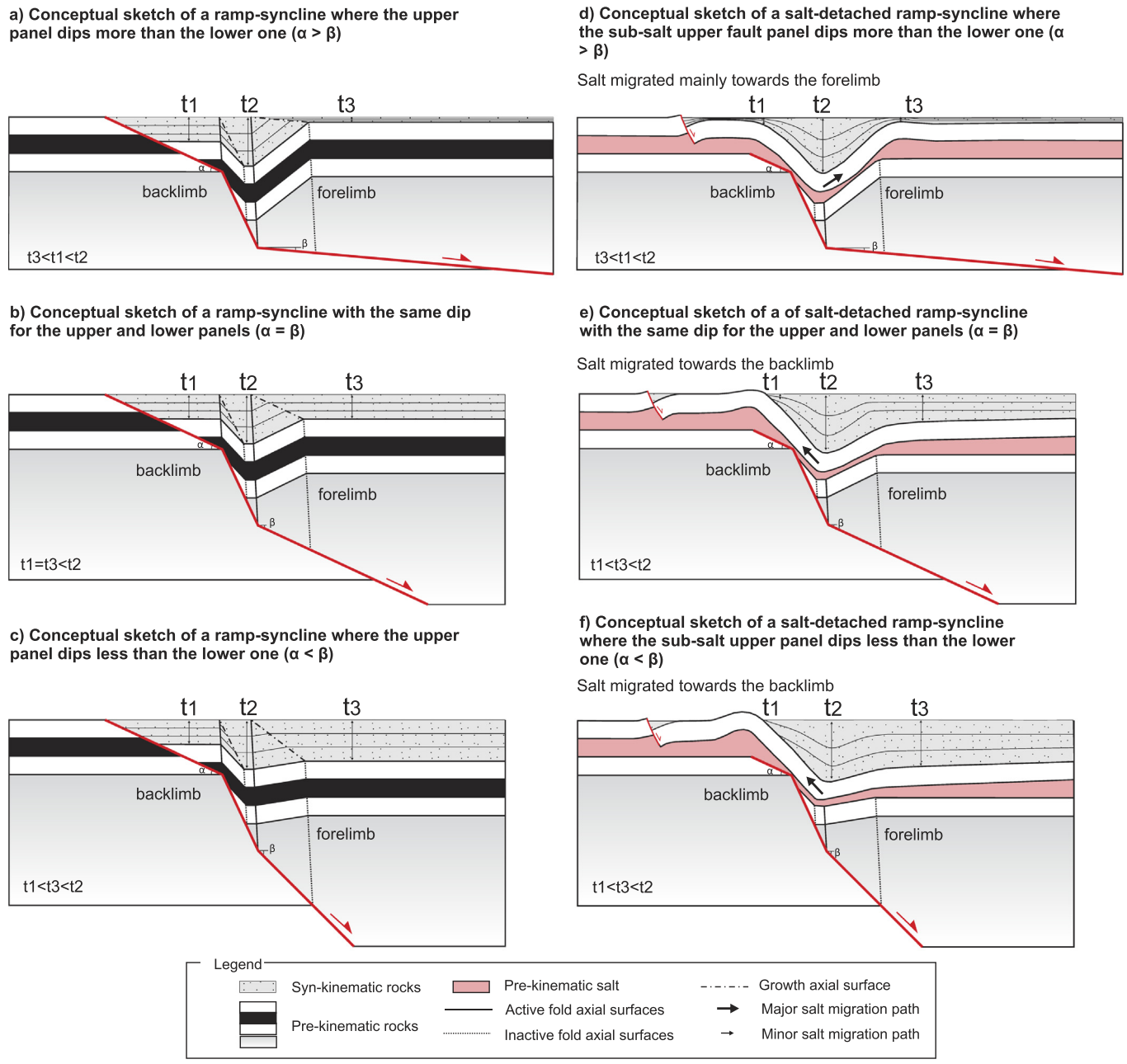

Fig. 14. Conceptual sketches showing the relationships between different kinked fault geometries, the overburden deformation thicknesses and the salt migration Note that the intermediate fault panel has the same length, position and dip in all figures.

shortening is mainly localized at the extensional rollover hinge rather than at the syncline backlimb, whereas the inherited diapirs and walls do not show any evidence for the formation of secondary welds.

5.4. Role of erosion during extension and inversion

The presence and evolution of diapiric structures during extension depends on: i) the regional extension, ii) the geometry of the sub-salt faults, iii) the thickness of the overburden and syn-kinematic sediments, and iv) erosion. Where the salt is preferentially migrated, salt inflation occurs. For buried salt to be diapirically emplaced, the overburden occupying the intruded space must be removed (Jackson and Hudec, 2017). Therefore, when salt inflation is removed by erosion, it may stretch the overburden, making room for a reactive diapir to rise. Later, when a weld develops at the syncline limb, the source layer that feeds the diapirs is interrupted—but welding favors extension in the cover, which further enhances diapir growth. Thus, four mixed diapiric mechanisms enhance salt diapir growth: salt inflation, erosion, reactive diapirism, and welding.

During inversion, the widening of pre-existing welds or the development of new ones, as occurs in Experiments 4 and 6 (Fig. 12b & d) are inhibited or delayed by surface processes such as erosion, by reducing the lithostatic load. Meanwhile, the non-weld development means that the structural style is partially coupled, hence hampering basin uplift (Fig. 12c).

6. Comparison with natural examples

6.1. Columbrets Basin

The comparison between the Columbrets Basin and the experimental results presented in this paper shows that the structure of this

basin is compatible with an inverted salt-detached ramp-syncline basin involving pre-kinematic salt, and a south-east dipping low angle fault that, according to our interpretation, includes three panels (Figs. 4a & 5).

The Columbrets Basin is filled by a succession of syn-extensional deposits that show a synclinal geometry (Figs. 4a & 5) with three dip domains similar to those observed in Experiments 4 and 8 (Fig. 12c). Those are characterized by a thick central domain with nearly horizontal pre- and syn-extensional strata (Fig. 5)—a southeast short domain equivalent to the syncline forelimb of the experiments (Fig. 12c), and a longer northwestern domain equivalent to the syncline backlimb of the experiments. As in the models, the NW-dipping syn-kinematic strata of the syncline forelimb gradually thins in the opposite direction (Fig. 5). In contrast, the syn-kinematic strata of the backlimb thins towards the NW (Fig. 5); another common feature is the migration of the basin depocenter with the ongoing extension (Fig. 4a). The syn-kinematic sedimentation is practically nil at the syncline edge above the lower fault panel. This implies that the Upper Triassic salt in Columbrets Basin preferentially migrates towards the syncline edge located above the lower fault panel (which is the one with the lowest dipping attitude), and where salt structures developed (southeastern syncline edge), equivalent to those located close to the rollover hinge in our models (Figs. 4a & 15).

More to the southwest of the basin (towards the Betic Cordillera) the salt thickens (Ortí et al., 2017), favoring the piercement of diapirs. The comparison between Experiments 4 and 6 (Fig. 12b & d) reveals the role of salt thickness on diapir development at the edges of the basin. In a similar way, the listric fan system of extensional faults that outcrop at the northwest part of the Columbrets Basin (Deset de les Palmes in Fig. 4a) is equivalent to the breakaway half-graben of our experiments. Such a listric fan coeval to the Columbrets Basin formation—rooted at the southeast-directed intracrustal low angle fault (Fig. 4a)—consumes a large amount of the Mesozoic extension. In contrast, a SE-verging thin-skinned backthrust detached on the Keuper evaporites in the syncline forelimb controls the inversion of the basin (Figs. 4a & 6) thus transporting the basin 6 km towards the SE. Such a displacement is inconsistent with our experimental results, where thin-skinned shortening is smaller. In this sense, we suggest that in the Columbrets Basin most of the shortening is related to the northwestward emplacement of a crustal thrust wedge (Fig. 6) bounded by the above mentioned backthrust (which acted as a passive roof thrust) and the south-east dipping floor thrust (Fig. 6). This last fault corresponds to an inherited structure inverted during the Paleogene. In addition, the seismic line shows a more recent extensional reactivation of this backthrust during Miocene times (Fig. 4a). This extensional episode has not been analyzed in our experimental program.

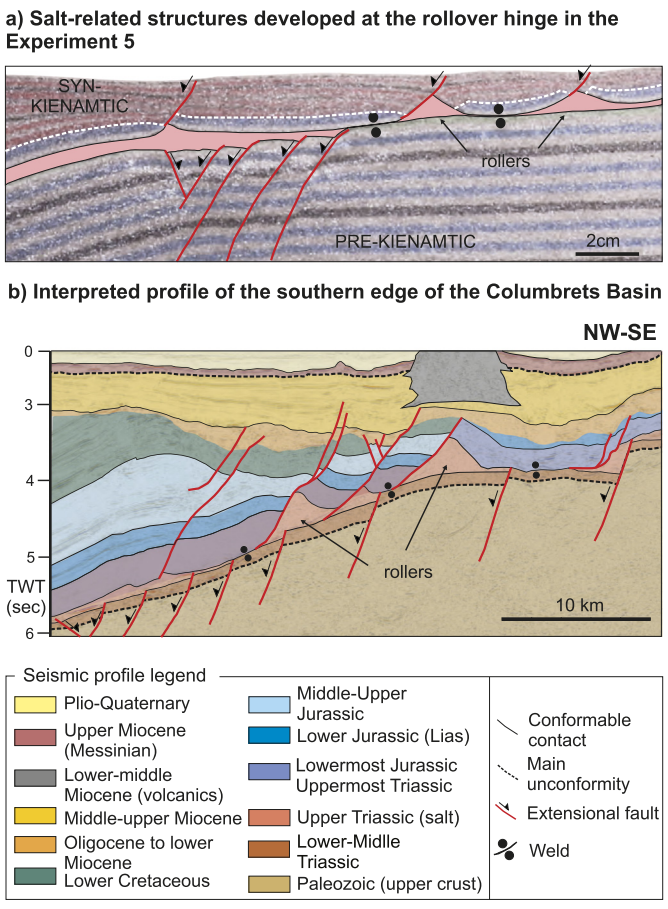

Fig. 15. Comparison between salt structures developed in Experiment 5 (thickpolymer) and a detail of a geoseismic section of the south-eastern edge of the Columbrets Basin (see Fig. 3 for location and Fig. 9 for the legend of the analog model).

6.2. Application to other salt-bearing basins

All mentioned deformation features can also be applied to the salt-bearing basins resulting from the widespread extensional deformation that took place in the Western Europe and North-Atlantic margins during Jurassic to Cretaceous times. Most of these extensional basins (Parentis, Orpheus, or Organyà basins; Durcanin, 2009, Ferrer et al., 2012; Mencos et al., 2015) (Fig. 1) show a broad synclinal-shape not bounded by major faults, detached on pre- or syn-kinematic salt, and filled by a thick sedimentary succession. Regardless of the presence of salt, the development of these basins has been controlled by the displacement and geometry of the extensional master fault.

Based on Withjack and Callaway (2000) seismic interpretation of the Jeanne d'Arc Basin (Fig. 1a), the geometry and displacement of the sub-salt master fault controls the dip and length of the salt-detached ramp-syncline limbs and determines the extensional accommodation space generated at both syncline edges. The accommodation space is also enhanced by salt migration from the hinge towards the syncline edges as occurs in Jeanne d'Arc or in the Parentis basins (Fig. 1a & c). As a result of salt migration, and if the extension is enough, primary welds can develop at syncline limbs leaving a salt remnant at the syncline hinge, as occurs in our experiments (Fig. 9b) and in the seismic interpretation of Parentis Basin in Ferrer et al. (2012) (Fig. 1c).

Part of these basins was subsequently inverted during Uppermost Cretaceous to Cenozoic times, developing a thick-skinned fault-bend anticline (e.g., cross-section of Cameros Basin; Soto et al., 2007) (Fig. 1e). In agreement with our experimental results, the contractional deformation promotes the formation of thin-skinned structures related to the syncline-shape changes during shortening. These are the geometric responses that are expected to occur in all inverted extensional basins containing an extensional rollover. An example of this occurs in the Cameros Basin (Fig. 1e), where the southern basin margin is characterized by an inverted thin-skinned backthrust developed above the extensional rollover and detached on the Upper Triassic salt (Soto et al. (2007) cross-section). Equivalent contractional structures can also be seen in the Parentis Basin (Fig. 1e), where the thin-skinned contraction produces the amplification of salt-cored anticlines by squeezing above the extensional rollover using the Upper Triassic salt as a contractional detachment (Ferrer et al., 2014). Consequently, it should not be ruled out that the contractional thin-skinned structures present in the rollover hinges of the inverted extensional basins might be linked to the same deformation mechanism (i.e., Feda Graben, Mid-Polish Trough, or Broad Fourteens Basin; Gowers et al., 1993; Nalpas et al., 1995; Burliga et al., 2012; Ferrer et al., 2014, 2016).

7. Conclusions

Our research supports previous modeling works in that the geometry and kinematics of salt-detached ramp-syncline basins are strongly controlled by the sub-salt master fault geometry. Nevertheless, our analog models show evidences of salt migration and decoupling during extension and inversion.

Whereas the kinked geometry of the sub-salt ramp-syncline is defined by the displacement and geometry of the extensional master fault, the supra-salt syncline appears significantly modified by salt migration. This mainly consists of a curved geometry of the supra-salt syncline and the development of salt walls or salt anticlines at the syncline edge related to the less dipping fault panel. When the salt unit is thin, the evolution of these diapiric structures is also favored by primary welding formations together with sliding of the supra-salt syncline, which uses the primary weld as a detachment. This sliding resulted in the formation of the primary weld at the syncline backlimb, consequently shifting the sub- and supra-salt syncline hinges. However when the salt unit is thick, the formations of primary welds are delayed and the shifting of syncline hinges is reduced.

The tectonic inversion of salt-detached ramp-syncline basins is mainly characterized by the formation of a major fault-bend anticline controlled by thick-skinned deformation.

The uplift of the thick-skinned fault-bend anticline is favored by the pre-existing primary welds or the new ones that developed during inversion. However, if the fault-bend anticline is eroded during the inversion phase, the reduction of the lithostatic load inhibits the widening of pre-existing welds and the development of new primary welds, and therefore hampers basin uplift.

Simultaneously, basin inversion also produces a reduction in the amplitude of the inherited syncline, which triggered thin-skinned shortening and reactivates the salt layer as an effective contractional detachment. Thin-skinned shortening produces the squeezing of the inherited salt walls; mainly the ones above the rollover hinge, thus increasing salt extrusion and favoring the development of secondary welds.

The results of the experimental program can be applied to reduce the uncertainty on the origin and kinematics of the Columbrets Basin and they suggest that it was inverted as a salt-detached ramp-syncline basin developed over a southeast-dipping low angle fault that included three different panels. The depocenter migration observed in this basin and the presence of contractionally squeezed diapiric structures at the syncline edge, such as occurs in the experiments, support our interpretation.

Acknowledgements

This work was carried out under the financial support of SALTECRES (CGL2014-54118-C2-1-R-MINECO/FEDER UE) and SALCONBELT (CGL2017-85532-P) projects and the “Grup de Recerca de Geodinàmica i Anàlisi de Conques” (2014SGR-467). Research by M. Roma is supported by an APIF pre-doctoral grant from Univeristat de Barcelona. Cairn Energy provided funding for the interpretation of the Columbrets Basin seismic dataset. The GEOMODELS Analog Modeling Laboratory was supported by a scientific infrastructure grant (UNBA08-4E-006) co-funded by the European Regional Development Fund of the “Ministerio de Ciencia e Innovación” of the Spanish government and by Statoil. Schlumberger, HS, and Midland Valley are also acknowledged for providing Petrel, The Kingdom Suite, and Move software respectively. The authors want to thank M.J. Aguilar for the logistical support during the experimental program. Finally we gratefully acknowledge the editor Philippe Agard as well as R. Soto, and one anonymous reviewer for the suggested improvements of the manuscript. English editing by Terranova Scientific.

References

Álvaro, M., Capote, R., Vegas, R., 1979. Un modelo de evolución geotectónica para la Cadena Celtibérica. Acta Geol. Hisp. 14, 172–177.

Ayala, C., Torne, M., Pous, J., 2003. The lithosphere-astenosphere boundary in the western Mediterranean from 3D joint gravity and geoid modeling: tectonic implications. Earth Planet. Sci. Lett. 209, 275–290. https://doi.org/10.1016/S0012-821X(03)00093-1.

Badley, M., Price, J.D., Backshall, L.C., 1989. Inversion, reactivated faults and related structures; seismic examples from the southern North Sea. Geol. Soc. Lond., Spec. Publ. 44, 201–219. https://doi.org/10.1144/GSL.SP.1989.044.01.12.

Bally, A.W., 1984. Tectogenése et sismique reflexion. Bull. Soc. Geol. Fr. 7 (2), 279–285. https://doi.org/10.2113/gssgfbull.S7-XXVI.2.279.

Benedicto, A., Séguret, M., Labaume, P., 1999. Interaction between faulting, drainage and sedimentation in extensional hanging-wall syncline basins: examples of Oligocene Matelles basin (Gulf of Lion rifted margin, SE France). In: Duran, B., Jolivet, L., Horváth, F., Séranne, M. (Eds.), The Mediterranean Basins: Tertiary Extension Within the Alpine Orogen. 156. Geological Society, London, Special Publications, pp. 81–108. https://doi.org/10.1144/GSL.SP.1999.156.01.06.

Biagi, R., 1988. Géométrie et cinématique des prismes d'accrétion sédimentaire: modélisation analogique. 76 Université de Montpellier II, Montpellier.

Buchanan, P.G., McClay, K.R., 1991. Sandbox experiments of inverted listric and planar fault systems. Tectonophysics 188 (1–2), 97–115. https://doi.org/10.1016/0040-1951(91)90317-L.

Burliga, S., Koyi, H.A., Krzywiec, P., 2012. Modelling cover deformation and decoupling during inversion, using the Mid-Polish trough as a case study. J. Struct. Geol. 42, 62–73.

Clark, J.A., Stewart, S.A., Cartwright, J.A., 1998. Evolution of the NW margin of the North Permian Basin, UK North Sea. Geol. Soc. Lond. Mem. 155 (4), 663–676. https://doi.org/10.1144/gsjgs.155.4.0663.

Couzens-Schult, B., Vendeville, B., Wiltschko, D., 2003. Duplex style and triangle zone formation: insights from physical modeling. J. Struct. Geol. 25, 1623–1644. https://doi.org/10.1016/S0191-8141(03)00004-X.

Coward, M., Stewart, S., 1995. Salt-influenced structures in the Mesozoic-Tertiary cover of the southern North Sea, U.K. In: Jackson, M.P.A., Roberts, D.G., Snelson, S. (Eds.), Salt Tectonics. A Global Perspective. 65. American Association of Petroleum Geologists Memoir, pp. 229–250.

De Ruig, M.J., 1995. Extensional diapirism in the eastern Prebetic fold belt, southeastern Spain. In: Jackson, M.P.A., Roberts, D.G., Snelson, S. (Eds.), Salt Tectonics: A Global Perspective. 65. American Association of Petroleum Geologists Memoir, pp. 353–367.

Dell' Ertole, T., Schellart, W., 2013. The development of sheath folds in viscously stratified materials in simple shear conditions: an analogue approach. J. Struct. Geol. 56, 129–141. https://doi.org/10.1016/j.jsg.2013.09.002.

Dooley, T., McClay, K.R., Hempton, M., Smit, D., 2005. Salt tectonics above complex basement extensional fault systems: results from analogue modelling. In: Doré, E.G., Vining, B.A. (Eds.), Petroleum Geology: North-West Europe and Global Perspectives – Proceedings of the 6th Petroleum Geology Conference. Geological Society, London, pp. 1631–1648. https://doi.org/10.1144/0061631.

Durcanin, M.A., 2009. Influence of Synrift Salt on Rift-basin Development. Application to the Orpheus Basin, Offshore Eastern Canada (M.S. thesis). The State University of New Jersey, Graduate School-New Brunswick Rutgers.

Ellis, P.G., McClay, K.R., 1988. Listric extensional fault system-results of analogue model experiments. Basin Res. 1, 55–70.

Escosa, F.O., Roca, E., Ferrer, O., 2018. Testing thin-skinned inversion of a prerift salt-bearing passive margin (Eastern Prebetic Zone, SE Iberia). J. Struct. Geol. 109, 55–73. https://doi.org/10.1016/j.jsg.2018.01.004.

Etheve, N., Mohn, G., Frizon de Lamotte, D., Roca, E., Tugend, J., Gómez-Romeu, J., 2018. Extreme Mesozoic crustal thinning in the eastern Iberia margin: the example of the Columbrets Basin (Valencia Trough). Tectonics 37, 636–662. https://doi.org/10.1002/2017TC004613.

Ferrer, O., Roca, E., Vendeville, B.C., 2008. Influence of a syntectonic viscous salt layer on the structural evolution of extensional kinked-fault systems. Boll. Geofis. Teor. Appl. 49 (2), 371–375.

Ferrer, O., Jackson, M.P.A., Roca, E., Rubinat, M., 2012. Evolution of salt structures during extension and inversion of the Offshore Parentis Basin (Eastern Bay of Biscay). In: Alsop, G.I., Archer, S.G., Hartley, A.J., Grant, N.T., Hodgkinson, R. (Eds.), Salt Tectonics, Sediments and Prospectivity. 363. Geological Society, London, Special Publications, pp. 361–380. https://doi.org/10.1144/SP363.16.

Ferrer, O., Roca, E., Vendeville, B.C., 2014. The role of salt layers in the hangingwall deformation of kinked-planar extensional faults. Insights from 3D analogue models and comparison with the Parentis Basin. Tectonophysics 636, 338–350. https://doi.org/10.1016/j.tecto.2014.09.013.

Ferrer, O., McClay, K.R., Sellier, N.C., 2016. Influence of fault geometries and mechanical anisotropies on the growth and inversion of hanging-wall synclinal basins: insights from sandbox models and natural examples. In: Child, C., Holdsworth, R.E., Jackson, C.A.L., Manzocchi, T., Walsh, J.J., Yieldings, G. (Eds.), The Geometry and Growth of Normal Faults. 439 Geological Society, London, Special Publications. https://doi.org/10.1144/SP439.8.

Ferrer, O., Gratacós, O., Roca, E., Muñoz, J.A., 2017. Modeling the interaction between presalt seamounts and gravitational failure in salt-bearing passive margins: the Messinian case in the northwestern Mediterranean Basin. Interpretation 5 (1), SD99–SD117. https://doi.org/10.1190/INT-2016-0096.1.

Gibbs, A.D., 1984. Structural evolution of extension basin margin. J. Geol. Soc. 141 (4), 609–620. https://doi.org/10.1144/gsjgs.141.4.0609.

Gowers, M.B., Holtar, E., Swensson, E., 1993. The structure of the Norwegian Central Trough (Central Graben area). In: Parker, J.R. (Ed.), Petroleum Geology of Northwest Europe: Proceedings of the 4th Conference. Geological Society, London, pp. 1245–1254. https://doi.org/10.1144/0041245.

Granado, P., Urgeles, R., Sàbat, F., Albert-Villanueva, E., Roca, E., Muñoz, J.A., Mazzuca,

N., Gambini, R., 2016. Geodynamical framework and hydrocarbon plays of a salt giant: the NW Mediterranean Basin. Pet. Geosci. 22 (4), 309–321. https://doi.org/10.1144/petgeo2015-084.
Groshong, R.H., 1989. Half-graben structures: balanced models of extensional fault-bend folds. Geol. Soc. Am. Bull. 101, 96–105. https://doi.org/10.1130/0016-7606(1989)101<0096:HGSBMO>2.3.CO;2.
Guimerà, J., Álvaro, M., 1990. Structure et évolution de la compression alpine dans le Chaîne Ibérique et la Chaîne Côtière Catalane (Espagne). Bull. Soc. Geol. Fr. 8, 339–348.
Guimerà, J., Alonso, Á., Mas, J.R., 1995. Inversion of an extensional-ramp basin by a newly formed thrust: the Cameros basin (N.Spain). Geol. Soc. Lond., Spec. Publ. 88 (1), 433–453. https://doi.org/10.1144/GSL.SP.1995.088.01.23.
Harding, R., Huuse, M., 2015. Salt on the move: multi stage evolution of salt diapirs in the Netherlands North Sea. Mar. Pet. Geol. 61, 39–55. https://doi.org/10.1016/j.marpetgeo.2014.12.003.
Hubbert, M.K., 1937. Theory of scale models as applied to the study of geologic structures. Geol. Soc. Am. Bull. 48, 1459–1519.
Hubbert, M.K., 1951. Mechanical basis for certain familiar geologic structures. Geol. Soc. Am. Bull. 62, 355–372.
Hudec, M.R., Jackson, M.P.A., 2007. Terra infirma: understanding salt tectonics. Earth-Sci. Rev. 82, 1–28. https://doi.org/10.1016/j.earscirev.2007.01.001.
Ings, S.J., Shimeld, J.W., 2006. A new conceptual model from the structural evolution of a regional salt detachment on the northeast Scotian margin, offshore eastern Canada. Am. Assoc. Pet. Geol. Bull. 90 (9), 1407–1423. https://doi.org/10.1306/04050605159.
Jackson, M.P.A., Hudec, M.R., 2005. Stratigraphic record of translation down ramps in a passive-margin salt detachment. J. Struct. Geol. 27, 889–911. https://doi.org/10.1016/j.jsg.2005.01.010.
Jackson, M.P.A., Hudec, M., 2017. Minibasins. In: Salt Tectonics: Principles and Practice. Cambridge University Press, Cambridge, pp. 155–180. https://doi.org/10.1017/9781139003988.010.
Jackson, M.P.A., Vendeville, B.C., 1994. Regional extension as a geologic trigger for diapirism. Geol. Soc. Am. Bull. 106, 57–73. https://doi.org/10.1130/0016-7606(1994)106<0057:REAAGT>2.3.CO;2.
Keppler, R., Rosas, F.M., Nagel, T.J., 2013. Thin viscous middle-crust and evolving fault distribution during continental rifting: insights from analog modeling experiments. Tectonophysics. https://doi.org/10.1016/j.tecto.2013.10.001.
Khele, R.O., 1988. The origin of salt structures. In: Schreiber, B.C. (Ed.), Evaporites and Hydrocarbons. Columbia University Press, New York, pp. 345–404.
Konstantinovskaia, E., Malavieille, J., 2005. Erosion and exhumation in accretionary orogens: experimental and geological approaches. Geochem. Geophys. Geosyst. 6. https://doi.org/10.1029/2004GC000794.
Koyi, H., Petersen, K., 1993. Influence of basement faults on the development of salt structures in the Danish Basin. Mar. Pet. Geol. 10, 82–94. https://doi.org/10.1016/0264-8172(93)90015-K.
Koyi, H., Jenyon, M.K., Petersen, K., 1993. The effect of basement faulting on diapirism. J. Pet. Geol. 16 (3), 285–312.
Krzywiec, P., 2012. Mesozoic and Cenozoic evolution of salt structures within the Polish basin: a review. In: Alsop, G.I., Archer, S.G., Hartley, A.J., Grant, N.T., Hodgkinson, R. (Eds.), Salt Tectonics, Sediments and Prospectivity. 363. Geological Society, London, Special Publications, pp. 381–394. https://doi.org/10.1144/SP363.17.
Liu, H., McClay, K.R., Powell, D., 1992. Physical models of thrust wedges. In: McClay, K.R. (Ed.), Thrust Tectonics. Chapman and Hall, London, pp. 71–81.
Mandl, G., De Jong, L.N.J., Maltha, A., 1977. Shear zones in granular material. Rock Mech. 9, 98–144.
Martín, P., Suriñach, E., 1988. Estructura de la corteza en la zona entre Ibiza y Castellón. Primeros resultados. In: C.I.R.I.T. Barcelona (Ed.), Xarxes sísmiques. Instrumentació i aplicació a la sismotectònica, pp. 521–537.
McClay, K.R., 1989. Analogue models of inversion tectonics. Geol. Soc. Lond., Spec. Publ. 44 (1), 41–59. https://doi.org/10.1144/GSL.SP.1989.044.01.04.
McClay, K.R., 1990. Extensional fault systems in sedimentary basins: a review of analogue model studies. Mar. Pet. Geol. 7 (3), 206–233. https://doi.org/10.1016/0264-8172(90)90001-W.
McClay, K.R., Scott, A.D., 1991. Experimental models of hangingwall deformation in ramp-flat listric extensional fault systems. Tectonophysics 188, 85–96. https://doi.org/10.1016/0040-1951(91)90316-K.
Medwedeff, D.A., Suppe, J., 1997. Multibend fault-bend folding. J. Struct. Geol. 19, 279–292. https://doi.org/10.1016/S0191-8141(97)83026-X.
Mencos, J., Carrera, N., Muñoz, J.A., 2015. Influence of rift basin geometry on the subsequent postrift sedimentation and basin inversion: the Organyà Basin and the Bóixols thrust sheet (south central Pyrenees). Tectonics 34 (7), 1452–1474. https://doi.org/10.1002/2014TC003692.
Mitra, S., 2002. Fold-accommodation faults. Am. Assoc. Pet. Geol. Bull. 86 (4), 671–693.
Mohr, M., Kukla, P.A., Urai, J.L., Bresser, G., 2005. Multiphase salt tectonic evolution in NW Germany: seismic interpretation and retro-deformation. Int. J. Earth Sci. 94, 917–940.
Nalpas, T., Le Douran, S., Brun, J.P., Untrnehr, P., Richert, J.P., 1995. Inversion of the Broad Fourteens Basin (offshore Netherlands), a small-scale model investigation. Sediment. Geol. 95, 237–250. https://doi.org/10.1016/0037-0738(94)00113-9.
Ortí, F., Pérez-López, A., Salvany, J.M., 2017. Triassic evaporites of Iberia: Sedimentological and palaeogeographical implications for the western Neotethys evolution during the Middle Triassic–Earliest Jurassic. Palaeogeogr. Palaeoclimatol. Palaeoecol. 471, 157–180. https://doi.org/10.1016/j.palaeo.2017.01.025.
Pascal, G., Torne, M., Buhl, P., Watts, A.B., Mauffret, A., 1992. Crustal and velocity structure of the Valencia trough (western Mediterranean), part II: detailed interpretation of five expanded spread profiles. Tectonophysics 203, 21–35. https://doi.org/10.1016/0040-1951(92)90213-P.
Ramberg, H., 1967. Model experimentation of the effect of gravity on tectonic processes. Geophys. J. R. Astron. Soc. 14, 307–329.
Rank-Friend, M., Elders, C.F., 2004. The evolution and growth of Central Graben salt structures, Salt Dome Province, Danish North Sea. In: Davies, R., Cartwright, J.A., Stewart, S.A., Lappin, M., Underhill, J.R. (Eds.), 3D Seismic Technology: Application to the Exploration of Sedimentary Basins. 29. Geological Society, London Memoir, pp. 149–163. https://doi.org/10.1144/GSL.MEM.2004.029.01.15.
Reston, T.J., 2007. The formation of non-volcanic rifted margins by the progressive extension of the lithosphere: the example of the West Iberian margin. Geol. Soc. Lond., Spec. Publ. 282 (1), 77–110. https://doi.org/10.1144/SP282.5.
Roca, E., 1996. La Cubeta mesozoica de las Columbrets: aportaciones al conocimiento de la estructura del surco de Valencia. Geogaceta 20 (7), 1711–1714.
Roca, E., 2001. The Northwest Mediterranean Basin (Valencia Trough, Gulf of Lions and Liguro-Provençal basins): structure and geodynamic evolution. In: Ziegler, P.A., Cavazza, W., Robertson, A.H.F., Crasquin-Soleau, S. (Eds.), Peri-Thetys Memoir 6: Peri-Tethyan Rift/wrench Basins and Passive Margins. 186. Mémoires du Muséum National d'Histoire Naturelle, pp. 671–706.
Roca, E., Guimerà, J., Salas, R., 1994. Mesozoic extensional tectonics in the southeast Iberian Chain. Geol. Mag. 131 (2), 155–168. https://doi.org/10.1017/S0016756800010694.
Roma, M., Vidal-Royo, O., McClay, K.R., Ferrer, O., Muñoz, J.A., 2018. Tectonic inversion of salt-detached ramp-syncline basins as illustrated by analog modeling and kinematic restoration. Interpretation 6 (1), 127–144. https://doi.org/10.1190/int-2017-0073.1.
Rowan, M.G., Jackson, M.P.A., Trudgill, B.D., 1999. Salt-related fault families and fault welds in the northern Gulf of Mexico. Am. Assoc. Pet. Geol. Bull. 83 (9), 1454–1484.
Salvany, J.M., Bastida, J., 2004. Análisis litoestratigráfico del Keuper surpirenaico central. Soc. Geol. Esp. 17 (1–2), 3–26.
Sanchis, E., Séranne, M., 2000. Structural style and tectonic evolution of a polyphase extensional basin of the Gulf of Lion passive margin: the Tertiary Ales basin, southern France. Tectonophysics 322 (3), 219–242. https://doi.org/10.1016/S0040-1951(00)00097-4.
Schellart, W.P., 2000. Shear test results for cohesion and friction coefficients for different granular materials: scaling implications for their usage in analogue modelling. Tectonophysics 324, 1–16.
Schettino, A., Turco, E., 2010. Tectonic history of the western Thetys since the Late Triassic. Geol. Soc. Am. Bull. 123, 89–105. https://doi.org/10.1130/B30064.1.
Soto, R., Casas-Sainz, M., Del Río, P., 2007. Geometry of half-grabens containing a midlevel viscous décollement. Basin Res. 19, 437–450. https://doi.org/10.1111/j.1365-2117.2007.00328.x.
Stewart, S.A., Clark, J.A., 1999. Impact of salt on the structure of the Central North Sea hydrocarbon fairways. In: Fleet, A.J., Boldy, A.R. (Eds.), Petroleum Geology of Northwest Europe. Proceedings of the 5th Conference. Geological Society, London, pp. 179–200. https://doi.org/10.1144/0050179.
Suppe, J., 1983. Geometry and kinematics of fault bend folding. Am. J. Sci. 283, 684–721.
Tavani, S., Storti, F., Salvini, F., 2005. Rounding hinges to fault-bend folding: geometric and kinematic implications. J. Struct. Geol. 27, 3–22. https://doi.org/10.1016/j.jsg.2004.07.005.
Torne, M., Pascal, G., Buhl, P., Watts, A.B., Mauffret, A., 1992. Crustal and velocity structure of the Valencia trough (western Mediterranean), part I. A combined refraction/wide angle reflection and near-vertical reflection study. Tectonophysics 203, 1–20. https://doi.org/10.1016/0040-1951(92)90212-O.
Vendeville, B.C., Jackson, M.P.A., 1992. The rise of diapirs during thin-skinned extension. Mar. Pet. Geol. 9, 331–353. https://doi.org/10.1016/0264-8172(92)90047-I.
Vendeville, B.C., Cobbold, P.R., Davy, P., Brun, J.P., Choukroune, P., 1987. Physical models of extensional tectonics at various scales. In: Coward, M.P., Dewey, J.F., Hancock, P.L. (Eds.), Continental Extensional Tectonics. 28. Geological Society, London, Special Publication, pp. 95–107.
Vidal, N., Gallart, J., Dañobeitia, J.J., 1998. A deep seismic crustal transect from the NE Iberian Peninsula to the western Mediterranean. J. Geophys. Res. 103, 12381–12396. https://doi.org/10.1029/98JB00076.
Weijermars, R., 1986. Flow behavior and physical chemistry of bouncing putties and related polymers in view of tectonic laboratory applications. Tectonophysics 123, 325–358. https://doi.org/10.1016/0040-1951(86)90208-8.
Weijermars, R., Jackson, M.P.A., Vendeville, B.C., 1993. Rheological and tectonic modeling of salt provinces. Tectonophysics 217, 143–174.
White, N., 1992. A method for automatically determining normal faults geometry at depth. J. Geophys. Res. 97, 1715–1733.
Withjack, M.O., Callaway, S., 2000. Active normal faulting beneath a salt layer: an experimental study of deformation patterns in the cover sequence. Am. Assoc. Pet. Geol. Bull. 84 (5), 627–651.
Withjack, M.O., Schlische, R.W., 2005. A review of tectonic events on the passive margin of eastern North America. In: Post, P. (Ed.), Petroleum Systems of Divergent Continental Margin Basins: 25th Bob S. Perkins Research Conference, Gulf Coast Section of SEPM, pp. 203–235.
Withjack, M.O., Schlische, R.W., 2006. Geometric and experimental models of extensional fault-bend folds. In: Buiter, S.J.H., Schreurs, G. (Eds.), Analogue and Numerical Modelling of Crustal-scale Processes. 235. Geological Society, London, Special Publications, pp. 208–305. https://doi.org/10.1144/GSL.SP.2006.253.01.15.
Withjack, M.O., Schlische, R.W., Olsen, P.E., 2002. Rift-basin Structure and Its Influence on Sedimentary Systems. 73. American Association of Petroleum Geologists, Special Publication of SEPM, pp. 57–81.
Xiao, H., Suppe, J., 1992. Origin of rollover. Am. Assoc. Pet. Geol. Bull. 76 (4), 509–529.
Zeyen, H.J., Banda, E., Gallart, J., Ansorge, J., 1985. A wide angle seismic reconnaissance survey of the crust and upper mantle in the Celtiberian Chain of eastern Spain. Earth Planet. Sci. Lett. 75, 393–402. https://doi.org/10.1016/0012-821X(85)90182-7.

APPENDIX II

Tectonic inversion of salt-detached ramp-syncline basins as illustrated by analog modeling and kinematic restoration

Roma, M., O. Vidal-Royo, K. McClay, O. Ferrer, J.A. Muñoz, 2018b. Interpretation. 6(1), T127-T144, doi: 10.1190/INT-2017-0073.1.

Tectonic inversion of salt-detached ramp-syncline basins as illustrated by analog modeling and kinematic restoration

Maria Roma[1], Oskar Vidal-Royo[2], Ken McClay[3], Oriol Ferrer[1], and Josep Anton Muñoz[1]

Abstract

Salt-detached ramp-syncline basins are developed in extensional settings and are characterized by wide synclinal sedimentary basins detached on salt and formed above the hanging wall of active ramp-flat-ramp extensional faults. They are rarely fault bounded; instead, they are bounded by salt structures that are in general parallel to the major subsalt structures. As such, the formation of these extensional systems requires the presence of (1) a subsalt extensional fault with significant dip changes and (2) an evaporitic unit above the extensional fault, which partially or completely decouples the basin from a subsalt extensional fault. Salt-detached ramp-syncline basins have a significant exploration potential when their extensional geometry is preserved and when they have undergone positive tectonic inversion and consequent uplift and fold amplification. However, in some cases, their subsalt geometry may not be fully recognizable, especially when subsalt seismic imaging is poor. To obtain a deeper understanding of the geometry and kinematic evolution of these salt-detached ramp-syncline basins, we performed a series of analog modeling experiments, in which the models' cross sections had been sequentially restored. Analog models and restoration results reveal that the kinematic evolution of the salt-detached ramp-syncline basins during extension and inversion depends on the interaction of different factors that may function simultaneously. Our results are used to improve the interpretation of seismic sections in inverted Mesozoic salt-detached ramp-syncline basins on the Atlantic margins, where subsalt faults are not well-imaged, and thus the suprasalt geometries must be used to infer the subsalt structure.

Introduction

Synclinal basins are defined as sedimentary basins that developed in the core of a syncline where synkinematic sediments are not bounded by major faults. Basins with synclinal geometries have been classically defined in contractional scenarios (e.g., piggy-back basins; Ori and Friend, 1984). Nevertheless, these basins can also develop via a range of mechanisms: (1) by extension above the hanging wall of active normal fault with dip variations (Figure 1a), (2) by salt evacuation (Figure 1b), or (3) by a combination of both (Figure 1c).

Synclinal basins may develop in the absence of salt when a ramp-flat-ramp extensional fault is involved; then a ramp-syncline basin is developed above its hanging wall (Figure 1a). The ramp synclines are characterized by asymmetric synclines with depocenters younging landward (McClay, 1990; Benedicto et al., 1999; Figure 1a). Where salt evacuation is the main mechanism controlling their growth, synclinal basins may develop as a consequence of sinking minibasins (Figure 1b). In this case, minibasins are small basins largely surrounded by salt walls and in the simplest cases, they contain vertically stacked depocenters (Jackson and Talbot, 1991; Rowan and Vendeville, 2006; Hudec et al., 2009; Callot et al., 2016; Figure 1b). Additionally, synclinal basins may also develop in hybrid systems (i.e., involving subsalt extensional faults and salt evacuation). In this scenario, when the extensional fault has a ramp-flat-ramp geometry, the resulting synclinal basin has been given numerous names: (1) extensional-ramp basins in Guimerà et al. (1995); (2) extensional hanging-wall syncline basins in Benedicto et al. (1999); and (3) hanging-wall synclinal basins in Ferrer et al. (2016) (Figure 1c). We propose that the term salt-detached ramp-syncline basin (Figure 1c) be used to describe all synclinal sedimentary basins that formed above active ramp-flat-ramp extensional faults and are detached on salt. In this case, the extensional salt tectonic system is characterized by (1) subsalt landward and basinward rollovers, (2) two wide salt-

[1]Universitat de Barcelona, Institut de Recerca GEOMODELS, Departament de Dinàmica de la Terra i de l'Oceà, Facultat de Ciències de la Terra, C/Martí i Franquès s/n, Barcelona, Spain. E-mail: mariaroma@ub.edu; joferrer@ub.edu; jamunoz@ub.edu.
[2]Terractiva Consulting SL, Barcelona, Spain. E-mail: oskar@terractiva.net.
[3]Royal Holloway University of London, Fault Dynamics Research Group, Earth Sciences Department, Egham, UK. E-mail: k.mcclay@rhul.ac.uk.
Manuscript received by the Editor 21 April 2017; revised manuscript received 8 September 2017; published ahead of production 02 November 2017; published online 21 December 2017. This paper appears in *Interpretation*, Vol. 6, No. 1 (February 2018); p. T127–T144, 12 FIGS., 1 TABLE.
http://dx.doi.org/10.1190/INT-2017-0073.1.

detached ramp-syncline basins, not bounded by normal faults but by salt-cored anticlines, and (3) the trend of the basins and bordering salt structures are generally parallel to the major subsalt structures (Figure 1c). However, if the amount of extension and decoupling is significant, the basin can be transported away from the subsalt fault ramp to above a subsalt fault flat (Carola, et al., 2015). Clearly, salt-detached ramp-syncline basins differ from the typical extensional minibasins because salt-detached ramp synclines can be a hundred times wider and the subsalt fault geometry is the main factor controlling these sedimentary basins, with or without the presence of salt. The salt acts as an effective décollement decoupling subsalt and suprasalt deformation (Vendeville, 1987, 1988; Koyi and Petersen, 1993; Nalpas and Brun, 1993; Vendeville et al., 1995; Steward and Clark, 1999; Withjack and Callaway, 2000; Ferrer et al., 2016), but such scenarios follow a partial coupling structural style, where the salt unit acts as a thin-skinned component in a thick-skinned deformation style. The basement fault does not penetrate the salt unit but is overlain by a draped fold over the master fault (Jackson and Hudec, 2017).

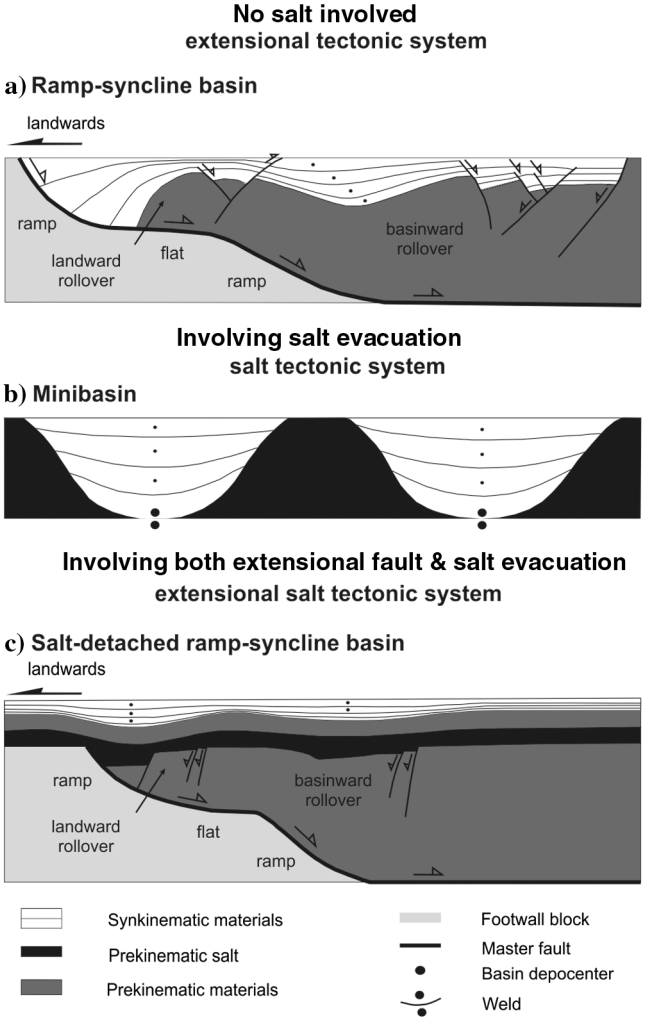

Figure 1. Conceptual models of (a) a ramp syncline developed in a salt-free extensional tectonic system, modified from McClay (1990), (b) a minibasin developed in a a salt tectonic system, and (c) a salt-detached ramp-syncline basin developed in an extensional salt tectonic system, modified from Ferrer et al. (2016).

Mesozoic extensional basins around western Europe, as well as in their equivalent North-American Atlantic margin, are characterized by synclinal geometries detached from subsalt faults by Late Triassic (Keuper and Dagorda) or Permian (Zechstein) evaporites, e.g., Parentis Basin (Ferrer et al., 2012, see Figure 2), Sogne Basin (Stewart and Clark, 1999), Jeanne d'Arc Basin (Tankard et al., 1989), Orpheus Basin (Withjack and Schlische, 2005), and the Lusitanian Basin (Alves et al., 2002). In these basins, the salt was deposited at the late stages of extensional deformation related to the breakup of Pangea during Permo-Triassic times (Coward, 1995; Glennie, 1995). As a result, the interaction between the subsalt fault structure and the main synrift depocenters is characterized by multiple rift events with deposition of salt during and after the extensional phase (Ziegler, 1988; Balkwill and Legall, 1989; Tankard et al., 1989; Dercourt et al., 1993; Rasmussen et al., 1998; Jackson et al., 2000; Alves et al., 2002). Consequently, the salt shows lateral variations in thickness (Jackson and Vendeville, 1994; Coward and Steward, 1995; Ferrer et al., 2008, 2014; Rowan, 2014). Furthermore, most of these basins were subsequently partially or totally tectonically inverted during the Late Cretaceous – Cenozoic, e.g., Parentis (Mathieu, 1986) or Lusitanian Basins (Alves et al., 2002) or incorporated into a fold-and-thrust belt, e.g., the Organyà (Muñoz, 1992) and Cameros Basins (Guimerà et al., 1995). Further complicating matters, the distribution and thickness of the evaporitic unit as well as the inherited structure at the end of the extensional phase determined the structural style during tectonic inversion of the mentioned examples. The complexity of this resulting geologic scenario together with the poor quality of the available seismic data, often hinder precise interpretation of subsalt data, and they consequently obscure the origin and kinematic development of the inverted basin. The use of scaled analog modeling allows reproducing an approximation of a natural geologic process. Thus, analog modeling can help in constraining the interpretation of the subsalt data, understanding the interaction between the subsalt fault and the evaporites during the extensional phase, and understanding the overprinted tectonic inversion phase.

For the past 80 years, analog modeling has been used to understand these complex geologic systems. For example, Roure et al. (1992) and McClay (1990) use a prekinematic sand pack (an analog of brittle materials in nature) over a rigid wooden footwall block and a plastic sheet (used to reproduce the fault geometry and fault motion) to study the formation of ramp synclines. Soto et al. (2007) and Ferrer et al. (2014) follow the previous technique, and they use different fault geometries — listric, ramp-flat listric, planar, and kinked — but they also tested the role of a shallow

prekinematic polymer layer (as an analog of salt in nature) within the brittle sand pack to simulate salt-detached ramp-syncline basins. More recently, Ferrer et al. (2014) consider a synkinematic ductile layer. Furthermore, McClay (1989), Buchanan and McClay (1991), and Yamada and McClay (2003) use different techniques to previously extend the model and then reverse the direction of motion to produce the subsequent inversion. Only the recent work of Durcanin (2009) and Ferrer et al. (2016) considers the inversion phase, including a polymer layer in the prekinematic configuration. They note the control of the inherited salt configuration and salt structures during inversion. But, they do not especially address it in large amounts of extension and inversion phases, in multiple rift events, in salt kinematics, and how salt influences the resulting structural style.

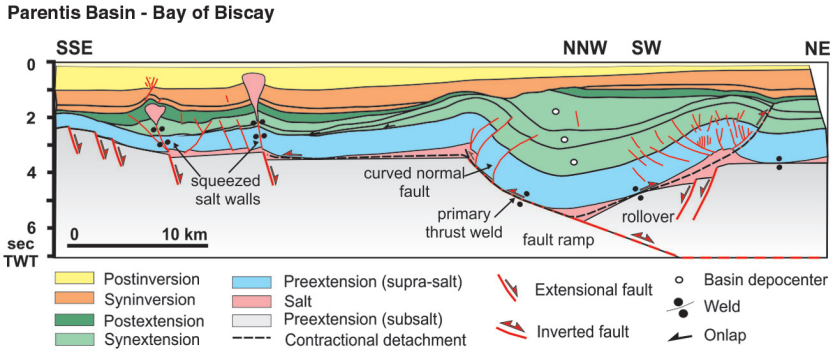

Figure 2. Natural example of an inverted salt-detached ramp-syncline basin. Line drawing of a seismic section of the inverted Parentis Basin (Bay of Biscay) with a prekinematic salt unit. Modified from Ferrer et al. (2012).

We have supplemented the works by Durcanin (2009) and Ferrer et al. (2016) by investigating the results of two analog models of salt-detached ramp-syncline basins developed above a ramp-flat-ramp rigid wooden footwall block. The models underwent two phases of extension with synkinematic salt deposited between them, and they were subsequently deformed by later inversion. We analyzed two representative sections across the model, illustrating domains with and without well-developed diapirism. The cross sections were then sequentially restored with geometric algorithms to illustrate the structural evolution as well as the variations in sectional area of the salt.

The experimental results are consistent with the interpretation of Ferrer et al. (2012) on the Parentis Basins (Figure 2), and they also lead to a new interpretation of the Lusitanian Basin, modifying the previous one by Alves et al. (2002). As such, our results can serve as a guide for improving the interpretation of seismic lines in other salt basins, where these styles of extensional salt tectonics develop.

Modeling methodology

Two experiments are presented in this paper. Both experiments simulate polyphase deformation. In detail, the models were initially extended by 7 cm, at which point our salt analog (silicone polymer) was added and followed by a further 8 cm of extension (15 cm of total extension). Experiment 1 was terminated at the end of the two extensional phases, whereas experiment 2 was inverted by 8 cm of shortening after the end of extension.

Experimental setup

The experimental setup was similar to that used by Yamada and McClay (2003) and Ferrer et al. (2016). The analog models were carried out in a 63 cm long, 30 cm wide, and 35 cm deep glass-sided deformation box (Figure 3a). A rigid wooden block with four kinked

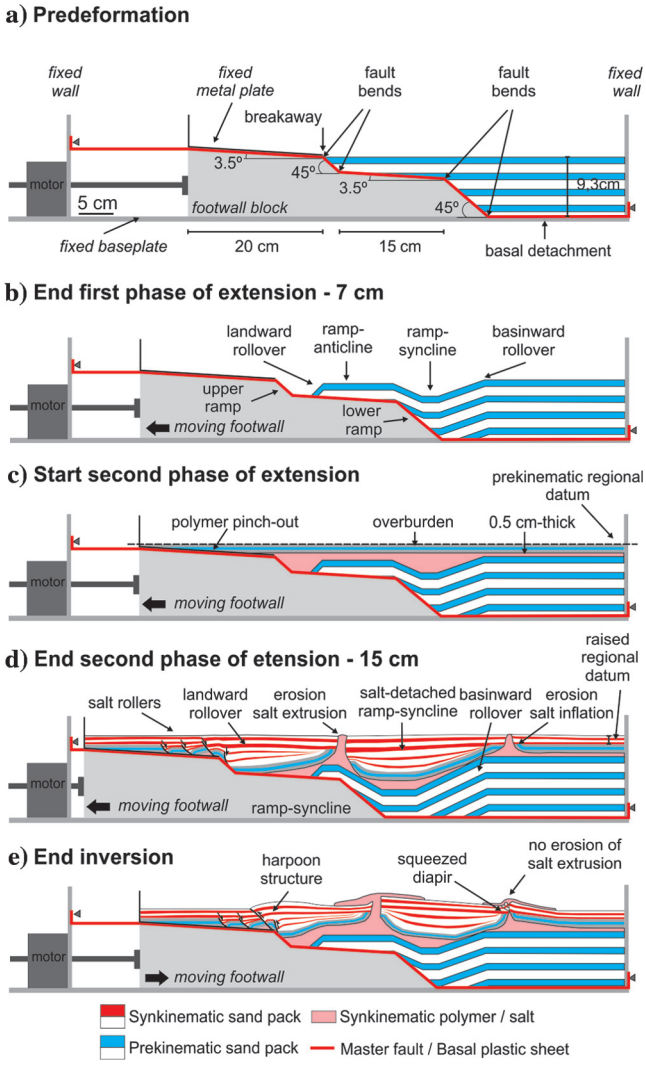

Figure 3. Simplified sketch illustrating the experimental apparatus: (a) predeformation geometry, (b) configuration of the experiments 1 and 2 at the end of first phase of extension — 7 cm, (c) experimental configuration prior to the second phase of extension for experiments 1 and 2, (d) configuration of the experiments 1 and 2 at the end of second phase of extension — 15 cm, and (e) configuration of the experiment 2 at the end of the inversion.

fault bends was used as a footwall geometry that imposed a ramp-flat-ramp geometry to the master fault. Both ramps dip at 45°, and they were separated by two panels dipping at 3.5° with an adjacent horizontal basal detachment at the base of the model (Figure 3a). We placed a plastic sheet above the footwall block to reproduce the master fault motion (Figure 3a, solid red line). The plastic sheet remained attached at both end walls during extension and inversion. We fixed a metal plate above the upper footwall flat to form the breakaway fault (Figure 3a); here, the plastic sheet went underneath the metal plate. Extension was achieved by pulling the footwall block away using a motor-driven worm screw (Figure 3d). For the inversion of experiment 2, the motion of the footwall block was reversed to produce contraction of the hanging wall section (Figure 3e).

Modeling materials

The materials used in the experimental program (Table 1) were well-sorted, subrounded dry silica sand and polydimethylsiloxane (PDMS) polymer. The dry sand was chosen to simulate the brittle deformation of upper crustal sedimentary rocks (Horsfield, 1977; McClay, 1990), and the PDMS polymer was used as our salt analog (Weijermars, 1986), as in most analog modeling studies (Koyi et al., 1993; Nalpas and Brun, 1993; Vendeville et al., 1995; Withjack and Callaway, 2000; Dooley et al., 2005; Soto et al., 2007; Ferrer et al., 2014, 2016). Silica sand has a Mohr-Coulomb behavior at moderate values of normal stress, and its mechanical properties were measured using a ring shear tester at the Fault Dynamics Research Group Laboratory. The poured dry sand had an average grain size of 250 μm, an angle of internal friction of 34.6°, a bulk density of 1500 $kg \cdot m^{-3}$, and a low apparent cohesive strength of 55 Pa. The polymer (PDMS) has a near-perfect Newtonian fluid behavior when deformed at a laboratory strain rate of 1.83×10^{-4} $cm \cdot s^{-1}$ (Weijermars, 1986). It has an effective viscosity of 1.6×10^4 $Pa \cdot s$ and a density of 972 $kg \cdot m^{-3}$ at 20°C. The coefficient of sliding friction between the plastic sheet and the sand pack was 0.37 (Huiqi et al., 1992).

Table 1. Scaling parameters used in the experimental program.

Quantity	Experiment	Nature	Model/nature
Length, L (m)	0.01	1000	10^{-5}
Density loose sand, ρ ($kg \cdot m^3$)	1500	2700	0.55
Gravity acceleration, g ($m \cdot s^{-2}$)	9.8	9.8	1
Angle of internal friction, φ (°)	34.6	40	0.87
Cohesion loose sand, σ (Pa)	55	10^7	5.5×10^{-6}
Density polymer, ρ ($kg \cdot m^3$)	972	2200	0.44
Viscosity, η (Pa·s)	1.6×10^4	10^{18}–10^{19}	$1.6 \times 10^{-14/-15}$

The experiments were geometrically, kinematically, and dynamically scaled (e.g., Hubbert, 1937; Schellart, 2000), such that with a length ratio of 10^{-5}, 1 cm in the model corresponds to approximately 1 km in nature (Table 1).

Experimental procedure

The layered prekinematic sand pack for both models was formed by pouring 3 mm thick, horizontal white and colored sand layers into the deformation box using a mechanical scraper. This prekinematic unit covered the entire model with a total thickness of 9.3 cm above the horizontal basal detachment (Figure 3a). The models were initially extended 7 cm at a displacement rate of 1 cm per 10 min. No synkinematic strata were added during this first phase of extension (Figure 3b). The accommodation space was then infilled by a polymer showing important variable thickness (Figure 3c). The polymer has a horizontal upper surface, a thickness of 0.5 cm on the right section of the model, and it pinches out on the upper footwall flat. The polymer was covered by a 1 cm thick sand layer prior to the second phase of extension (overburden in Figure 3c).

The second 8 cm of extension (15 cm in total) was applied to both models at a rate of 1 cm per hour (Figure 3d). During this phase, synkinematic layers were added by pouring alternating layers of red, white, and black sand after every 0.5 cm of extension, keeping the prekinematic regional datum constant (Figure 3c). The models were paused for 15 min during the deposition of each second extensional phase synkinematic sand layer. Any topographic highs that had formed by polymer inflation were eroded during the synkinematic layering (Figure 3d), thus removing the overburden and enhancing subsequent polymer rise. When the polymer reaches the surface of the model on these inflated areas, the regional datum was raised by 3 mm for each subsequent synkinematic layer, thus simulating the passive growth of the salt wall (Figure 3d). Any polymer surface extrusion was manually removed with a sharpened knife (it has only removed the entire polymer overhang without affecting the diapir stem) during the second phase of extension (simulating salt dissolution and erosion in nature) before adding a new synkinematic layer (Figure 3d). The polymer surface extrusions are also removed to avoid Christmas-tree structures (repeated salt extrusion over the underlying strata, which create stacked salt wings forming a serrated contact). Removing the polymer extrusion, we simplify the extensional geometry of the salt structures and we also reduce the complexity of the subsequent inverted salt structures.

Experiment 2 followed the same procedure as experiment 1, but was in-

verted 8 cm after the end of the second phase of extension (Figure 3e) at a shortening rate of 1 cm per hour, until reaching the null point of the second extensional phase. Nonerosion and synkinematic layers were added during the inversion phase.

At the end of both experiments, the models were covered by a thick postkinematic sand layer to preserve the final topography and to inhibit any undesired movement of the polymer. Then, the models were preserved and serially sectioned at a spacing of 0.3 cm.

The tops and the sides of the models were recorded by high-resolution digital time-lapse photography. The final cross sections were also recorded using digital photography.

Restoration procedure

Two final cross sections of experiment 2 were sequentially restored to illustrate the structural evolution of the two main domains across areas with well-developed salt walls and across areas without extruded salt walls. The sequential restoration shows (1) the change in basin geometry due to extension, positive inversion, and diapirism, and it highlights the different responses to deformation of the subsalt and suprasalt units and (2) the variations in the area of the salt section between the subsalt and suprasalt units at each phase.

The subpolymer and suprapolymer units in the analog models were restored independently using different strain transformations (i.e., restoration methods) for each. The suprapolymer deformation is characterized by folding and faulting as a consequence of extension and compression — triggering polymer mobilization — and therefore flexural slip, unfolding to a known datum (regional) was applied, allowing conservation of the line length and area (Dahlstrom, 1969; Groshong et al., 2012; Lingrey and Vidal-Royo, 2015). The deformation of the subpolymer sand pack was generated by slip along the master fault, and was restored using the fault parallel flow algorithm in Move by applying the measured fault offsets between consecutive restoration phases.

Modeling limitations

The main limitation of our experimental setup is that the rigid footwall block that constrains the geometry of the extensional fault (Figures 4 and 5) prevented the formation of basement-involved footwall shortcuts and horses, as in Nalpas et al. (1995) and in Eisenstadt and Sims (2005). Besides, higher friction between the glass-side walls and the polymer/sand pack produced a border effect on the structures (Ferrer et al., 2016). As a consequence, there was preferred polymer inflation at the central part of the model during the second extensional phase. In addition, the polymer produces smearing against the glass side walls, which obscures the detailed evolution of structures at these phases. Consequently, the evolution of the models was determined by the analysis of vertical cross sections at the end of the experiments and their sequential restoration combined with overhead time-lapse photographs. The restored sections in Figures 6 and 7 show differences in restored line lengths between the subpolymer and suprapolymer units. To explain the differential line length, the actual geologic processes that have been described in nature and are replicated by sandbox models include (1) internal shear and readjustment of particles because of the ongoing deformation regime; and (2) out-of-section movement due to salt tectonics and transpression (Casas et al., 1996; Koyi, 2000; Koyi and Sans, 2006; Burberry, 2015). Consequently, we consider internal shear as the main factor to take into account when it comes to considering bed length and area conservation in the restoration of compressional structures. During the analysis of the cross sections and the overhead photographs, we omitted a 3 cm wide section to avoid the border effects.

Modeling results

Experiment 1 and 2 — Two phases of extension

The results of the first and second extensional phases can be seen in experiments 1 and 2.

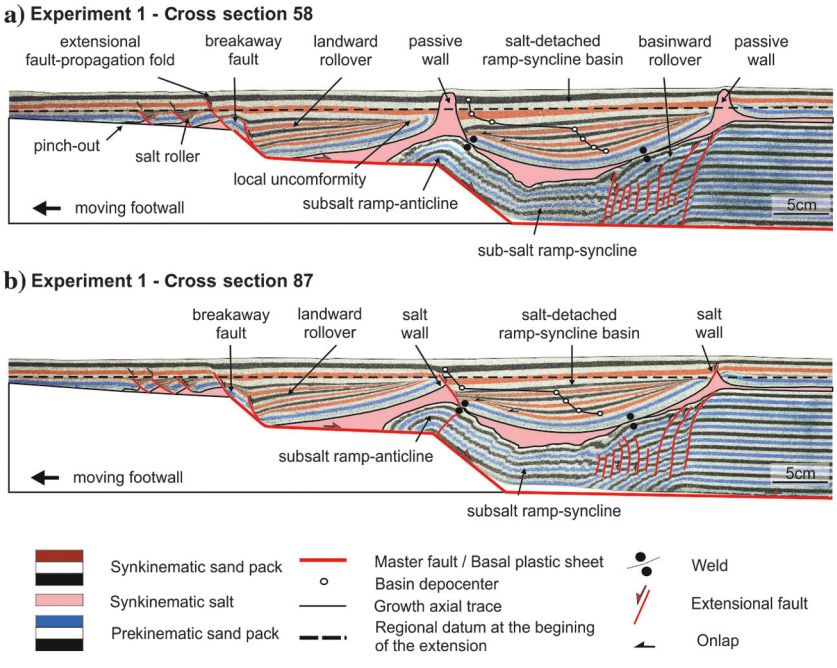

Figure 4. Interpreted cross section of the structures observed in experiments 1 and 2 at the end of the second phase of extension (after 15 cm of lengthening) and with the terminology used in this paper. (a) Cross section 58 and (b) cross section 87. The location of the cross sections is shown in Figure 5.

First phase: 0–7 cm of extension

The first phase of extension produced translation of the prekinematic strata over the master fault, which generated fault-related folding of the hanging wall (Figure 3b). This formed a landward rollover, together with a fault-bend fold ramp anticline and a ramp syncline over the major footwall ramp. In addition, a basinward rollover anticline formed where the master fault flattened out into the horizontal basal detachment on the right side of the model (Figure 3b). Minor antithetic normal faults developed within this large rollover panel. All these structures were covered by a salt unit (i.e., polymer) of variable thickness at the end of the first extensional phase (Figure 3c).

Second phase: 7–15 cm of extension

The second phase of the extension reactivated the main master fault. The subsalt structures developed during the first phase of extension are still recognized during the entire second phase of extension (Figure 4). The width of the subsalt ramp anticline decrease as the extension progressed; in contrast, the subsalt ramp syncline was amplified as a result (Figure 4). With continued extension, an extensional forced fold developed at the breakaway fault (Figures 5a, 6b, and 7b), evolving into an extensional fault-propagation fold (Figures 4a, 6c, and 7c). During this process, the salt thinned above the upper ramp favoring the upward propagation of this fault into the synextensional sand pack (Figures 4 and 6c). Once subsalt and suprasalt units were completely coupled, a curved normal fault nucleated on the upper ramp (Figure 5b). At the early stages of the second phase of extension, several small listric faults with triangular footwall salt rollers were formed in the upper footwall flat to the left of the breakaway (Figures 4 and 5a).

Upward fault propagation was inhibited, where the salt was the thickest (above the lower ramp). Continued extension was accommodated by the formation of a salt-detached ramp-syncline basin lying above the salt unit and above the subsalt ramp syncline (Figures 4, 6c, and 7c). The lithostatic load produced by synkinematic sedimentation — combined with the subsalt fault slip — triggered salt flow from the areas with high vertical load (basin depocenter) to the edges of the salt-detached ramp-syncline basin, where the vertical load was lower (e.g., Kehle, 1988; Koyi et al., 1993; Hudec and Jackson, 2007; Ferrer et al., 2014). This gave rise to salt-inflated areas bounding the salt-detached ramp syncline (Figure 7c). The erosion of salt-inflated areas (local unconformity in Figures 4 and 6d) above the regional datum (Figure 5a), as well as the effective decoupling of subsalt and suprasalt materials, favored the growth of reactive (Figure 6b) to passive salt walls (Figure 6e) at the edges of the salt-detached ramp-syncline basin (Figure 4a and 4b). The salt walls only pierced the cover in the center and along the glass-side walls of the experiment (cross section 58, Figures 4a, 5a, and 6f). The continuity of the source layer was interrupted after the formation of basin welds gave rise to coupled deformation near the end of the extensional phase (Figures 4 and 6f).

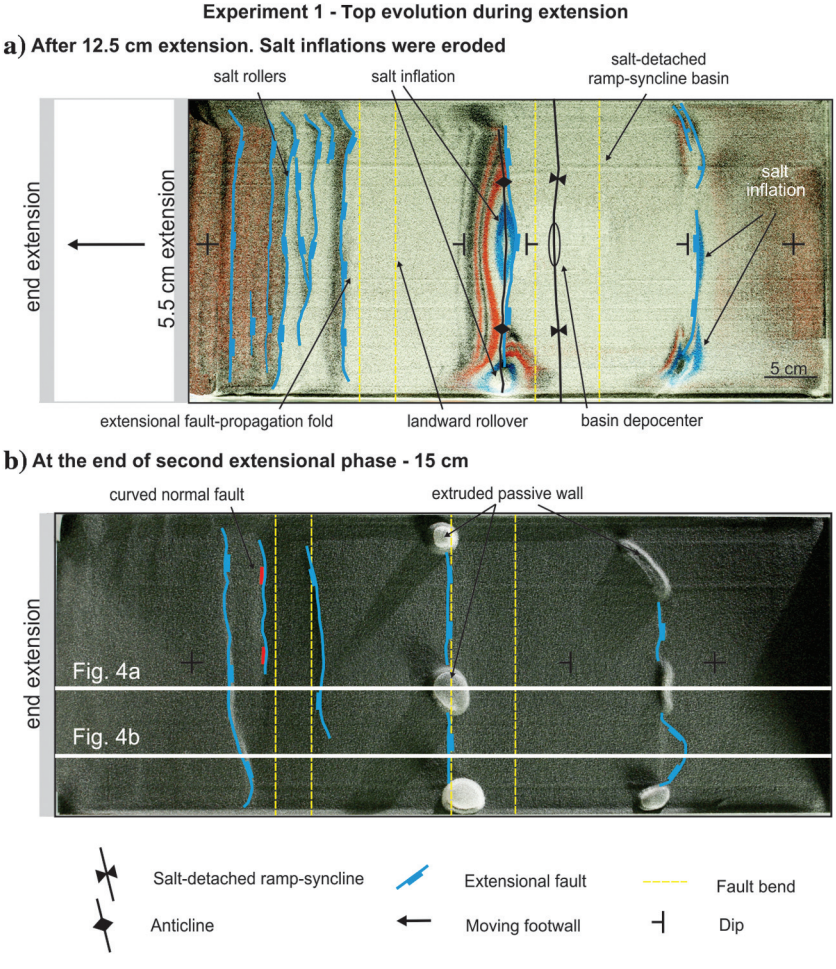

Figure 5. Interpreted overhead photographs illustrating the structural evolution of experiments 1 and 2 during extension. (a) After 12.5 cm extension and (b) at the end of the extension (15 cm total), the horizontal white lines indicate the location of the experiment 1 cross sections in Figure 4.

Experiment 2 — Two phases of extension followed by inversion

Figure 8 shows the result of 8 cm of bulk shortening superimposed on two phases of extension similar to those described in experiment 1. Inversion produced the reactivation of the master fault and the salt flow. Both cross sections in Figure 8 show a broad frontal harpoon structure (see Buchanan and McClay, 1991) formed by contractional

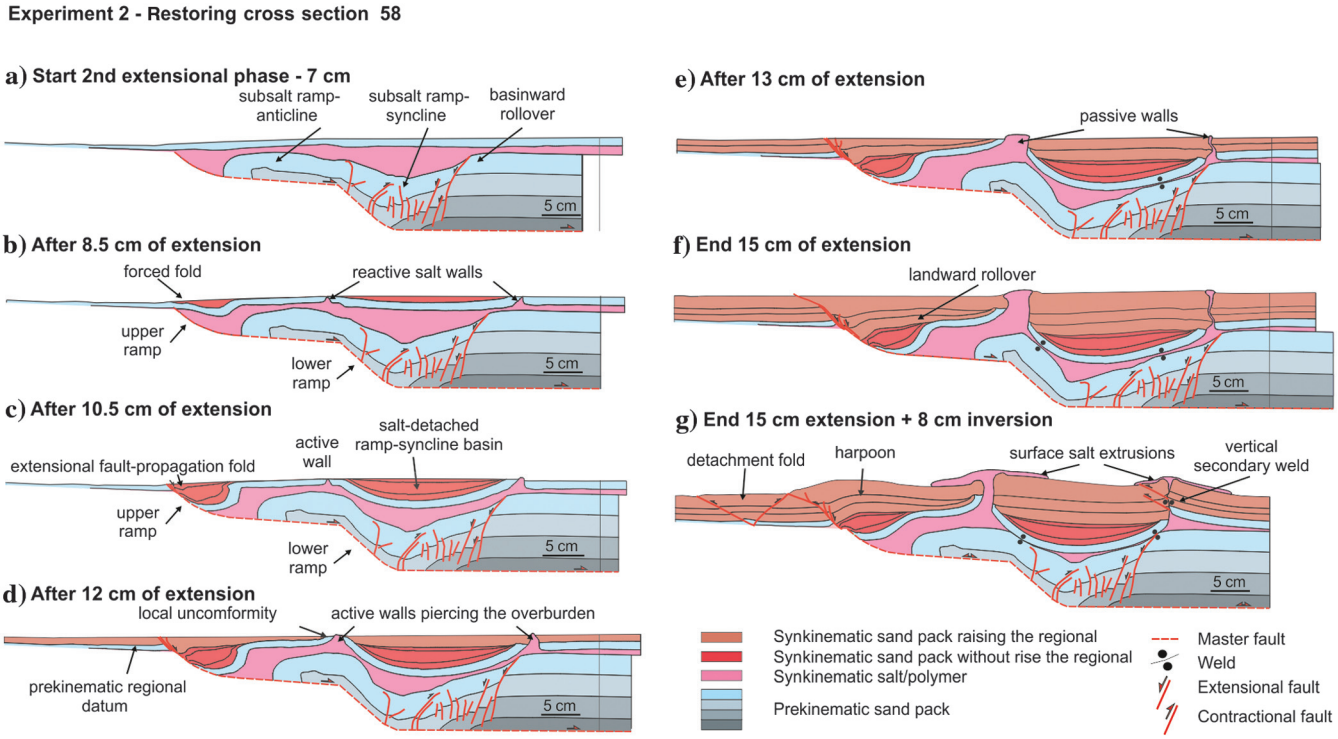

Figure 6. Sequential restoration of cross section 58 from experiment 2 illustrating the structural evolution during the second phase of extension. (a) Prior to the second phase of extension where is shown the subsalt structures developed during the first phase of extension; (b) after 8.5 cm of extension, there is suprasalt forced fold above the upper ramp and two reactive salt walls developed at both basin edges; (c) after 10.5 cm of extension, the suprasalt forced fold become an extensional fault-propagation fold and the reactive salt wall become an active salt wall; (d) after 12 cm of extension, the active salt walls pierced the overburden and consequently the prekinematic regional datum was raised; (e) after 13 cm of extension, the active salt walls become passive; (f) after 15 cm of extension, the salt-detached ramp syncline has already welded against the subsalt structures; and (g) at the end of 8 cm of inversion — net contraction with regard to the second phase of extension.

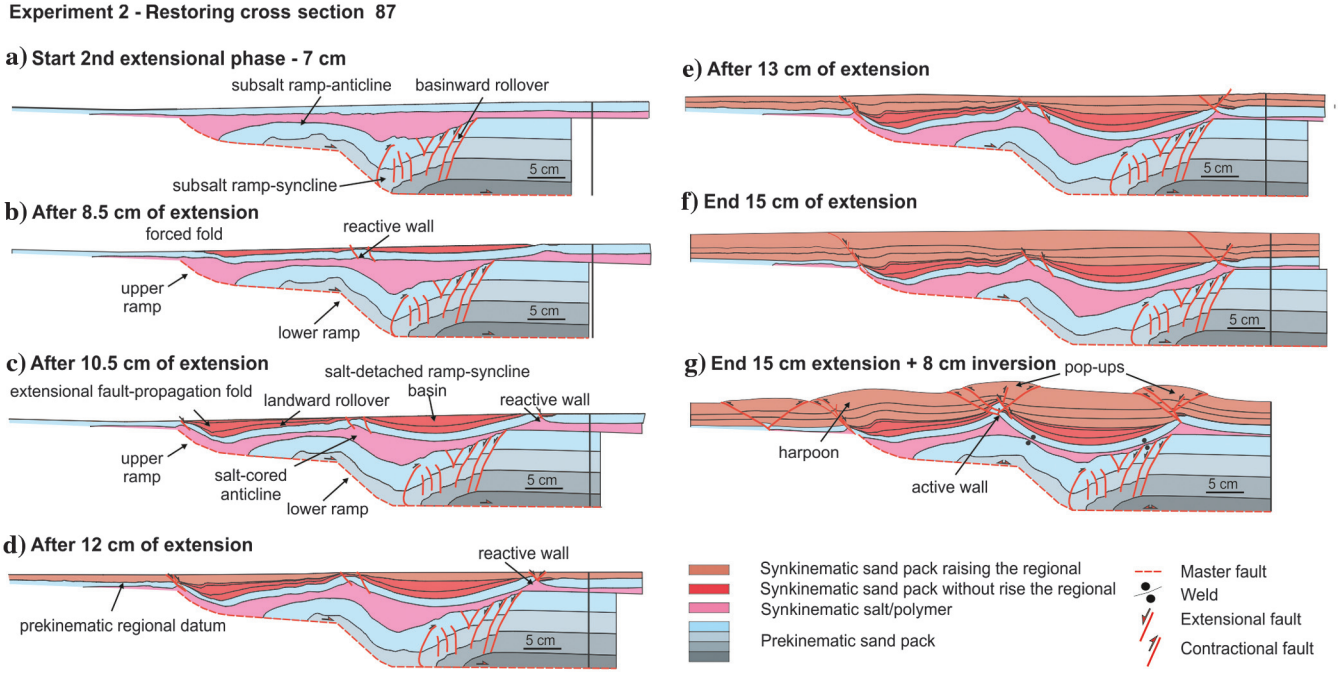

Figure 7. Sequential restoration of cross section 87 from experiment 2 illustrating the structural evolution during the second phase of extension. (a) Prior to the second phase of extension; (b) after 8.5 cm of extension, a suprasalt forced fold and a reactive salt wall were developed; (c) after 10.5 cm of extension, the suprasalt forced fold become an extensional fault-propagation fold; (d) after 12 cm of extension, the prekinematic regional datum was raised; (e) after 13 cm of extension; (f) after 15 cm of extension; and (g) at the end of 8 cm of inversion — net contraction regard to the second phase of extension.

reactivation of the breakaway fault (structure 1 in Figure 9a). In the footwall of the harpoon structure, minor displacement at the base of the thin salt resulted in a small amplitude faulted detachment fold (Figure 8 and structures 7 and 9 in Figure 9c). The subsalt ramp anticline and ramp syncline in the prekinematic units were pushed back up along the master fault (Figure 8a and 8b). The salt-detached ramp-syncline basin was welded against the subsalt structures during the inversion phase and became rapidly uplifted, tightened, and narrowed during the inversion. At the end of extension, the weld surfaces at both syncline limbs were narrow and local (Figure 4). In contrast, at the same point at the end of the inversion (Figure 8), the joining area of the welds increases. The inherited salt wall, above the basinward rollover, at the end of extension was squeezed shut with the consequent development of secondary welds and the formation of a thrust at the salt wall pedestal (Rowan and Vendeville, 2006; Dooley et al., 2015) (Figure 8a). At this point, subsalt and suprasalt deformations became coupled. In contrast, the left side polymer walls were squeezed, thereby forcing salt extrusion, but not the development of secondary welds.

The top surface of experiment 2 constrains the temporal evolution of the inversion phase (Figure 9). The first phase of contraction reactivated the breakaway fault resulting in the frontal harpoon fold and thrust (structure 1 in Figure 9a). The squeezing of the inherited salt walls increased salt extrusion at this phase of shortening. Continued shortening produced more uplift and folding, together with elongate-shaped salt-surface extrusions (Figure 9b). The formation of secondary welds at approximately 7–8 cm of shortening is indicated by a broad uplift above the regional datum (Figures 8, 9c, and 9d) and the formation of thrusts (Figures 8a and 9d) that nucleated at the top of the salt wall pedestals.

Discussion

The analog models presented in this paper have successfully simulated the evolution of partial coupling models during the two extension and subsequent inversion phases.

Interaction of factors during the extensional phase

In the illustrated analog models, the salt distribution after the first extensional phase relies on the steepened geometry of the subsalt fault. During the second extensional phase, the degree of decoupling between subsalt and suprasalt units and the salt withdrawal due to sediment loading mainly depends on salt thickness (e.g., Koyi and Petersen, 1993; Koyi et al., 1993; Vendeville et al., 1995; Richardson et al., 2005). Although a thinner salt unit promotes the development of extensional fault-propagation folds and premature welds by salt depletion, a thicker salt unit allows a partially coupled deformation, which results in further salt migration and the development of wide salt-detached ramp-syncline basins (Figure 4). Synkinematic sediment loading triggered salt expulsion that contributed to the development of the wide salt-detached ramp-syncline bounded by salt walls.

Some salt rollers also developed detached on the thin salt unit (Figure 4) because (1) the salt flows toward the space created by the upper ramp and (2) the basinward tilt of the footwall flat promotes gravitational gliding.

The final salt-detached ramp-syncline basin depocenters are laterally shifted toward the ramp anticline (see the growth axial trace formed by the shifted depocenters dipping basinward in Figure 4). This markedly differs from the salt distribution and stratal geometry associated with extensional forced folds (Withjack and Callaway, 2000; Tavani et al., 2013; Tavani and Granado, 2014), whereby they are characterized by wide monoclines with often vertically stacked depocenters, and where the salt walls are only developed at the monocline hinge. Moreover, the basinward rollover structure present in the salt-detached ramp syncline does not exist in extensional forced folds.

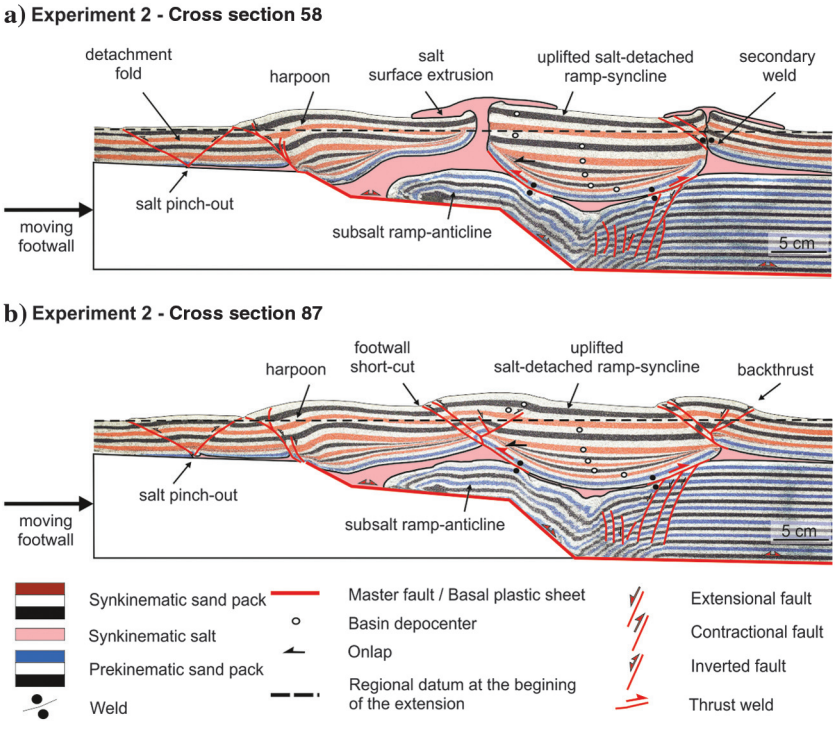

Figure 8. Interpreted cross section of the structures observed in experiment 2 at the end of the inversion (after two phases of extension followed by 8 cm of contraction) and with the terminology used in this paper. (a) Cross section 58 and (b) cross section 87. The location of cross sections is shown in Figure 9.

The growth axial trace (formed by the lateral stacking depocenters) dipping basinward is the result of the displacement of the synclinal basin from the lower ramp to the horizontal basal detachment (as occurs in McClay [1990]; see Figure 1a). In our models, such displacement was coeval with salt withdrawal, which is being preferentially expelled toward the adjacent left side salt wall (Figure 4a). This preferential migration promotes the decrease of the dip of the growth axial trace (Figure 4). During extension, the salt-detached ramp-syncline basin was tilted landward and some onlap geometries were formed (Figure 4). Both features observed together mean that there is a thin-skinned component and the main salt-detached ramp-syncline basin was decoupled and horizontally translated above the salt. Our models also show that in the shallowest synkinematic layers of the salt-detached ramp syncline, the depocenters appear totally shifted from the previous path (Figure 4a and 4b). This means that the salt-detached ramp-syncline basin becomes coupled with subsalt structures, and this occurs when welds form at the syncline limbs where salt is expelled, and the salt layer is exhausted (Figure 4).

Overall, in our models, we can observe through the synkinematic architecture, the interaction of four factors during extension: (1) the subsalt fault geometry and fault displacement, (2) the initial thickness of the salt unit and its distribution, (3) the salt withdrawal due to sediment loading, and (4) the degree of coupling between subsalt and suprasalt units (Ellis and McClay, 1988; Koyi et al., 1993; Withjack and Callaway, 2000). When the influence of one of those factors is dominant, the other factors may stay masked; e.g., the fault displacement is masked by salt migration when the synrift depocenters appear vertically stacked in salt-detached ramp-syncline basins (Figure 1c). Deciphering the contribution of each factor relies on the recognition of the stacking pattern of the depocenters and the stratal geometries within the synkinematic unit.

Role of salt during inversion phase

Most of the literature of analog models with rigid footwalls subject to inversion does not contemplate the presence of viscous detachments. Only the works of Durcanin (2009) (synextension polymer on the hanging wall of a listric fault) or Ferrer et al. (2016) (preextension polymer covering the entire models with different faults geometries) analyzed the role of salt during inversion using rigid footwalls. These authors pointed that subsalt and suprasalt contractional deformation could be partially coupled or completely decoupled depending on the inherited polymer configuration and the presence of primary welds at the beginning of the inversion. They also denote that preexisting salt structures (diapirs and walls) preferentially absorb contractional deformation during early inversion. The analog models presented in this manuscript, with more extension and inversion, support these statements, but also illustrate the salt kinematics during inversion and how salt influences the resulting structural style.

Despite the ductile layer, the inversion of the landward rollover was totally coupled (Figure 8), being similar to those described by Buchanan and McClay (1991) using isotropic models without a ductile layer. In this

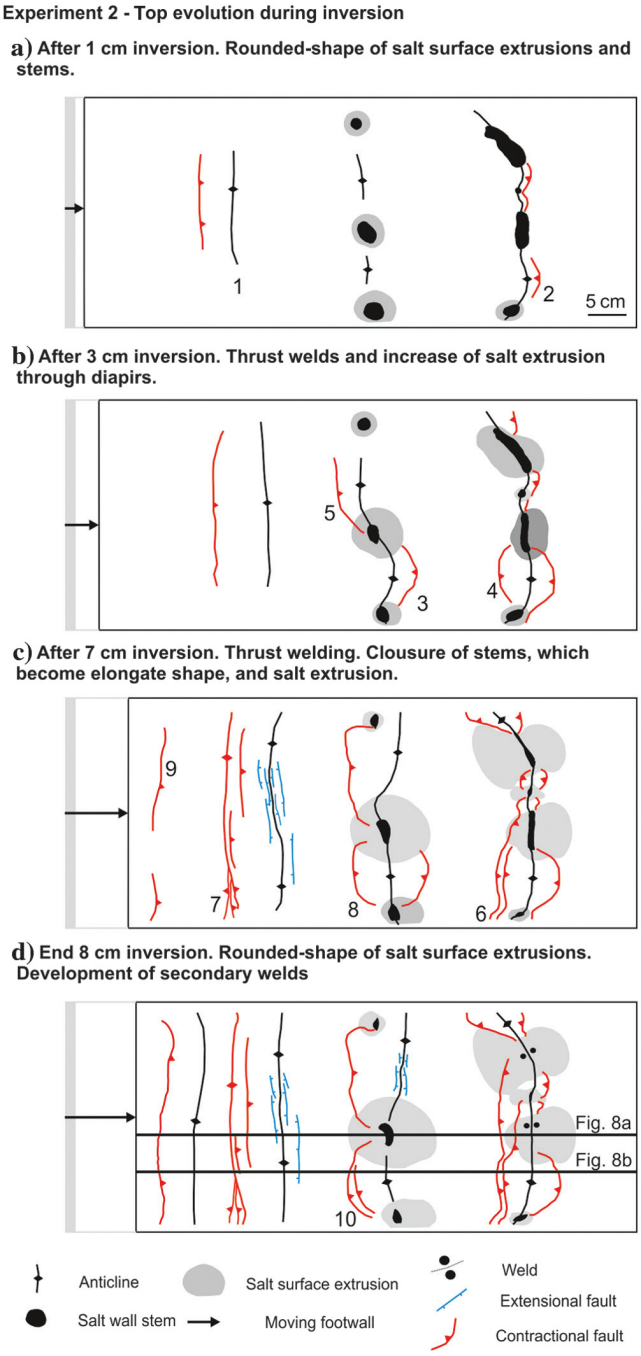

Figure 9. Interpreted overhead photographs illustrating the structural evolution of experiment 2 during the inversion: (a) after 1 cm of inversion, (b) after 3 cm of inversion, (c) after 7 cm of inversion, and (d) at the end of the inversion. The solid black line indicates the location of experiment 2 cross sections in Figure 8.

case, the master fault reactivation produced basin uplift with the development of a harpoon structure (Figure 6g). The upper ramp of the master fault propagated as a thrust into the synextensional sand pack. In the central part of the models, the presence of primary welds at the beginning of the inversion disrupts the source layer and prevents salt withdrawal from the salt-detached ramp-syncline depocenter toward the preexisting salt walls (Figure 4a). At this point, the system becomes wholly coupled and the up-slip contractional displacement of the subsalt unit along the lower ramp of the master fault is transferred into the suprasalt unit uplifting, tilting, and rotating clockwise the salt-detached ramp-syncline basin (Figure 8a). The inversion of the subsalt unit entails a progressive width lessening of the subsalt ramp syncline related to the draping of the sand pack over the master fault geometry and salt evacuation out of section (compare Figure 6f and 6g). As a consequence, primary welds are contractionally reactivated as thrust welds. This primary thrust weld has not been described previously in any natural case; e.g., in Rowan et al. (1999), a thrust weld will develop from a secondary weld. This reactivation implies an increasing of the welded area with respect to the beginning of the inversion (compare Figures 4a and 8a). In regions where salt structures are well-developed, these primary thrust welds transmit the shortening to the inherited passive salt walls that are progressively squeezed triggering salt extrusion (Figures 8a, 9b, and 9c). Despite that both salt walls are squeezed, only the one located above the basinward rollover hinge (Figure 4a) develops a secondary weld (Figure 8a). This is related to the 3D geometry and size of the welded area, larger and wider above the basinward rollover than in the ramp anticline. Whereas the salt wall located above the ramp anticline was fed by out-of-section polymer during inversion, the larger weld of the basinward rollover sector hampered out-of-section salt migration to feed the other salt wall during inversion (Figure 9c). Although the sections with reactive salt walls (Figure 8b) show slight differences in comparison with the previous ones, the regional structure after inversion is relatively similar with coupled deformation due to the inherited primary welds (Figure 4b). In a similar way, the basins developed as a consequence of the upper and lower ramps were progressively uplifted and tilted during inversion. Despite the absence of salt structures piercing the suprasalt sand-pack confining the salt (Figure 8b), the progressive loss of salt volume during inversion (Figure 10) indicates out-of-section salt migration. This difference in salt volume feeds the squeezed salt walls at the central part of the model during inversion (see the following section for more details). The reactive diapirs inherited from the extensional phase are preferentially deformed as the shortening propagates. Different thrust faults nucleate at the apex of the reactive diapirs developing an imbricate thrust system detached at the viscous layer (Figure 8b). The normal faults that controlled the growth of these reactive diapirs during the extension were involved in the hanging wall of these thrusts.

As occurs during extension, the interaction of different factors during inversion is also evident: (1) the subsalt fault geometry and fault displacement, (2) the inherited salt configuration, (3) the presence and geometry of preexisting salt structures, (4) the salt migration, and (5) the degree of coupling between subsalt and suprasalt units. In our models, these factors may function simultaneously. The subsalt master fault geometry and displacement are the main factors controlling the inversion phase in our models, also because the system is partially coupled by the welds. However, those fac-

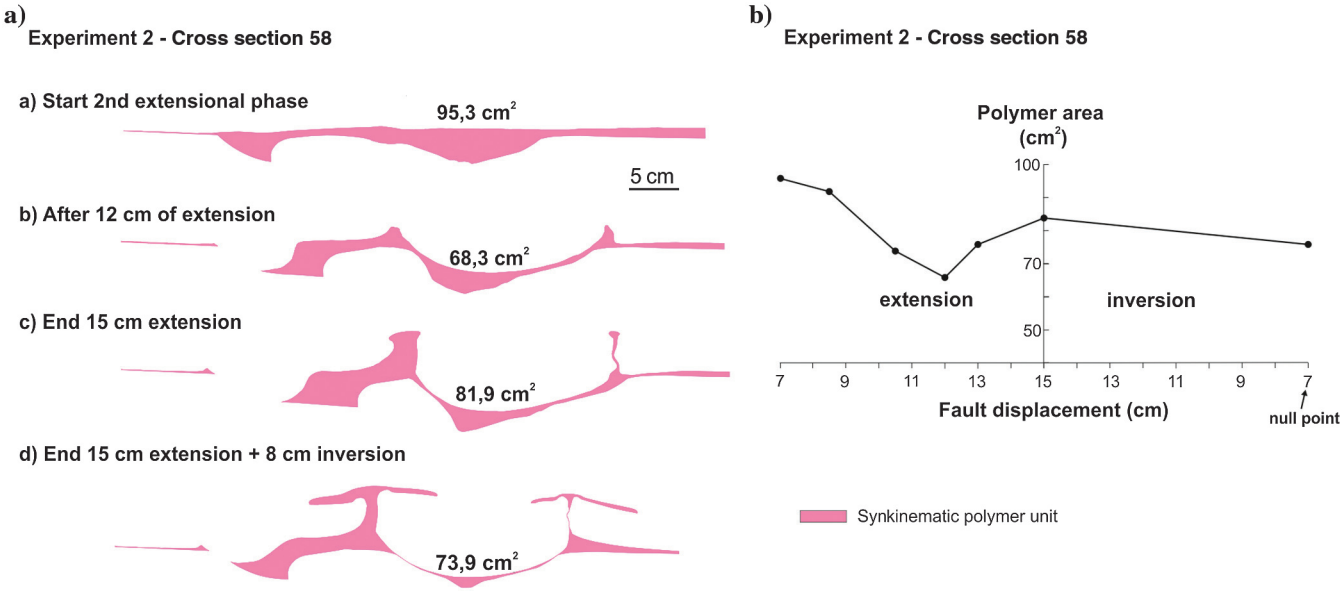

Figure 10. (a) Restoration of polymer area for section 58 from experiment 2 and (b) plot of polymer area versus fault displacement during extension (left side of the graph) and inversion (right side of the graph).

tors were coeval with the basin translation above the primary thrust welds, the reactivation of the salt structures and also the shortening accommodation toward the salt pinch-out, whereby denotes that the salt unit was reactivated.

Salt mobilization

The evolution in geometry and volume (the area in the section plane) of the salt is strictly related to the formation (or lack) of pierced salt walls in the model. Figures 10 and 11 illustrate the variation of salt area through extension and shortening for sections 58 and 87, respectively. The estimated initial polymer area on each section should be approximately 98.5 cm^2, assuming that the initial 2773 cm^3 volume of polymer was evenly distributed over the 30 cm wide, homogeneously folded, prekinematic units.

With the onset of the second phase of extension in section 58 (the central section of the model) (Figure 10a), the main subsided part of the salt-detached ramp-syncline basin caused a progressive loss of salt (Figure 10b). Due to border effects, we can determine that the basin geometry is almost conical (Figure 5a) (i.e., noncylindrical); therefore, the basin depocenter coincides with the central part of the model (Figures 4a and 5a from cross section 58). As a consequence, the salt tends to migrate radially. In this central section 58, the area of available salt reached its minimum at 12 cm of extension, losing approximately 28.3% (27 cm^2) of the salt in the form of out-of-section salt mobilization (Figure 10b); it coincided with the end of the reactive diapirism and also with the onset of passive diapirism. At 12 cm of the second extensional phase, the triangular shapes (reactive diapirsm) become open salt walls (passive diapirism), and they grow in width and height. At the end of this second extensional phase (15 cm), the area of available salt has increased by a total of 19.9% (13.6 cm^2 — including all material lost by the effects of extrusion and erosion, which corresponds to 455 cm^3 or 16% of the initial volume of salt volume lost through diapirs during the second extensional phase) (Figure 10c). This value indicates a large volume of salt that mobilized along-strike into the central section from the neighbouring areas (from Figure 11c to 10c). Finally, after the inversion of the basin, the salt area went out of the section, which resulted in a decrease of 8.7% (8 cm^2) (Figure 10d). This area of variation is surprisingly low. At this stage (Figure 10d), we would expect to quantify a great loss of salt because (1) the surface of joining primary welds was increased, (2) the formation of secondary welds, and (3) the large amount of salt being extruded. However, the key to understanding the small variation in salt volume in section 58 lies in the neighboring cross section 87 (Figure 11). At this particular stage, there is a large decrease in the salt area where no extrusion takes place (Figure 11d): from 98.9 cm^2 at the end of the second extensional event (Figure 11c), down to 50.8 cm^2 of salt available at the end of the compressional phase (Figure 11d). The difference totals up to 48.6% of the salt area lost (48.1 cm^2) during the inversion of the basin. This indicates that during the extension and inversion phases, a large volume of salt migrates across the model from outer areas (cross section 87, Figures 8b and 11) toward the central parts (cross section 58, Figures 8a and 10) of the model to feed the piercing salt walls. Beyond this, we can observe how the regions without diapirs, welds, and salt extrusion (cross section 87, Figures 8b and 11) are at the end of the regions that have lost more salt volume.

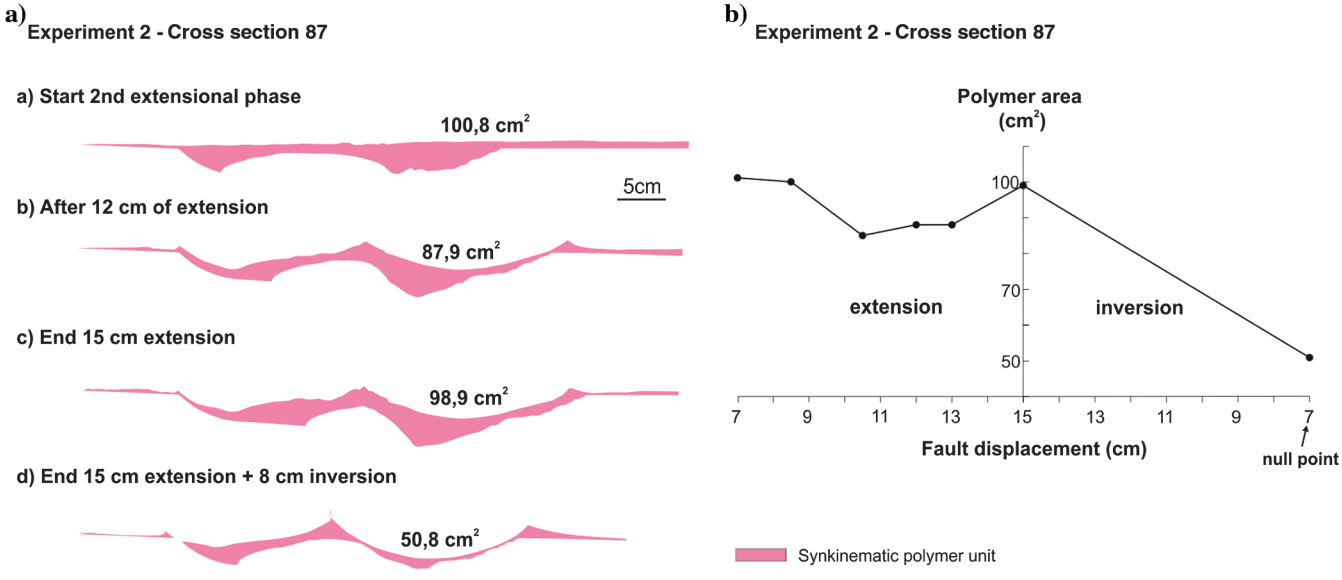

Figure 11. (a) Restoration of polymer area through the extension and inversion phases for section 87 from experiment 2 and (b) plot of the polymer area versus fault displacement during extension (left side of the graph) and inversion (right side of the graph).

Comparison between the analog model results and a natural example (Parentis Basin, Bay of Biscay)

The Parentis Basin (Figure 2) is a clear and published example of a salt-detached ramp-syncline basin, and our experimental results show some similar structural features and kinematic evolution. Although, Ferrer et al. (2014) try to support their interpretation using analog models, they only contemplate the evolution of the models during the extensional episode, without taking into account the Late Cretaceous-Middle Miocene inversion of the Parentis Basin. The analog experimental program of Ferrer et al. (2016) tests the influence of the inversion phase. However, they apply lesser extension than the calculated in the Parentis Basin. In this sense, our experiments include two large extensional phases with salt deposited between them and the later contractional episode, elucidating the role of the inherited extensional structure and salt during inversion.

The Parentis Basin (Figure 2) in the eastern Bay of Biscay is a moderately inverted extensional basin (Tugend et al., 2014) developed above a flat-ramp-flat fault with a Late Triassic salt unit (Keuper facies) in the lower part of the synrift sequence (Ferrer et al., 2012). The salt unit was deposited between the extensional deformation related to the Permo-Triassic breakup of Pangea and the main Early Cretaceous extension of the Bay of Biscay (Ziegler, 1988; Dercourt et al., 1993; Rowan, 2014). During the main rift phase (Early Cretaceous), the salt partially decouples the subsalt and suprasalt structures. In a similar manner to our experiments, the migration of the salt forced by thick-skinned extension led to the development of a wide salt-detached ramp syncline bounded by salt-cored anticlines and with similar laterally stacked depocenters formed in experiment 1. Actually, the Parentis Basin is welded above the hanging wall rollover panel and the footwall fault ramp (Figure 2); in contrast, in our experiments (Figure 4) the salt-detached ramp syncline is welded during the extensional phase against the subsalt ramp anticline and the basinward rollover (compare the location of the primary welds between the case study and experiment 1 in Figures 2 and 4, respectively). In the Parentis Basin, Ferrer et al. (2012) do not interpreted a subsalt ramp anticline, but eventually in our models, the process that developed the landward rollover (welded against the upper ramp) together with the salt-detached ramp syncline, could explain the structures observed in the Parentis Basin. The evolution of the models suggests that the development of welds in the Parentis Basin have been done during the extension phase and not during inversion. In the Parentis Basin, welding at the fault ramp (Figure 2) forced the development of curved normal faults and modified the trend of the synextensional depocenter path (Figure 2). Similar curved normal faults can be observed detached on the upper ramp in experiment 1 during the extensional phase (Figures 4a and 5b).

In the eastern Parentis Basin (Figure 2), the salt-cored anticlines bounding the basin did not become piercing diapirs. This disagreement between our models result and the Parentis Basin is related to (1) the thickness of the prekinematic overburden (Withjack and Callaway, 2000), (2) the effect of the erosion, and (3) the synextension sediment supply. First, in the Parentis Basin, the suprasalt prekinematic isopach layer (unit blue in Figure 2) is thicker than the prekinematic overburden in our experiments (Figure 3c). Second, in the Parentis Basin, the synkinematic materials raise the prekinematic regional datum at the beginning of the extension, whereas, in our models, the regional datum was raised after the diapirs pierced the cover. Third, the interpreted seismic section of the Parentis Basin does not show any erosion during the extensional phase at both salt-cored anticlines. Contrarily, in our models, we can observe an important unconformity generated by the erosion of the salt inflations (Figures 4a and 5a). This thinner cover and the erosion are the principal mechanisms triggering the piercing salt walls in our analog models (Coward and Stewart, 1995).

Later, the ongoing Pyrenean shortening during Late Cretaceous to Middle Miocene times produced contractional reactivation of the subsalt extensional fault that resulted in the uplift of the Parentis Basin. The presence of a major Late Cretaceous unconformity on the top of the basin infill denotes that the Parentis Basin was tectonically inverted. During this episode, the Parentis Basin was slightly inverted compared with other basins located further south, which were incorporated into the Pyrenean orogeny.

Unfortunately, our models do not include erosion during inversion phase; therefore, we are not able to test changes in the kinematic evolution and in the uplift of the basin due to erosion effect (Konstantinovskaya and Malavieille, 2011). However, similar processes have been done in analog experiment 2 and the Parentis Basin. In experiment 2 (Figure 8) and the Parentis Basin (Figure 2), the salt-layer configuration, at the onset of the inversion phase, appears offset (without continuity) by the welds. Nevertheless, our models show that shortening produces the contractional reactivation of the source layer through the primary thrust welds. A similar process could occur in the Parentis Basin, giving rise to the contraction of the basin-bounding salt-cored anticlines (Figure 2). The Parentis Basin also shows that squeezed salt walls developed above the footwall fault (Figure 2), whereas in experiment 2, there are well-developed detachment folds detached at the salt pinch-out (Figures 8a and 9d). These structures are also the result of the reactivation of the salt layer as a contractional detachment above the footwall master fault (Figures 2 and 8).

Our model results provide insights into the processes that can explain the geometries observed in Ferrer et al. (2012), and the previous comparison lends support to their work.

Analog model application to improving seismic interpretation (Northern Lusitanian Basin, offshore Portugal)

The northern Lusitanian Basin is a good example of a basin developed via hybrid thick- and thin-skinned structural styles during extension and subsequent inversion, but the available seismic imaging data in this salt-bearing region are quite poor. This occurs because seismic waves refract when passing between media having different velocities (salt usually has a higher P-wave velocity than the surrounding sediments) (Jackson and Hudec, 2017). A wavefront passing through salt encased in sediments is distorted at the top and the base of the salt before reflecting off subsalt units and distorting further if returning to receivers through the salt. Seismic processing attempts to unscramble this returning wave to produce a coherent image of the subsalt section. However, limitations in seismic acquisition may still leave a poor subsalt image (Jackson and Hudec, 2017). In this sense, although the suprasalt and shallow structures are well-characterized, the interpretation of the subsalt structures are problematic and make it difficult to understand the origin and kinematic evolution of salt-bearing basins. In fact, the analog modeling provides one of the most powerful and visual tool to understand the 4D structural evolution as well as providing possible poorly imaged geometries of the subsalt basins in seismic data.

Although the suprasalt geometry of the Lusitanian Basin published by Alves et al. (2002) is comparable with our experimental results, the subsalt interpretation could be improved. However, according to the processes and control factors that our analog models demonstrate in relation to the coupling-decoupling between the subsalt and suprasalt structures, the use of suprasalt features obtained in analog results can help to constrain the subsalt fault geometry and provide an alternative kinematic evolution of the Lusitanian Basin.

The Lusitanian Basin (Figure 12a) is related to the rifting that led to the breakup of Iberia and northeastern North America (Alves et al., 2002). Multiple rift events, from Late Triassic to Early Cretaceous, were developed (Stapel et al., 1996; Jackson et al., 1998) with the deposition of the Dagorda salt Formation during the Late Triassic. Subsequently, the second Late Jurassic rift phase was the main triggering event for salt tectonics. Where the salt was thin, subsalt faults propagated into suprasalt units and promoted the development of extensional forced folds and fault-propagation folds (compare the analog models of Figure 4 with the seismic sections published by Alves et al. [2002], notably, their Figure 3). However, where the salt was thick, subsalt and suprasalt deformation was partially decoupled, as well as the suprasalt and subsalt interpretation (Figure 12a). It is at this point where the subsalt extensional master faults could be misinterpreted. Together with the original interpretation by Alves et al. (2002) (Figure 12a), we are providing a new interpretation (Figure 12b), based on what the analog models show. In this last scenario, where the salt was thick, the statements of Alves et al. (2002) (Figure 12a) do not fit with the extensional forced fold analog models published by Withjack and Callaway (2000) for two reasons. First, its synclinal geometry and, second, the developed onlaps (Figure 12a and 12b) require a thin-skinned deformation style with significant horizontal displacement of the suprasalt units above the subsalt fault steps — similar to the models presented in this paper. Furthermore, the synclinal geometry in Figure 12a had been interpreted by Alves et al. (2002) as the result of salt withdrawal. However, our experimental results indicate that the development of the salt-detached ramp-syncline basin was mainly controlled by the geometry of the subsalt fault (Figure 12b), similar to our models (ramp-flat-ramp). The decoupling effect of the salt is also revealed by the thin-skinned structural style of the Lusitanian Basin during the Miocene inversion, which is related to Pyrenean-Alpine shortening. Our experimental results suggest that the salt-cored anticlines nucleated on inherited salt structures (from the second phase of extension) during the Miocene inversion (compare the analog models of Figure 4 with the seismic sections published by Alves et al. [2002], in our Figure 12a). Alves et al. (2002)

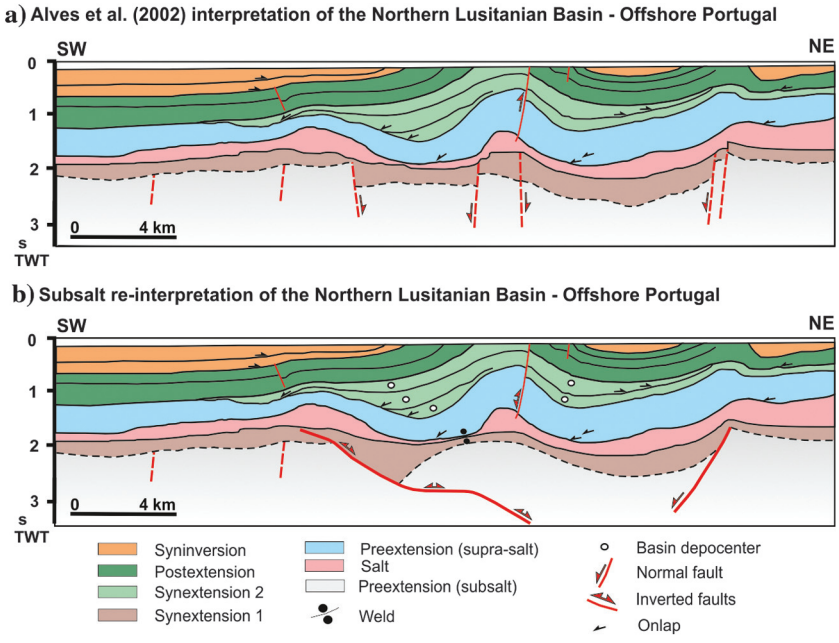

Figure 12. (a) Interpreted seismic line S84-23, modified from Alves et al. (2002), of the Northern Lusitanian Basin (offshore Portugal) containing synstretching salt according to Rowan (2014) and subsequent pronounced period of inversion according to Alves et al. (2002) and (b) reinterpretation of the subsalt structure of seismic line S84-23 from Alves et al. (2002) in the northern Lusitanian Basin (offshore Portugal).

say that the Lusitanian Basin was resolved by a thin-skinned structural style during inversion, as evidenced by the seismic data, but the subsalt faults were interpreted by Alves et al. (2002) following a thick-skinned style, and according to the structural relief shown by the sedimentary basin, as explained by high-angle subsalt faults underneath the salt.

Therefore, the suprasalt deformation patterns resemble those observed in our model results. In this sense, we offer an alternative interpretation based on the insights found in the subsalt and suprasalt deformation coupling in the analog models. Therefore, new constraints for the interpretation of subsalt extensional master fault were presented in this paper (Figure 12b).

Conclusion

Our physical models illustrate the role of salt during the development of salt-detached ramp-syncline basins in areas that have undergone multiple rifting events and subsequent inversion. Therefore, the analog results can be useful (1) to support published interpretations where geometries similar to the ones in our models can be observed, (2) assist in the reinterpretation of seismic sections in subsalt areas where imaging is problematic, and (3) serve as a guide for other similar salt basins.

The experimental results at the end of the extension reveal that suprasalt hanging wall structures are controlled by the interaction of (1) the subsalt fault geometry and fault displacement, (2) the initial thickness of the salt unit and its distribution, (3) salt withdrawal, and (iv) the degree of coupling between the subsalt and suprasalt units. The ramp-flat-ramp subsalt fault constrained three variables: the development of the ramp-syncline basin related to the concave-up fault bend during the first extensional phase, the thickness of the salt layer after the first extensional phase, and the salt flow during the second subsequent extensional phase. The variable salt thickness akin to its synrift nature promotes decoupling between suprasalt and subsalt units, with the development of wide salt-detached ramp-syncline basins when the salt is thicker. This is similar to what was observed on the development of the Parentis Basin in the eastern Bay of Biscay, the Matelles, and Ales Basins in the Gulf of Lion, the Angola passive margin, West Africa, and the Nordkapp Basin. In contrast, early extensional forced folds evolving to extensional fault-propagation folds develop when the salt is thinner, thus favoring coupled deformation and the upward propagation of subsalt faults. Equivalent structures have been interpreted in the Lusitanian Basin, offshore Portugal, the Stavenger fault system in North Sea, and in the central Suez rift or the Haltenbanken area in offshore Norway. The interaction between the extension rate, basin subsidence, salt withdrawal, and decoupling between the subsalt and suprasalt units enhances the development of salt ridges and walls at the edges of the salt-detached ramp-syncline basin. They also constrain the stacking pattern of synrift depocenters and stratal geometries in the basin.

The interaction of different factors during inversion is also evident in analog models and natural examples: (1) the subsalt fault geometry and fault displacement, (2) the inherited extensional structure and salt configuration, (3) the presence and geometry of preexisting salt structures, (4) the salt migration, and (5) the degree of coupling between subsalt and suprasalt units. The subsalt faults were inverted, thereby forcing the arching and uplift of suprasalt units along with the development of harpoon structures, or the uplifting and tilting of the salt-detached ramp syncline. Despite the ductile layer, the presence of primary welds at the beginning of the inversion disrupts the source layer and the system becomes completely coupled. Nevertheless, shortening promotes the squeezing of the salt structures and at passive walls increases the salt extrusion rate (see the Essaouira Basin, the western Atlas system). We highlight that our analog model results show that during the uplift of the cover, some primary welds are contractionally reactivated as thrust welds, transferring the contractional deformation to the suprasalt unit. This has not been described in any natural case. The restoration of some cross sections also illustrates the along-strike salt migration to feed the extruded salt bodies. When these salt structures are squeezed shut, vertical secondary welds develop and vergent thrusts nucleate at the salt pedestal (e.g., in the Loberbus diapir, northwestern Tunisia and in thrusted diapirs from offshore Angola). This contractional evolution is consistent with the structure of different salt-bearing inverted basins, such as the eastern part of the Parentis Basin or the Cameros Basin, where arching, uplift, and squeezing have been identified using seismic data.

The models and their restorations indicate that 2D and 3D changes in salt thicknesses and salt dispositions must be taken into account when interpreting these complex hanging-wall and salt structures in the extensional and inverted salt-bearing basins.

Acknowledgments

This research is part of the first author's Ph.D. thesis and has been supported by the SALTECRES (CGL2014-54118-C2-1-R MINECO/FEDER, UE) project and the Group of Geodynamics and Basin Analysis (2014SGR-467). The analog experiments were funded by the STAR Research Consortium, sponsored by the BG Group, BHPBilliton, ConocoPhilips, Eni, MarathonOil, Nexen, Shell, Talisman Energy, and YFP. We also thank K. D´Souza, J. Morris, and F. Lehane for logistical support in the modeling laboratory. The authors wish to thank Midland Valley Exploration Ltd. for providing academic licenses for the software Move used in the restoration of the cross sections. Reviews and suggested improvements by T. Dooley, O. Duffy, and S. Tavani were greatly appreciated. We are thankful for the English editing by G. G. Buffett.

References

Alves, T. M., R. L. Gawthorpe, D. W. Hunt, and J. H. Monteiro, 2002, Jurassic tectono-sedimentary evolution of the Northern Lusitanian Basin (offshore Portugal): Marine and Petroleum Geology, **19**, 727–754, doi: 10.1016/S0264-8172(02)00036-3.

Balkwill, H. R., and F. D. Legall, 1989, Whale Basin, offshore Newfoundland: Extension and salt diapirism. Extensional tectonics and stratigraphy of the North Atlantic Margins: AAPG Memoir, **46**, 233–246.

Benedicto, A., M. Séguret, and P. Labaume, 1999, Interaction between faulting, drainage and sedimentation in extensional hanging-wall syncline basins: Examples of Oligocene Matelles basin (Gulf of Lion rifted margin, SE France), *in* B. Duran, L. Jolivet, F. Horváth, and M. Séranne, eds., The mediterranean basins: Tertiary extension within the Alpine Orogen: Geological Society of London, Special Publications, 81–108, doi: 10.1144/GSL.SP.1999.156.01.06.

Buchanan, P. G., and K. R. McClay, 1991, Sandbox experiments of inverted listric and planar fault Systems: Tectonophysics, **188**, 97–115, doi: 10.1016/0040-1951(91)90317-L.

Burberry, C. M., 2015, Spatial and temporal variation in penetrative strain during compression: Insights from analog models: Lithosphere, **7**, 611–624, doi: 10.1130/L454.1.

Callot, J. P., J. F. Salel, J. Letouzey, J. M. Daniel, and J. C. Ringenbach, 2016, 3D evolution of salt controlled minibasins: Interactions, folding and megaflap development: AAPG Bulletin, **20**, 160–518, doi: 10.1306/03101614087.

Carola, E., J. A. Muñoz, and E. Roca, 2015,The transition from thick-skinned to thin-skinned tectonics in the Basque-Cantabrian Pyrenees: The Burgalesa Platform and surroundings: International Journal of Earth Sciences, **104**, 2215–2239, doi: 10.1007/s00531-015-1177-z.

Casas, J. M., J. D. Durney, J. Ferret, and J. A. Muñoz, 1996, Determinación de la deformación finita en la vertiente sur del Pirineo oriental a lo largo de la transversal del rio Ter: Geogaceta, **20**, 803–805.

Coward, M., and S. Stewart, 1995, Salt-influenced structures in the Mesozoic-Tertiary cover of the Southern North Sea, UK, *in* M. P. A. Jackson, D. G. Roberts, and S. Snelson, eds., Salt tectonics: A global perspective: AAPG, 229–250.

Coward, M. P., 1995, Structural and tectonic setting of the Permo-Triassic basins of northwest Europe: Geological Society of London, Special Publications, 7–39.

Dahlstrom, C. D. A., 1969, Balanced cross sections: Canadian Journal of Earth Sciences, **6**, 743–757, doi: 10.1139/e69-069.

Dercourt, J., L. E. Ricou, and B. Vrielynck, 1993, Atlas tethys palaeoenvironmental maps: Gauthier-Villars.

Dooley, T. P., M. P. A. Jackson, C. A. L. Jackson, M. R. Hudec, and C. R. Rodriguez, 2015, Enigmatic structures within salt walls of the Santos Basin — Part 2: Mechanical explanation from physical modeling: Journal of Structural Geology, **75**, 163–187, doi: 10.1016/j.jsg.2015.01.009.

Dooley, T. P., K. R. McClay, M. Hempton, and D. Smit, 2005, Salt tectonics above complex basement extensional fault systems: Results from analogue modelling, *in* A. G. Dore and B. A. Vining, eds., Petroleum geology: North-west Europe and global perspectives: Proceedings of the 6th Petroleum Geology Conference: Petroleum Geology Conferences Ltd. and the Geological Society, 1631–1648, doi: 10.1144/0061631.

Durcanin, M. A., 2009, Influence of synrift salt on rift-basin development: Application to the Orpheus Basin, offshore Canada: M.S. thesis, The State University of New Jersey.

Eisenstadt, G., and D. Sims, 2005, Evaluating sand and clay models: Do rheological differences matter?: Journal of Structural Geology, **27**, 1399–1412, doi: 10.1016/j.jsg.2005.04.010.

Ellis, P. G., and K. R. McClay, 1988, Listric extensional fault system-results of analogue model experiments: Basin Research, **1**, 55–70, doi: 10.1111/j.1365-2117.1988.tb00005.x.

Ferrer, O., 2012, Salt tectonics in the Parentis Basin (Eastern Bay of Biscay): Origin and Kinematics of salt structures in a hyperextended margin affected by subsequent contractional deformation: M.S. thesis, Universitat de Barcelona.

Ferrer, O., M. P. A. Jackson, E. Roca, and M. Rubinat, 2012, Evolution of salt structures during extension and inversion of the Offshore Parentis Basin (Eastern Bay of Biscay), *in* G. I. Alsop, S. G. Archer, A. J. Hartley, N. T. Grant, and R. Hodgkinson, eds., Salt tectonics, sediments and prospectivity: Geological Society of London, Special Publications, 361–380, doi: 10.1144/SP363.16.

Ferrer, O., K. R. McClay, and N. C. Sellier, 2016, Influence of fault geometries and mechanical anisotropies on the growth and inversion of hangingwall synclinal basins: Insights from sandbox models and natural examples, *in* C. Child, R. E. Holdsworth, C. A. L. Jackson, T. Manzocchi, J. J. Walsh, and G. Yieldings, eds., The geometry and growth of normal faults: Geological Society of London, Special Publications, 439, doi: 10.1144/SP439.8.

Ferrer, O., E. Roca, and B. C. Vendeville, 2008, Influence of a syntectonic viscous salt layer on the structural evolution of extensional kinked-fault systems: Bollettino di Geofisica Teorica ed Applicata, **49**, 371–375.

Ferrer, O., E. Roca, and B. C. Vendeville, 2014, The role of salt layers in the hangingwall deformation of kinked-planar extensional faults: Insights from 3D analogue models and comparison with the Parentis Basin: Tectonophysics, **636**, 338–350, doi: 10.1016/j.tecto.2014.09.013.

Glennie, K. W., 1995, Permian and Triassic rifting in northwest Europe: Geological Society of London, Special Publications, 1–5.

Groshong, R. H., Jr., C. Bond, A. Gibbs, R. Ratliff, and D. V. Wiltschko, 2012, Preface: Structural balancing at the

start of the 21st century: 100 years since Chamberlin: Journal of Structural Geology, **41**, 1–5, doi: 10.1016/j.jsg.2012.03.010.

Guimerà, J., Á. Alonso, and J. R. Mas, 1995, Inversion of an extensional-ramp basin by a newly formed thrust: The Cameros basin (N. Spain): Geological Society of London, Special Publications, 433–453.

Horsfield, W. T., 1977, An experimental approach to basement controlled faulting: Geologie en Mijnbouw, **56**, 363–370.

Hubbert, M. K., 1937, Theory of scaled models as applied to the study of geological structures: Geological Society of America Bulletin, **48**, 1459–1520, doi: 10.1130/GSAB-48-1459.

Hudec, M. R., and M. P. A. Jackson, 2007, Terra infirma: Understanding salt tectonics: Earth Science Reviews, **82**, 1–28, doi: 10.1016/j.earscirev.2007.01.001.

Hudec, M. R., M. P. A. Jackson, and D. D. Schultz-Ela, 2009, The paradox of minibasin subsidence into salt: Clues to the evolution of crustal basins: Geological Society of America Bulletin, **121**, 201–221, doi: 10.1130/B26275.1.

Huiqi, L., K. R. McClay, and D. Powell, 1992, Physical models of thrusts wedges, *in* K. R. McClay, ed., Thrust tectonics: Chapman and Hall, 71–81.

Jackson, M. P. A., C. Cramez, and J. M. Fonck, 2000, Role of subaerial volcanic rocks and mantle plumes in creation of South Atlantic margins: Implications for salt tectonics and source rocks: Marine and Petroleum Geology, **17**, 477–498, doi: 10.1016/S0264-8172(00)00006-4.

Jackson, M. P. A., and M. R. Hudec, 2017, Salt tectonics: Principles and practice: Cambridge University Press.

Jackson, M. P. A., D. D. Schultz-Ela, M. R. Hudec, I. A. Watson, and M. L. Porter, 1998, Structure and evolution of Upheaval Dome: A pinched-off salt diapir: Geological Society of America Bulletin, **110**, 1547–1573, doi: 10.1130/0016-7606(1998)110<1547:SAEOUD>2.3.CO;2.

Jackson, M. P. A., and C. J. Talbot, 1991, A glossary of salt tectonics: Bureau of Economic Geology.

Jackson, M. P. A., and B. C. Vendeville, 1994, Regional extension as a geologic trigger for diapirism: Geological Society of America Bulletin, **106**, 57–73, doi: 10.1130/0016-7606(1994)106<0057:REAAGT>2.3.CO;2.

Kehle, R. O., 1988, The origin of salt structures, *in* B. C. Schreiber, ed., Evaporites and hydrocarbons: Columbia University Press, 345–403.

Konstantinovskaya, E., and J. Malavieille, 2011, Thrust wedges with décollement levels and syntectonic erosion: A view from analog models: Tectonophysics, **502**, 336–350, doi: 10.1016/j.tecto.2011.01.020.

Koyi, H., M. K. Jenyon, and K. Petersen, 1993, The effect of basement faulting on diapirism: Journal of Petroleum Geology, **16**, 285–312, doi: 10.1111/j.1747-5457.1993.tb00339.x.

Koyi, H., and K. Petersen, 1993, Influence of basement faults on the development of salt structures in the Danish Basin: Marine and Petroleum Geology, **10**, 82–94, doi: 10.1016/0264-8172(93)90015-K.

Koyi, H. A., 2000, Towards dynamic restoration of geologic profiles: Some lessons from analogue modeling, *in* W. Mohriak and M. Taiwani, eds., Atlantic rifts and continental margins: American Geophysical Union, Geophysical Monograph Series 115, 317–329, doi: 10.1029/GM115p0317.

Koyi, H. A., and M. Sans, 2006, Deformation transfer in viscous detachments: Comparison of sandbox models to the South Pyrenean Triangle Zone: Geological Society of London, Special Publications, 117–134, doi: 10.1144/GSL.SP.2006.253.01.06.

Lingrey, S., and O. Vidal-Royo, 2015, Evaluating the quality of bed length and area balance in 2D structural restorations: Interpretation, **3**, no. 4, SAA133–SAA160, doi: 10.1190/INT-2015-0126.1.

Mathieu, C., 1986, Histoire géologique du sous-bassin de Parentis: Bulletin des Centres Recherche Exploration-Production Elf-Aquitaine, **10**, 22–47.

McClay, K. R., 1989, Analogue models of inversion tectonics: Geological Society of London, Special Publications, 41–59, doi: 10.1144/GSL.SP.1989.044.01.04.

McClay, K. R., 1990, Extensional fault systems in sedimentary basins: A review of analogue model studies: Marine and Petroleum Geology, **7**, 206–233, doi: 10.1016/0264-8172(90)90001-W.

Muñoz, J. A., 1992, Evolution of a continental collision belt: ECORS-Pyrenees crustal balanced cross-section, *in* K. R. McClay, ed., Thrust tectonics: Chapman and Hall, 235–246.

Nalpas, T., and J. P. Brun, 1993, Salt flow and diapirism related to extension at crustal scale: Tectonophysics, **228**, 349–362, doi: 10.1016/0040-1951(93)90348-N.

Nalpas, T., S. Le Douran, J. P. Brun, P. Untrnehr, and J. P. Richert, 1995, Inversion of the broad fourteens basin (offshore Netherlands): A small-scale model investigation: Sedimentary Geology, **95**, 237–250, doi: 10.1016/0037-0738(94)00113-9.

Ori, G. G., and P. F. Friend, 1984, Sedimentary basins formed and carried piggyback on active thrust sheets: Geology, **12**, 475–478, doi: 10.1130/0091-7613(1984)12<475:SBFACP>2.0.CO;2.

Rasmussen, E. S., S. Lomholt, C. Andersen, and O. V. Vejbæk, 1998, Aspects of the structural evolution of the Lusitanian Basin in Portugal and the shelf and slope area offshore Portugal: Tectonophysics, **300**, 199–225, doi: 10.1016/S0040-1951(98)00241-8.

Richardson, N. J., J. R. Underhill, and G. Lewis, 2005, The role of evaporite mobility in modifying subsidence patterns during normal fault growth and linkage, Halten Terrace, Mid-Norway: Basin Research, **17**, 203–223, doi: 10.1111/j.1365-2117.2005.00250.x.

Roure, F., J. O. Brun, B. Colletta, and J. Van Den Driessche, 1992, Geometry and kinematics of extensional structures in the Alpine foreland basin of southeastern

France: Journal of Structural Geology, **14**, 503–519, doi: 10.1016/0191-8141(92)90153-N.

Rowan, M. G., 2014, Passive-margin salt basins: Hyperextension, evaporite deposition, and salt tectonics: Basin Research, **26**, 154–182, doi: 10.1111/bre.12043.

Rowan, M. G., M. P. A. Jackson, and B. D. Trudgill, 1999, Salt-related fault families and fault welds in the northern Gulf of Mexico: AAPG Bulletin, **83**, 1454–1484.

Rowan, M. G., and B. C. Vendeville, 2006, Foldbelts with early salt withdrawal and diapirism: Physical model and examples from the northern Gulf of Mexico and the Flinders Ranges, Australia: Marine and Petroleum Geology, **23**, 871–891, doi: 10.1016/j.marpetgeo.2006.08.003.

Schellart, W. P., 2000, Shear test results for cohesion and friction coefficients for different granular materials: Scaling implications for their usage in analogue modeling: Tectonophysics, **324**, 1–16, doi: 10.1016/S0040-1951(00)00111-6.

Stapel, G., S. Cloetingh, and B. Pronk, 1996, Quantitative subsidence analysis of the Mesozoic evolution of the Lusitanian basin (western Iberian margin): Tectonophysics, **266**, 493–507, doi: 10.1016/S0040-1951(96)00203-X.

Stewart, S. A., and J. A. Clark, 1999, Impact of salt on the structure of the Central North Sea hydrocarbon fairways: Geological Society of London,Petroleum Geology Conference Series, 179–200.

Soto, R., M. Casas-Sainz, and P. Del Río, 2007, Geometry of half-grabens containing a mid-level viscous décollement: Basin Research, **19**, 437–450, doi: 10.1111/j.1365-2117.2007.00328.x.

Tankard, A. J., H. J. Welsink, and W. A. M. Jenkins, 1989, Structural styles and stratigraphy of the Jeanne d'Arc Basin, Grand Banks of Newfoundland. Extensional tectonics and stratigraphy of the North Atlantic margins: AAPG Memoir, **46**, 265–282.

Tavani, S., E. Carola, P. Granado, A. Quintà, and J. A. Muñoz, 2013, Transpressive inversion of a Mesozoic extensional forced fold system with an intermediate décollement level in the Basque-Cantabrian Basin (Spain): Tectonics, **32**, 146–158, doi: 10.1002/tect.v32.2.

Tavani, S., and P. Granado, 2014, Along-strike evolution of folding, stretching and breaching of supra-salt strata in the Plataforma Burgalesa extensional forced fold system (northern Spain): Basin Research, **27**, 573–585, doi: 10.1111/bre.12089.

Tugend, J., G. Manatschal, N. J. Kusznir, E. Masini, G. Mohn, and I. Thinon, 2014, Formation and deformation of hyperextended rift systems: Insights from rift domain mapping in the Bay of Biscay-Pyrenees: Tectonics, **33**, 1239–1276, doi: 10.1002/2014TC003529.

Vendeville, B., 1987, Champs de failles et tectonique en extension: Modélisation expérimentale: M.S. thesis, Université de Rennes.

Vendeville, B., 1988, Modèles expérimentaux de fracturation de lat couverture controlée par des failles normales dans le socle: Comptes Rendus Académie des Sciences Paris, **307**, 1013–1019.

Vendeville, B. C., H. Ge, and M. P. A. Jackson, 1995, Scale models of salt tectonics during basement-involved extension: Petroleum Geoscience, **1**, 179–183, doi: 10.1144/petgeo.1.2.179.

Weijermars, R., 1986, Flow behavior and physical chemistry of bouncing putties and related polymers in view of tectonic laboratory applications: Tectonophysics, **124**, 325–358, doi: 10.1016/0040-1951(86)90208-8..

Withjack, M. O., and S. Callaway, 2000, Active normal faulting beneath a salt layer: An experimental study of deformation patterns in the cover sequence: AAPG Bulletin, **84**, 627–651.

Withjack, M. O., and R. W. Schlische, 2005, A review of tectonic events on the passive margin of eastern North America, *in* P. Post, ed., Petroleum systems of divergent continental margin basins: 25th Bob S. Perkins Research Conference, Gulf Coast Section of SEPM, 203–235.

Yamada, Y., and K. R. McClay, 2003, Application of geometric models to inverted listric fault systems in sandbox experiments. Paper 1: 2D hanging wall deformation and section restoration: Journal of Structural Geology, **25**, 1551–1560, doi: 10.1016/S0191-8141(02)00181-5.

Ziegler, P. A., 1988, Evolution of the Arctic-North Atlantic and the Western Tethys: A visual presentation of a series of paleogeographic-paleotectonic maps: AAPG Memoir, **43**, 164–196.

Maria Roma received a B.S. (2012) in geology and an M.S. (2013) in reservoir geology and geophysics from the University of Barcelona. During her Ph.D., she did a research internship (2014) at the Fault Dynamics Research Group (Royal Holloway University of London). In 2015, she built up the analog modeling laboratory at the University of Dodoma, and she gave lessons in the M.S. petroleum geosciences division at the University of Dodoma. She now is pursuing a Ph.D. supported by an APIF predoctoral grant from the University of Barcelona, about the formation and inversion of extensional basins with syncline geometries in GEOMODELS Research Institute at the University of Barcelona.

Oskar Vidal-Royo received an M.S. (hons; 2006) in exploration, analysis, and modeling of basins and orogenic systems and a Ph.D. (high hons; 2010) in earth sciences from the University of Barcelona. After eight years with GGAC and the Geomodels Research Institute at the University of Barcelona, he joined Midland Valley Exploration in early 2013, working as a structural geologist carrying out consultancy, training, and research tasks for

oil and gas, mining, and carbon storage companies worldwide. In 2016, he cofounded Terractiva to deliver geologic consulting and advice for the hydrocarbon and mining industries at the regional, basin, and prospect/deposit scales. His research interests include seismic interpretation of complex structural styles, kinematic and geomechanical modeling of geologic bodies in two and three dimensions, salt tectonics, and tectonosedimentary relationships guiding fold-and-fault kinematics.

Ken R. McClay received a B.S. (honors) and D.S. from Adelaide University and an M.S. and Ph.D. from Imperial College, London. He is a professor of structural geology and the director of the Fault Dynamics Research Group at Royal Holloway University of London. His research has focused upon the dynamics of inverted, extensional, and strike-slip terrains and fault systems in fold-thrust belts. This involves the integration of field studies, seismic interpretation, and scaled physical modeling to develop quantitative 4D models for fault systems in sedimentary basins.

Oriol Ferrer received a B.S. and a Ph.D. in earth sciences from the University of Barcelona. He also did a postdoc at the Fault Dynamics Research Group (Royal Holloway University of London). Since 2010, he has been in charge of the GEOMODELS Analog Modeling Laboratory, UB. He is a tenured lecturer at UB. His research interests include salt tectonics of rift systems, inverted basins, and salt-bearing passive margins using outcrop, subsurface, and analog modeling.

Josep Anton Muñoz received a Ph.D. (1985) from the University of Barcelona and worked for the Servei Geologic de Catalunya from 1985 to 1990, when he joined the University of Barcelona. He is a professor of structural geology at UB. He is the director of the GEOMODELS Research Institute. His research interests include the structure of thrust-and-fold belts, tectonosedimentary relationships, tectonics of collisional orogens, and construction of 3D structural models.

APPENDIX III

Weld kinematics of synrift salt during basement-involved extension and subsequent inversion: Results from analog models

Roma, M., O. Ferrer, K.R. McClay, J,A. Muñoz, E. Roca, O. Gratacós, P. Cabello, 2018c.. Geologica Acta. 16(4), 391-410, doi: 10.1344/GeologicaActa2018.16.4.4

Geologica Acta, Vol.16, Nº 4, December 2018, 391-410
DOI: 10.1344/GeologicaActa2018.16.4.4

geologica acta

Weld kinematics of synrift salt during basement-involved extension and subsequent inversion: Results from analog models

M. ROMA[1] O. FERRER[1] K.R. MCCLAY[2] J.A. MUÑOZ[1] E. ROCA[1] O. GRATACÓS[1] P. CABELLO[1]

[1]Departament de Dinàmica de la Terra i de l'Oceà-Institut de Recerca GEOMODELS, Facultat de Ciències de la Terra, Universitat de Barcelona
C/ Martí i Franquès s/n 08028, Barcelona, Spain. Roma E-mail: mariaroma@ub.edu

[2]Fault Dynamics Research Group, Earth Sciences Department
Royal Holloway University of London. TW20 0EX, Egham, United Kingdom

ABSTRACT

Scaled analog models based on extensional basins with synrift salt show how basement topography exerts a control factor on weld kinematics during the extension and inversion phases. In the case of basement-involved extension, syn-rift salt thickness differences may lead to variable degrees of extensional decoupling between basement topography and overburden, which in turn have a strong impact on the development of salt structures. With ongoing extension and after welding, the basin kinematics evolves toward a coupled deformation style. The basin architecture of our experimental results record the halokinetic activity related to growing diapirs and the timing of weld formation during extension. Moreover, the structures that result from any subsequent inversion of these basins strongly depends on the inherited welds and salt structures. While those basins are uplifted, the main contractional deformation during inversion is absorbed by the pre-existing salt structures, whose are squeezed developing secondary welds that often evolve into thrust welds. The analysis of our analog models shows that shortening of diapirs is favored by: i) basement topography changes that induce reactivation of primary welds as thrust welds; ii) reactivation of the salt unit as a contractional detachment and iii) synkinematic sedimentation during basin inversion. Finally, in this article, we also compare two natural examples from the southern North Sea that highlight deformation patterns very similar to those observed in our analog models.

KEYWORDS | **Extension and inversion. Salt tectonics. Syn-rift salt. Analog modeling. Southern North Sea.**

INTRODUCTION

The timing of salt deposition, pre-, syn-, or post-kinematic, during the evolution of the salt-bearing rift basins is one of the main factors controlling their structural style (Jackson and Vendeville, 1994; Rowan, 2014). In fact, the development of salt structures in this scenario is influenced by salt thickness differences or by its lateral continuity, which in turn is controlled by basement topography prior to salt deposition (Fig. 1A). Although, the most important thickness differences occur with syn-rift salt, the presence of previous topographic irregularities can also favor salt thickness differences in pre-rift salt. The origin of these subsalt salt irregularities could be diverse but may be related to the irregular erosion of basement rocks or to the different slip of rift faults (Dooley *et al*., 2017; Ferrer *et al*., 2017).

Salt and overburden thickness differences, cohesive strength/ductility of the overburden, displacement amount and displacement rate or salt viscosity can also have a strong impact on the degree of coupling over time (Coward and Stewart, 1995; Stewart and Clark, 1999; Withjack and Callaway, 2000). The important strength contrasts between

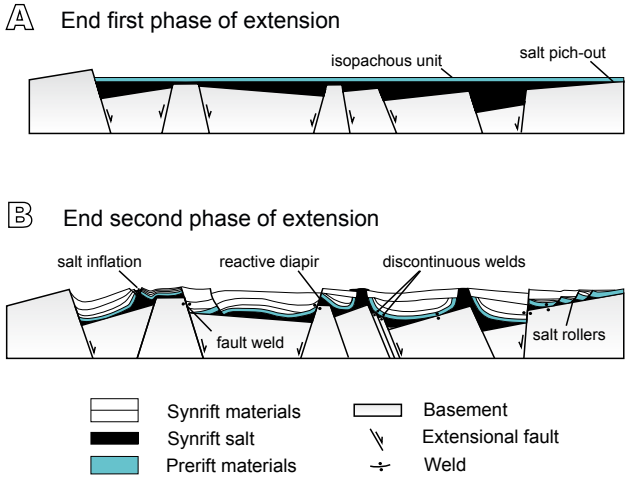

FIGURE 1. Conceptual model on the structural style of syn-rift salt basins. A) During the first extensional phase syn-rift salt accumulates in grabens and half-grabens so salt thickness varies and B) salt rollers, reactive diapirs, passive diapirs and fault welds form in the syn-kinematic overburden; modified from Jackson and Hudec, 2017.

salt and other sedimentary rocks favor a partial to fully decoupled deformation between basement and overburden during rift, where salt acts as a highly efficient décollement (*e.g.* Koyi *et al.*, 1993; Jackson and Vendeville, 1994; Pascoe *et al.*, 1999; Withjack and Callaway, 2000; Dooley *et al.*, 2005; among others). The most common scenario in nature for basement-involved extension is partial coupling (Jackson and Hudec, 2017), in which the structure of the overburden is an indirect reflection of the underlying basement structural patterns. The basement topographic differences created by fault slip causes salt withdrawal from the main depocenters towards the margins of the different subbasins where different salt structures develop (Fig. 1B). Their growth will be influenced by different factors such as the sedimentation rate, salt continuity or welding, erosion and regional extension and shortening (Vendeville and Jackson, 1992; Vendeville, 2002). Among these salt structures, the development of primary welds is common, either below the sub-basins' depocenters or above their margin faults. In this case, fault offset leads to basinwards-dipping discontinuous welds, and if the stretching continues, basement faults can propagate upwards into the overburden (Fig. 1B). After welding, the deformation becomes coupled, and this has an intense influence in the basin architecture which records the evolution and location of welds.

If these rift basins are subsequently inverted, the syn-kinematic sedimentation, the inherited structure and the continuity of the salt layer or its welded equivalent, strongly influences the propagation of contractional deformation. Salt structures are inherently weaker than other parts of the basin; because of this weakness diapirs react sensitively to contraction long before any surrounding rocks (Letouzey *et al.*, 1995, Letouzey and Sherkati, 2004; Rowan and Vendeville, 2006; Callot *et al.*, 2007; Callot *et al.*, 2012; Dooley *et al.*, 2015). Initial shortening is visibly focused on diapirs which displace salt upwards and squeeze the diapir whereas surrounding areas deform by lateral compaction (Vendeville and Nilsen, 1995; Nilsen *et al.*, 1995; Cramez and Jackson, 2000; Rowan *et al.*, 2000, 2004).

While much has been written on rift basins with pre-rift salt (*e.g.* Koyi and Petersen, 1993, Nalpas *et al.*, 1995; Vendeville *et al.*, 1995; Brun and Nalpas, 1996; Withjack and Callaway, 2000; Dooley *et al.*, 2005; Soto *et al.*, 2007; Burliga *et al.*, 2012; Ferrer *et al.*, 2016), there is little published about the role of synrift salt during extension and subsequent inversion. Koyi *et al.* (1993) used a centrifuge to study the influence of basement faults on diapirism in sedimentary basins. Their models showed that, when syn-rift salt only occupied half-grabens and the overburden covered the entire model the development of salt structures is constrained by the major faults. Jackson and Vendeville (1994) documented a close link between the onset of diapirism and regional extension considering different world' salt basins with syn-rift salt, which in turn influence the distribution of resulting diapirs. Del Ventisette *et al.* (2005) explored the influence of positive inversion on diapirism in previously extended basins with syn-rift salt. Using an experimental approach based on the western Central Graben (North Sea), Dooley *et al.* (2005) investigated the 3D geometries and kinematics of deformation in the overburden above intersecting basement fault systems that were separated by a salt layer. In this work they indicate that this intersecting fault set generates complex 3D flap structures in the overburden that localize diapiric activity. Ferrer *et al.* (2014, 2016) used a rigid footwall to simulate different basement fault geometries with pre- and syn-rift salt to understand the main factors controlling the overburden deformation and salt tectonics during extension and inversion. Our investigation agrees with their regarding the presence of a salt layer acting as an effective decoupling unit, and the effect of basement geometry controlling the location of salt structures. However, our work differs from Dooley *et al.* (2005) and Ferrer *et al.* (2014) because they did not apply inversion (or if so, very few). Finally, despite the experiments of Ferrer *et al.* (2016) considered the effect of inversion, the small amount of previous extension applied did not allow the development of diapirs.

The present work expands the experimental program and the methodological analysis of Roma *et al.* (2018) in order to provide insights into welding kinematics in basins with syn-rift salt during both extension and inversion phases. Despite some authors pointing that salt thinned by welding during extension in nature become less effective

to act as a detachment, our experimental results show that primary welds can be forced to reactivate as thrust welds by basement topography variation during inversion. Moreover, our models demonstrate that syn-inversion sedimentation clearly favors the development of vertical secondary welds, decapitated diapirs or even thrust welds. Those features are well recognized at the north-eastern edge of the Broad Fourteens Basin (BFB) and at the northern edge of the Dutch Central Graben (DCG), in the southern North Sea.

EXPERIMENTAL METHODOLOGY

This contribution is part of a wider experimental program including 5 different experiments (Table 1) and they complement the recent work of Roma *et al.* (2018) which characterized the kinematics of salt-detached ramp-syncline basins during extension and subsequent inversion. Here, we have selected three end-member experiments to illustrate the evolution of salt structures during extension and inversion, paying special attention to the role of syn-kinematic sedimentation.

Experimental design and material properties

Our analog models were designed using the same experimental setup as Yamada and McClay (2003a, b) and subsequently improved by Ferrer *et al.* (2016). Analog models were carried out in a 63cm-long, 30cm-wide and 35cm-deep, glass-sided deformation box (Fig. 2A). A rigid wooden footwall block with double ramp-flat faults constrained the footwall geometry. Above the almost flat section of the footwall, a metal plate was fixed to form the breakaway of the extensional fault system (Fig. 2A). Between the rigid footwall and this metal plate, and covering the entire footwall, a flexible (but not stretchable) plastic sheet was attached to the fixed end walls (Fig. 2A). It acted as a major detachment during both extension and inversion. Lengthening or shortening were transmitted to the hanging wall sand pack with a motor-driven worm screw attached to the footwall block (Fig. 2A). The extensional and contractional displacement rates of the moving footwall remained constant during the experimental program

TABLE 1. Summary table showing the main characteristics of the experimental program

Experiments	Amount Extension		Stretching rate ($cm \cdot s^{-1}$)	Amount inversion	Shortening rate ($cm \cdot s^{-1}$)	Sedimentation rate during inversion
	phase 1	phase 2				
Exp. 1*	7cm	8cm	$2.75 \cdot 10^{-5}$	-	-	-
Exp. 2*	7cm	8cm	$2.75 \cdot 10^{-5}$	8cm	$2.75 \cdot 10^{-5}$	-
Exp. 3*	7cm	8cm	$2.75 \cdot 10^{-5}$	8cm	$2.75 \cdot 10^{-5}$	5mm thick / 1cm
Exp. 4	7cm	8cm	$1.27 \cdot 10^{-4}$	-	-	-
Exp. 5	-	9cm	$2.75 \cdot 10^{-5}$	every 5mm of extension the deformation box was tilted 0.5°		

* Experiments presented in detail in this study

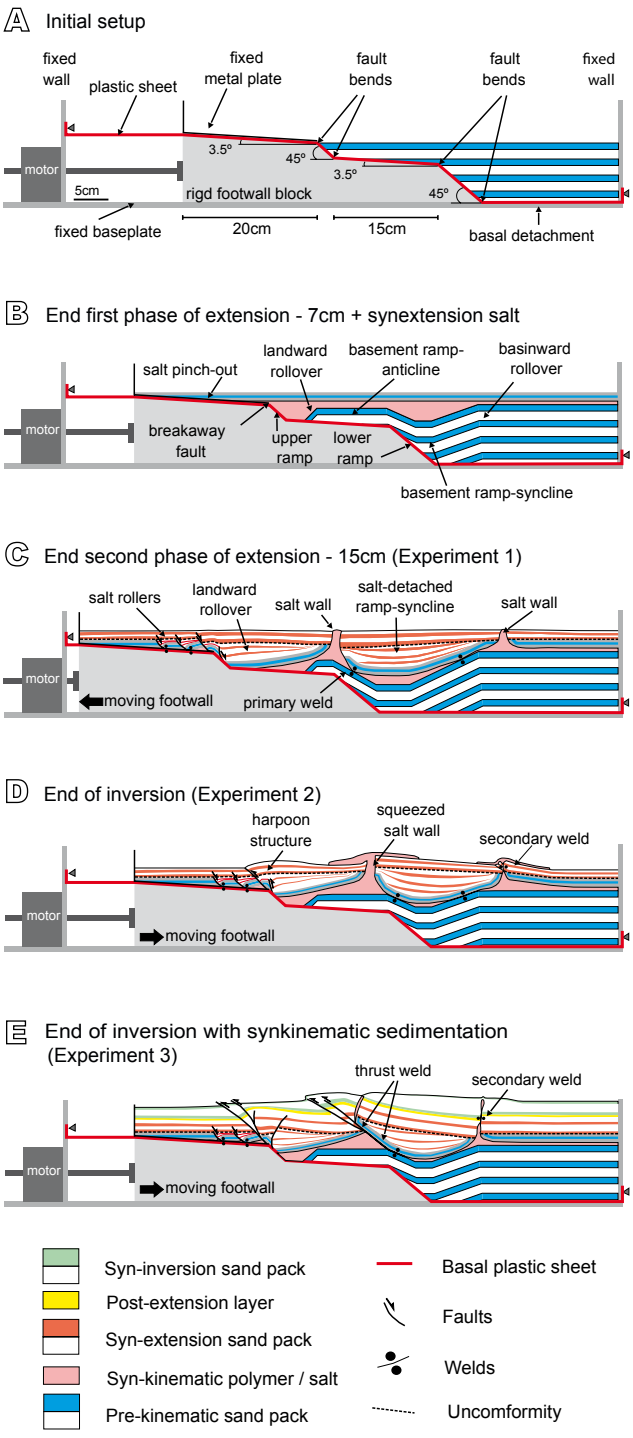

FIGURE 2. Synoptic sketches showing the experimental procedure with the terminology used in the description of the models (modified after Roma *et al.*, 2018). A) pre-deformation configuration, B) structural pattern at the end of the first extensional phase (after 7cm of stretching), C) experimental configuration at the end of the second extensional phase (after an additional 8cm of stretching), red and white layers represent syn-kinematic sedimentation, D) configuration at the end of the inversion (after 7cm of shortening) and E) structural pattern at the end of the inversion (after 7cm of shortening), green and white layers represent syn-inversion sedimentation.

TABLE 2. Scaled parameters used in the experimental program

Quantity	Experiment	Nature	Model/Nature
Length, L (m)	0.01	1000	10^{-5}
Density loose sand, ρ (kg·m^{-3})	1500	2700	0.55
Gravity acceleration, g (m·s^{-2})	9.8	9.8	1
Angle of internal friction, ϕ (º)	34.6	40	0.87
Cohesion loose sand, σ (Pa)	55	10^{7}	$5.5{\cdot}10^{-6}$
Density polymer, ρ (kg·m^{-3})	972	2200	0.44
Viscosity, η (Pa s)	$1.6{\cdot}10^{4}$	10^{18}–10^{19}	$1.6{\cdot}10^{-14/-15}$

($2.75x10^{-5}$cm s^{-1}). These deformations and syn-kinematic sedimentation rates were selected after two testing models in order to favor polymer flow, such as the salt in nature.

The materials used in the experimental program are summarized in Table 2. Dry silica sand with an average grain size of 250μm simulates the brittle sedimentary rocks of the upper crust and a polydimethylsiloxane polymer (PDMS) is the analog for salt (Weijermars, 1986). Silica sand has a Mohr-Coulomb behavior at moderate values of normal stress (McClay, 1990). The mechanical properties of poured sand were measured using a ring shear tester at the Fault Dynamics Analog Modeling Laboratory at Royal Holloway University of London, resulting in an angle of internal friction of 34.6º, a bulk density of 1500kg m^{-3} and a low apparent cohesive strength of 55Pa. In contrast, the polymer (PDMS) has a near-perfect Newtonian fluid behavior when deformed at a laboratory strain rate of 1.83x104cm s^{-1} (Dell'Ertole and Schellart, 2013). It has an effective viscosity of $1.6x10^{4}$Pas and a density of 972kg m^{-3} at 20ºC. The coefficient of sliding friction between the basal plastic sheet and the sand pack was 0.37 (Huiqi *et al.*, 1992; Konstantinovskaia and Malavieille, 2005).

As shown in Table 2, the experiments were dynamically scaled (*e.g.* Hubbert, 1937; Schellart, 2000) in such a way that 1cm in the model is equivalent to ~1km in nature (see McClay, 1990, for the details of the scaling).

Experimental procedure

The pre-kinematic sand pack was formed by pouring 3mm-thick, white and colored sand horizontal layers covering the footwall block and the plastic sheet, with a total thickness of 9.3cm above the horizontal basal detachment (Fig. 2A). The models were initially extended by 7cm at a displacement rate of $1.6x10^{-3}$cm s^{-1}. After this first phase of extension, the resultant hangingwall ramp-anticline and the ramp-syncline basin were filled by a polymer layer of variable thickness ranging from 0cm (at salt pinch-out) to 3.7cm (at the deepest depocenter) (Fig. 2B). Prior to the second phase of extension the polymer was overlaid by a 1cm-thick sand layer. Subsequent stretching was applied at a rate of $2.75x10^{-5}$cm s^{-1}with up to 8cm of total extension (15cm, considering both phases) (Fig. 2C). During this stage, syn-kinematic sediments were added for every 5mm of extension keeping a constant regional datum equal to the one existing at the beginning of the second extensional phase (Fig. 2C). Syn-kinematic sedimentation increased the differential load between basin depocenters and their edges enhancing polymer flow and localizing diapirism. Once the polymer reached the surface of the experiment through passive diapirs, the regional datum was raised by 3mm for each new syn-kinematic layer. Overhangs formed by polymer extrusion onto the model's surface were manually removed to simulate salt dissolution in nature, before adding a syn-kinematic layer (Rowan and Vendeville, 2006).

While Experiment 1 ended after the second extensional phase, Experiments 2 and 3 were subsequently inverted by 8cm (Fig. 2D, E) at a shortening rate of $2.75x10^{-5}$cm s^{-1} until recover of the second extensional phase. Experiment 2 did not consider syn-kinematic sedimentation during the inversion stage (Fig. 2D). However, in Experiment 3, green, white and black syn-inversion sand layers were added after each 1cm of shortening raising the regional datum to 5mm-thick (Fig. 2E).

Completed models were covered by a thick post-kinematic sand layer to preserve the final topography and inhibit any undesired polymer movement. They were subsequently gelled and serially sectioned into 3mm-thick vertical slices.

Modeling limitations

Although the use of rigid blocks to force the geometry of normal faults has been widely employed in analog modeling (McClay, 1989, 1995; Buchanan and McCLay, 1991; Roure and Colleta, 1996; Yamada and McCLay, 2003a, b), the main disadvantage of this technique is the inability of rigid footwalls to deform (McClay, 1995; Bonini *et al.*, 2012). This fact prevents the formation of basement-involved footwall structures as shortcuts, or horses, as occurs in nature (*e.g.* McClay, 1989, 1995; Nalpas *et al.*, 1995; Eisenstadt and Sims, 2005). Despite this limitation, we combined the rigid footwall and a brittle pre-salt sand pack to impose topographic variations during deformation, and both were considered to be the basement. We focus the analysis of our experimental results on how these basement topographic variations affect salt kinematics and the evolution of welds during both extension and inversion.

Data capture, analysis and visualization techniques

In addition to the foregoing limitations, the presence of polymer enhances friction and produces smearing against the glass sidewalls. This masks the structures' evolution through the glass due to the edge effects. For this reason,

the evolution of our experiments during both extension and inversion was documented using top-view time-lapsed photographs taken every 60 seconds with high-resolution digital cameras. To analyze the along-strike variations of structures, the vertical sections sliced at the end of the experiments were also recorded using digital cameras. In order to avoid the edge effects, a 5cm-wide section was neglected along each side of the experiments during their analyses.

To constrain the structural analysis, we used the final serial cross-sections of each experiment to build Voxel models in image-processing software, which allow the creation of virtual strike and depth slices (Dooley *et al.*, 2009; Ferrer *et al.*, 2016, 2017). In addition, following the methodology proposed by Hammerstein *et al.* (2014) we also converted the cross-section photographs into SEG-Y format to be loaded into seismic interpretation software to create a seismic volume (Fig. 3A). This allowed an accurate interpretation of each of the horizons and faults, paying special attention to the top and bottom of the polymer layer to characterize the along-strike variation of salt structures (Fig. 3B). The 3D seismic interpretation was carried out with Petrel (Schlumberger) and the maps were built using Gocad (Paradigm).

MODELING RESULTS

In this section, we summarize the main results of the three end-member experiments (Table 1). We begin with the experiment affected by extension (Experiment 1) and then, with the two experiments that were also subjected to inversion (Experiments 2 and 3). In the first case, we illustrate how the combination of a major basement fault and a syn-rift salt layer with significant thickness differences affects salt migration and the rise of salt structures during extension. In contrast, the second set of experiments depicts the inherited configuration (salt and basement faults) as being contractionally reactivated and rejuvenated during inversion, in addition to the role of syn-kinematic sedimentation during inversion.

Extension above a ramp-flat-ramp basement fault with syn-rift salt

The hanging wall geometry at the end of the first extensional phase was characterized by two major depocenters (landward rollover and basement ramp-syncline, Fig. 2B) flanking a structural high (basement ramp-anticline, Fig. 2B). The space created by the extensional motion of the rigid footwall was carefully filled with polymer simulating syn-kinematic salt and preserving the topography of the pre-kinematic sequence. Thus, the salt exhibits important variations in thickness, being thicker in the two depocenters, constant above the horizontal panels, and pinching out against the rigid footwall upper flat. These thickness differences simulate different sub-basins with syn-rift salt or post-rift salt units filling the topography generated during the rift in nature.

With ongoing extension during the second phase, two different deformation styles characterized the evolution of the overburden above the upper and the lower basement fault ramps. These two styles are clearly controlled by the salt thickness differences inherited from the first extensional phase (*e.g.* Jackson and Vendeville, 1994; Jackson *et al.*, 1994; Vendeville *et al.*, 1995). So, the thin salt layer above the breakaway fault favored strong coupling between basement and overburden extension, with the early development of an extensional forced fold that rapidly evolved into an extensional fault-propagation fold (Figs. 4A; 5A). This led to the upwards propagation of the breakaway basement fault through the salt into the overburden, which constrained the development of a landward rollover at the hanging wall block (Fig. 5A, B). As extension progressed, the growth of this rollover forced

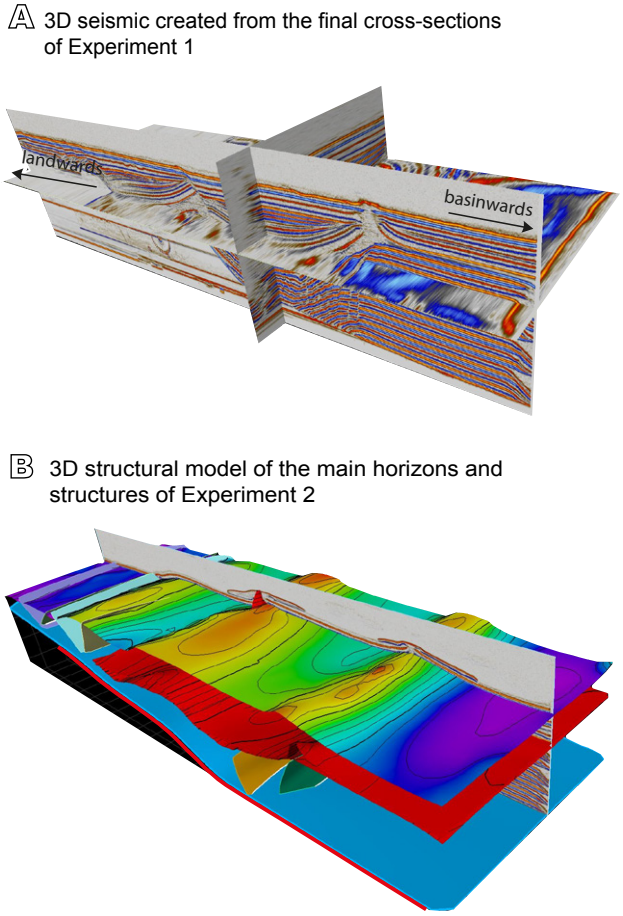

FIGURE 3. A) 3D seismic cube obtained from the final cross-sections of Experiment 1 and B) the 3D structural model resulting from the interpretation of the 3D seismic of Experiment 2.

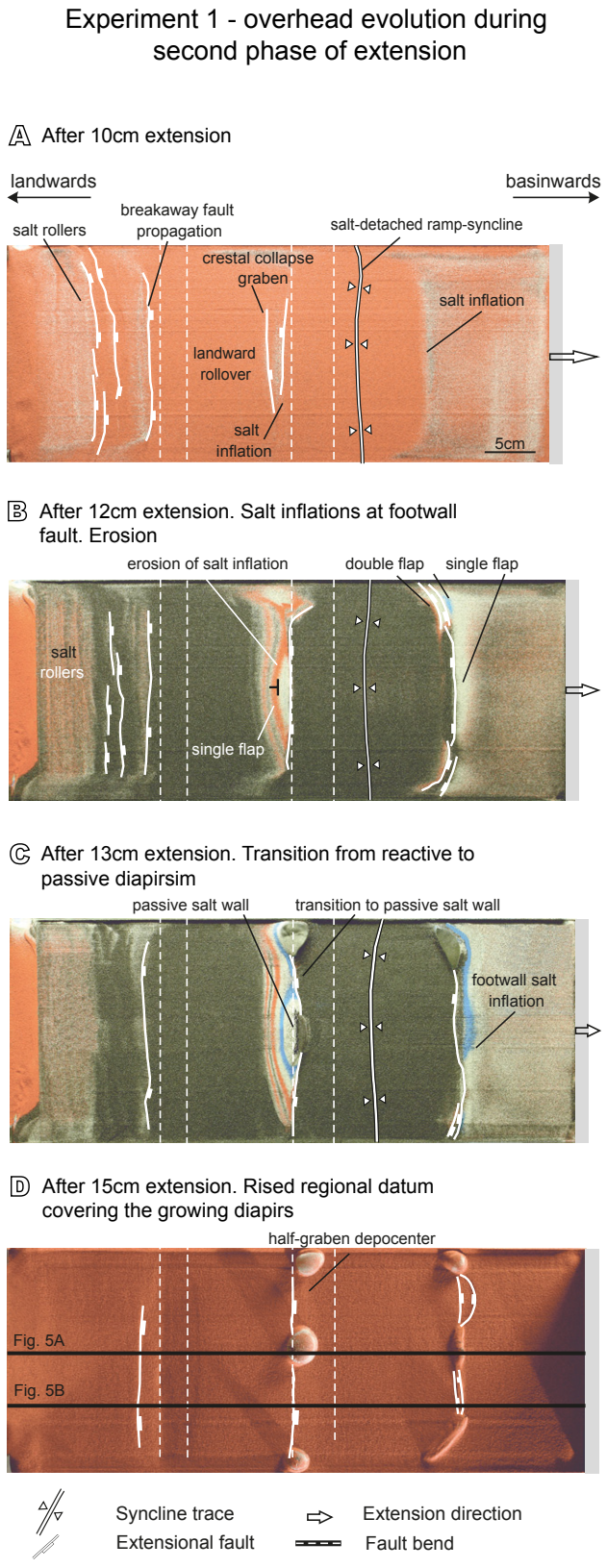

FIGURE 4. Interpreted top-view photographs showing the extensional evolution of Experiment 1 (illumination is from the right) after A) 10cm, B) 12cm, C) 13cm and D) 15cm of extension. Continuous black lines in Figure 4D correspond to the cross-section locations of Figure 5.

the salt evacuation towards the rollover hinge, thus arching the overburden above the pre-extension regional datum by inflation (Fig. 4A). Extension also produced the early downdip translation of the overburden over the gently-dipping upper flat panel of the rigid block. Consequently, different basinwards-dipping salt-detached listric faults controlled the rise of asymmetric reactive diapirs and salt rollers close to the salt pinch-out (Figs. 4A; 5A, B).

In contrast, above the lower ramp, where the salt layer was thicker, the overburden deformation was initially decoupled from basement extension. In this case, most of the subsidence related to the basement ramp-syncline was filled by salt that triggered the development of two drape monoclines bounding a salt-detached ramp-syncline in the overburden (Roma *et al.*, 2018). Figure 5C illustrates a structural map of Experiment 1 at the top of the salt unit that defines the main features detached on salt, whereas the map of Figure 5D illustrates the basement structure. Note the differences in structural styles between both horizons, which mean that the salt layer acts as a markedly effective decoupling layer during extension (*e.g.* Koyi *et al.*, 1993; Vendeville *et al.*, 1995; Stewartand Clark, 1999; Withjack and Callaway, 2000). As extension progressed, the interplay between basement extension and lithostatic load produced by syn-kinematic sedimentation forced salt migration from the sub-basin depocenters towards their edges where salt-inflated ridges developed (*e.g.* Kehle, 1988; Koyi *et al.*,1993; Hudec and Jackson, 2007; Ferrer *et al.*, 2014) (Fig. 6A, B). After 10cm of extension, overburden stretching in the inflated areas produced crestal collapse grabens (Fig. 6C) which evolved into a half graben as extension progressed (Fig. 6D). The basinward-dipping normal faults of these half grabens controlled the growth of reactive walls (Fig. 6D) in the central part of the experiment where both the extensional fault slip and the salt flow were maximum. The geometry of the basement ramp-anticline enhanced salt migration towards the inflated area located above it in comparison with the ridge at the basinward edge of the basin (Fig. 4A, B). This fact is clearly visible in the top-view photographs of Experiment 1 after 12cm of extension (Fig. 4B). Here, the erosion related to salt inflation is higher in the footwall of the normal fault located above the basement ramp-anticline than at the basinward edge of the basin (erosion of pre-kinematic white and blue sand layers in Fig. 4B). This different timing of salt extrusion is caused by the progressive erosion of any topographic high formed by salt inflation during syn-kinematic sedimentation, which enhanced salt rising and the formation of single or double vertical flaps of pre-kinematic sand. These flaps flank the reactive wall above the basement ramp-anticline (Ge *et al.*, 1995). After 13cm of extension, the intense erosion at the edges of the salt-detached ramp-syncline basin favors salt piercement and extrusion (Figs. 4C; 6E). From this moment

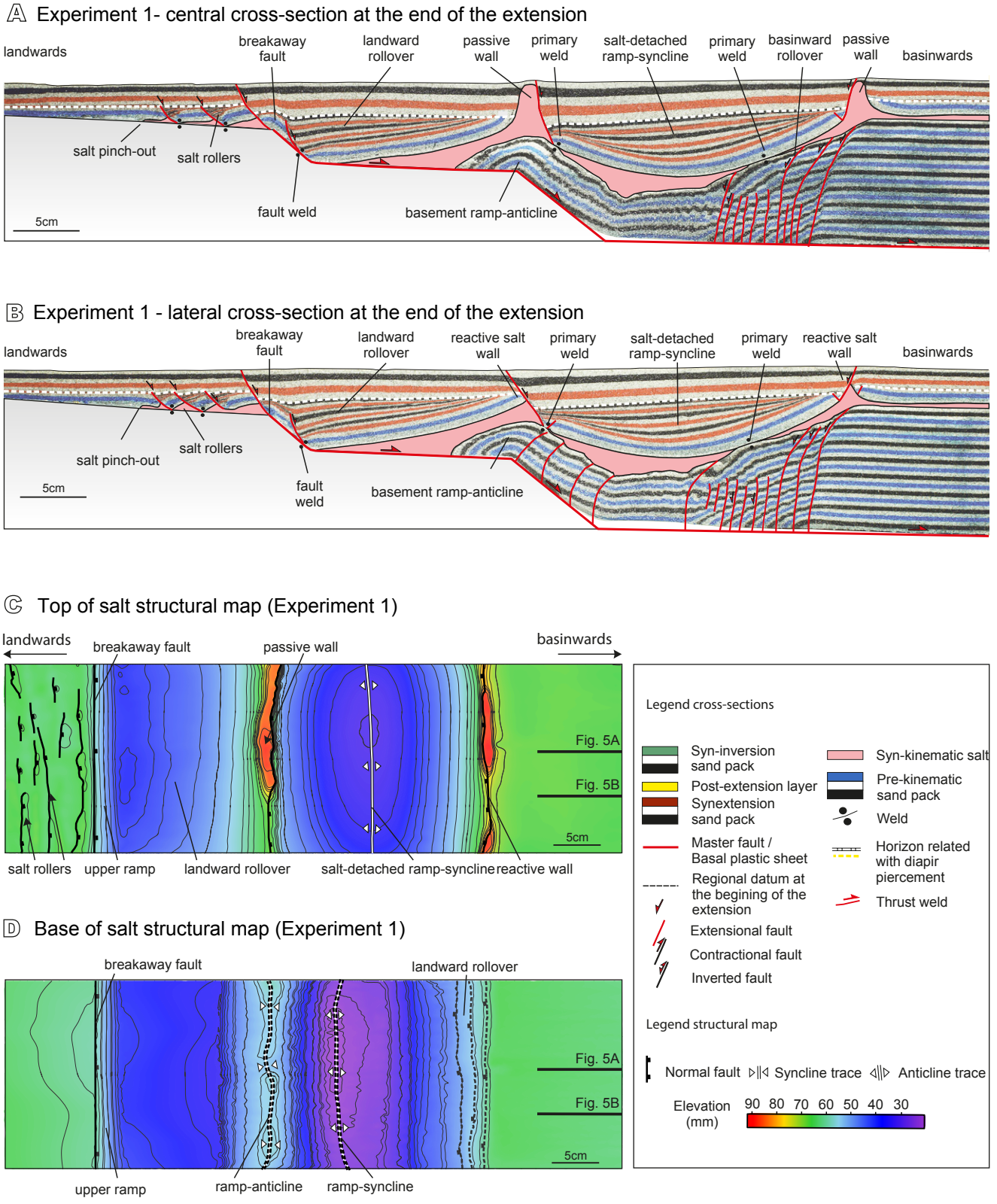

FIGURE 5. Interpreted cross-sections and structural maps of Experiment 1 showing the different style of salt structures along-strike: A) cross-section at the central part of the experiment at the end of the extension, B) lateral cross-section at the end of extension, C) structural map of the suprasalt structures and D) structural map of the subsalt structures (contours in mm). Reddish color indicates a structural high and blue, structural lows. Structures marked with a continuous line correspond to the faults affecting the overburden whereas dashed structures are those affecting the basement. See Figure 4D for cross-section location.

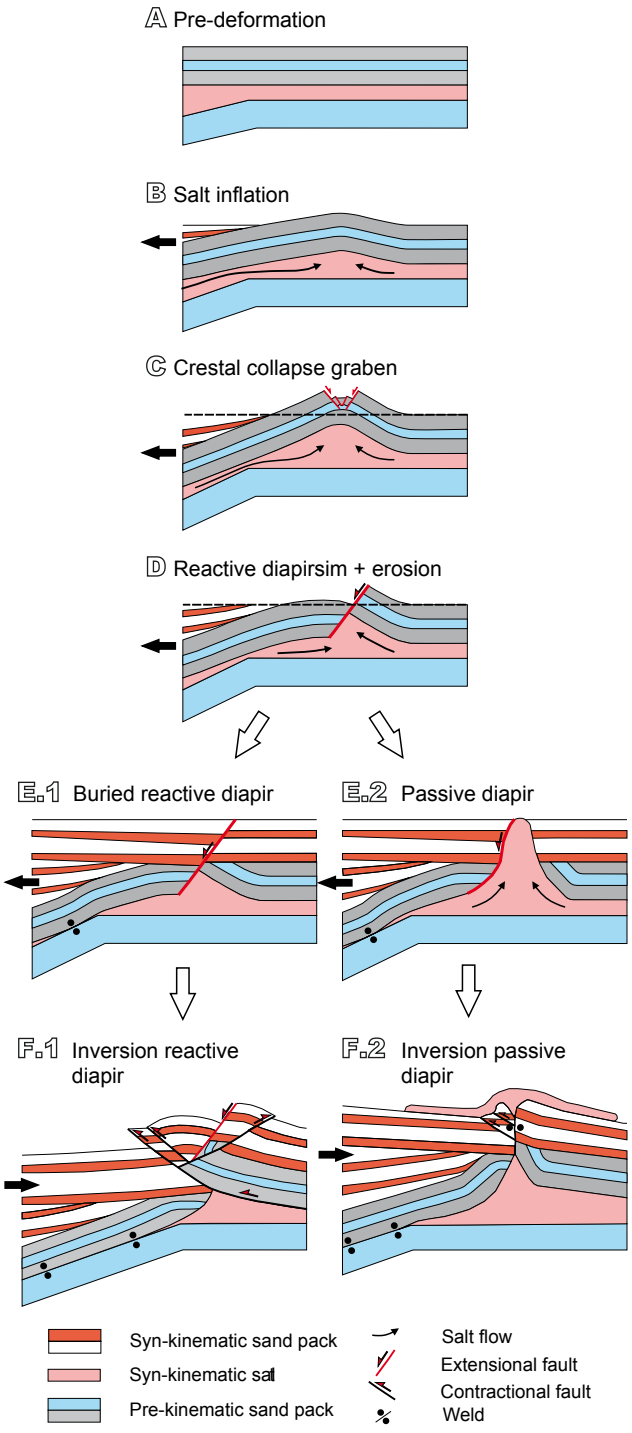

FIGURE 6. Synoptic model showing the different stages of salt structures evolution at the edges of the salt-detached ramp-syncline basin: A) Pre-deformational stage, B) at the beginning of extension with salt inflated areas fed by the flow from below the basin towards its edges, C) as extension progressed, the collapse grabens developed at the crest of these anticlines, D) evolving into basinward-dipping normal faults like a reactive diapir. From this point the reactive diapir could be buried (E.1) or could have evolved to a passive diapir (E.2). With ongoing inversion, an early pop-up structure flanked by opposite-verging thrusts developed above the buried reactive diapir (F.1). As shortening progressed the right flank of this diapir was thrusted basinward. In contrast, the passive diapir was squeezed, developing a secondary weld (F.2).

the regional datum was progressively raised to preserve the passive diapirs. This maximum fault slip at the central part of the experiments generate along-strike transition of both salt walls, from the passive salt wall in the central part of the model (Figs. 5A; 6E.2) to the reactive salt wall towards the glass-side (Figs. 5B; 6E.1).

During extension, the source layer was progressively stretched, thinned and finally depleted with the development of primary welds (Jackson and Cramez, 1989) (Fig. 5A, B). Different weld types developed in our experiments associated with the salt rollers (primary welds), below the landwards rollover at the hanging wall of the upper ramp (fault weld) and at both limbs of the salt-detached ramp-syncline (primary welds). The formation of these welds, especially at the upper ramp and below the salt-detached ramp-syncline favored coupling between overburden and basement deformation (Fig. 5A, B).

Inversion of a ramp-flat-ramp basement fault with syn-rift salt

The analog models described in this section were partially inverted (Bally, 1984). This inversion recovered the 8cm of stretching, which occurred during the second extensional phase. The inherited extensional architecture, the location of salt structures and the presence of primary welds dramatically controlled the evolution of the contractional structures during this episode. Independent of the syn-inversion sedimentation (Experiment 3), shortening produced the contractional reactivation of the main basement faults, the uplift of the two basins (the landward rollover and the salt-detached ramp-syncline), and the squeezing of salt structures that increased salt flow and extrusion (Fig. 7A).

As soon as inversion began, the inherited weak salt walls at both edges of the salt-detached ramp-syncline reactivated their growth. After 1cm of inversion (Fig. 7C.1), the partial closure of the stems drives a significant increase of upwards salt flow rates producing lateral extrusion and small overhangs on the model surface. During this initial stage, the reactive sectors of the salt walls were contractionally rejuvenated by squeezing, developing anticlines or thrust anticlines on top of them (Fig. 7C.1, C.2). The new topography forces the extruding salt flow, thereby developing salt sheets. At this point the breakaway fault was partly reactivated and propagated upwards into the syn-extensional cover as a reverse fault (Fig. 7C.1, C.2). This arched, folded and uplifted the landwards rollover and developed an asymmetric anticline that verged landward (Fig. 7C.1, C.2).

With the ongoing inversion, salt extrusion continued and part of the coalesced salt sheets was amalgamated developing symmetric allosutures (Dooley *et al.*, 2012)

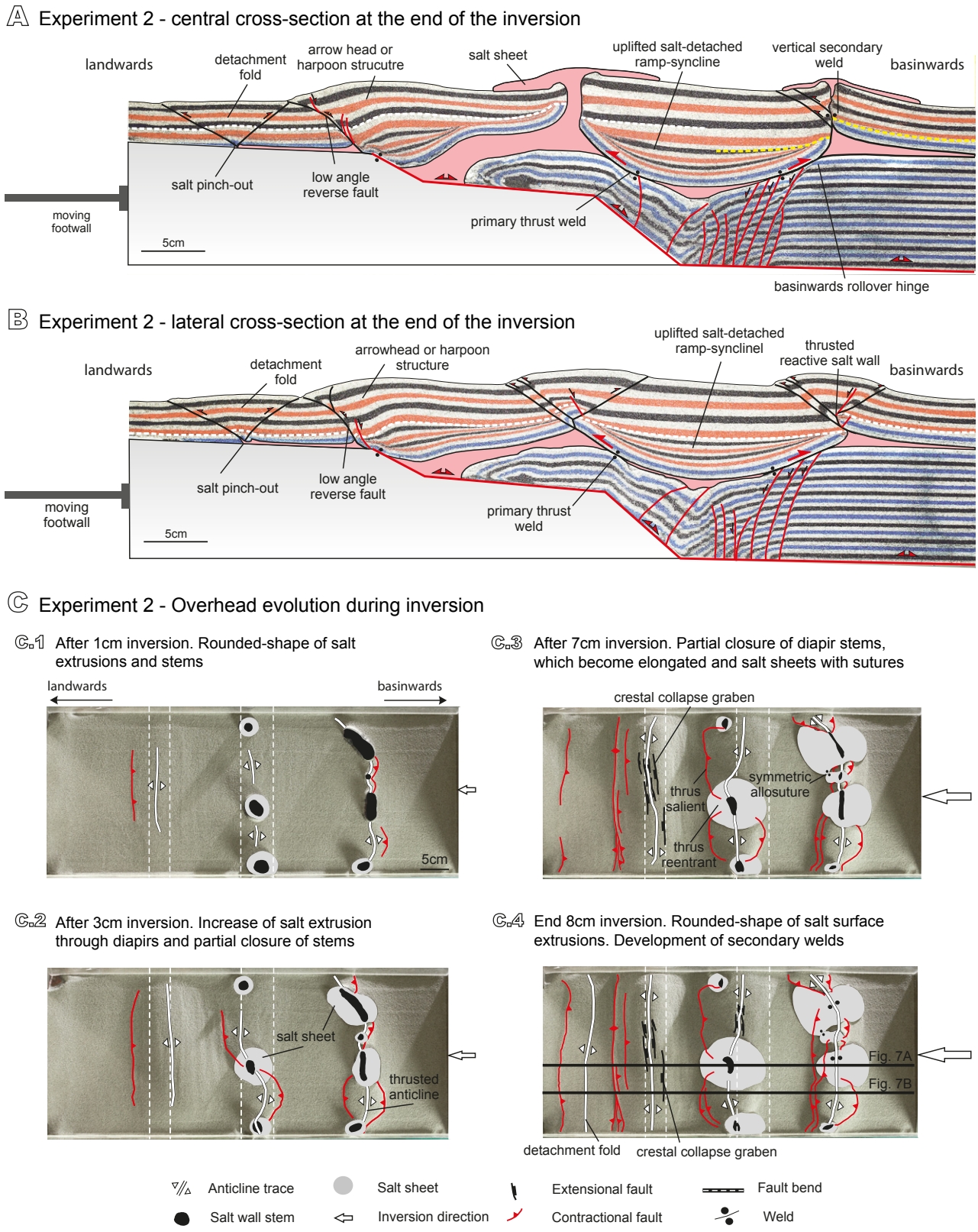

FIGURE 7. Interpreted cross-sections of Experiment 2 showing the main structural elements and the different style of salt structures along-strike: A) central cross-section at the end of the inversion, B) lateral cross-section at the end of the inversion. C) Interpreted top-view photographs showing the evolution of Experiment 2 during inversion without syn-inversion sedimentation after 1cm (C.1), 3cm (C.2), 7cm (C.3) and 8cm (C.4) of inversion. Continuous white lines in Figure 7C.4 correspond to the cross-sections locations of Figure 7A, B. In all the photographs illumination is from the right and surfaces in shadow are dipping to the left. See Figure 5 for legend.

(Fig. 7C.3). The different contractional strength along-strike in the salt walls results in curved thrusts (thrust salient at reactive salt walls) that form reentrants towards the squeezed passive walls (Fig. 7C.1, C.4) (Dooley *et al.*, 2009). Top-view photographs clearly illustrate how much of the salt walls have an elongated shape, thus indicating partial closure of the stems with associated secondary welds (Fig. 7C.4). The development of secondary welds is not coeval at both syncline-edging salt walls and it depends on the salt available at the source layer, the presence of primary welds, their reactivation and the width of the pre-contractional salt body. The surface that was primarily welded at the end of the extension at both syncline limbs is larger above the basinward rollover (Fig. 5A, B). This clearly limited the volume of salt available to be expulsed during shortening, and therefore, favors a faster secondary welding of the salt wall above the basinward rollover hinge (Fig. 7A). Secondary welding is also enhanced by the reactivation of primary welds as thrust welds that cause the uplift of the salt-detachment ramp-syncline (Fig. 7A).

After 7–8cm of shortening, the uplift of the landwards rollover produced an arrowhead or harpoon structure (Badley *et al.*, 1989) with a crestal collapse graben (Fig. 7C.3, C.4). Part of this shortening propagated above the upper flat panel of the major fault using the salt as a contractional detachment. As a result, a faulted detachment fold nucleated at the salt pinch-out (Fig. 7A, B, C.4). The salt-detached ramp-syncline was also uplifted with a clockwise rotation pushed by the widening of the basement ramp-anticline as inversion progressed (Fig. 7A, B). At this point, the contractional deformation at the secondary welds developed small thrusts nucleated at the upper part of salt pedestals (Figs. 6F.2; 7A). In contrast, asymmetric anticlines developed along-strike on the hanging wall of the thrusts that nucleated at the apex of the reactive salt wall (Figs. 6F.1; 7B). The complexity of the fault pattern of these anticlines depends on the geometry of the inherited salt wall at the beginning of the inversion.

Inversion of a ramp-flat-ramp basement fault with syn-rift salt and syn-inversion sedimentation

At the end of extension Experiment 3 was covered by a 5mm-thick post-extensional layer made of yellow sand (Fig. 8A, B). This layer buried the different salt structures at the salt-detached ramp-syncline edges. The evolution of the experiment with syn-inversion sedimentation (Experiment 3) during an early shortening episode is similar to the one previously described for Experiment 2. After 1cm of inversion, the buried passive diapirs were contractionally rejuvenated as active diapirs. Shortening reactivated the upwards salt migration, arching and uplifting the thin diapirs roof above their surroundings. A linear thrust developed after 2cm of shortening by the inversion of the breakaway fault (Fig. 8C). Thrust salients and reentrants also developed by the squeezing of the two salt walls at both salt-detached ramp-syncline edges (Fig. 8C.1). The stem of the central passive wall gradually lengthened by squeezing, stretching its plan section orthogonally to the shortening direction (Fig. 8C.1, C.2).

As inversion progressed, between 3–5cm of shortening, the salt extrusion rate significantly decreased. This fact is related to the squeezing of diapir stems and the development of secondary welds, isolating the feeder from the source layer (Fig. 8A). During mild shortening (4.5–5cm), the salt-detached ramp-syncline is intensely uplifted by the strong basement topography variations; this was forced by the hanging wall accommodation to the rigid footwall geometry. This produces diapir stem closure and concentrates deformation at the two curved thrusts (with opposite vergence at both basin edges). With between 5–6cm of shortening, secondary welds evolve into thrust welds. The salt walls' pinch-off above the basement ramp-anticline create an allochthonous teardrop that is decapitated by thrust welds (Fig. 8C.2). Short-cuts nucleated into the thrust weld and then propagated contractional deformation into the overburden. These short cuts produced a landward offset of the contractional deformation front and the thrust reentrant became inactive (Fig. 8C.3). At this point, the gradual thickness increase of the syn-inversion package hinders the contractional propagation of the breakaway fault being finally buried as a blinded thrust (Fig. 8A, B, C.3). In contrast to Experiment 2, the shortening propagation at the footwall of this thrust and the reactivation of the salt pinch-out is totally inhibited by the thick syn-kinematic unit (Fig. 8A, B, C.3).

After intense shortening (7–8cm), the only active contractional structure is the thrust related to the salt wall above the basement ramp-anticline (Fig. 8C.3). The allochthonous teardrop located at the hanging wall of the thrust weld is displaced by up to 4cm from its original position above its pedestal (Fig. 8A). In contrast, the syn-inversion sedimentation buried the salt wall at the opposite basin edge (Fig. 8A, C.3). It was partially squeezed while developing vertical secondary welds and faulted pop-ups above the diapir (Fig. 8A, B). The welding kinematic differences between the two edges of the salt-detached ramp-syncline basin forced the clockwise rotation of the basin at the hanging wall of the thrust weld (Fig. 8A, B).

DISCUSSION

Welding kinematics

The subsidence of the salt-detached ramp-syncline basin during extension drives salt flow from the basin

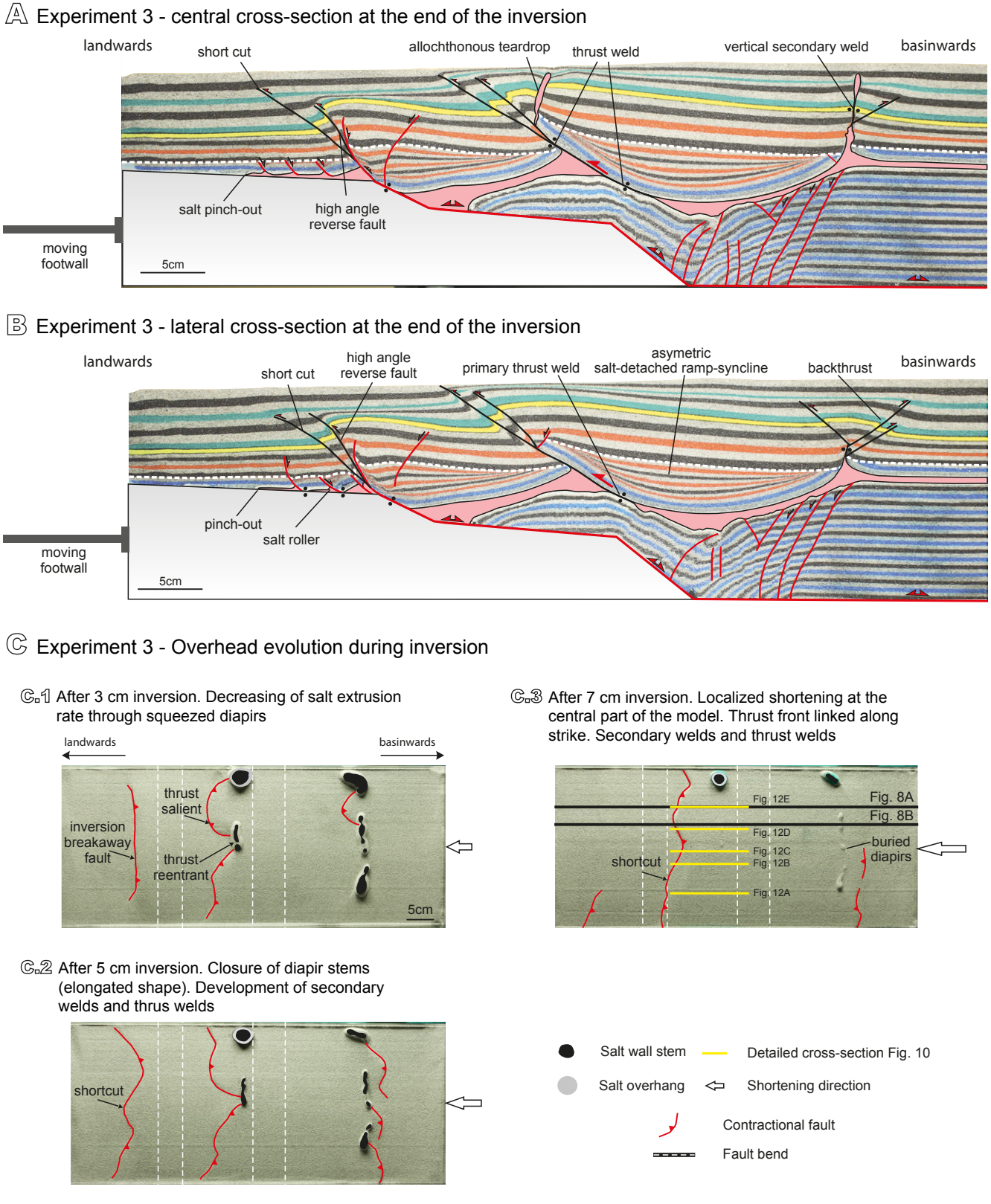

FIGURE 8. Interpreted cross-sections of the Experiment 3 showing the main structural elements and the different style of salt structures along-strike: A) central cross-section at the end of the inversion, B) lateral cross-section at the end of the inversion, C) interpreted top-view photographs showing the evolution of Experiment 3 (with syn-inversion sedimentation) after 3cm (C.1), 5cm (C.2) and 7cm (C.3) of inversion. Continuous black lines in Figure 8C.3 correspond to the cross-section locations of Figure 8A, B. Yellow lines correspond to the different detailed cross-sections of Figure 12. In all the photographs illumination is from the right and surfaces in shadow are dipping to the left. See Figure 5 for legend.

depocenter towards its edges where salt inflated anticlines evolve into salt walls. While this occurs, the overburden gradually approaches the underlying basement by thinning the source layer until they eventually come into contact, developing a primary weld. However, unlike what happens when the base of the salt unit is horizontal, the existence of basement topography constraints welding kinematics.

Syn-kinematic infill layers show a syncline basin with different sedimentary architectures at both edges (Fig. 5A, B). Whereas these layers progressively onlap against the syncline limb located above the basement ramp-anticline, they form a wedge with different internal unconformities at the other syncline limb (Fig. 5A, B). This architecture completely changes with the formation of the first primary weld at the basinward rollover. From here, the salt-detached ramp-syncline basin subsides asymmetrically towards the unwelded limb, expelling salt landward to the adjacent passive diapir. This produces a counter-clockwise rotation of the salt-detached ramp-syncline basin that modifies the basin fill architecture to a half-graben and slightly folds the unconformity (white dashed line in Fig. 5A, B). This rotation, favored by salt expulsion, also widens the primary weld at the basinward rollover hinge (Fig. 5A). Sinking ceases with the development of the second primary weld at the landward limb of the basement syncline. Despite the length of this new weld, it is shorter than the previous one (Fig. 9A), but it is enough to interrupt diapir feeding. This is demonstrated by a significant reduction of the salt extrusion rate (Fig. 4D).

At this point the overburden is stuck to the basement. Further extension then increases the width of the basement ramp-syncline, thus dragging the overburden and widening the passive diapir (cryptic extension).

Primary welds at the end of the extension strongly contrast with those observed at the end of the inversion (Fig. 7A, B). The comparison of salt thickness maps between Experiments 1 and 2 (Fig. 9) clearly depicts that: i) the

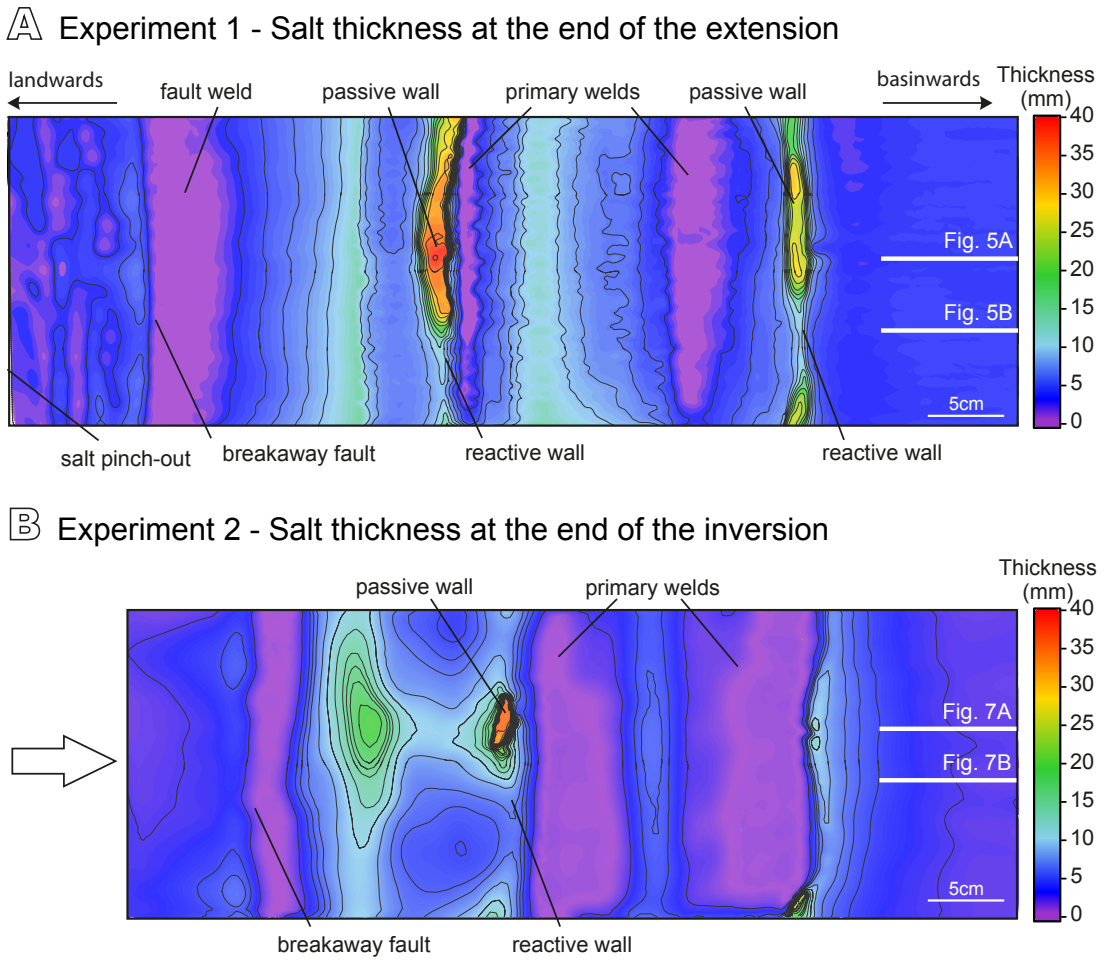

FIGURE 9. A) Thickness maps of salt at the end of the extensional phase for Experiment 1 and B) at the end of the inversion for Experiment 2. Purple colors indicate the areas where salt was depleted thus developing primary welds, whereas yellowish colors correspond to the salt walls with maximum salt thicknesses. White lines correspond to the cross-section locations of Figures 5A, B and 7A, B.

length of the primary welds below the salt-detached ramp-syncline progressively increase during shortening and ii) it is reduced for the fault weld related to the breakaway fault. Inversion implies important basement topographic variations, such as the gradual uplift of the basin. This uplift is associated with a width reduction of the basement ramp-syncline (compare this to the width of the basement syncline between Figs. 5A–7A; 5B–7B). Width reduction implies an asymmetric uplift of the salt-detachment ramp-syncline basin pushed by basement topographic variations above the lower ramp (Fig. 7A). These processes lead to a change in the weld kinematics. That is, pre-existing primary welds are reactivated as thrust welds (Roma *et al.*, 2018) involving shear along their surfaces. Both the uplift and the progressive primary welds' contractional reactivation favors the squeezing of passive diapirs located at the basin edges. These structures could be totally squeezed hence developing secondary vertical welds (Fig. 7A).

Reactivation of sub-horizontal primary welds as thrust welds during later contraction is common in fold-and-thrust belts of convergent or passive margins with pre-existing diapirs and welded minibasins (*e.g.* Basque Pyrenees, La Popa Basin, Flinder Ranges, Angola Margin) (Brun and Fort, 2004; Rowan and Vendeville, 2006; Hudec and Jackson, 2007). Gottschalk *et al.* (2004, figs. 7 and 11) and Rowan and Vendeville (2006, fig. 9) show some restorations that illustrate sub-horizontal primary welds serving as thrust welds. Nevertheless, only scarce examples of dipping primary welds reactivated as thrust welds have been provided in the literature. These types of structures should develop in inverted rift basins with syn-rift salt or post-rift salt filling pre-existing relief in which the source layer can have an original dip. This is typical at the margins of the rift where topographic relief is more important or is located between sub-basins. Similar structures have been found at the north-eastern edge of the BFB and at the northern edge of the DCG (Fig.10). These salt-bearing rift basins developed during Jurassic–Early Cretaceous times and were later inverted during the Late Cretaceous–Early Tertiary (De Jager, 2003). In both cases, Zechstein salt acted as a decoupling layer during basement-involved rifting. The differential loads created by syn-rift sedimentation triggered salt migration towards the edges of the basins (NE edge of the BFB and at both edges in the DCG) feeding the growth of diapirs above the major faults (Fig. 10). The depletion of the source layer, especially above the basin-bounding faults, probably resulted in a discontinuous primary weld that dipped towards the basin with a steeped geometry that is controlled by the offset of basement faults and the topographic relief.

Despite the fact that the degree of inversion was stronger in the BFB than in the DCG (compare Fig. 10A, B), due to BFB strike at high angles to the direction of compression (Letouzey *et al.*, 1995) salt structures show similar kinematic evolutions. The inversion of the northern sector of the BFB resulted in folding, uplift and erosion (Nalpas *et al.*, 1995). Zechstein salt inhibited the basement fault propagation into the overburden (Dronkers and Mrozek, 1991) and favored the development of a striking thrust weld detached on this salt (De Jager, 2003) probably from an inherited squeezed salt structure. The hanging wall of this thrust weld, formed by Upper Jurassic–Lower Cretaceous rocks (basin infill), was carried onto the footwall of the major inverted extensional fault thus bounding the rift basin (Fig. 10A). This major fault disconnects the salt unit during the extension; note how the inversion of the basin perfectly fits with the harpoon structure that developed in our experiment (Fig. 7A, B). In contrast, the southern margin of the DCG (Fig. 10B) shows a salt-detached ramp-syncline basin that is flanked by collapsed salt diapirs, mainly developed by a major kinked basement fault. Just as it occurred in our experiments, the basinward dipping salt remnants and their equivalent primary welds located at the edge of the basin above the major basement fault probably served as thrust welds during the early stages of

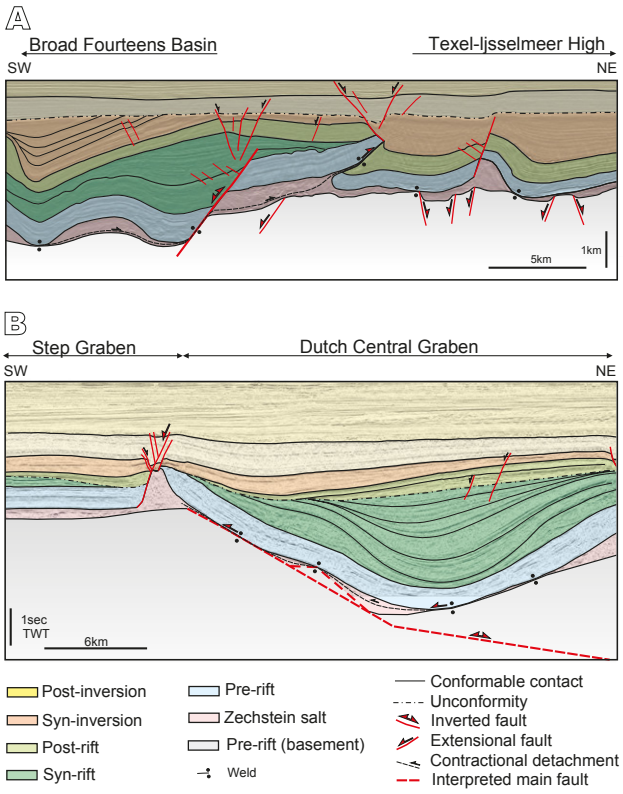

FIGURE 10. Natural examples of inverted salt basins. A) Line drawing of the SW-NE seismic profile in the Dutch offshore at the transition from the offshore extension of the Texel-Ijsselmeer High to the Broad Fourteens Basin (southern North Sea) (modified from De Jager, 2003) and B) line drawing of the regional SW-NE profile through salt structures across the eastern part of the Dutch Central Graben (southern North Sea - Netherlands). Seismic image obtained from Virtual Seismic Atlas (VSA) by Fugro.

inversion. However, we have not had the opportunity to study recently reprocessed seismic data from the area, so this hypothesis is for the moment, merely speculative.

How does syn-inversion sedimentation affect regional structure and salt tectonics?

The comparison between Experiments 2 and 3 (Figs. 7A–8A; 7B–8B) shows that in addition to the structural architecture inherited from the extensional episode, the syn-kinematic sedimentation plays a key role in strain localization and the evolution of salt structures during inversion. Furthermore, it is also critical to the timing of contractional structures.

In both models, the contractional reactivation of the breakaway fault forced an asymmetrical uplift of the landward rollover. This formed a harpoon structure due to the propagation of this fault into the cover in a coupled deformation style. However, as documented for fold-and-thrust belts, syn-inversion sedimentation controls the dip and the shape of the reverse fault that propagates into the cover (Baby *et al.*, 1995; Storti and McClay, 1995; Barrier *et al.*, 2013). While Experiment 2 shows a low angle curved reverse fault flattening upwards (Fig.7A, B), this fault is planar and has a high angle in Experiment 3, which had syn-kinematic sedimentation (Fig. 8A, B). Another important point is how syn-kinematic sedimentation favors the back-rotation of the salt-detached ramp-syncline basin during uplift (Fig. 8A, B) (McClay, 1989, 1995; Buchanan and McClay, 1991; Bonini *et al.*, 2012; Ferrer *et al.*, 2016). In a similar manner to the experiments of Ferrer *et al.* (2016), who used a rigid footwall to constrain the geometry of different faults -and considering pre-extension salt- in our models the salt acted as a decoupling layer that transferred contractional deformation landward above the upper flat panel. This décollement was extremely efficient in the experiment without syn-inversion sedimentation where a detachment fold was flanked by two reverse faults that were developed at the salt pinch-out (Fig. 11A). In contrast, it was not effective in the experiments with syn-inversion sedimentation where contractional deformation was absorbed by a footwall short-cut and did not propagate landward (Fig. 11B). Similar examples have been described in fault-and-thrust belts where, despite the existence of a décollement, syn-kinematic sedimentation can inhibit the outwards propagation of the deformation front into the foreland (Bonini, 2001; Bonini *et al.*, 2012).

Our experimental results also demonstrate how the thickening of the syn-inversion unit directly controls where and how deformation localizes and therefore the timing of the contractional kinematics. Figure 8C illustrates how the growth of contractional structures is constrained by syn-kinematic sedimentation. During early inversion the deformation was preferentially absorbed by the upward propagation of the fault breakaway as a reverse fault and by the central salt wall (Fig. 8C.1). Incremental syn-kinematic sedimentation buried the reverse fault related to the breakaway fault propagation and the contractional deformation switched backwards to the central salt wall. This was favored by the salt layer that acts as a shear zone that transfers the deformation basinward developing a fish-tail structure (Letouzey *et al.*, 1995) (Fig. 11B). Similar structures have been interpreted in contractional scenarios with different detachment layers (Pichot and Nalpas, 2009). The central salt wall absorbed the main contractional deformation and it was squeezed shut. Squeezing forms thrusts and folds, which trend away in map view due to the 3D strain compatibility differences between salt and adjacent rocks (Fig. 8C.1, C.2). These differences constrain the development of reverse faults where the inherited salt wall was reactive (Fig. 12A, E) and that progressively curve towards the diapirs, creating thrust reentrants where the inherited salt wall was passive (Fig. 12B, C, D). If the inversion continues after secondary welding (Fig. 12C), the diapir separates from their original pedestal (decapitated diapir) (Fig. 12B) or develops a thrust weld (Fig. 12C, D). This change in the structural style is

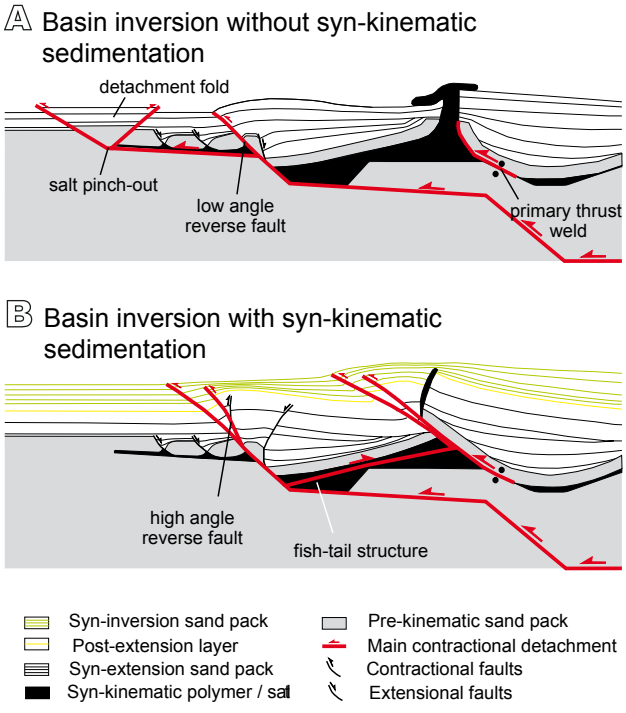

FIGURE 11. Conceptual sketch on the effect of syn-kinematic sedimentation during inversion: A) basin inversion without syn-kinematic sedimentation, where the contractional deformation propagates towards the salt pinch-out and it is mainly absorbed by the frontal thrust related to the harpoon structure and B) basin inversion with syn-kinematic sedimentation where the thrust front has a high angle and the main contractional deformation is absorbed by the pre-existing salt wall also favored by the salt layer transferring deformation towards the salt wall, while developing a fish-tail.

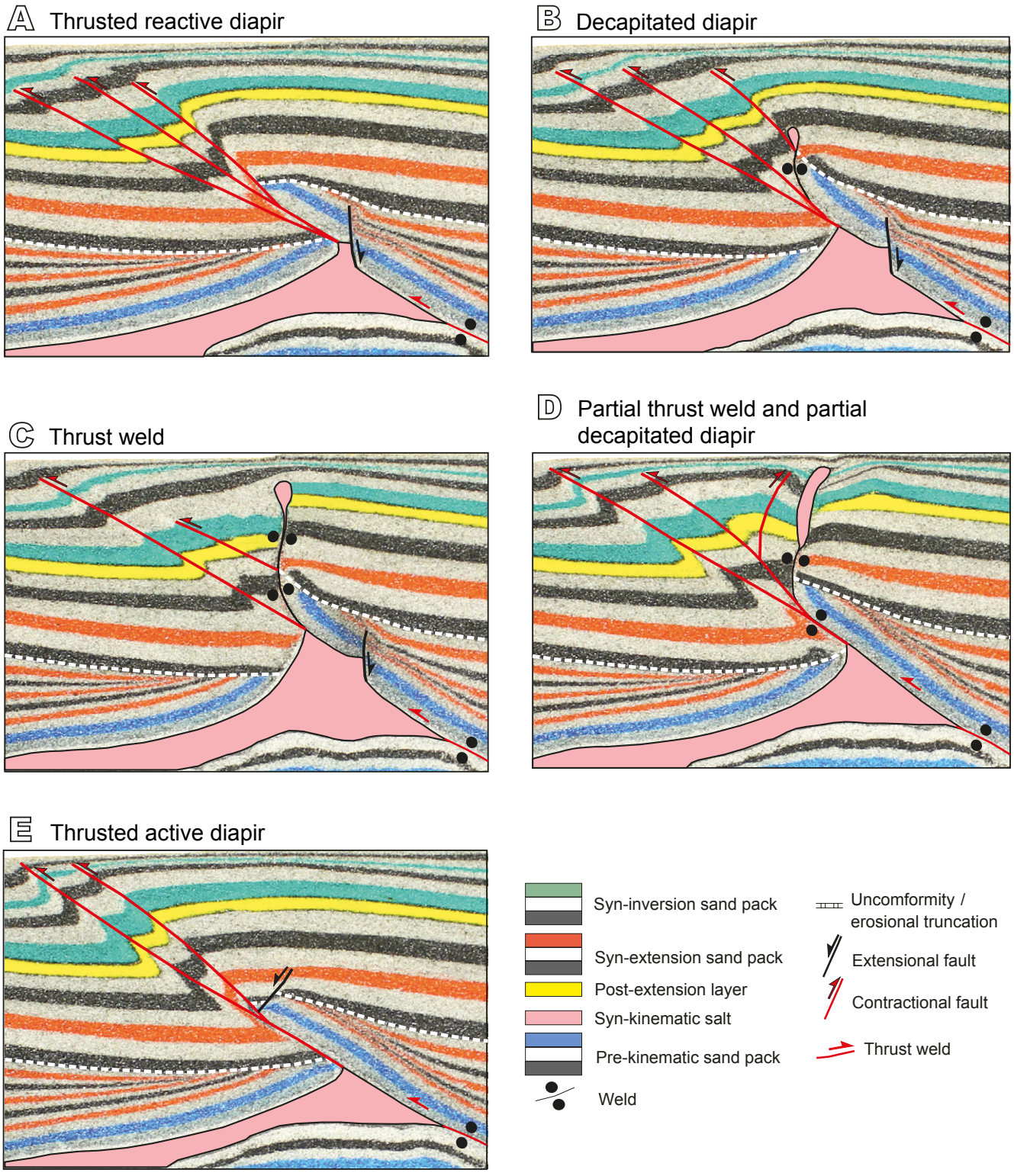

FIGURE 12. Serial detailed cross-sections of Experiment 3 showing how inversion increases towards the weak diapir inherited from the extensional phase where shortening was focused. Note the along-strike variation of the inverted salt wall above the basement ramp-anticline. A) Thrusts nucleating at the apex of a pre-existing reactive diapir, B) squeezed passive diapir with a vertical secondary weld subsequently decapitated, C) squeezed passive diapir with a vertical secondary weld that evolves to a thrust weld when shortening continues, D) partial thrust weld and decapitated diapir and E) thrusts nucleating at the apex of a pre-existing reactive diapir. The inherited structure (reactive or passive diapir) and syn-inversion sedimentation are the main factors controlling the structural evolution during inversion. See Figure 8C.3 for location.

so critical to the thrust's geometry that it is progressively smoothed until it develops a straight thrust front (Fig. 8C.3). This evolution is consistent with the models presented by Rowan *et al.* (1999) or Dooley *et al.* (2009). Figure 8A, B illustrate how the growth of the frontal short-cut ends after the sedimentation of the second green layer. This is practically coeval to the age of the pop-up structure above the squeezed diapir at the basinward rollover.

Despite the effect of the syn-kinematic sedimentation during inversion, we should not rule out the influence of different sedimentation rates as well as the erosion, on the evolution of these tectonic processes. These two factors tend to favour or inhibit the landward propagation of contractional deformation (Storti and McClay, 1995; Graveleau *et al.*, 2012) as well as the squeezing and extrusion rates of salt structures.

CONCLUSIONS

We have used analog models to investigate the influence of welding kinematics on the deformation patterns associated with extended and inverted basins with syn-rift salt and how basement topography variations impact it. Our work shows that while salt distribution and basement topography constrain welding kinematics during extension, the inherited structures, the continuity of the salt layer or its welded equivalent, and the syn-inversion sedimentation is what drive the welds' evolution during late inversion. In this sense, the main conclusions of this research are:

i) The interaction of basement fault offsets and syn-rift salt thickness variations between different sub-basins determines coupled/decoupled deformation during extension. The thin salt layer favors the upwards propagation of basement faults into the overburden in a coupled deformation. When this occurs, the continuity of the source layer is interrupted and can halt the growth of salt structures. In contrast, a thick salt layer favors the development of a salt-detached ramp-syncline basin partially decoupled from basement fabrics.

ii) Salt thickness also has an impact on the salt structures' style during extension. While salt rollers dipping basinward develop where the salt is thinner, salt walls develop at the edges of the salt-detached ramp-syncline as salt thickness increases.

iii) Primary welding enhances basement and overburden coupling in areas with thin and thick salt layers. The interplay between basement topography, salt thinning by expulsion and sedimentation load as extension progresses, constrains the complex welding kinematics. The asymmetrical sinking of the salt-detached basin infers the timing of welding. Welding kinematics can be also noticed by basin rotations and by the depocenter's trajectory variations in syn-extension sediments.

iv) The pre-existing structure (basement faults, salt continuity and the presence of primary welds) plays a key role during inversion. Changes to basement topography during inversion control welding kinematics, where dipping primary welds are reactivated as thrust welds. Depending on the geometry of the inherited salt bodies (reactive or passive salt walls), the contractional reactivation of these primary welds favor: i) the rejuvenation of the reactive salt wall as a thrust salient and ii) the formation of thrust reentrants towards the squeezed passive walls, developing secondary vertical welds and small thrusts nucleated at their pedestals.

v) Syn-kinematic sedimentation during inversion is a key factor controlling where, when, and how the strain is localized, and it therefore controls the evolution of inherited salt structures. While salt pinch-outs usually serve as nucleation points, syn-kinematic sedimentation during inversion inhibits the propagation of the contractional deformation towards the pinch-out. In that case, the thrust front is translated backwards and is characterized by high angle reverse faults. For instance, syn-kinematic sedimentation during inversion also seals the thrust front and therefore forces contractional deformation to switch further backwards, where pre-existing salt structures can absorb the main shortening. Meanwhile, salt layers and primary thrust welds act as contractional detachments and also transfer deformation towards these inherited diapirs until the development of secondary welds and thrust welds.

These types of structures are found in inverted salt basins with syn- or post-rift salt that experiences pre-existing relief in which the salt unit can have an original dip. The Broad Fourteens Basin and Dutch Graben are two clear examples that follow similar kinematic evolutions as our analog models. Seismic line interpretation of these basins shows basinward dipping salt remnants and their equivalent welds are located at the edges of the basin above the major bounding faults. These primary welds served as thrust welds during the early stages of inversion. Consequently, we cannot rule out that some reactivation of primary welds as thrust welds may be present, and even more so when syn-kinematic sedimentation is involved during the inversion stage.

ACKNOWLEDGMENTS

The experimental program presented in this manuscript was carried out at the Fault Dynamics Research Group laboratory of

the Royal Holloway University of London and was supported by the STAR Research Consortium. This Consortium was sponsored by the following companies: BG Group, BHPBilliton, ConocoPhillips, Eni, MarathonOil, Nexen, Shell, Talisman Energy and YPF. Part of this research has also been supported by the SALCONBELT Project (CGL2017-85532-P), the GEOMODELS Research Institute and the Grup de Geodinàmica i Anàlisi de Conques (2014SGR-467). Research of M. Roma was partially funded by APIF-PhD program of the Universitat de Barcelona. We thank J. Hammerstein for the construction of the 3D seismic from the cross-sections and K. D'Souza, J. Morris and F. Lehane are also acknowledged for logistical support in the modeling laboratory. We thank Schlumberger and Midland Valley Exploration Ltd.for providing the academic licenses of Petrel and Move software, respectively, used in the interpretation of the models. Also, thanks are due to Fugro for sharing the seismic data of the Dutch Central Graben (Dutch sector of the southern North Sea Basin) through Virtual Seismic Atlas (VSA). Finally we gratefully acknowledge the editor J.M. Casas as well as M. Moragas, G. Zamora and one anonymous reviewer for the suggested improvements of the manuscript. English editing by Terranova Scientific.

REFERENCES

Baby, P., Colletta, B., Zubieta, D., 1995. Etude géométrique et expérimentale d'un bassin transporté: exemple du synclinorium de l'Alto Beni (Andes centrales). Bulletin de la Société Géologique de France, 166(6), 797-811.

Badley, M., Prince, J.D., Backshall, L.C., 1989. Inversion, reactivated faults and related structures, seismic examples from the Southern North Sea. The Geological Society of London, 44 (Special Publications), 201-219. DOI: 10.1144/GSL.SP.1989.044.01.12

Bally, A.W., 1984. Tectonogénese et sismique de réflexion. Bulletin Société Géologique de France, 7(2), 279-285. DOI: 10.2113/gssgfbull.S7-XXVI.2.279

Barrier, L., Nalpas, T., Gapais, D., Proust, J.-N., 2013. Impact of synkinematic sedimentation on the geometry and dynamics of compressive growth structures: Insights from analogue modelling. Tectonophysics, 608, 737-752. DOI: 10.1016/j.tecto.2013.08.005

Bonini, M., 2001. Passive roof thrusting and forelandward fold propagation in scaled brittle-ductile physical models of thrust wedges. Journal of Geophysical Research, 106(B2), 2291-2311.

Bonini, M., Sani, F., Antonielli, B., 2012. Basin inversion and contractional reactivation of inherited normal faults: a review based on previous and new experimental models. Tectonophysics, 522-523, 55-88. DOI: 10.1016/j.tecto.2011.11.014

Brun, J.P., Nalpas, T., 1996. Graben inversion in nature and experiments. Tectonics,15(3), 677-687. DOI: 10.1029/95TC03853

Brun, J.P., Fort, X., 2004. Compressional salt tectonics (Angola margin). Tectonophysics, 382, 129-150. DOI: 10.1016/j.tecto.2003.11.014

Buchanan, P.G., McClay, K.R., 1991. Sandbox experiments of inverted listric and planar fault systems. Tectonophysics, 188, 97-115. DOI: 10.1016/0040-1951(91)90317-L

Burliga, S., Koyi, H.A., Krzywiec, P., 2012. Modelling cover deformation and decoupling during inversion, using the Mid-Polish Trough as a case study. Journal of Structural Geology, 42, 62-73. DOI: 10.1016/j.jsg.2012.06.013

Cramez, C., Jackson, M.P.A, 2000. Superposed deformation straddling the continental-oceanic transition in deep-water Angola. Marine and Petroleum Geology, 17(10), 1095-1109. DOI: 10.1016/S0264-8172(00)00053-2

Callot, J.P., Jahani, S., Letouzey, J., 2007. The role of pre-existing diapirs in fold and thrust belt development. In: Lacombe, O., Roure, F., Lavé, J., Vergés, J. (eds.). Thrust Belts and Foreland Basins. Frontiers in Earth Sciences. Berlin, Heidelberg, Springer, 309-325. DOI:10.1007/978-3-540-69426-7_16

Callot, J.P., Trocmé, V., Letouzey, J., Albouy, E., Jahani, S., Sherkati, S., 2012. Pre-existing salt structures and the folding of the Zagros Mountains. The Geological Society of London, 363 (Special Publications), 545-561. DOI: 10.1144/SP363.27

Coward, M., Stewart, S., 1995. Salt-influenced structures in the Mesozoic-Tertiary cover of the southern North Sea, U.K. In: Jackson, M.P.A., Roberts, D.G., Snelson, S. (eds.). Salt tectonics: a global perspective. American Association of Petroleum Geologists (AAPG), 65 (Memoir), 229-250.

De Jager, J., 2003. Inverted basins in the Netherlands, similarities and differences. Netherlands. Journal of Geoscienes/Geologie em Miijnnown, 82(4), 355-366.

Dell'Ertole, D., Schellart, W.P., 2013. The development of sheath folds in viscously stratified materials in simple shear conditions: an analogue approach. Journal of Structural Geology, 56, 129-141. DOI: 10.1016/j.jsg.2013.09.002

Del Ventisette, C.D., Montanari, D., Bonini, M., Sani, F., 2005. Positive fault inversion triggering 'intrusive diapirism': an analogue modelling perspective. Terra Nova,17(5),478-485. DOI: 10.1111/j.1365-3121.2005.00637.x

Dooley, T.P., McClay, K.R., Hempton, M., Smit, D., 2005. Salt tectonics above complex basement extensional fault systems: Results from analogue modelling In: Dore, A.G., Vining, B.A. (eds.). Petroleum geology: North-west Europe and global perspectives. Proceedings of the 6th Petroleum Geology Conference, London, Petroleum Geology Conferences Ltd. and the Geological Society, 1631-1648. DOI: 10.1144/0061631

Dooley, T.P., Jackson, M.P.A., Hudec, M.R., 2009. Inflation and deflation of deeply buried salt stocks during lateral shortening. Journal of structural geology, 31, 582-600. DOI: 10.1016/j.jsg.2009.03.013

Dooley, T.P., Hudec, M.R., Jackson, M.P.A., 2012. The structure and evolution of sutures in allochthonous salt. American Association of Petroleum Geologists Bulletin, 96, 1045-1070. DOI: 10.1306/09231111036

Dooley, T.P., Jackson, M.P.A., Jackson, C.A.L., Hudec, M.R., Rodriguez, C.R., 2015. Enigmatic structures within salt walls of the Santos Basin—Part 2: Mechanical explanation from physical modelling. Journal of Structural Geology, 75,163-187. DOI: 10.1016/j.jsg.2015.01.009

Dooley,T.P., Hudec, M.R., Carruthers, D., Jackson, M.P.A., Luo, G., 2017. The effects of base-salt relief on salt flow and suprasalt deformation patterns—Part 1: Flow across simple steps in the base of salt. Interpretation, 5(1), SD1-SD23. DOI: 10.1190/INT-2016-0087.1

Dronkers, A.J., Mrozek, F.J., 1991. Inverted basins of The Netherlands. First Break, 9, 409-418.

Eisenstadt, G., Sims, D., 2005. Evaluating sand and clay models: do rheological differences matter? Journal of Structural Geology, 27, 1399-1412. DOI: 10.1016/j.jsg.2005.04.010

Ferrer, O., Roca, E., Vendeville, B.C., 2014. The role of salt layers in the hangingwall deformation of kinked-planar extensional faults: insights from 3D analogue models and comparison with the Parentis Basin. Tectonophysics, 636, 338-350. DOI: 10.1016/j.tecto.2014.09.013

Ferrer, O., McClay, K., Sellier, N., 2016. Influence of fault geometries and mechanical anisotropies on the growth and inversion of hangingwall synclinal basins: Insights from sandbox models and natural examples. In: Child, C., Holdsworth, R.E., Jackson, C.A.L., Manzocchi, T., Walsh, J.J., Yieldings, G. (eds.). The geometry and growth of normal faults. The Geological Society of London, 439 (Special Publications), 487-509. DOI: 10.1144/SP439.8

Ferrer, O., Gratacós,O., Roca, E., Muñoz, J.A., 2017. Modeling the interaction between presalt seamounts and gravitational failure in salt-bearing passive margins: The Messinian case in the northwestern Mediterranean Basin. Interpretation,5(1), SD99-SD117. DOI: 10.1190/INT-2016-0096.1

Ge, H., Jackson, M.P.A., Vendeville, B.C., 1995. Extensional origin of breached Paradox Basin diapirs, Utah and Colorado: Field observations and scaled physical models. In: Huffman, A.C., Lund, W.R.Jr., Godwin, H.L. (eds.). Geology and resources of the Paradox basin: Salt Lake City, UT, Utah Geological Association, Guidebook 25, 285-293.

Gottschalk, R.R., Anderson, A.V., Walker, J.D., Da Silva, J.C., 2004. Modes of contractional salt tectonics in Angola Block 33, Lower Congo basin, West Africa: In Salt-sediment interactions and hydrocarbon prospectivity. Concepts, applications and case studies for the 21st century: Society of Economic Paleontologist and Mineralogist Gulf Coast Section, 24th annual research conference, 705-734.

Graveleau, F., Malavieille, J., Dominguez, S., 2012. Experimental modelling of orogenic wedges: A review. Tectonophysics, 538, 1-66. DOI: 10.1016/j.tecto.2012.01.027

Hammerstein, J., Truelove, L., McClay, K.R., 2014. Additional methods for the analysis of seismic data and risk reduction through the interpretation and reservoir modelling of scaled analogue models. American Association of Petroleum Geologists (AAPG), Houston (Texas, USA),Annual Convention and Exhibition, April 6-9, Datapages/Search and Discovery Article #90189, last accessed: October 2018, website: http://www.searchanddiscovery.com/abstracts/html/2014/90189ace/abstracts/1841538.html

Hubbert, M.K., 1937. Theory of scaled models as applied to the study of geological structures. Geological Society of America Bulletin, 48, 1459-1520. DOI: 10.1130/GSAB-48-1459

Hudec, M.R., Jackson, M.P.A., 2007. Terra infirma: understanding salt tectonics. Earth Science Reviews, 82, 1-28. DOI: 10.1016/j.earscirev.2007.01.001

Huiqi, L., McClay, K.R., Powell, D., 1992. Physical models of thrusts wedges. In: McClay, K.R. (ed.). Thrust Tectonics. London, Chapman and Hall, 71-81.

Jackson, M.P.A., Cramez, C., 1989. Seismic recognition of salt welds in salt tectonics regimes, In: Gulf of Mexico salt tectonics, associated processes and exploration potential. Society of Economic Paleontologists and Mineralogists Gulf Coast Section, 10th annual research conference program and abstracts, 66-71.

Jackson, M.P.A., Vendeville, B.C., 1994. Regional extension as a geologic trigger for diapirism. Geological society of America bulletin, 106(1), 57-73. DOI: 10.1130/0016-7606(1994)106<0057:REAAGT>2.3.CO;2

Jackson, M.P.A., Hudec, M., 2017. Salt Stocks and Salt Walls. In Salt Tectonics: Principles and Practice. Cambridge, Cambridge University Press, 76-118. DOI: 10.1017/9781139003988.008

Jackson, M.P.A., Vendeville, B.C., Schultz-Ela, D.D., 1994. Structural dynamics of salt systems. Annual Review of Earth and Planetary Sciences, 22, 93-117.

Kehle, R.O., 1988. The origin of salt structures. In: Schreiber, B.C. (ed.). Evaporites and Hydrocarbons. Columbia University Press, 345-403.

Konstantinovskaia, E., Malavielle, J., 2005. Erosion and exhumation in acreationary orogens. Experimental and geological approaches. Geochemistry, Geophysics and Geosystems, 6(2), 1-25. DOI: 10.1029/2004GC000794

Koyi, H., Jenyon, M.K., Petersen, K., 1993. The effect of basement faulting on diapirism. Journal of Petroleum Geology, 163, 285-312. DOI: 10.1111/j.1747-5457.1993.tb00339.x

Koyi, H., Petersen, K., 1993. Influence of basement faults on the development of salt structures in the Danish Basin. Marine and Petroleum Geology, 10, 82-94. DOI: 10.1016/0264-8172(93)90015-K

Letouzey, J., Sherkati, S., 2004. Salt Movement, Tectonic Events, and Structural Style in the Central Zagros Fold and Thrust Belt (Iran). Salt-sediments interactions and hydrocarbon prospectivity: Concepts, applications, and case studies for the 21st century. Society of Economic Paleontologist and Mineralogist Gulf Coast Section, 24th annual research conference, 753-778.

Letouzey, J., Colletta, B., Vially, R., Chermette, J.C., 1995. Evolution of Salt-Related Structures in Compressional Settings. In: Jackson, M.P.A., Roberts, D.G., Snelson, S., (eds.). American Association of Petroleum Geologists Memoir 65 on Salt Tectonics: a global perspective, 41-60.

McClay, K.R., 1989. Analogue models of inversion tectonics. In: Cooper, M.A., Williams, G.D. (eds.). Inversion Tectonics. The Geological Society of London, 44 (Special Publications), 44, 41-59. DOI: 10.1144/GSL.SP.1989.044.01.04

McClay, K.R., 1990.Deformation mechanics in analogue models of extensional fault systems. The Geological Society of London, 54 (Special Publications), 445-453. DOI:10.1144/GSL.SP.1990.054.01.40

McClay, K.R., 1995. The geometries and kinematics of inverted fault systems: a review of analogue models studies. In: Buchanan, J.G., Buchanan, P.G. (eds.). Basin Inversion. The Geological Society of London, 88 (Special Publications), 97-118. DOI: 10.1144/GSL.SP.1995.088.01.07

Nalpas, T., Le Douaran, S., Brun, J.-P., Unternehr, P., Richert, J.-P., 1995. Inversion of the Broad Fourteens Basin (offshore Netherlands), a small-scale model investigation. Sedimentary Geology, 95, 237-250.

Nilsen, K.T., Vendeville, B.C., Johansen, J.-T., 1995. Influence of regional tectonics on halokinesis in the Nordkapp Basin, Barents Sea. In: Jackson, M.P.A, Roberts, D.G., Snelson, S. (eds.). Salt tectonics: a global perspective. American Association of Petroleum Geologists (AAPG), 65 (Memoir), 413-436.

Pascoe, R., Hooper, R., Storhaug, K., Harper, H., 1999. Evolution of extensional styles at the southern termination of the Nordland Ridge, Mid-Norway: a response to variations in coupling above Triassic salt. In: Fleet, A.J., Boldy, S.A.R. (eds.). Petroleum Geology of northwest Europe: Proceeding of the 5th Conference.The Geological Society of London, 5,83-90.

Pichot, T., Nalpas, T., 2009. Influence of synkinematic sedimentation in a thrust system with two décollement levels; analogue modelling. Tectonophysics, 473, 466-475. DOI: 10.1016/j.tecto.2009.04.003

Roma,M.,Vidal-Royo,O., McClay, K.R., Ferrer, O., Muñoz, J.A., 2018. Tectonic inversion of salt-detached ramp-syncline basins as illustrated by analog modeling and kinematic restoration. Interpretation, 6(1), T127-T144. DOI: 10.1190/INT-2017-0073.1

Roure, F., Colletta, B., 1996. Cenozoic inversion structures in the foreland of the Pyrenees and Alps. Mémoires du Muséum national d'histoire naturelle,170, 173-209.

Rowan, M.G., 2014. Passive-margin salt basins: Hyperextension, evaporite deposition, and salt tectonics. Basin Research, 26, 154-182. DOI:10.1111/bre.12043

Rowan, M.G., Vendeville, B.C., 2006. Foldbelts with early salt withdrawal and diapirism: Physical model and examples from the northern Gulf of Mexico and the Flinders Ranges, Australia. Marine and Petroleum Geology, 23, 871-891. DOI: 10.1016/j.marpetgeo.2006.08.003

Rowan, M.G., Jackson, M.P.A., Trudgill, B.D., 1999. Salt-related fault families and fault welds in the northern Gulf of Mexico. American Association of Petroleum Geologists (AAPG) Bulletin, 83(9), 1454-1484.

Rowan, M.G., Trudgill, B.D., Fiduk, J.C., 2000. Deep-water, salt-cored foldbelts: Lessons from Mississippi fan and Perdido foldbelts; northen Gulf of Mexico. In: Mohriak, W., Talwani, M. (eds.). Atlantic rifts and continental margins. Washington D.C., American Geophysical Union, Geophysical Monograph, 115, 173-191.

Rowan, M.G., Peel, F.J., Vendeville, B.C., 2004. Gravity-driven fold belts on passive margins. In: McClay, K.R. (ed.). Thrust tectonics and hydrocarbon sustems. Tulsa(OK), American Association of Petroleum Geologist (AAPG), 82 (Memoir), 157-182.

Schellart, W.P., 2000. Shear test results for cohesion and friction coefficients for different granular materials: scaling implications for their usage in analogue modelling. Tectonophysics, 324, 1-16. DOI: 10.1016/S0040-1951(00)00111-6

Soto, R., Casas-Sainz, A.M., Del Río, P., 2007. Geometry of half-grabens containing a mid-level viscous décollement. Basin Research, 19, 437-450.DOI: 10.1111/j.1365-2117.2007.00328.x

Stewart, S.A., Clark, J.A., 1999. Impact of salt on the structure of the Central North Sea hydrocarbon fairways. In: Fleet, A.J., Boldy, S.A.R. (eds.). Petroleum Geology of northwest Europe. Proceeding of the 5th Conference. The Geological Society of London, 5, 179-200. DOI: 10.1144/0050179

Storti, F., McClay, K., 1995. Influence of syntectonic sedimentation on thrust wedges in analogue models. Geology, 23(11), 999-1002. DOI: 10.1130/0091-7613(1995)023<0999:IOSSOT>2.3.CO;2

Vendeville, B.C., 2002. A new interpretation of Trusheim's classic model of salt-diapir growth. Gulf Coast Association of Geological Societies Transaction, 52, 943-954.

Vendeville, B.C., Jackson, M.P.A., 1992. The rise of diapirs during thin-skinned extension. Marine and Petroleum Geology, 9, 331-353.

Vendeville, B.C., Nilsen, K.T., 1995. Episodic growth of salt diapirs driven by horizontal shortening. In: Salt, sediment, and hydrocarbons. Society of Economic Paleontologist and Mineralogist Gulf Coast Section, 16th annual research conference program and extended abstracts, 285-295.

Vendeville, B.C., Ge, H., Jackson, M.P.A., 1995. Scale models of salt tectonics during basement-involved extension. Petroleum Geoscience, 1(2), 179-183. DOI: d10.1144/petgeo.1.2.179

Weijermars, R., 1986. Flow behavior and physical chemistry bouncing putties and related polymers in view of tectonic laboratory applications. Tectonophysics, 124, 325-358. DOI: 10.1016/0040-1951(86)90208-8

Withjack, M.O., Callaway, S., 2000. Active normal faulting beneath a salt layer: an experimental study of deformation patterns in the cover sequence. American Association of Petroleum Geologists Bulletin, 84(5), 627-651.

Yamada, Y., McClay, K.R., 2003a. Application of geometric models to inverted listric fault systems in sandbox experiments. Paper 2: insights for possible along strike

migration of material during 3D hanging wall deformation. Journal of Structural Geology, 25(9), 1551-11560. DOI: 10.1016/S0191-8141(02)00181-5

Yamada, Y., McClay, K.R., 2003b. Application of geometric models to inverted listric fault systems in sandbox experiments. Paper 1: 2D hanging wall deformation and section restoration. Journal of Structural Geology, 25(8), 1331-1336. DOI: 10.1016/S0191-8141(02)00160-8

Manuscript received February 2018;
revision accepted May 2018;
published Online November 2018.